Supplementary information for:

Determinants of lithium-ion battery technology cost decline

Micah S. Ziegler,[†] Juhyun Song,[†] and Jessika E. Trancik[†,‡,*]

October 2021

Contents

[†]Institute for Data, Systems, and Society, Massachusetts Institute of Technology, Cambridge, MA, USA.
[‡]Santa Fe Institute, Santa Fe, NM, USA.
[*]trancik@mit.edu

1 Additional methodological details

1.1 Methods flowchart

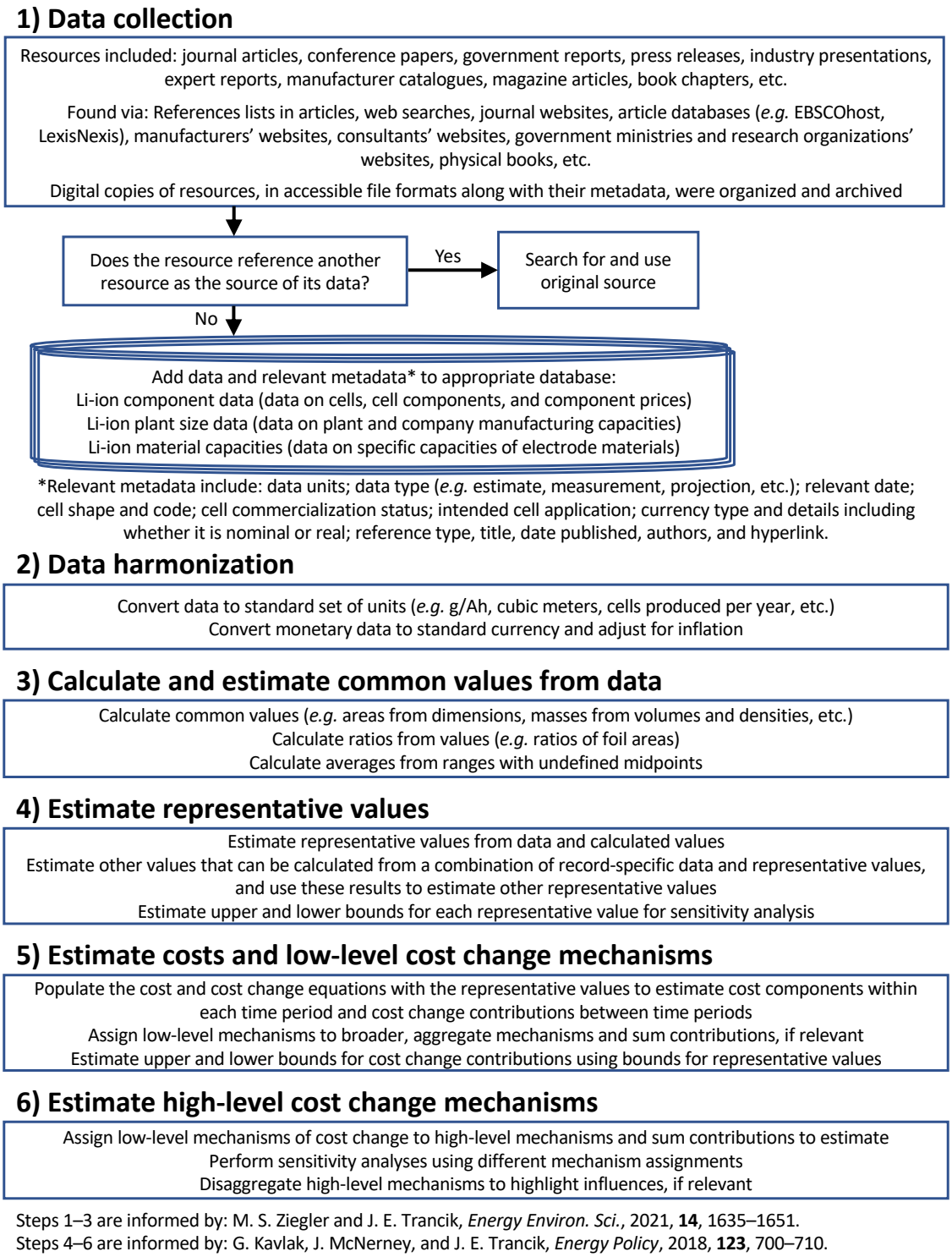

Figure S1: Flowchart summarizing our general data collection, harmonization, and analysis approach.

1.2 Data extraction from previously published plots

Data collection focused on numerically presented data when available. When data underlying plots were unavailable, values were extracted from plots digitally using WebPlotDigitizer (v 4.1, released January 8, 2018).[1]

2 Cell component analyses and assumptions

2.1 Cell component geometry calculations and assumptions

In many cases, a few measures were reported for cell components, such as thicknesses or volumes, and a set of assumptions allowed other metrics to be calculated. One key geometric assumption is that all active material layers, foils, and separators are rectangular prisms with external dimensions governed by:

$$\text{volume} = \text{length} \times \text{width} \times \text{thickness} \tag{1}$$

and areas given by:

$$\text{area} = \text{length} \times \text{width}. \tag{2}$$

Similarly, "jelly rolls" composed of rolled layers of cathode, anode, and a separator, and sometimes rolled around a mandrel, are assumed to be cylinders with geometries governed by:

$$\text{volume} = \pi \times \text{radius}^2 \times \text{height}. \tag{3}$$

The "jelly roll" dry volume was assumed to be the sum of the volumes of the coated cathode material, coated anode material, current collector foils, separator(s), and mandrel, if present. Unless otherwise specified, cylindrical cells were assumed to contain one sheet each of a cathode foil, anode foil, and separator. When the length and width of an unrolled "jelly roll" were given and current collectors' dimensions were not, the foils' lengths and widths were assumed to be equal to those of the "jelly roll." Separators' widths were similarly assumed to be the same as the "jelly roll" widths, as has been assumed previously.[2] Moreover, unless explicitly stated otherwise, cathodes and anodes were assumed to have the same exterior dimensions for length and width. When the extent of a current collector foil coated with cathode or anode material was not specified, the entire foil area was assumed to be coated. In addition, if not specified, mandrel height was assumed to be equal to the widest foil or separator.

2.2 Cell component masses and densities

Many studies that include breakdowns of commercial cells indicate that components were rinsed and dried, and then massed. When this was the case and sufficient data were available, the electrolyte solution mass was estimated by subtracting the sum of the dried components' masses from the overall unopened cell mass. In addition, when possible, material densities were calculated by dividing measured masses of materials by

measured volumes. Meanwhile, the densities of copper and aluminum current collector foils were taken from the Handbook of Chemistry and Physics.[3]

2.3 Cell voltage calculations and assumptions

In some cases, cell capacity (in Ah or Wh) or nominal voltage were unreported. If two of the three values were available, the third was calculated using the equation:

$$\text{energy capacity (Wh)} = \text{charge capacity (Ah)} \times \text{nominal voltage (V)}\,. \tag{4}$$

3 Development of representative physical values

3.1 Electrode active materials and their specific charge capacities

We collected specific charge capacities for a range of possible "active" or "lithium-hosting" or "lithium-storage" electrode materials and categorized them by value type, including "theoretical", "experimental", "initial", "reversible", "practical", "commercial", and "unclear". In this work, we are primarily concerned with the capacities of electrode materials relevant to their use in commercially available lithium-ion cells, which are often denoted "reversible", "practical", or "commercial". In a few cases, "unclear" values were incorporated if their use in context suggested that they approximate "reversible" or "practical" values. If ranges for a specific material were given, the average was employed. When blends of materials, typically cathode materials, were reported without specific mass or volume ratios, 1:1 mass ratios were assumed.

Practical specific charge capacity values are not necessarily time-independent because different cell chemistries, material modifications, electrolyte solution additives, and formation processes can alter capacity utilization. For example, the values collected for lithium cobalt oxide are plotted in Figure S2 and those for "graphite" in Figure S3.

3.1.1 Cathode

For values collected and representative values estimated, see Figure S2 and Figures S4–S6.

Period 1. The cathode material for cells in period 1 was taken to be lithium cobalt oxide ($LiCoO_2$, LCO) as the records we collected, among a variety of references,[4–6] indicate that $LiCoO_2$ was the primary cathode material used in the 1990s to construct commercial high energy density cells. The specific capacity was estimated by averaging the values reported between 1995 and 2000 (inclusive) that were "reversible", "practical", or "commercial". The representative value obtained is: 0.139 Ah/g. For the data-informed sensitivity analysis, the uncertainty range for this value comprises the minimum and maximum values reported for $LiCoO_2$ during the period.

Period 2. As lithium-ion technologies have improved, different cathode compositions have been employed to construct high energy density cylindrical cells and reduce costs. In this work, the period 2 technological representation focuses on data collected from high energy density cells that use either 2:1 $LiCoO_2$/$Li(Ni_{0.50}Mn_{0.25}Co_{0.25})O_2$ or $Li(Ni_{0.80}Co_{0.15}Al_{0.05})O_2$ (NCA) as cathode materials. Thus, the period 2 cathode specific capacity was estimated by averaging the specific capacities of these two cathode compositions. To incorporate slightly more data from reliable references, specific capacities reported in 2009 were also included in the development of this representative value. In addition, a value for $Li(Ni_{0.50}Mn_{0.25}Co_{0.25})O_2$ was not available so instead the average of $Li(Ni_{0.5}Mn_{0.3}Co_{0.2})O_2$ and $Li(Ni_{0.6}Mn_{0.2}Co_{0.2})O_2$ capacities, including those reported in 2018 and 2019, was used. The representative value obtained is: 0.180 Ah/g.

The uncertainty range for this value is informed by estimates of which cathode materials were employed industry-wide during period 2, which indicate considerable use of $LiCoO_2$, NCA, $LiMn_2O_4$ (LMO), and various compositions of $Li(Ni_xMn_yCo_{(z\,=\,1\,-\,x\,-\,y)})O_2$ (NMC-XYZ where $X = x\times10$, etc., or when the ratios of the first-row transition metals were unspecified simply NMC).[7,8] While we also obtained data describing cells with cathode materials containing $LiFePO_4$ (LFP), these were excluded from the development of our representative values as per our focus on high energy density cells in period 2. Considering this focus on cells with high energy density, the lower end of the range is the average specific capacity reported during the period for $LiCoO_2$. We note that these values might reflect active materials composed primarily of $LiCoO_2$ with various coatings or other modifications employed to increase its practical specific capacity. The upper bound of the range reflects the capacities reported for $Li(Ni_{1/3}Mn_{1/3}Co_{1/3})O_2$ (NMC-333) and $Li(Ni_{0.80}Co_{0.15}Al_{0.05})O_2$ and is the average of the average specific capacities reported for these two cathode materials between 2009 and 2015.

3.1.2 Anode

For values collected and representative values estimated, see Figure S3.

Period 1. The records we collected evidence the use of various carbonaceous materials through the 1990s, notably "soft carbon", "hard carbon", and "graphite". More detailed material descriptions, such as "petroleum coke", were provided in a few cases. The detailed cell composition data we use to develop a representative technology for period 1 are derived primarily from cells whose anode material is simply described as "graphite". We decided to focus on cells containing graphite-based anodes both because reports suggest graphite anodes became common by the late 1990s and because their flat-discharge curves make them more comparable to cells in the second period.[9,10] As such, we averaged values reported for "graphite", including those that were specifically labeled as natural or synthetic, over the course of period 1, giving a representative value of: 0.334 Ah/g. The uncertainty range for this value comprises the 25^{th} and 75^{th} percentiles of the values employed to calculate the average.

Period 2. We were unable to find many records of commercially relevant specific capacities for "graphite" published between 2010 and 2015, so we expanded the window to include 2009 through 2018. (Many references instead cited the theoretical maximum of 0.372 Ah/g.) Averaging collected specific capacities reported for graphite, including the natural and synthetic subcategories, yielded a value of 0.348 Ah/g, which is inconsistent with reports of higher practical values (ca. 0.360 Ah/g) having been achieved years earlier.[9] The average was found to be brought down by values obtained from papers surveying ranges of available graphite materials, not necessarily focusing on those materials commonly used in commercial cells, especially those cells with high energy density. As a result, the 95^{th} percentile of the specific capacities was used, yielding a representative value of: 0.361 Ah/g. For the uncertainty range, the 80^{th} percentile of the aforementioned set of values is taken as the lower bound. Meanwhile, the highest "practical", "commercial", or "reversible" value reported after 2009 for a graphite anode material is used as the upper bound.

3.2 Electrode materials and their mass fractions

3.2.1 Cathode

Very few resources gave direct measurements of the mass fraction of active, or "lithium-hosting", material used in cathode material mixtures. Thus, these representative values also rely on estimates employed by researchers studying commercially relevant cell chemistries. For values collected and representative values estimated, see Figures S7–S15.

Period 1. For the first period, we only found one reported measurement[6] of the mass fraction of lithium cobalt oxide in the cathode material of a commercial lithium-ion cell: 0.905. The other values found for $LiCoO_2$-based cells described during this period, which included 0.78 and 0.85, were reported for experimental or prototype cells or appeared to be rough estimates. The same report[6] also provided the mass fraction of poly(vinylidene fluoride) (PVDF) binder in the positive electrode material for the same cell. The average binder mass fraction (0.028) is used as our representative value. This value is similar to the mass fraction (0.02) reported by researchers at Bellcore for a $LiMn_2O_4$-based prototype cell constructed by Moli Energy.[11] Similarly, the aforementioned report[6] also provided the mass fraction of carbon, very likely added as the conductive material for the positive electrode. The average mass fraction was 0.067.

Considering the paucity of data, a relatively wide range is employed for our data-informed sensitivity analysis. Based on estimates provided in a variety of sources,[12,13] the lower bound is set at 0.85 and the upper bound at 0.95. The uncertainty bounds for the mass fractions of the other materials are obtained by subtracting the bounds for the lithium-hosting material mass fraction from 1 and splitting the remainder using the ratio of binder to conductive material calculated from the central representative values.

Period 2. For the second period, more values were available and ranged from 0.80 to 0.962. Of the

records describing commercial cells, only two were identified as cells designed to have high energy capacity, as determined by their charge capacities (*e.g.* 3.35 Ah for an 18650 cell) and corresponding energy densities (*e.g.* greater than or equal to 550 Wh/L). Other cells appear to have been specifically designed for power applications or long cycle lifetimes, as suggested by their charging voltage limits (*e.g.* limiting charging to 4.0 V) or cathode materials (*e.g.* $LiFePO_4$). The two high energy capacity cells were estimated or assumed to have metal oxide mass fractions of 0.95 and 0.96, which is consistent with the estimates Marks *et al.*[14] and others[15,16] reported to be commercially relevant by 2010 (0.96). Based on these estimates, the representative mass fraction for period 2 was taken to be: 0.960.

To develop representative mass fractions for binder and conductive materials, we again focused on commercial cells with a high energy capacity, specifically those cells with NMC- or NCA-containing cathode materials that, based on the data available, were not specifically designed for high power or electric vehicle applications. (In this case, we did not use a strict energy density cutoff as energy density details were not available for otherwise useful records.) The average fraction of binder (PVDF) to total binder and conducting material was found to be nearly 0.54. This fraction was then used to apportion the 0.04 mass fraction remaining after subtracting the metal oxide mass fraction from 1. The resulting representative values are 0.022 for binder mass fraction and 0.018 for conducting material mass fraction. These values are very similar to the estimates (0.02 for both mass fractions) reported by Marks *et al.*[14]

Considering the reliability of the references that indicate commercial cells had an active material percentage of about 96% during and around period 2, the uncertainty range assigned to this value is small (± 0.01). The uncertainty bounds for the mass fractions of the other materials are obtained by subtracting the bounds for the lithium-hosting material mass fraction from 1 and splitting the remainder using the fractions of binder and conductive material calculated from the primary values for period 2.

3.2.2 Anode

As with cathode materials, few reports provided mass fractions of the components of anodes. Thus, for the development of these representative values, we rely on measurements and estimates for experimental, prototype, and commercially available cells. We are also not explicitly accounting for the mass faction of any accumulated surface-electrolyte interphase (SEI) layer. For values collected and representative values estimated, see Figures S16–S24.

Period 1. For the first period, the same report[6] that provided mass fractions for cathode materials provided mass fractions for anode materials. For a 1996-vintage lithium-ion cell, the average mass fraction of PVDF binder was reported as: 0.07852, leaving 0.92148 for "carbon". However, the report's analysis does not appear to distinguish lithium-hosting carbonaceous materials from conductive carbonaceous materials. A prototype $LiMn_2O_4$-based cell reported by Bellcore researchers in 1995[11] had lithium-hosting/binder/conducting ma-

terial mass fractions of 0.84:0.12:0.04. However, a cell constructed by LG Chem using "standard procedure" and reported just after period 1 reportedly had no "conductive" carbonaceous material added to the anode material mixture.[17] Given this uncertainty, we average the two values (0.04 and 0.00), resulting in an estimate of 0.02 for the mass fraction of conductive material and subtract this value from the carbon mass fraction reported by Isaacs *et al.*[6] The resulting representative anode material mass fractions are 0.901 for lithium-hosting material (*i.e.* graphite, *vide supra*), 0.079 for PVDF binder, and 0.020 for conductive carbon material.

The upper bound for the mass fraction of lithium-hosting material was obtained from the same report describing an experimental LG Chem cell: 0.94. Given the paucity of data, a moderately large uncertainty range was desired so the lower bound was set to 0.86. For anode conducting material, the bounds are the values averaged to obtain the representative value. For anode binder material, a range of ± 0.03 was employed, which covers nearly all values collected for the years during and around period 1.

Period 2. For the second period, more mass fraction values and estimates were available. However, once the data were limited to commercial cells with graphite anode materials, and cells designed for long cycle life or electric vehicles were rejected along with a low reliability estimate, lithium-hosting material mass fractions ranged from 0.92 to 0.954 (average: 0.941), binder mass fractions from 0.033 to 0.051 (average: 0.045), and conducting material from 0 to 0.03 (average: 0.014). (Note: the values reported by Golubkov *et al.*[18] are adjusted to compensate for their added consideration of the SEI mass fraction.) In these cases, the binder material was reported to be carboxymethylcellulose, sometimes specified as its sodium salt and sometimes mixed with styrene-butadiene rubber. The conducting material was typically assumed or reported to be carbon black. This shift away from PVDF binders is consistent with other reports.[19] The average for the lithium-hosting material (*i.e.* graphite, *vide supra*) mass fraction was taken as the representative value. The average fraction of the binder material mass fraction to the sum of the binder and conductor material mass fractions was determined and applied to the remainder after subtracting the lithium-hosting material mass fraction from 1 to obtain 0.046 for binder, and 0.013 for conductive carbon material. The uncertainty bounds for each components' mass fraction are taken from the minimum and maximum values, as given above.

3.3 Calculating charge capacities for active (or "lithium-hosting") materials

For records that contain an estimate or measure of the total mass of electrode material but no estimate of the mass or mass fraction of lithium-hosting material, the representative mass fractions were employed to estimate the mass of lithium-hosting material. For values before the first period, the representative mass fraction for the first period was used. For values after the second period, the representative mass fraction for the second period was used. For values between the two periods, the average of the two periods' representative mass fractions was used.

Then, for records of cells that contain both (1) a measure or estimate of the mass of lithium-hosting material and (2) details on the chemical composition of cathode active material, but no value for the lithium-hosting materials' charge capacities, these materials' charge capacities were estimated. In these cases, the specific charge capacities employed were chemistry-specific, not simply the representative values estimated above, and were estimated by averaging the data collected on the specific capacities of each lithium-ion hosting material for the appropriate time range.

3.4 N/P Ratios

For the cell records for which sufficient data were available or could be calculated from other reported data or representative values, N/P ratios were calculated by dividing the charge capacity of the lithium-hosting anode material by the charge capacity of the lithium-hosting cathode material. These N/P ratios represent "initial" values and rely on reversible, practical specific capacities for the cathode and anode materials; they do not consider cell aging or degradation. For values collected and representative values estimated, see Figures S25–S26.

Period 1. As the representative anode material and specific capacity for period 1 were limited to graphite-based anode chemistry, the N/P ratio was also limited to cells using graphite-based anodes, for which we have a handful of records during period 1. A record meant to represent average, practical N/P ratio values was also included.[20] One of the calculated N/P ratios was very low and attributed to an anode-limited cell design and excluded from this analysis. The remaining values were averaged to give a representative N/P ratio for period 1. The uncertainty bounds are the minimum and maximum of the values averaged to obtain the representative value.

Period 2. For the second period, considering the diversification of cell types, we limited the sample used to cells designed to have high energy density (*i.e.* restricting the analysis to cells with nameplate energy density greater than or equal to 550 Wh/L). (The N/P ratios derived from the values reported by Golubkov *et al.*[18,21] were estimated by using the representative values derived herein as opposed to using the charge capacities estimated in their work.) The resulting values were averaged to give a representative N/P ratio for period 2. For the uncertainty range, the lower bound was taken to be 1 (representing a perfectly balanced cell), and the upper bound was set to the maximum of those values averaged to give the representative value.

3.5 Electrolyte solution mass to cathode charge capacity ratios

In nearly all collected records, the electrolyte solution in non-experimental lithium-ion cells was composed of lithium hexafluorophosphate ($LiPF_6$) dissolved in organic carbonates, such as ethylene carbonate, propylene

carbonate, dimethyl carbonate, ethyl methyl carbonate, etc. or a mixture of these, with concentrations of approximately 1 M. The wide prevalence of electrolyte solutions composed primarily of $LiPF_6$ in mixtures of organic carbonates is consistent with early and recent reports that describe electrolyte solution composition in commercial lithium-ion cells.[7,22–28]

For the cell records for which sufficient data were available or could be calculated from other reported data and/or representative values, the ratios of electrolyte solution mass to cathode charge capacity (in units of g/Ah) were calculated by dividing the electrolyte solution mass by the charge capacity of the lithium-hosting cathode material. Ratios of electrolyte solution mass to cathode charge capacity are plotted in Figure S27. A second plot, in which only cells considered to have high energy density during period 2 are shown, is provided as Figure S28. The ratios of electrolyte solution volume to cathode charge capacity, sometimes estimated by assuming an electrolyte solution density of 1.27 g/mL, are plotted in Figure S29. In addition, electrolyte solution masses for commercial 18650-sized cells are plotted in Figure S30 along with the electrolyte solution masses obtained by multiplying the representative electrolyte solution mass to cathode charge capacity ratios by the representative cathode charge capacities for a fixed volume for each period.

Period 1. The estimated values for commercial, cathode-limited, 18650-sized cells from period 1 were averaged to give a representative ratio of electrolyte solution mass to cathode charge capacity for period 1. The uncertainty range comprises the minimum and maximum of the averaged values.

Period 2. Considering this work's focus on high energy density cells, cells with energy density less than 550 Wh/L were excluded. The remaining estimates for commercial, 18650-sized cells were averaged to give a representative ratio of electrolyte solution mass to cathode charge capacity for period 2. The uncertainty range comprises the minimum and maximum of the averaged values.

3.6 Electrode foil areas

In nearly all collected records for commercial cells, the cathode material was coated on aluminum foil while the anode material was coated on copper foil. Areas of electrode foils from commercial 18650-sized cells are plotted in Figures S31 and S32. These areas only reflect one side of the electrode foils. Most of the collected records describe cells with electrodes coated on both sides of the foil, with coated areas typically close to double the single-side values. For this cost change analysis, the single-side areas are used, along with the electrode foil thicknesses.

Period 1. The measured and estimated values for commercial 18650-sized cells from period 1 were averaged to give representative electrode foil areas for period 1. The lower uncertainty bound is the 25^{th}percentile of the values. However, as there is one considerably higher value in the set, the 75^{th} percentile is lower than

the mean. Thus, an upper uncertainty bound is estimated by taking the difference of the representative value and the lower bound and adding the difference to the representative value to generate a symmetric uncertainty range.

Period 2. A pair of values, both the cathode and anode foil areas for a single record, which were unreasonably low (by an order of magnitude), was excluded from the analysis. The remaining values for commercial 18650-sized cells were averaged to give representative electrode foil areas for period 2. The uncertainty bounds comprise the 25^{th} and 75^{th} percentiles of the values.

3.7 Anode to cathode foil area ratios

The same data used to develop representative values for cathode and anode foils' areas were used to calculate the ratio between the foils' areas. For records where both anode and cathode foil areas were reported or could be calculated from other reported values, their ratios were determined by

$$\text{Anode to cathode foil area ratio} = \frac{\text{anode foil area}}{\text{cathode foil area}} \tag{5}$$

and the results are plotted in Figure S33. The ratios were then averaged within periods to give representative ratios for periods 1 and 2. For the first period, the uncertainty range comprises the minimum and maximum of the averaged values. For the second period, the range's minimum was set to 1, while the maximum was set to the highest value.

3.8 Separator to cathode foil area ratios

For nearly all collected records of commercial cylindrical cells, the separators' compositions were reported to be polyethylene (PE) or polypropylene (PP). One cell contained a layered PP/PE/PP separator while another had one PP separator and a second PE separator. Separator areas of commercial 18650-sized cells are plotted in Figure S34. As with the electrode foils, these areas only reflect one side of the separator. For records where separator and cathode foil areas were both reported, or could be calculated from reported values, their ratios were calculated using

$$\text{separator to cathode foil area ratio} = \frac{\text{separator area}}{\text{cathode foil area}} \tag{6}$$

and the results are plotted in Figure S35.

Period 1. The ratios for commercial 18650-sized cells from period 1 were averaged to give a representative separator to cathode area ratio. The uncertainty range comprises the minimum and maximum of the averaged values.

Period 2. A pair of values, both the cathode and anode foil areas for a single record, which were unreasonably low (by an order of magnitude), was excluded from the analysis. The remaining ratios for commercial 18650-sized cells were averaged to give a representative separator to cathode area ratio for period 2. The uncertainty range comprises the minimum and maximum of the averaged values.

3.9 Cathode foil, anode foil, and separator thicknesses

Thicknesses of cathode foils, anode foils, and separators were reported by a variety of sources. While all three thicknesses were typically reported as part of cell breakdown or modeling studies, separator thicknesses were also sometimes reported in reviews of separator materials. In this work, the representative values were developed from the values found specifically for commercial 18650-sized cells. Values from the aforementioned record with unreasonably low foil areas were also excluded from this analysis. Collected and representative values are plotted in Figures S36–S38.

Period 1. The thicknesses for foils and separators for commercial 18650-sized cells from period 1 were averaged to give representative thicknesses for all three materials. The uncertainty ranges comprise the minima and maxima of the averaged values.

Period 2. The thicknesses for foils and separators for commercial 18650-sized cells from period 2 were averaged to give representative thicknesses for all three materials. The uncertainty ranges comprise the minima and maxima of the averaged values.

3.10 Separator densities

Separator densities were reported by a few sources. However, most separators extracted from commercial cells were reported to simply be composed of polyethylene or polypropylene. More detailed composition information, for example whether or not they included a coating, was often not included in reports. As such, separator densities for the two periods are estimated empirically and are plotted in Figure S39. These values are not included in the final cost equation but are used in later calculations.

Period 1. The separator densities calculated from mass and volume values measured for commercial, cylindrical cells from period 1 were averaged to give a representative density value.

Period 2. The separator densities calculated from mass and volume values measured for commercial, cylindrical cells from period 2 were averaged to give a representative density value.

3.11 Charge capacity utilization

Reports suggest that in the early-to-mid 1990s, manufacturers of cylindrical lithium-ion cells produced cells whose charge capacities were limited by either the cathode or anode (*i.e.* cathode- or anode-limited cells) and that over time manufacturers shifted toward producing cathode-limited cells.[5,29–36] Considering the two time periods being compared, this work focuses on cathode-limited cells. To determine how much of the cathode charge capacity is employed to provide usable energy storage, the ratio of a cell's typical nameplate charge capacity to the total cathode active material charge capacity was calculated for cells for which both values were available or could be estimated from other data and details. The ratio was calculated by dividing the typical cell charge capacity (in Ah) by the cathode material charge capacity (also in Ah), and the results are plotted in Figure S40. Some values are a few percent above 1, an error we attribute to the approximations required to estimate some of these values. Notably, the mass fraction and specific charge capacity of the lithium-hosting cathode materials are estimated based on a variety of details and roughly time-specific averages. In addition, to simplify slightly, we are not explicitly accounting for excess cathode material that might have be included to aid SEI formation.[37]

Period 1. For the period 1 records, cells with N/P ratios lower than 0.95 (likely anode-limited) were excluded along with non-commercial, non-18650–sized cells. The remaining cathode capacity utilization values were averaged to give the representative cathode charge capacity utilization for the period. The minimum and maximum values compose the uncertainty bounds.

Period 2. For the second period, considering the diversification of cell types, we limited the sample used to commercial 18650-sized cells designed to have high energy density (*i.e.* restricting the analysis to cells with nameplate energy density greater than or equal to 550 Wh/L). For results derived from Golubkov *et al.*,[21] utilization ratios were estimated using representative values derived in this work as opposed to using the charge capacities estimated in their work. The cathode charge capacity utilization values estimated for high energy density cells were averaged to yield a representative value for period 2. The minimum and maximum values compose the uncertainty bounds.

3.12 Cathode charge capacity

Representative cathode charge capacity estimates were determined from records collected in the previously described lithium-ion technology database.[38] In both periods, the database was restricted to records containing nameplate descriptions of 18650-sized, commercially available lithium-ion cells (Fig. S41). As different numbers of records were collected for different years, trending toward more data collected for more recent years, the average charge capacity was calculated for each year within period 1 or period 2 and the mean of these averages was taken as the representative nameplate value for each period. This nameplate charge

capacity was then divided by the representative charge capacity utilization percentage estimated for the given period.

Period 1. For period 1, the average nameplate charge capacity was estimated to be 1.443 Ah, which after division by the cathode capacity utilization ratio, gives a representative cathode charge capacity of 1.726 Ah. The minimum nameplate charge capacity values for each year were similarly averaged and divided by the representative cathode charge capacity utilization percentage to give the lower uncertainty bound. Analogously, the maximum values for each year gave the upper bound.

Period 2. For period 2, the database was further limited to those cells with energy densities greater than 550 Wh/L. The average nameplate charge capacity was estimated to be 2.978 Ah, which after division by the capacity utilization ratio, gives a representative cathode charge capacity of 3.129 Ah. As more data were available, the uncertainty bounds were based on 25^{th} and 75^{th} percentiles. For each year, these percentiles were calculated for the set of nameplate charge capacity values. The average of the annual 25^{th} percentile values was divided by the representative cathode charge capacity utilization percentage to give the lower bound while the upper bound was similarly calculated from the average of the annual 75^{th} percentile values.

3.13 Nominal operating voltage

Representative nominal operating voltage values were determined from records collected in the previously described lithium-ion technology database.[38] In both periods, the database was restricted to records containing nameplate descriptions of commercially available cylindrical lithium-ion cells (Fig. S42). As different numbers of records were collected for different years, trending toward more data collected for more recent years, the average nominal operating voltage was calculated for each year within period 1 or period 2 and the mean of these averages was taken as the representative value for each period.

Period 1. For period 1, the averaging described above afforded a representative value of: 3.642 V. The average of the annual minimum values was taken as the lower bound while the average of the annual maximum values was taken as the upper bound.

Period 2. For period 2, the database was further limited to those cells with energy densities greater than 550 Wh/L. The averaging described above afforded a representative value of: 3.659 V. As more data were available for the second period, the average of the annual 25^{th} percentile values was taken as the lower bound while the average of the annual 75^{th} percentile values was taken as the upper bound.

4 Development of representative price values

4.1 Electrode active materials' prices

We collected a variety of specific price values for "active" or "lithium-hosting" electrode materials. Duplicate and projected values were excluded from this analysis, as were sample prices[39] and values assigned for defense-related stockpiling.[40,41]

4.1.1 Cathode

For the specific price values collected for a variety of metal oxides and the representative price values estimated, see Figure S43.

Period 1. The cathode material for cells in period 1 was taken to be lithium cobalt oxide ($LiCoO_2$) (*vide supra*). The representative specific price was estimated by averaging the values reported for $LiCoO_2$ between 1995 and 2000 (inclusive), giving: 0.0868 2018USD/g. Given the small number of prices obtained for this period, the uncertainty range comprises the minimum and maximum prices.

Period 2. As discussed previously, the period 2 technological representation focuses on data collected from high energy density cells that use either 2:1 $LiCoO_2$/$Li(Ni_{0.50}Mn_{0.25}Co_{0.25})O_2$ or $Li(Ni_{0.80}Co_{0.15}Al_{0.05})O_2$ as cathode materials. Just as the period 2 cathode specific capacity was estimated by averaging the two cathode compositions, the price was similarly estimated. First, the prices for a range of metal oxides were estimated by averaging the values obtained for the years between 2010 and 2015 (inclusive): $LiCoO_2$ (0.0472 2018USD/g, n = 7 values); $Li(Ni_{0.80}Co_{0.15}Al_{0.05})O_2$ (0.0363 2018USD/g, n = 9 values); $Li(Ni_{1/3}Mn_{1/3}Co_{1/3})O_2$ (0.0354 2018USD/g, n = 21 values); and $Li(Ni_{0.60}Mn_{0.20}Co_{0.20})O_2$ (0.0321 2018USD/g, n = 2 values). Meanwhile, the price of $Li(Ni_{0.50}Mn_{0.25}Co_{0.25})O_2$ was estimated by averaging the average prices of $Li(Ni_{1/3}Mn_{1/3}Co_{1/3})O_2$ and $Li(Ni_{0.60}Mn_{0.20}Co_{0.20})O_2$. The resulting representative price value for the average of 2:1 $LiCoO_2$/$Li(Ni_{0.50}Mn_{0.25}Co_{0.25})O_2$ and $Li(Ni_{0.80}Co_{0.15}Al_{0.05})O_2$ is: 0.0395 2018USD/g. The lower and upper bounds were estimated analogously, except that the lower bound was composed of the 25^{th} percentile of the collected $LiCoO_2$, $Li(Ni_{1/3}Mn_{1/3}Co_{1/3})O_2$, and $Li(Ni_{0.80}Co_{0.15}Al_{0.05})O_2$ prices and the minimum $Li(Ni_{0.60}Mn_{0.20}Co_{0.20})O_2$ price, and the upper bound was composed of the 75^{th} percentile of the collected $LiCoO_2$, $Li(Ni_{1/3}Mn_{1/3}Co_{1/3})O_2$, and $Li(Ni_{0.80}Co_{0.15}Al_{0.05})O_2$ prices and the maximum $Li(Ni_{0.60}Mn_{0.20}Co_{0.20})O_2$ price.

4.1.2 Anode

For the specific price values collected for a variety of anode materials and representative values estimated, see Figure S44.

Period 1. The representative anode material for period 1 was taken to be graphite. The specific price was estimated by averaging the values collected for graphite, including those categorized as "natural" and "synthetic", as well as "mesocarbon microbeads" (MCMB) and non-specific listings, between 1995 and 2000 (inclusive). The representative price value obtained is: 0.0442 2018USD/g (n = 6). Given the number of prices obtained for this period, the uncertainty range comprises the 25^{th} and 75^{th} percentiles of the prices.

Period 2. The representative anode material in period 2 was also taken to be graphite. The specific price was estimated by averaging the values collected for graphite, including "natural", "synthetic", and non-specific listings, between 2010 and 2015 (inclusive). No MCMB-categorized values were obtained for period 2. The representative price value obtained is: 0.0189 2018USD/g (n = 19). Given the number of prices obtained for this period, the uncertainty range comprises the 25^{th} and 75^{th} percentiles of the prices.

4.2 Electrode binder materials' prices

We similarly collected a variety of specific price values for electrode binder materials. Duplicate and projected values were excluded from this analysis.

4.2.1 Cathode

Nearly all collected records describing commercial cells' cathode materials in both periods indicate that PVDF was employed as the cathode binder. For the specific price values collected, see Figure S45.

Period 1. No price values for PVDF were found for period 1 (1995 through 2000, inclusive). Thus, the representative value was estimated from a record dated 2002, giving a representative binder price of 0.0136 2018USD/g. A wide uncertainty range (± 30%) was employed for this value.

Period 2. Three specific prices for PVDF were found for period 2, with an average price of 0.0165 2018USD/g. This average was taken to be the representative binder price for period 2 even though it is higher than that estimated for period 1. It is unclear whether this upward trend is a consequence of our data collection's limitations or represents an actual increase in binder price. The uncertainty range comprises the minimum and maximum values collected.

4.2.2 Anode

Records describing commercial cells' anode materials suggest that through the 1990s and early 2000s, PVDF was the primary anode binder material. Toward the end of the 2000s and into the 2010s, carboxymethylcellulose (CMC), sometimes mixed with styrene-butadiene rubber, was more commonly observed in records of cell composition (*vide supra*). For the specific price values collected and representative values estimated, see Figure S46.

Period 1. As with cathode binder materials, no price values for PVDF were found for period 1 (1995 through 2000, inclusive). Thus, the representative value was estimated from a record dated 2002, giving a representative binder price of 0.0136 2018USD/g. A wide uncertainty range (± 30%) was employed for this value.

Period 2. Carboxymethylcellulose was taken as the representative anode binder material for period 2. One specific price for CMC for period 2 was found and used as the representative binder price: 0.0115 2018USD/g. A wide uncertainty range (± 30%) was employed for this value.

4.3 Electrode conducting materials' prices

We similarly collected a variety of specific price values for conducting materials added to electrode material mixtures. Duplicate and projected values were excluded from this analysis, as were sample prices.[39] Our collected data suggest that the same range of conducting materials, and their mixtures, was generally used in both cathodes and anodes. These were often reported as "carbon", "carbon black", "graphite", and "acetylene black". For the specific price values collected and representative values estimated, see Figure S47.

Period 1. No price values for conducting material were found for period 1 (1995 through 2000, inclusive). Thus, the representative value was estimated from a record dated 2002, giving a representative conducting material price of 0.00929 2018USD/g. A wide uncertainty range (± 30%) was employed for this value.

Period 2. Four specific prices for carbon black were found for period 2, with an average price of 0.00838 2018USD/g. This average was taken to be the representative conducting material price for period 2. The uncertainty bounds comprise the minimum and maximum prices collected for the period.

4.4 Electrolyte solution prices

We also collected electrolyte solution prices, which were typically reported in either USD/kg or USD/liter. We focused on collecting values that estimate the price for bulk purchases in the context of lithium-ion cell production in an effort to avoid prices for less pure (or more pure) solutions and smaller orders. Duplicates

and projections were rejected. If additional details on the electrolyte solute, solvent, and molarity were provided, we used composition-specific densities, typically obtained from Sigma-Aldrich, to convert USD/liter prices into USD/kg. If these details were unavailable, a density of 1.27 g/mL was employed. The resulting prices, in USD/g, are plotted along with the representative values in Figure S48.

Period 1. The specific electrolyte solution prices for period 1 were averaged to give a representative price of: 0.0737 2018USD/g. Considering the number of prices collected, the uncertainty bounds comprise the minimum and maximum prices collected for the period.

Period 2. The specific electrolyte solution prices for period 2 were averaged to give a representative price of: 0.0191 2018USD/g. Considering the number of prices collected, the uncertainty bounds comprise the 25^{th} and 75^{th} percentiles of the prices.

4.5 Foil prices

Current collector foil prices were collected and were typically reported in either USD/kg or USD/m^2. Both sets of values were converted to units of 2018USD/g. To convert USD/m^2 values to USD/g, foil thicknesses and metal densities were employed. As most reports of foil prices did not specify foil thicknesses, average cathode and anode foil thicknesses for the periods 1990–2000 (inclusive), 2001–2010 (inclusive), and 2011–2020 (inclusive) were developed using the collected values for all shapes of cells, and these averages were employed to estimate prices of current collector foils with unspecified thicknesses. Obvious duplicates and projections and an unreliable value were rejected. The resulting prices, in 2018USD/g, are plotted along with the representative values in Figures S49 and S50.

Period 1. The only foil specific prices collected for cells in period 1 were taken as the representative prices, 0.0283 2018USD/g for the cathode foil and 0.0212 2018USD/g for the anode foil. A wide uncertainty range ($\pm$ 30%) was employed for both foil prices

Period 2. The foil specific prices for period 2 were averaged to give a representative price of: 0.0146 2018USD/g for the cathode foil and 0.0196 2018USD/g for the anode foil. Considering the number of prices collected for both foils, the uncertainty bounds comprise the 25^{th} and 75^{th} percentiles of the prices.

4.6 Separator prices

Most collected separator prices were reported in USD/m^2, while a few prices were reported in USD/g. Both were converted to 2018USD/m^3. Separator prices in USD/m^2 were converted to 2018USD/m^3 using separator thicknesses. If a given record did not specify the separator thickness, as many did not, an average

separator thickness for the decade (*i.e.* 1990–2000 (inclusive), 2001–2010 (inclusive), or 2011–2020 (inclusive)) was calculated and used. These averages were calculated using the same approach employed to develop representative foil thicknesses for the same three decades (*vide supra*). To convert the few prices reported in USD/g, representative separator densities were also required. For separator prices reported for 1990–2000 (inclusive), the period 1 representative separator density was employed. For prices reported for 2001–2010 (inclusive), the average of the first and second periods' representative separator densities was employed. For prices reported for 2011–2020 (inclusive), the period 2 representative separator density was employed. The resulting prices, in 2018USD/m^3, are plotted along with the representative values in Figure S51. Nearly all records of separator prices did not include details regarding separator composition (*e.g.* the number of layers, whether they included a ceramic coating, etc.), precluding analysis of more specific improvements in separator technologies.

Period 1. The separator price densities for period 1 were averaged to give a representative price of: 0.200 $\times 10^6$ 2018USD/m^3. Considering the number of prices collected, the uncertainty bounds comprise the minimum and maximum prices collected for the period.

Period 2. The separator price densities for period 2 were averaged to give a representative price of: 0.0772 $\times 10^6$ 2018USD/m^3. Considering the number of prices collected, the uncertainty bounds comprise the 25^{th} and 75^{th} percentiles of the prices.

4.7 Can, header, safety component, and other hardware costs and prices

Few data were found detailing the prices of cell cans, headers, safety components, and other hardware, and their overall cost contribution. As the hardware yield is taken to be 1 (*vide infra*), the "other hardware" component cost is equal to the total purchase price of the various hardware components.

Period 1. For period 1, the estimated combined cost of these components was derived from a cost breakdown provided by Juzkow and Mayer,[5] which suggests that hardware costs (including, "the header or cap, can, current collectors and tabs") compose 20.1% of cell-level material costs. This percentage can be combined with other estimates to provide a cost estimate of these combined components in units of USD/cell. First, we can employ Gaines and Cuenca's cost estimate of 2 USD/cell.[13] As the value was an upper bound estimate, we will assume it was not inflation adjusted and is in 1999USD, based on the year given for the reference, giving a cost of 2.89 2018USD/cell. Subtracting Gaines and Cuenca's mid-range estimates of non-material costs gives: 2.31 2018USD, 20.1% of which is 0.464 2018USD/cell. A second approach would be to calculate the cost of non-hardware materials employing the representative values estimated herein and assuming that approximately 25.1% of that cost would approximately equal the hardware costs. This approach gives an estimate of 0.653 2018USD/cell. The average of these two estimates (0.559 2018USD/cell) is employed as

the representative combined hardware cost for period 1. The uncertainty range comprises the two averaged estimates.

Period 2. For period 2, we can use estimates provided by Brodd and Helou[42] as well as Ciez and Whitacre.[43] Brodd and Helou report a per cell bill of materials that includes a line for "Can, headers and terminals." However, they also include an "Other (including scrap)" category. As yield is considered separately in this work, we can only use the first line, and we employ it as a rough estimate. Ciez and Whitacre provide much more detail, including costs for a cell container, polymer insulator, and header that includes both a polymer insulator and charge interrupting device. The individual costs, using the averages of the ranges, provided by Ciez and Whitacre are summed to give the representative combined hardware cost for period 2, which is corroborated by its rough similarity to the estimate provided by Brodd and Helou. The lower bound of the uncertainty range was developed by summing the minima of the ranges provided by Ciez and Whitacre while the upper bound was developed by summing the maxima.

5 Development of representative yield estimates

We collected process yield estimates from sources including peer-reviewed articles and industry and government reports that examine and model lithium-ion cell manufacturing processes. In the data analysis, when possible, cell-level yields, which typically represented the number of cells that passed formation or quality-checking stages, are separated from component-level yields. We also focused on including values that reflected what was observed in commercial cell manufacturing.

Manufacturing yields were difficult to estimate and validate using publicly available data, resulting in considerable data uncertainty. Very few reliable data were available, and the data that we did collect were not always consistent. For example, early quantitative yield estimates vary widely,[13,44] while other early estimates are non-specific (*i.e.* one report suggested that by 1999, "producers must have simultaneously reached high yields in their production processes (exceeding 90%) as well as accepting [sic] very thin margins"[45]). Even more recent estimates exhibited considerable variability. For example, a study published in 2017 reported a survey of industry experts who provided central estimates of cell-level yield from 80% to 98%, with a lower bound of 60% and upper bound of 99.5%.[46] Moreover, estimates from a series of reports suggest that material yields might have decreased over time, which could represent a real trend or more accurate information being incorporated into later iterations of models. Plots of the yields collected are presented in Figures S52–S58.

5.1 Material yield estimates

Period 1. Considering the wide discrepancies between early estimates of yields, IIT's values specific to commercial, cylindrical cells were chosen as the representative material yields for period 1.[47] Distinct yields were available for cathode material, including cathode current collector foil; anode material, including anode current collector foil; electrolyte solution, separator material; and hardware components.

For the uncertainty range, the upper bounds were taken as the values presented by Henriksen *et al.* in 2002,[44] except in the case of electrolyte solution and separator where the values provided by Henriksen *et al.* were used as lower bounds. The differences between these bounds and the representative values were used to generate the other bounds, assuming that the uncertainty ranges are symmetric around the representative values. For the hardware cost component, a lower bound of 95% was employed.

Period 2. For the second period, material yield estimates employed are the same as those published by Nelson *et al.*,[48] which are also used by Ciez and Whitacre in their study of the manufacturing process of 18650-sized cells.[43] No estimates of hardware component yields were found for period 2, possibly reflecting the assumption that the value is near 1. As the hardware yield for period 1 was assumed to be 100%, the same estimate was employed for period 2.

The uncertainty ranges for the second period were based on the values reported by Nelson *et al.* in 2009.[49] In the cases where the yields reported by Nelson *et al.* in 2009 were higher than the representative yields, they were employed as upper bounds, and the differences between the upper bounds and representative values were subtracted from the representative values to provide lower bounds. In the case that these values were lower than the representative values, they were employed as lower bounds and the differences were added to the representative values to afford upper bounds. For the hardware cost component, a lower bound of 95% was employed.

5.2 Overall cell-level yield estimates

Period 1. Cell-level yields presented by both Gaines and Cuenca (ca. 99%)[13] and the aforementioned IIT report[47] are consistent and very high. For period 1, the Gaines and Cuenca estimate is employed as the representative value. The uncertainty range's lower bound is 90%, drawing from a general estimate,[45] and its upper bound is 100%.

Period 2. Cell-level yields collected during the second period vary widely, both as a result of the incorporation of survey results, and the diversification of cell types. Notably, many of the later studies focused on prismatic and pouch cell designs. Considering that for 18650-sized cells, earlier reports suggest very high cell-level yields, some of these lower values appeared unreasonable. As such, the higher value from the

aforementioned IIT report[47] was employed as the representative value for period 2. The uncertainty range's lower bound is drawn from the estimate reported by Nelson *et al.* in 2009,[49] and the upper bound is 100%.

6 Development of representative plant sizes and plant size–dependent values

6.1 Development of plant size database

Using the same approach described previously for the development of the reported database of lithium-ion technology characteristics[38] and herein for the database of cell component details, we similarly collected and organized records of production capacities for plants that manufacture lithium-ion cells. Records were mostly collected from newspaper articles, press releases, companies' websites and annual reports, and similar sources. We focused on records of plant-level production capacity measured in units of "cells per month" or "cells per year" because plant size estimates in these units were found throughout the time range for which data were collected. In one case, specifically Sony's early plant in Fukushima Prefecture, we assumed production "units" referred to "cells". Some data were also collected that estimated plant capacity in units of MWh or GWh (see Figure S59). However, as early estimates tended to be in units of "cells" per month or year, estimates using these units were used to develop the representative plant sizes for both periods in order to provide a consistent comparison (*vide infra*).

When available, additional details were collected for each record including:

1. Whether the plant capacity estimates referred to plants in operation or plants currently being planned for a future date (see Figure S60)
2. What lithium-ion cell shape was being manufactured or planned to be manufactured (see Figure S61)
3. Where the plant was located (see Figure S62)

Sometimes reports referenced a given company's production capacity for lithium-ion or lithium-ion polymer cells. These estimates were collected but excluded from this analysis unless additional sources corroborated that the capacity estimate referred to an individual plant.

6.2 Development of representative plant size estimates

Period 1. Our collected data for period 1 contains two estimates for production capacities for plants reported to produce cylindrical cells during that period. The average of the annual production capacities of these plants is employed as the representative plant size. The estimate was corroborated by other estimates of the capacities of existing or planned plants that were producing or expected to produce either prismatic cells or a combination of cylindrical and prismatic cells. The lower bound of the uncertainty range is the lower of the two averaged values. The upper bound is the capacity of a plant expected to produce cylindrical cells and planned for 1999.

Period 2. Our collected data for period 2 contains one estimate for a plant, owned by Panasonic, that was reported to produce cylindrical cells during that period, which is employed as the representative plant size. Period 2 contains a much wider range of plant sizes. However, according to the limited information on the intended applications of the manufactured cells (see Figure S63), at least some of the smaller plants were reported to specifically produce cells for automotive applications. Considering the representative technologies being compared in this study, the Panasonic plant production capacity estimate is likely more representative of the production capacity of a plant manufacturing 18650-sized cells with high energy capacity during period 2. The uncertainty range's lower bound is the capacity of a plant at which LG Chem expected to start production of cylindrical cells by the end of 2004. The uncertainty range's upper bound is the capacity of a plant at which Panasonic expected to start production in 2011.

6.3 Development of representative material and non-material cost fractions

In our collection of cell component quantities and costs, we also compiled data on non-material costs. These data were typically presented as the results of cost modeling efforts, with varying categories of non-material costs. For example, some studies split non-material costs into 'labor, overhead, and depreciation' while others include details on the 'equipment, building, labor, energy, auxiliary equipment, maintenance, and overhead.' Other references simply provide an estimate of the contribution of materials costs to overall cell-level manufacturing costs. The one consistent demarcation was between material and non-material costs so we similarly focus this data analysis on the ratios of material and non-material costs to overall cell costs (Figures S64 and S65). Whenever possible, material and non-material fractions of manufacturing *cost* were carefully distinguished from fractions of *price*, with the latter being excluded from this analysis.

Period 1. We only have one estimate of the fractions of material and non-material costs for a cylindrical lithium-ion cell in period 1 — the estimate provided by Gaines and Cuenca.[13] Based on their "rough estimate" of costs for an 18650-sized cell, they approximate that 75% of total manufacturing costs are material costs, and this percentage is used as the representative value for period 1. This percentage could also be an

overestimate, because their total manufacturing cost was, to the best of our knowledge, only corroborated by an industry estimate of 18650-sized cells costing "under $2 each." The lower bound estimate was also determined from their analysis, assuming the same material cost (1.28 nominal USD per cell) and their maximum cost of 2 nominal USD per cell, giving a material cost percentage of ≈65%. The difference between the representative value and the lower bound was used to estimate an upper bound of 85%.

Period 2. Cost estimates strictly within period 2 are relatively consistent, suggesting that material costs compose between approximately 70 and 85% of total costs of cylindrical cells. However, cell cost breakdown estimates published just after period 2,[43] suggest a much lower contribution of material costs. Ostensibly, this difference could result from the reported model's boundary; the primary model reported includes manufacturing costs from "in-house preparation of cathode active material." Shifting cathode material production "in-house" would increase the non-materials costs, by considering more manufacturing steps, while decreasing material costs, by removing any profit made by the cathode active material suppliers, and possibly transportation costs. However, the same report also provided estimates assuming purchased cathode materials, which similarly suggested a much lower contribution of material costs to overall costs. To further investigate the impact of these estimates of the material cost fraction, we estimated cell-level costs per kWh using the representative material costs developed herein. The results, along with a representative price series for cylindrical lithium-ion cells,[38] are plotted in Figure S66. Considering these results, only the data within period 2 were employed to estimate the representative value.

The multiple estimates for 2010 refer to different cylindrical cell charge capacities.[50] Keeping with the approach of focusing on cells with reasonably high energy density, only those estimates for cells with greater than 550 Wh/L were employed in this analysis. To prevent over-reliance on this one report, the percentages for the high energy density cells in the 2010 report were averaged, as were the two estimates provided in the 2012 report.[42] The resulting averages were themselves averaged to provide the final representative value for period 2. The averages for each individual report were used as the lower and upper uncertainty bounds.

6.4 Development of representative non-material, plant size–dependent cell costs

For each period, the material costs per cell are calculated using the final cost equation (eq. 21) considering the various material-specific yields but not the overall cell-level yield. The result is divided by the material cost percentages (as fractions out of 1) estimated for each period to yield the overall cell cost for each period. Subtracting the sum of the material costs per cell from this overall cell cost estimate provides an estimate of the non-material costs per cell.

6.5 Estimation of scaling factor

The scaling factor (b) was estimated using BatPaC (v. 4.0).[51] Using various distributions, 200 random combinations of cell and manufacturing characteristics were developed. These characteristics included:

- Cathode materials, with LCO, LMO, NMC333, NMC532, NMC622, NMC811, and NCA considered with equal probabilities using a discrete uniform distribution with min=1 and max=7
- Plant size, which was varied between 10^6 and 10^9 cells manufactured per year using a truncated base-10 lognormal distribution with a mean of 7.5 and standard deviation of 1, in log-10 space
- Pack energy capacity, which was varied between 40 and 100 kWh with a truncated normal distribution with a mean of 60 and a standard deviation of 20
- Pack power-to-energy ratio, which was varied between 1 and 10 (1/hr) with a truncated base-10 lognormal distribution with a mean of 1 and standard deviation of 1

All characteristics were varied independently. BatPaC was employed to calculate the costs of manufacturing cells with these characteristics, and the non-material manufacturing costs per cell (excluding profit) were summed. A power law model was fit to data describing the relationship between these non-material costs per cell and plant size, as measured in number of cells manufactured (see Fig. S67). Specifically, the exponent (b) was estimated by fitting a line to the data in log-log space and then rounded. Our estimate of b for lithium-ion cells is: 0.30 with 95% confidence bounds of 0.29 and 0.31. These confidence bounds are not used for our data-informed sensitivity analysis as they represent the results of a single model of cell production processes. Based on a comparison with an estimate of b obtained using results reported by Brodd and Helou,[42] a wider range ($\pm$ 30%) is instead employed in the data-informed sensitivity analysis.

7 Supplementary data and representative values figures

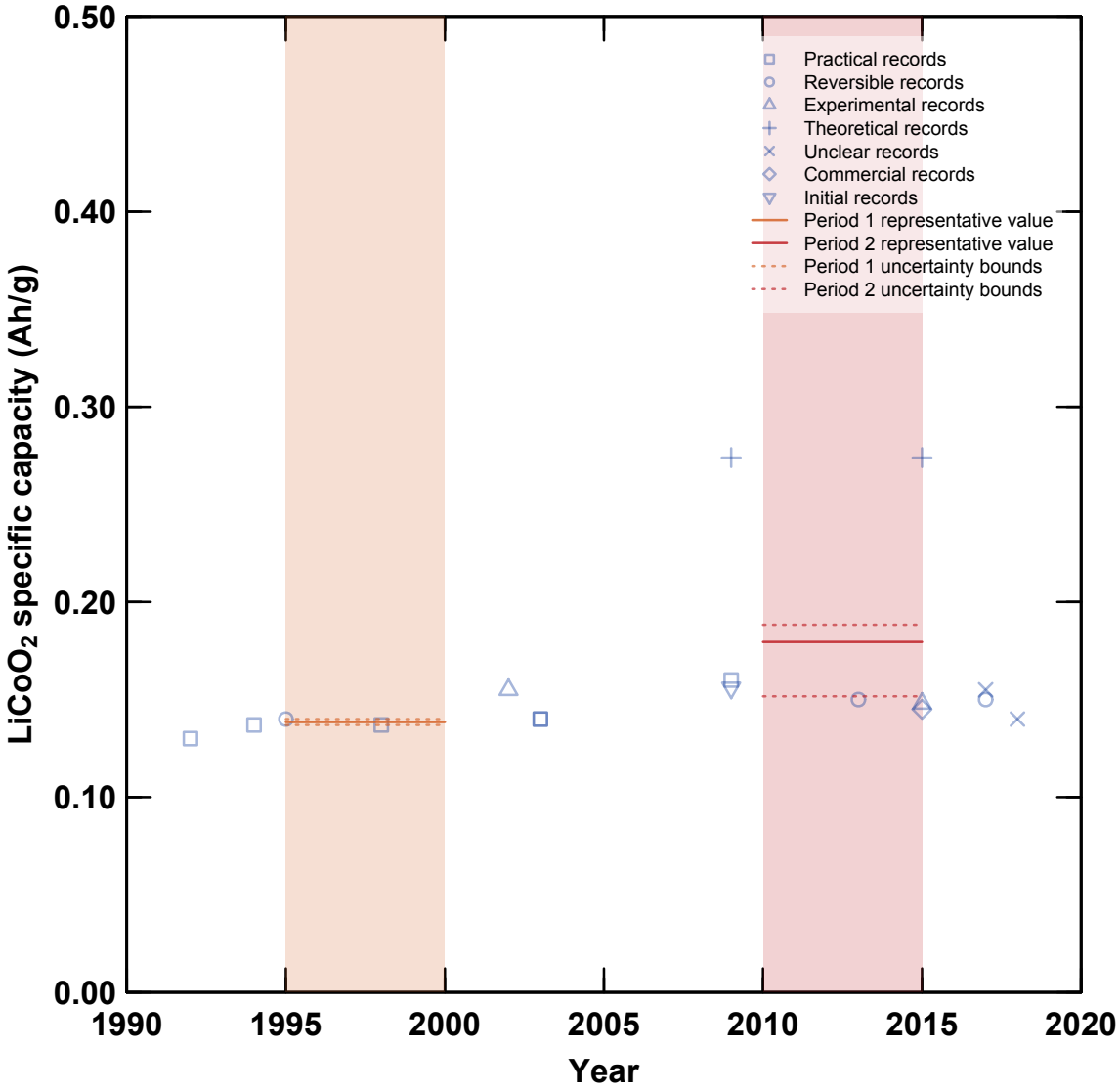

Figure S2: Plot of lithium cobalt oxide specific capacities categorized by value type and versus publication year. Representative values plotted are of cathode active material specific capacities in the first and second periods, whose compositions are not necessarily the same material as depicted by the plotted data points.

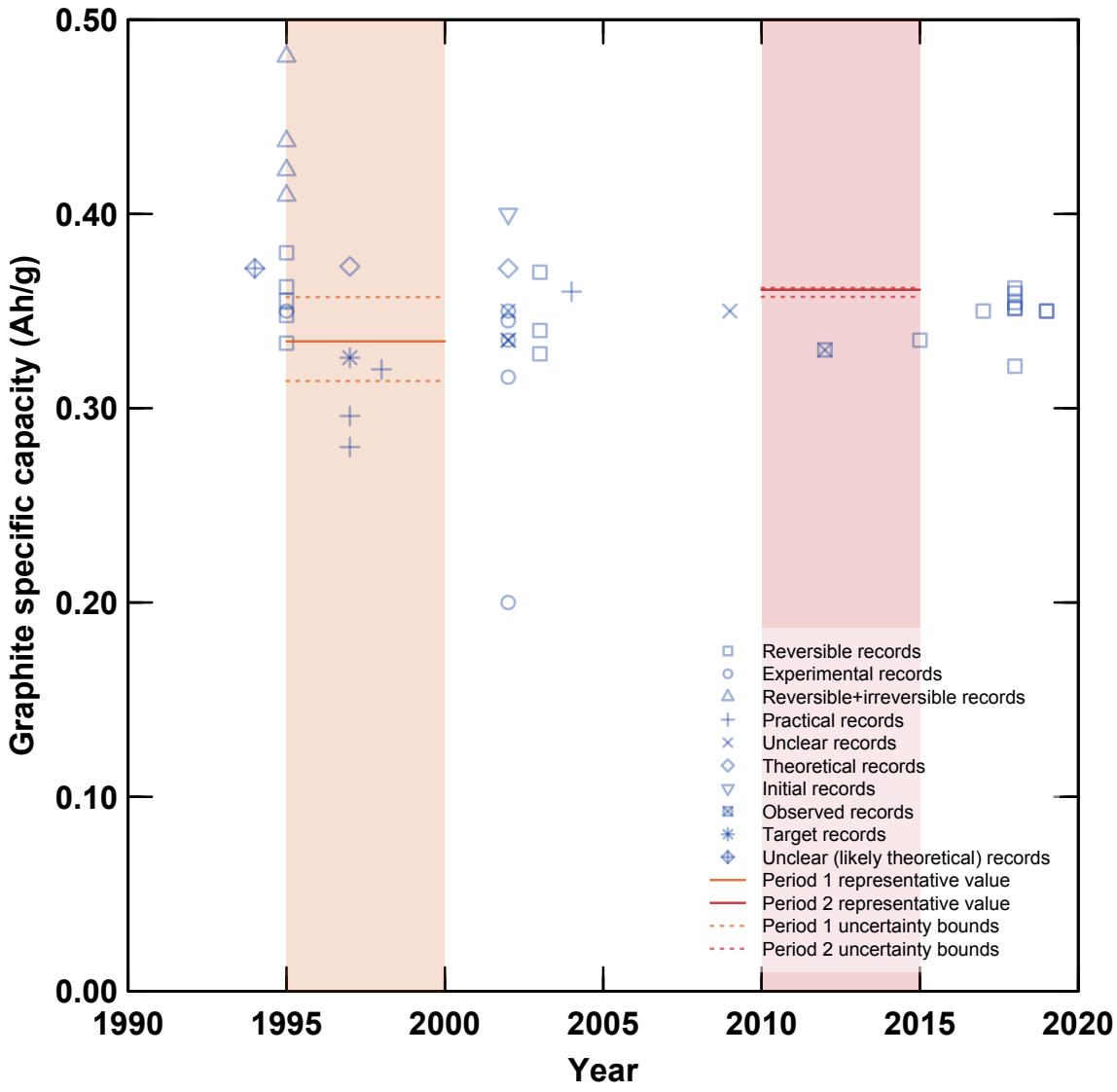

Figure S3: Plot of graphite specific capacities categorized by value type and versus publication year. Representative values plotted are of anode active material specific capacities in the first and second periods, whose compositions are not necessarily the same material as depicted by the plotted data points.

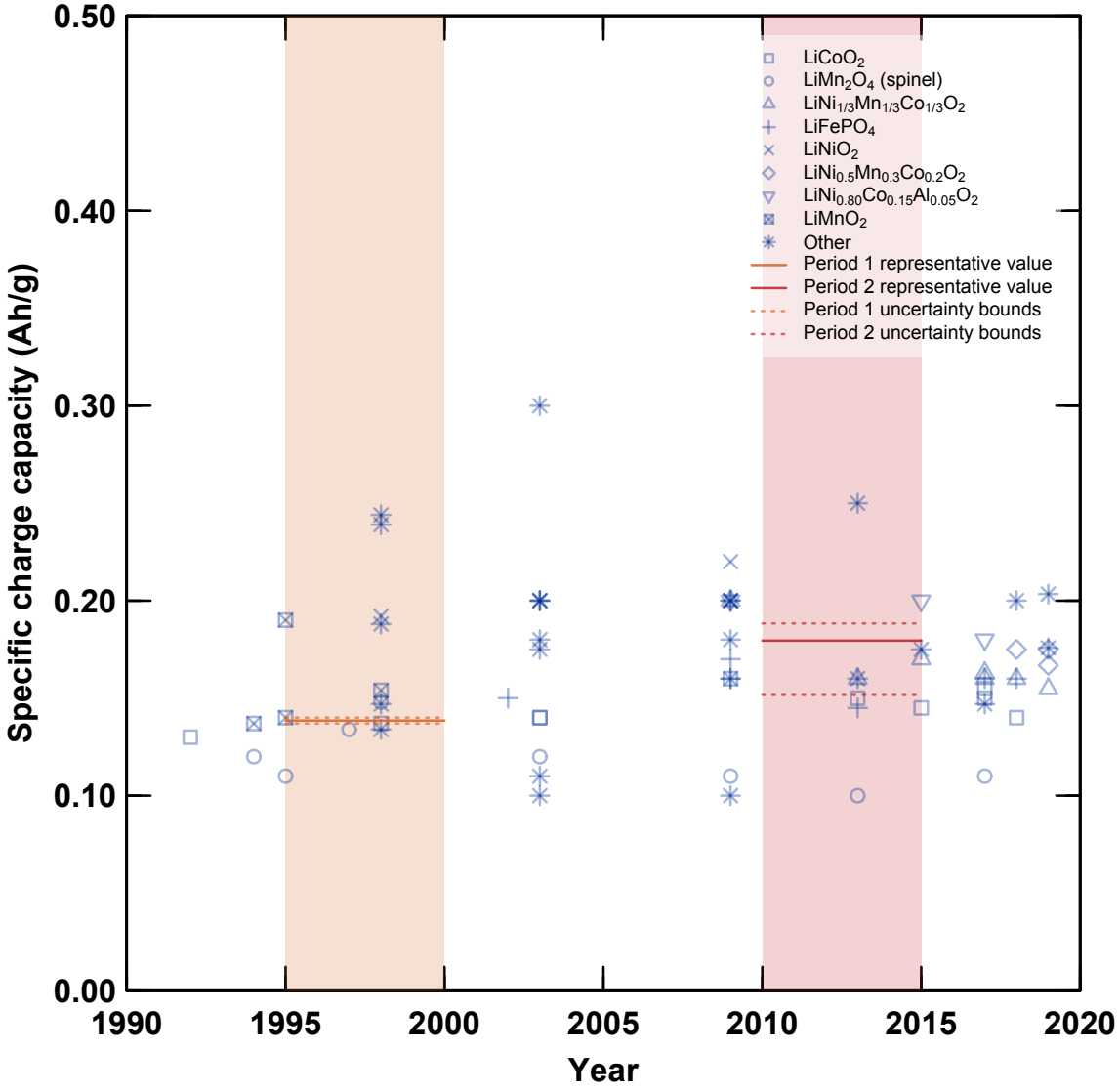

Figure S4: Plot of cathode material specific capacities categorized by material type and versus publication year.

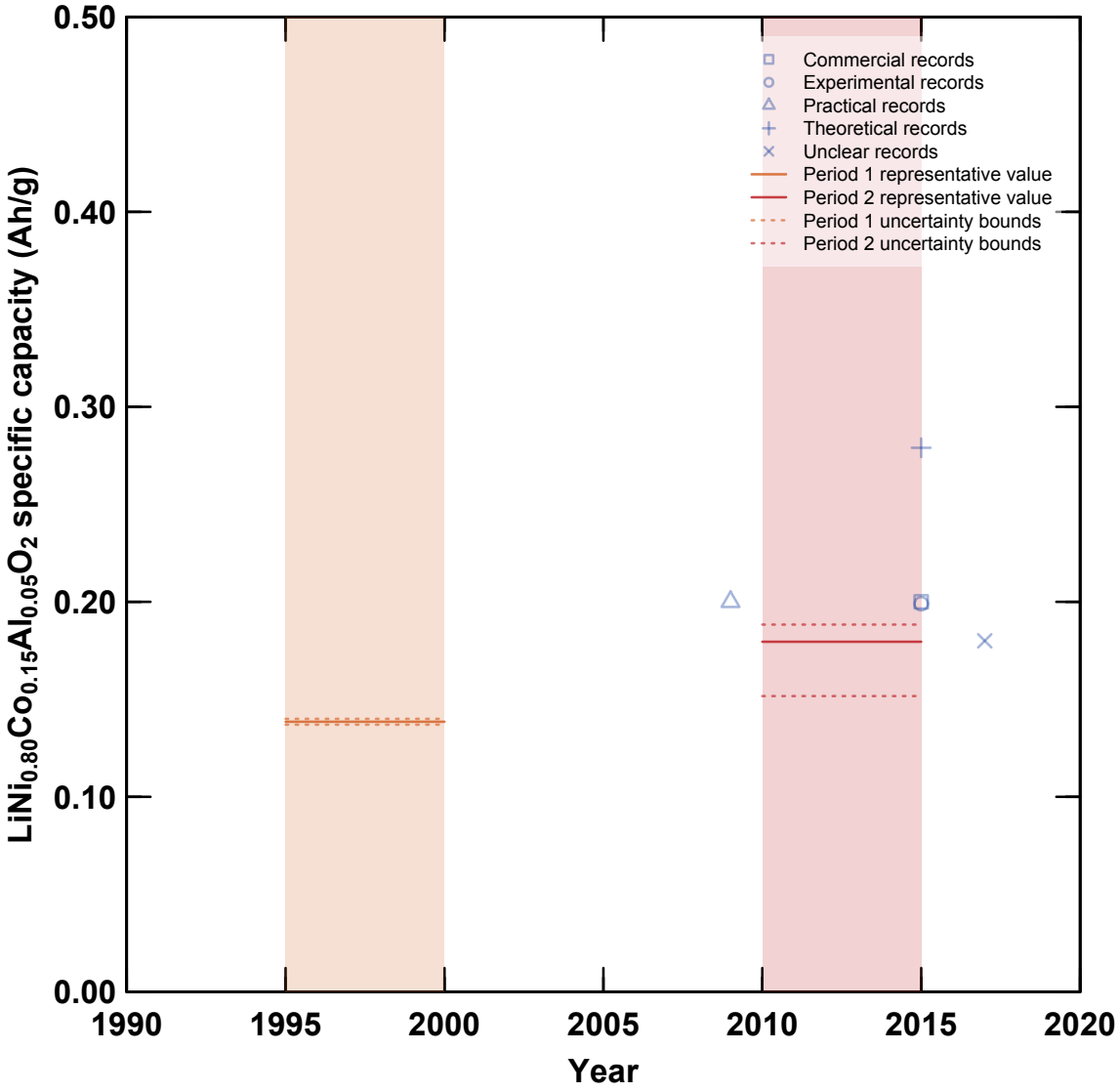

Figure S5: Plot of $LiNi_{0.80}Co_{0.15}Al_{0.05}O_2$ specific capacities categorized by value type and versus publication year. Representative values plotted are of cathode active material specific capacities in the first and second periods, whose compositions are not necessarily the same material as depicted by the plotted data points.

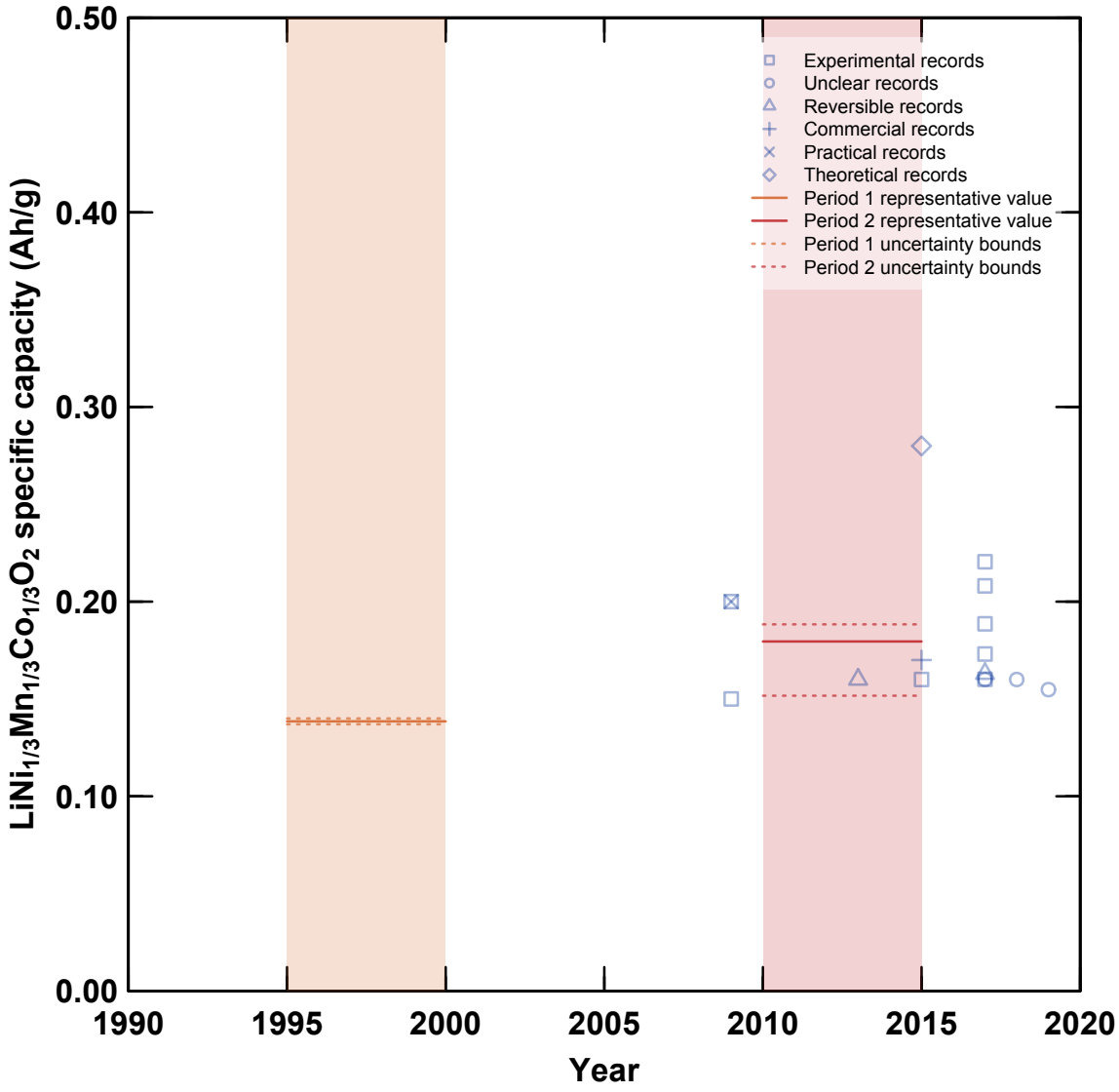

Figure S6: Plot of $LiNi_{1/3}Mn_{1/3}Co_{1/3}O_2$ specific capacities categorized by value type and versus publication year. Representative values plotted are of cathode active material specific capacities in the first and second periods, whose compositions are not necessarily the same material as depicted by the plotted data points.

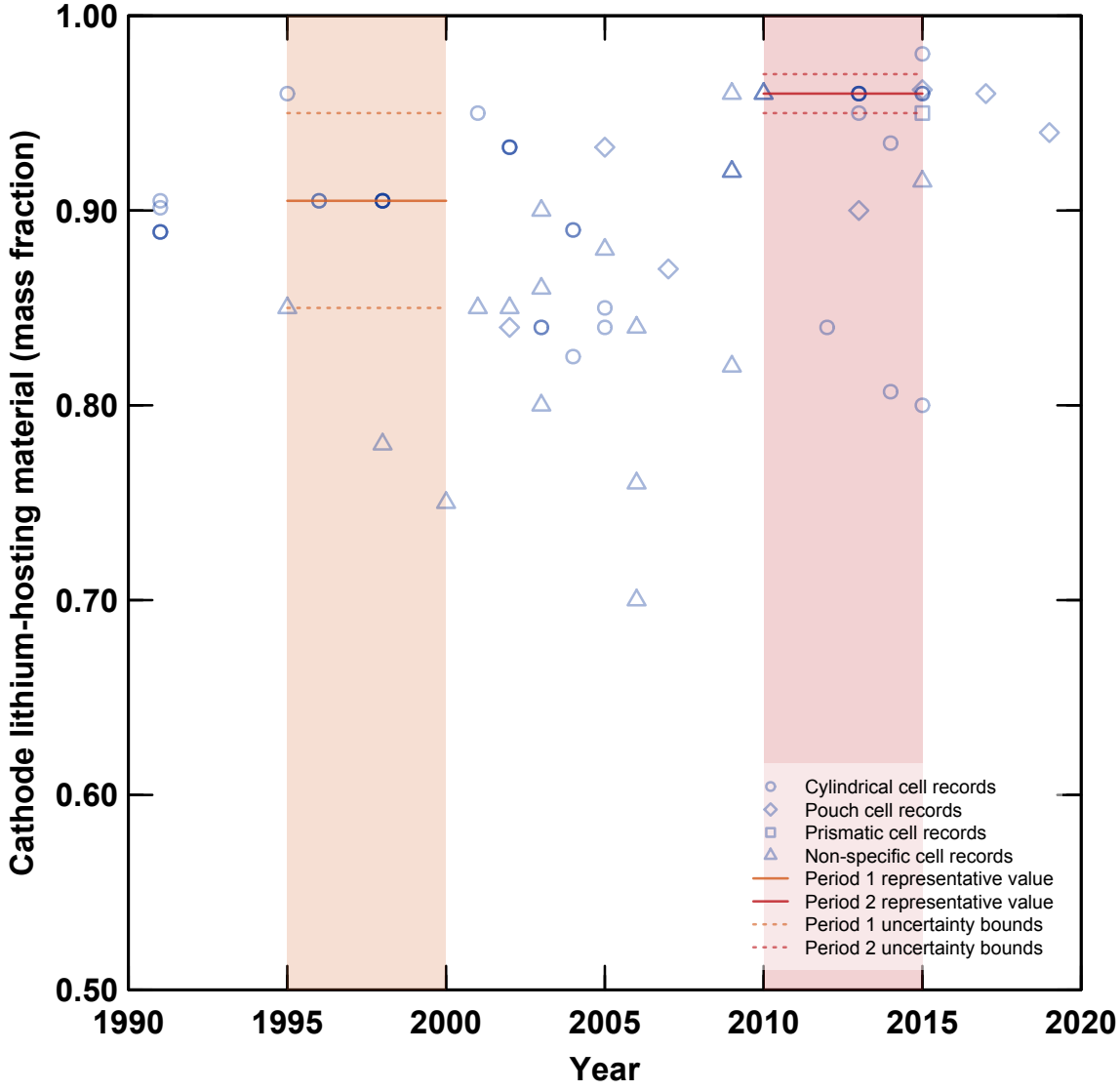

Figure S7: Mass fractions of cathode active (or "lithium-hosting") material in total cathode material, by cell shape.

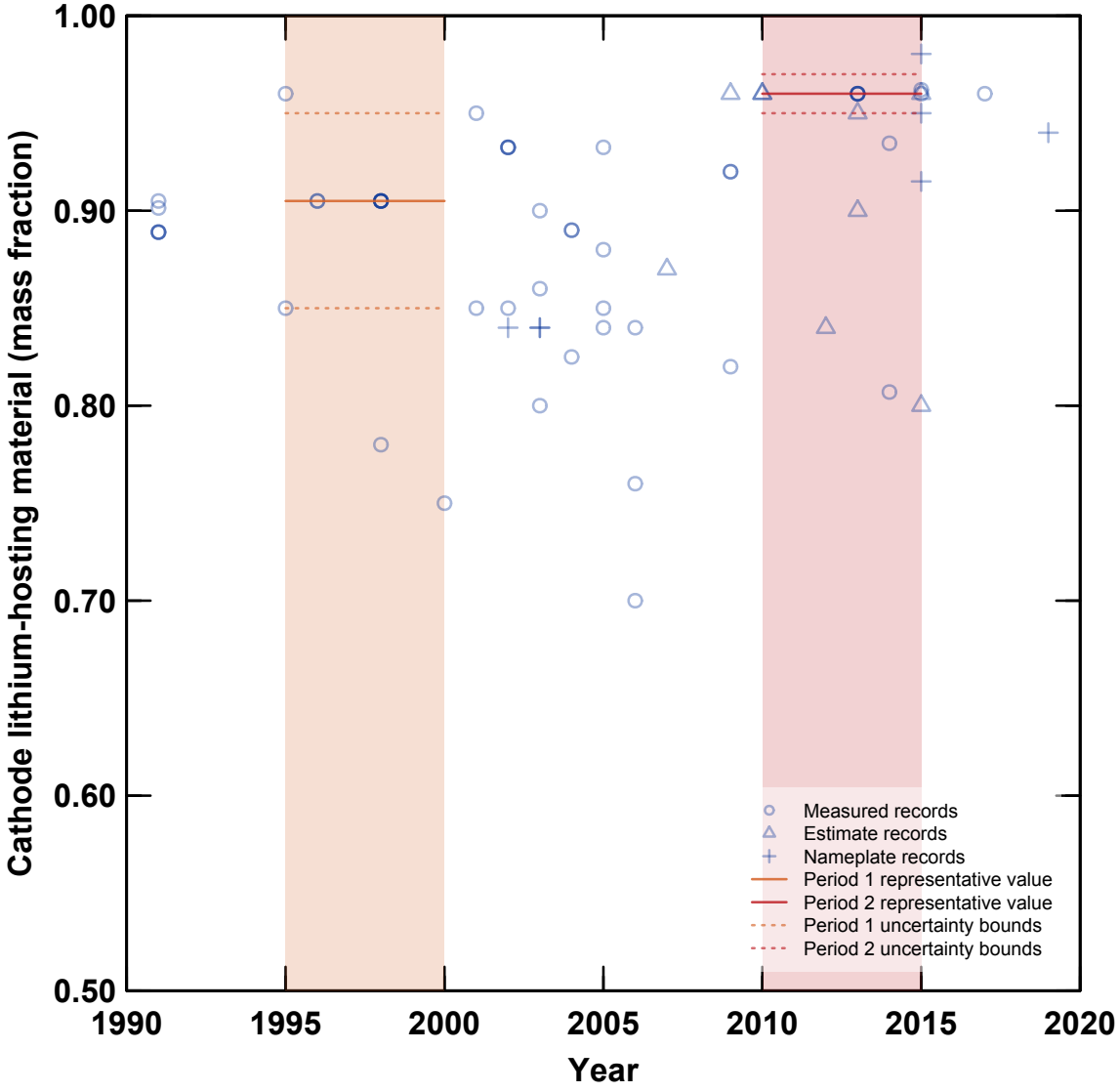

Figure S8: Mass fractions of cathode active (or "lithium-hosting") material in total cathode material, by record type.

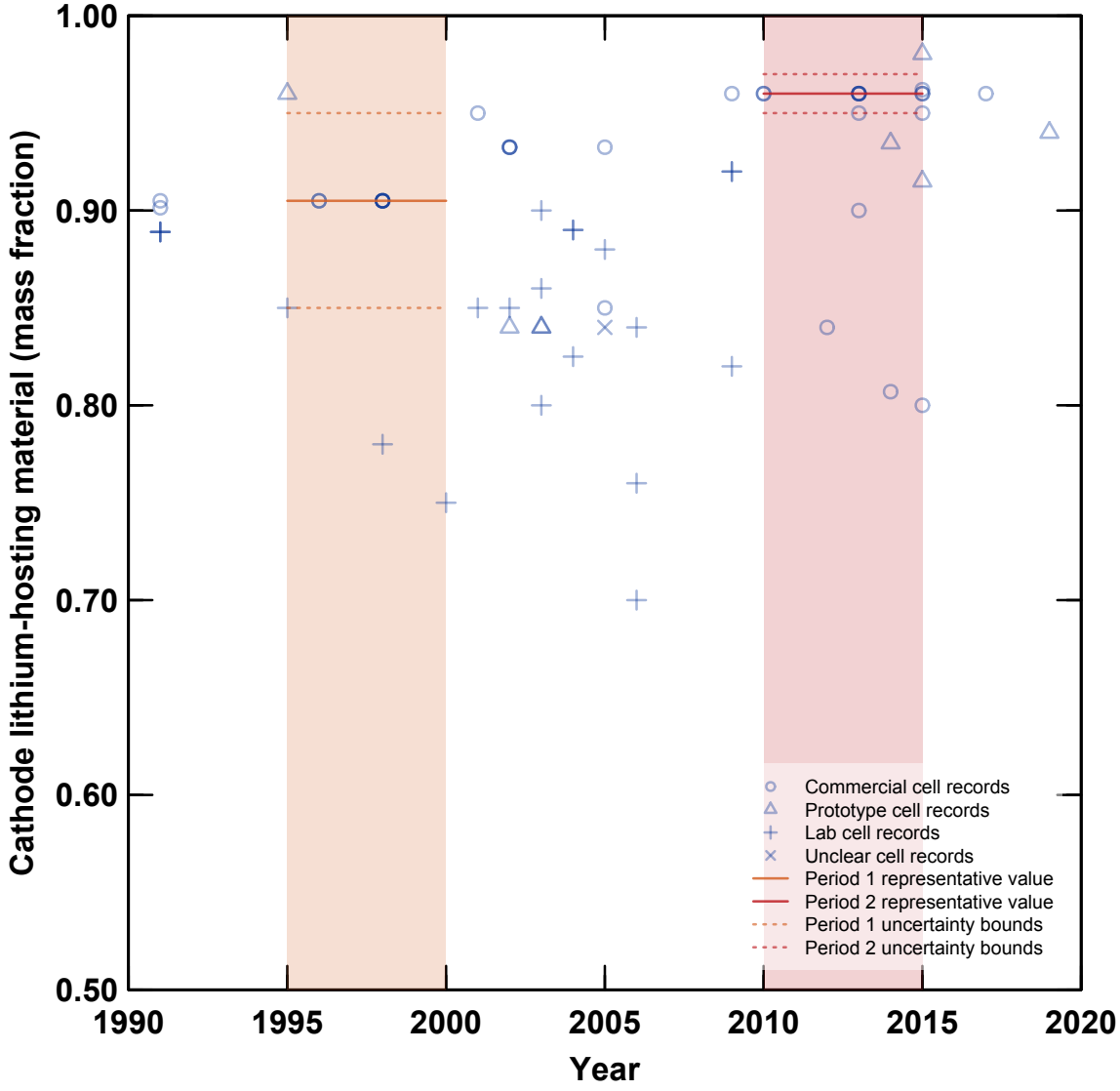

Figure S9: Mass fractions of cathode active (or "lithium-hosting") material in total cathode material, by cell type.

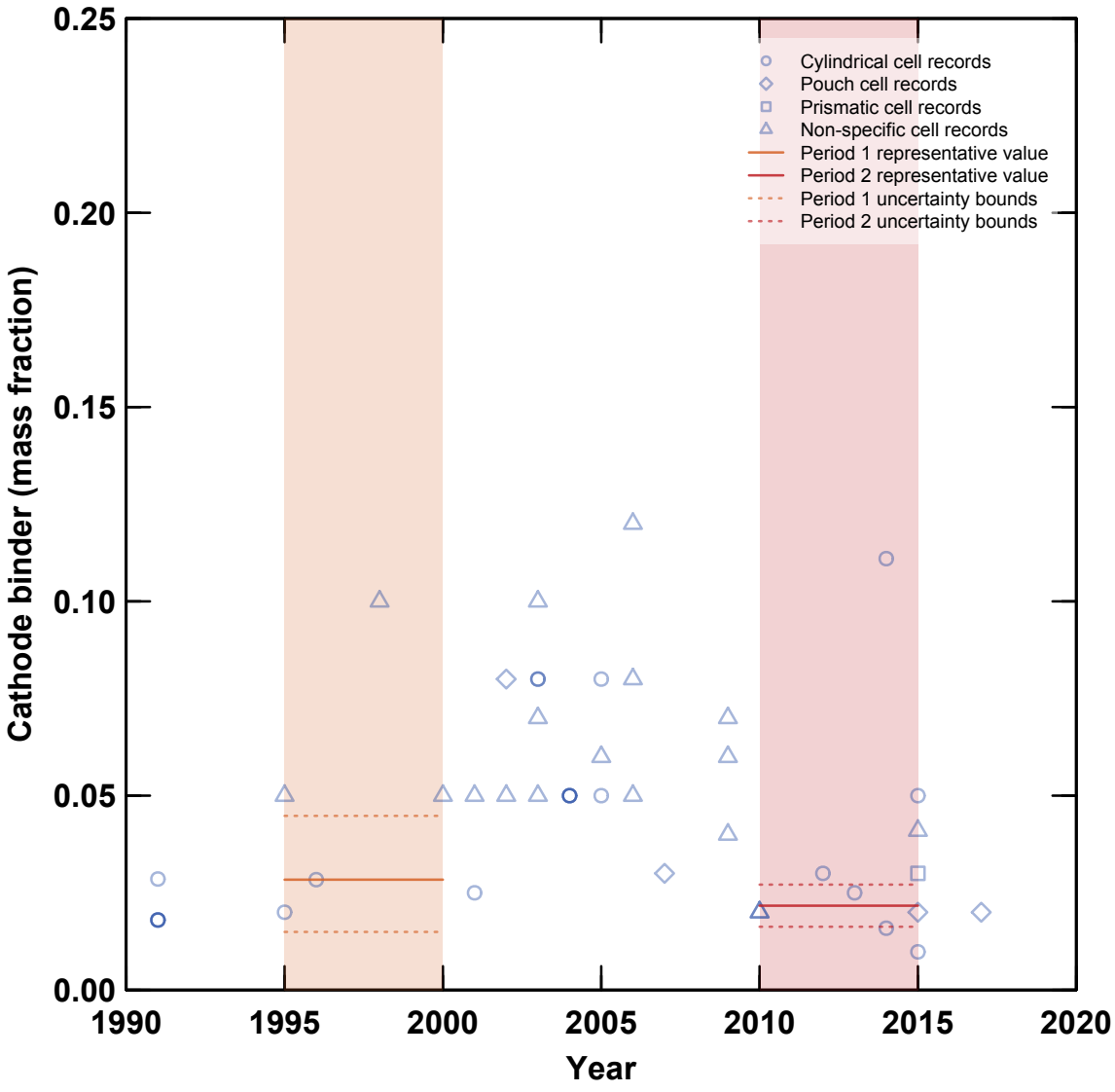

Figure S10: Mass fractions of binder material in total cathode material, by cell shape.

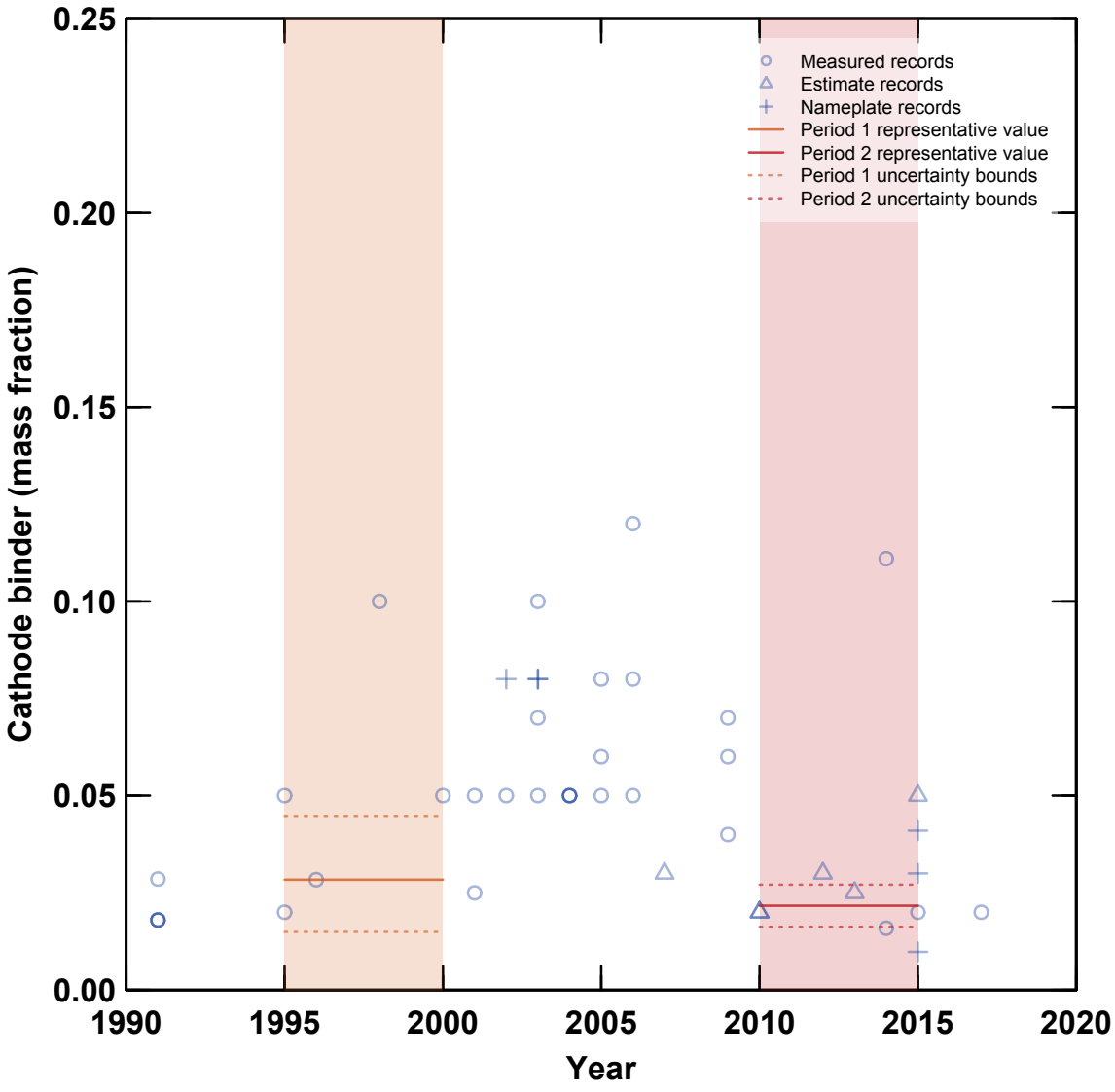

Figure S11: Mass fractions of binder material in total cathode material, by record type.

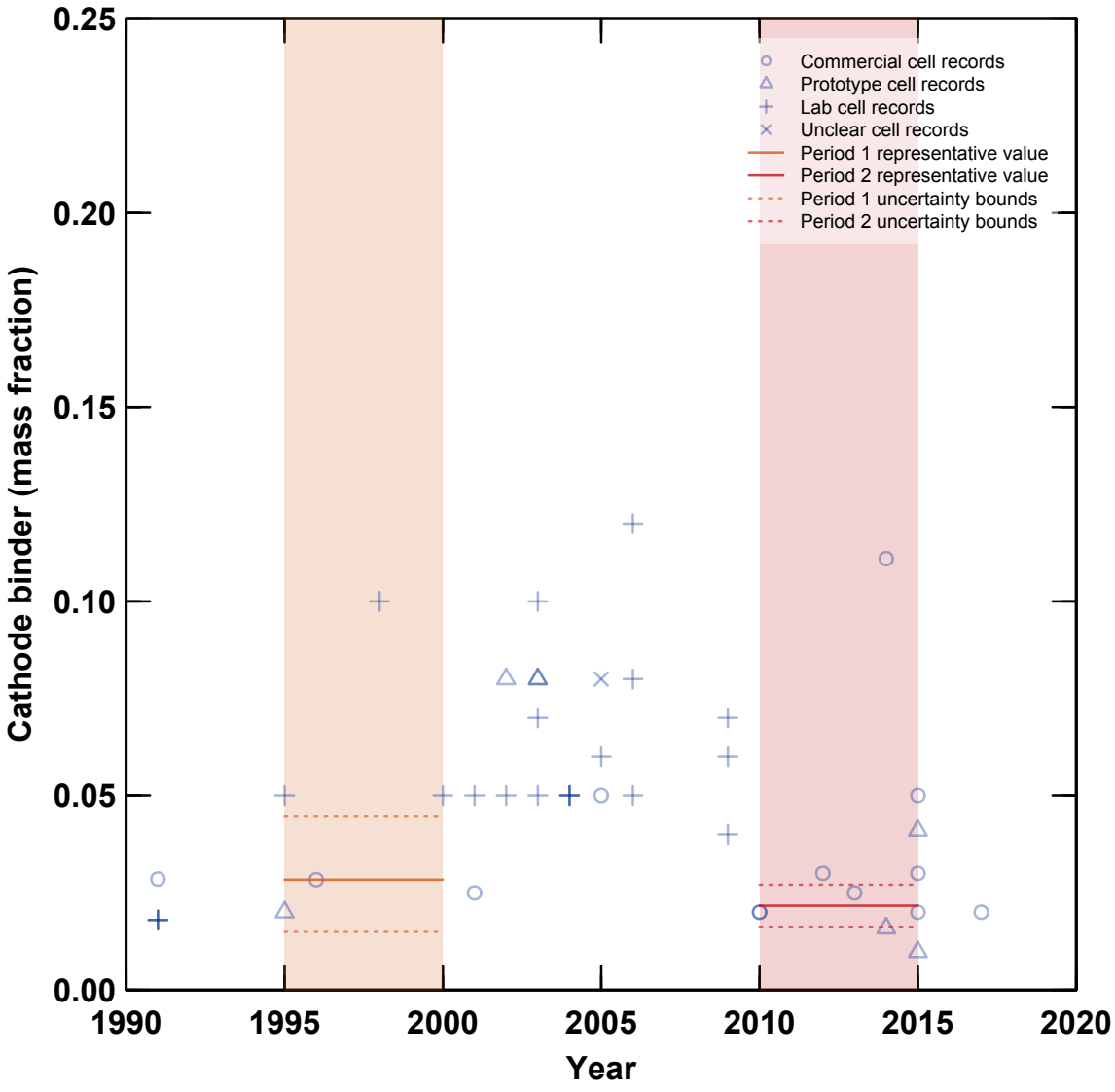

Figure S12: Mass fractions of binder material in total cathode material, by cell type.

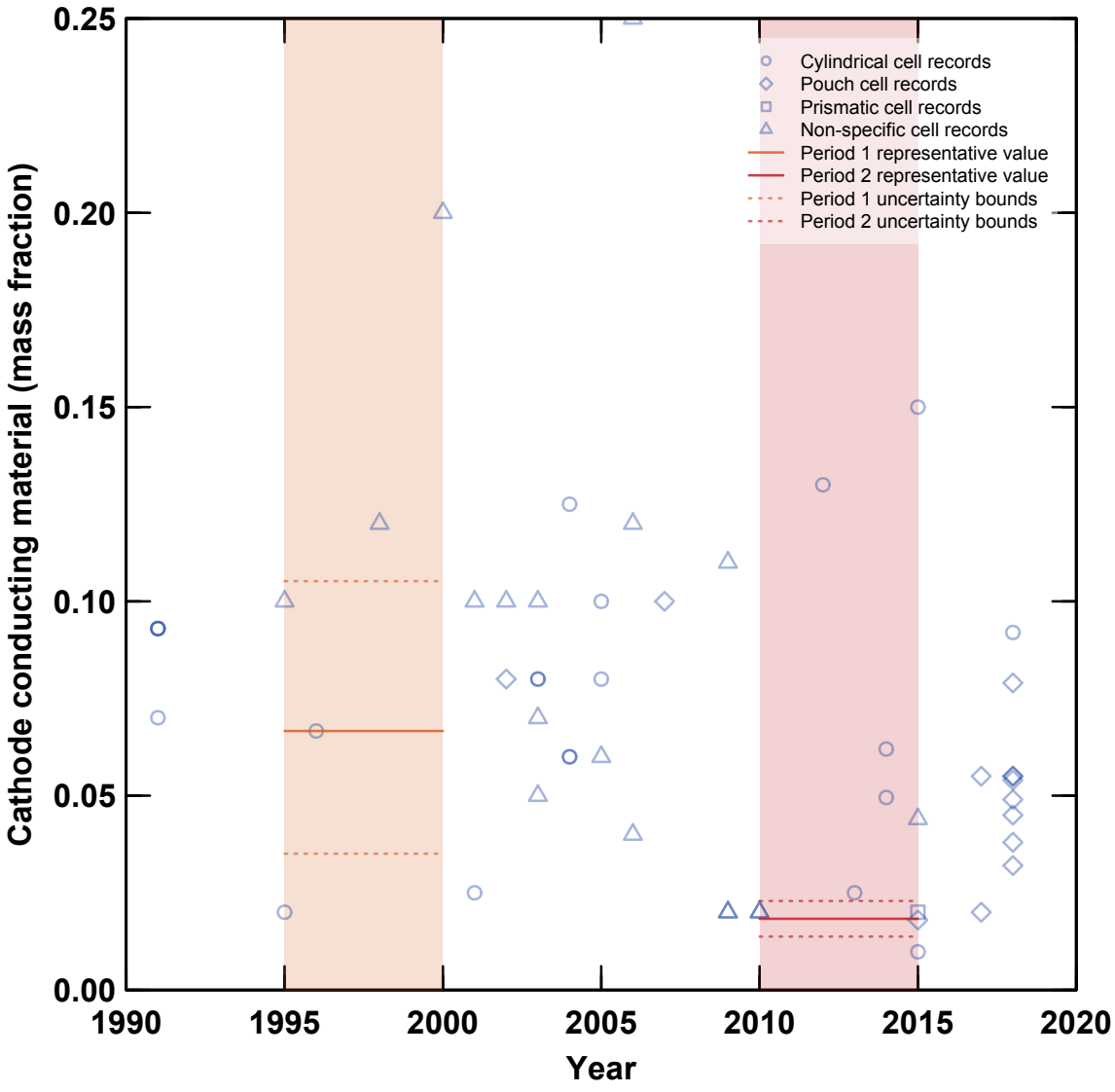

Figure S13: Mass fractions of conducting material in total cathode material, by cell shape.

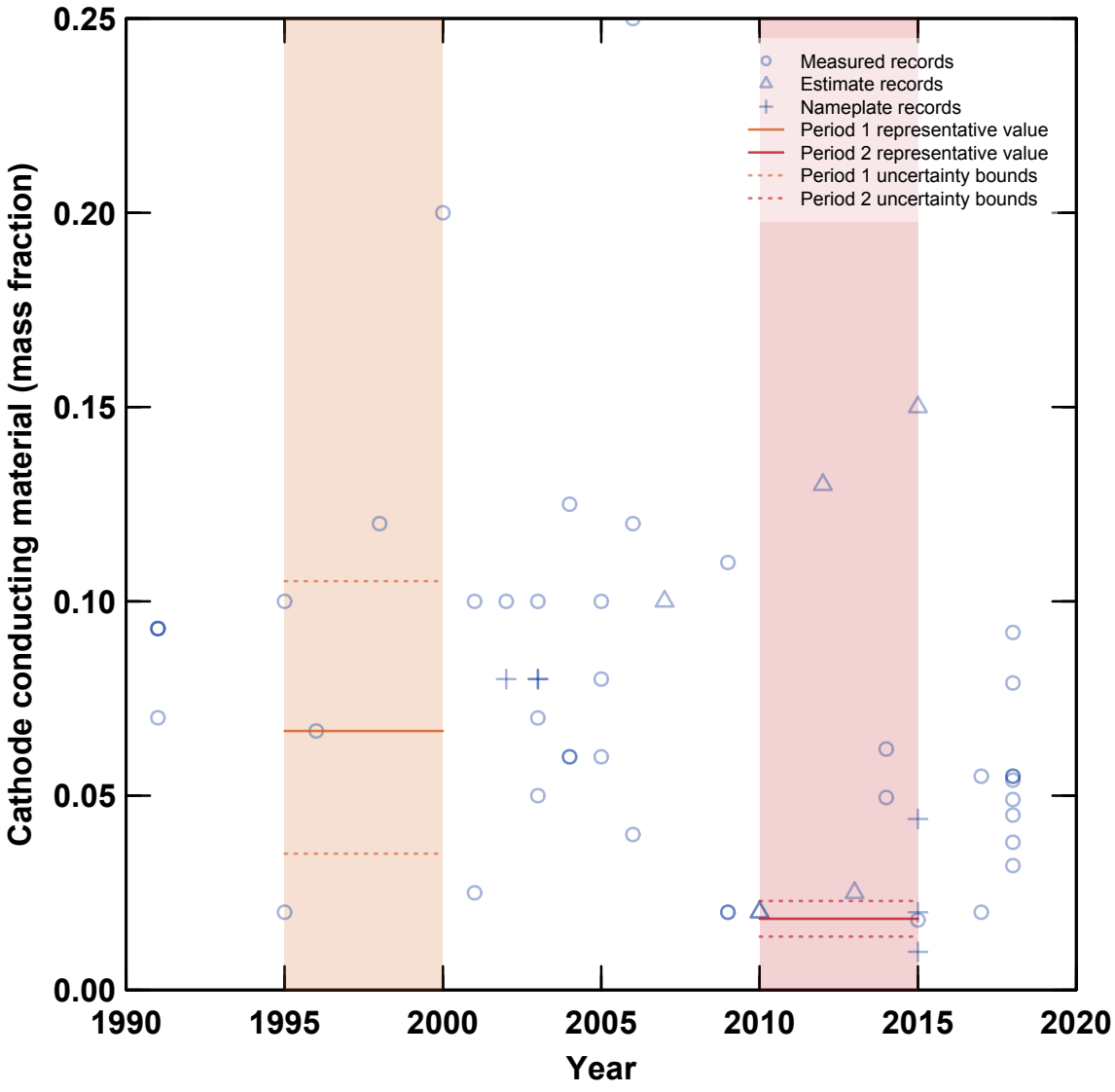

Figure S14: Mass fractions of conducting material in total cathode material, by record type.

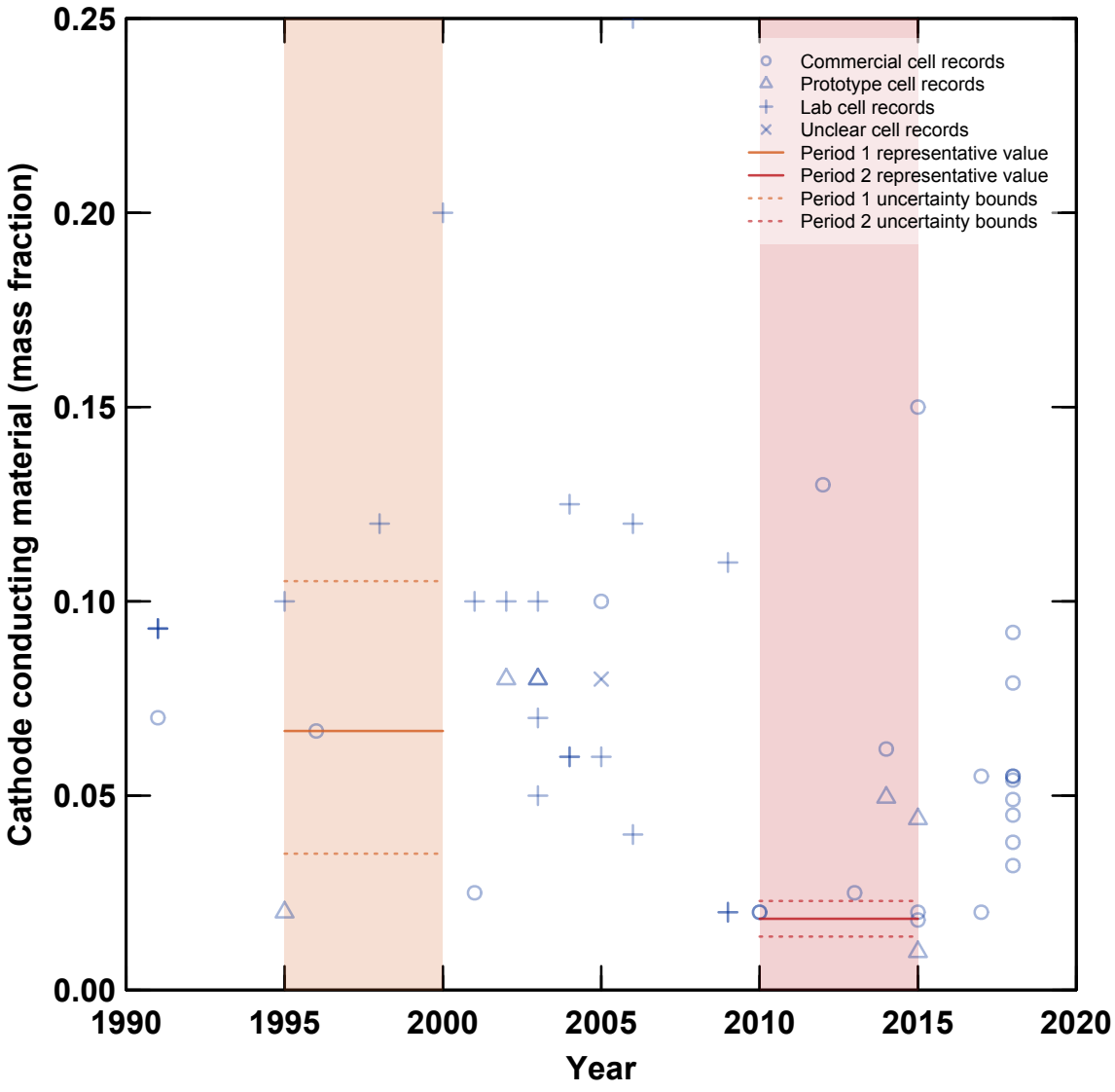

Figure S15: Mass fractions of conducting material in total cathode material, by cell type.

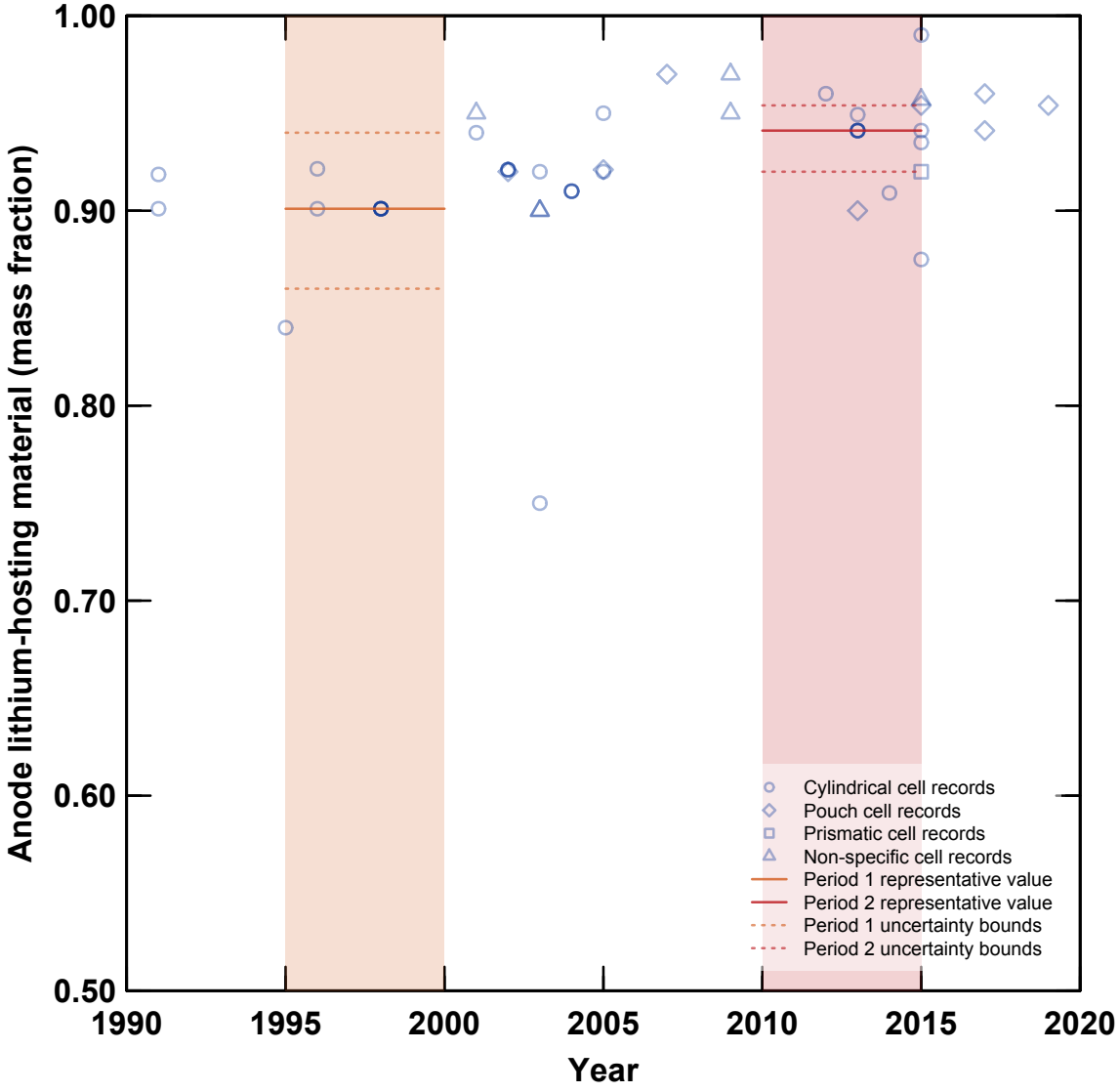

Figure S16: Mass fractions of anode active (or "lithium-hosting") material in total anode material, by cell shape.

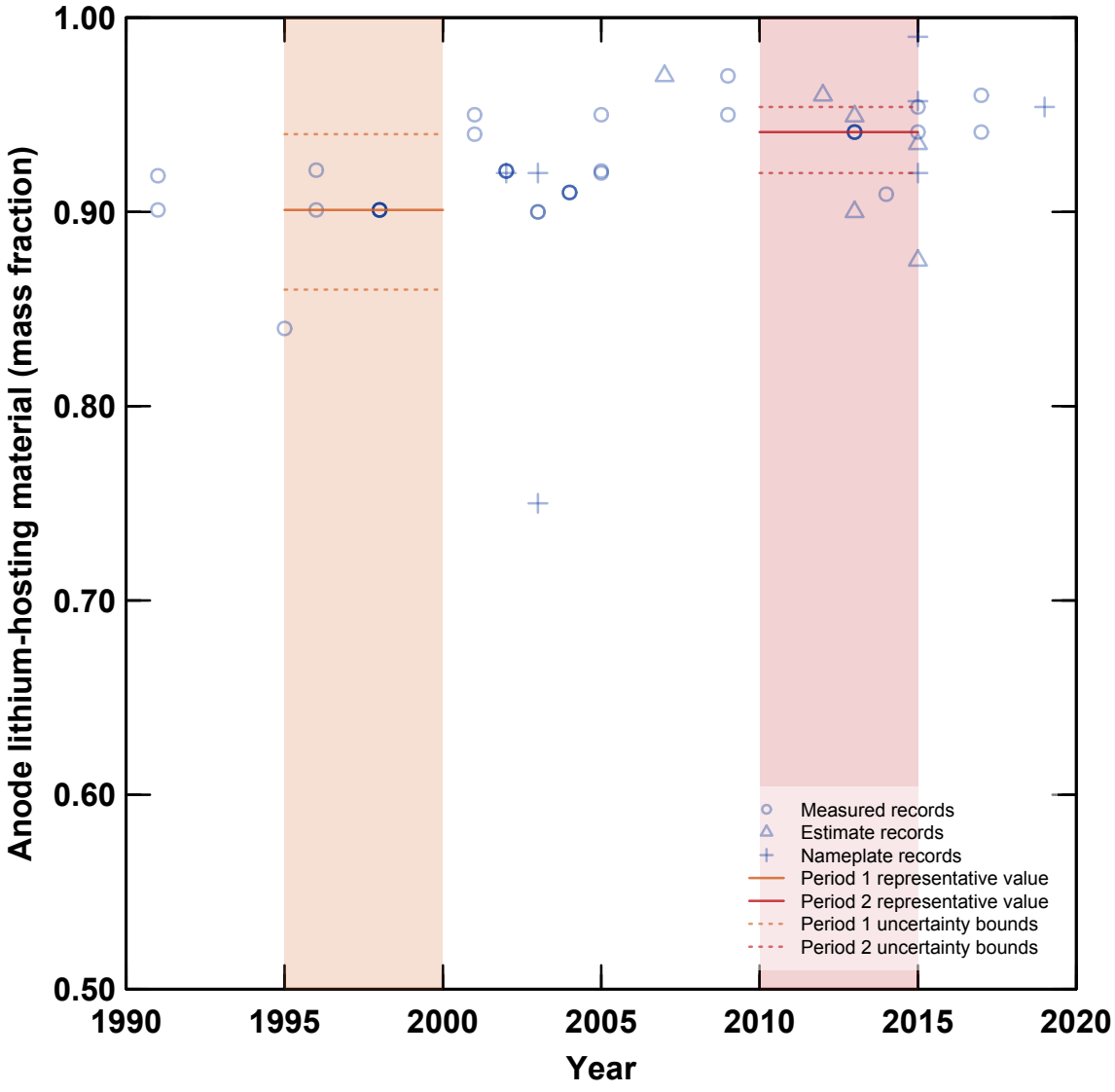

Figure S17: Mass fractions of anode active (or "lithium-hosting") material in total anode material, by record type.

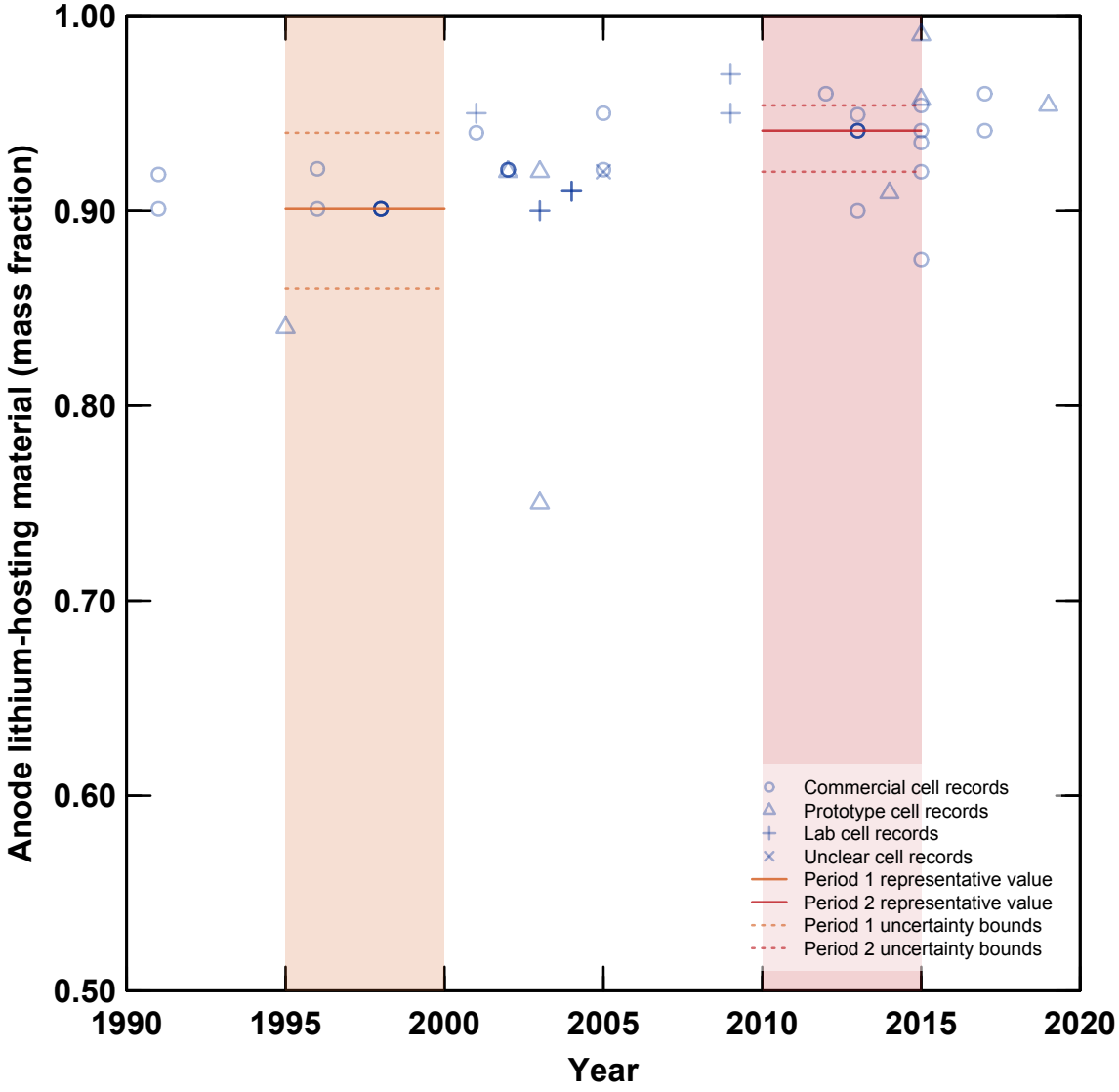

Figure S18: Mass fractions of anode active (or "lithium-hosting") material in total anode material, by cell type.

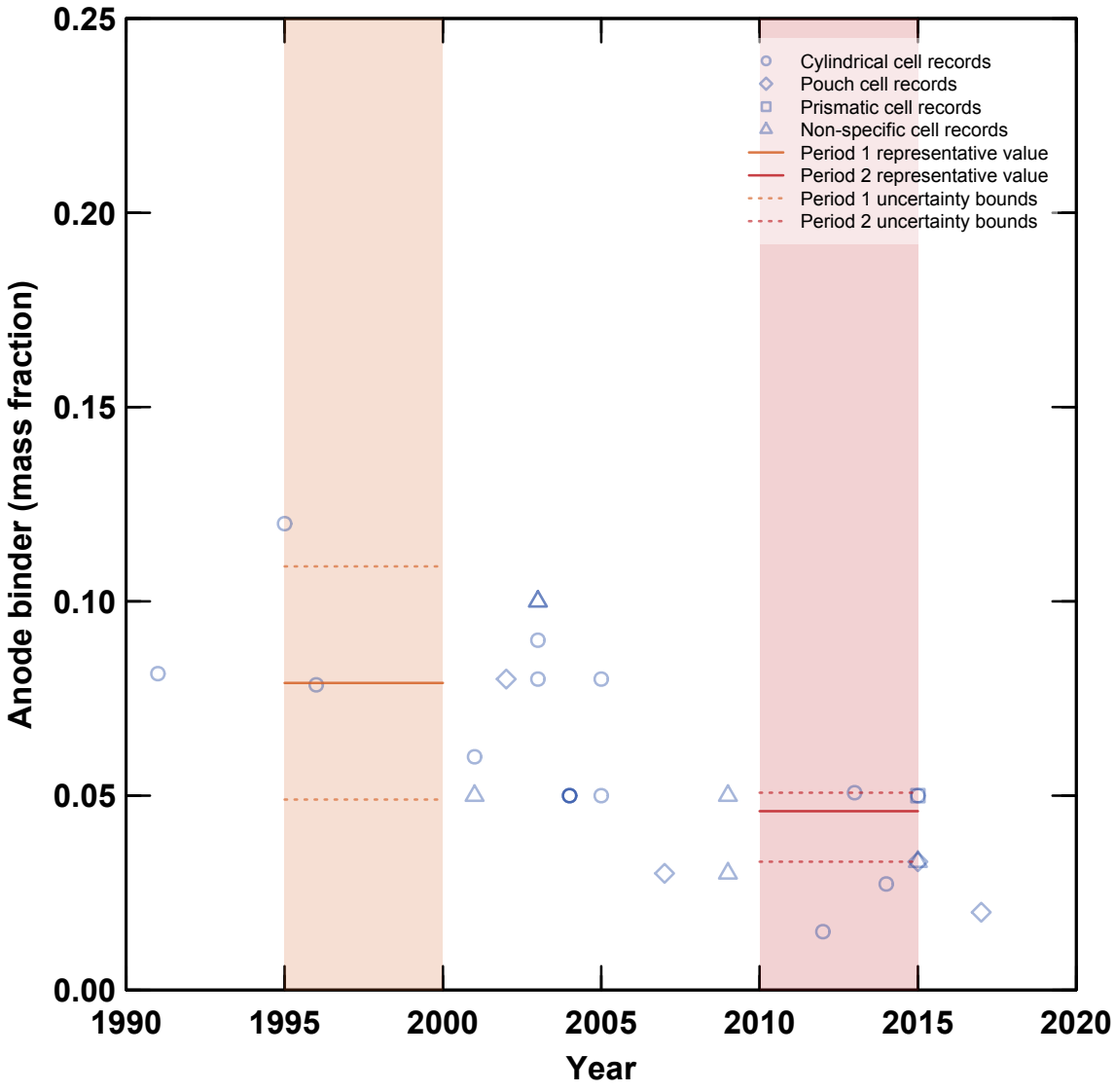

Figure S19: Mass fractions of binder material in total anode material, by cell shape.

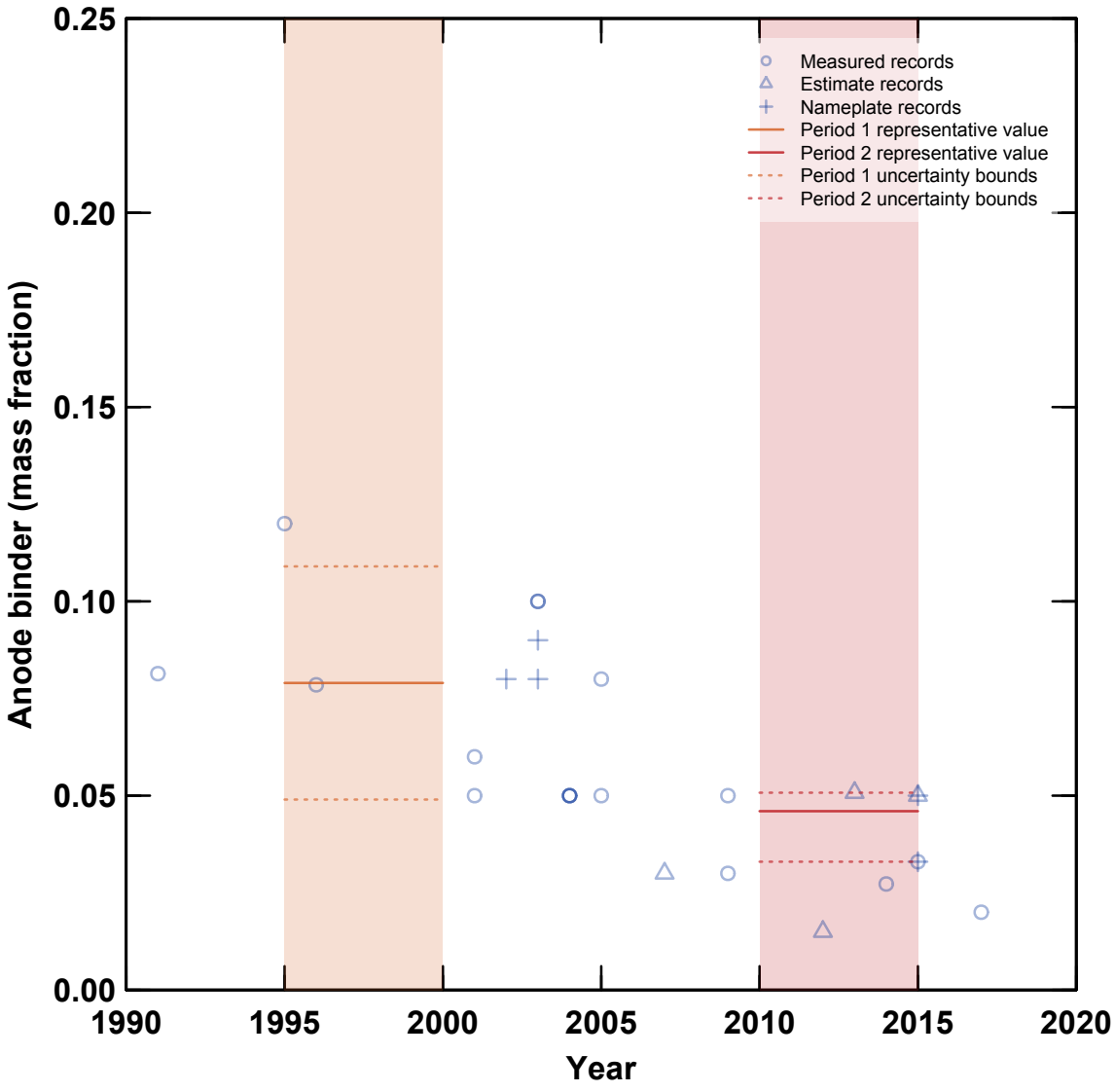

Figure S20: Mass fractions of binder material in total anode material, by record type.

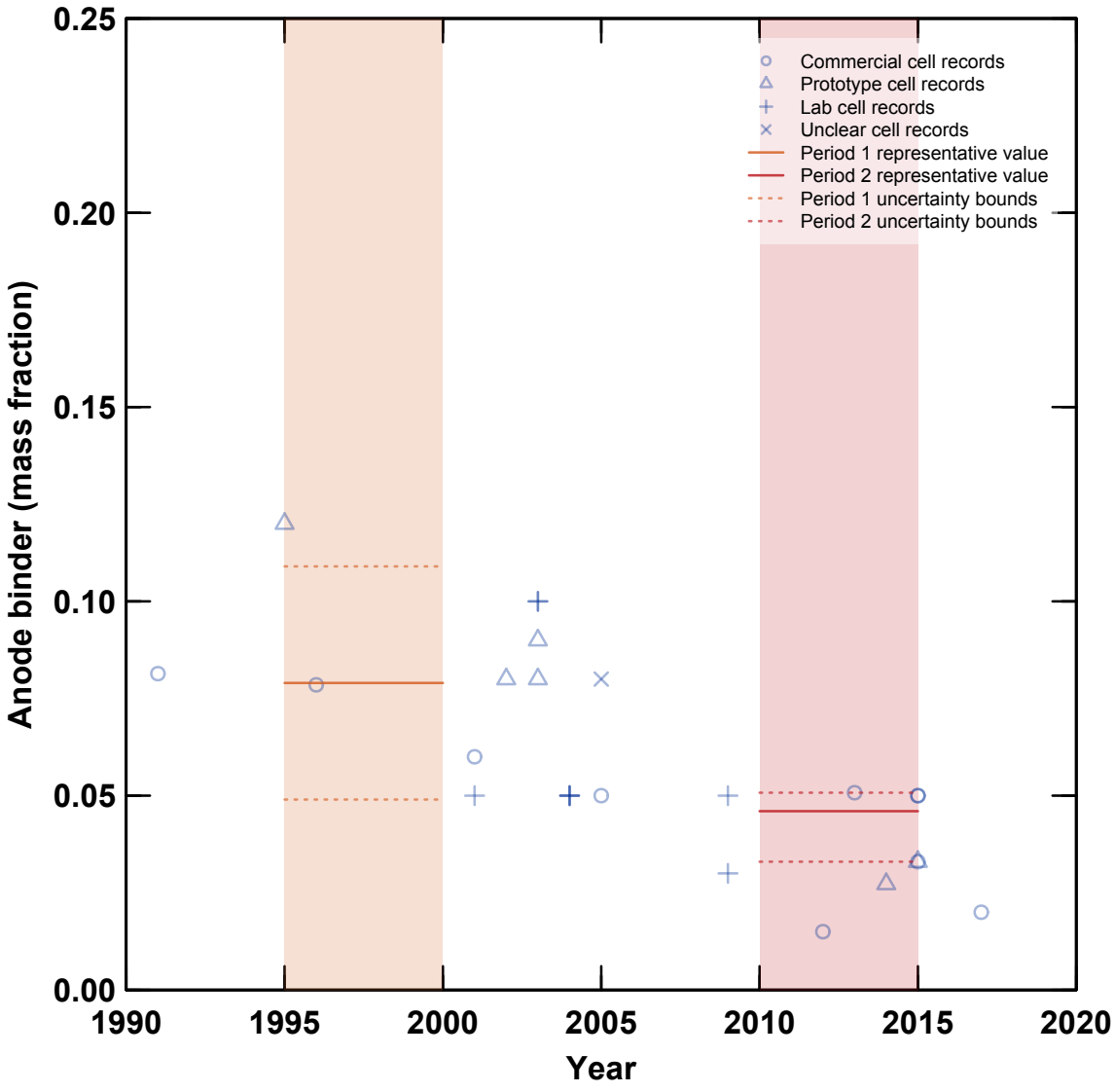

Figure S21: Mass fractions of binder material in total anode material, by cell type.

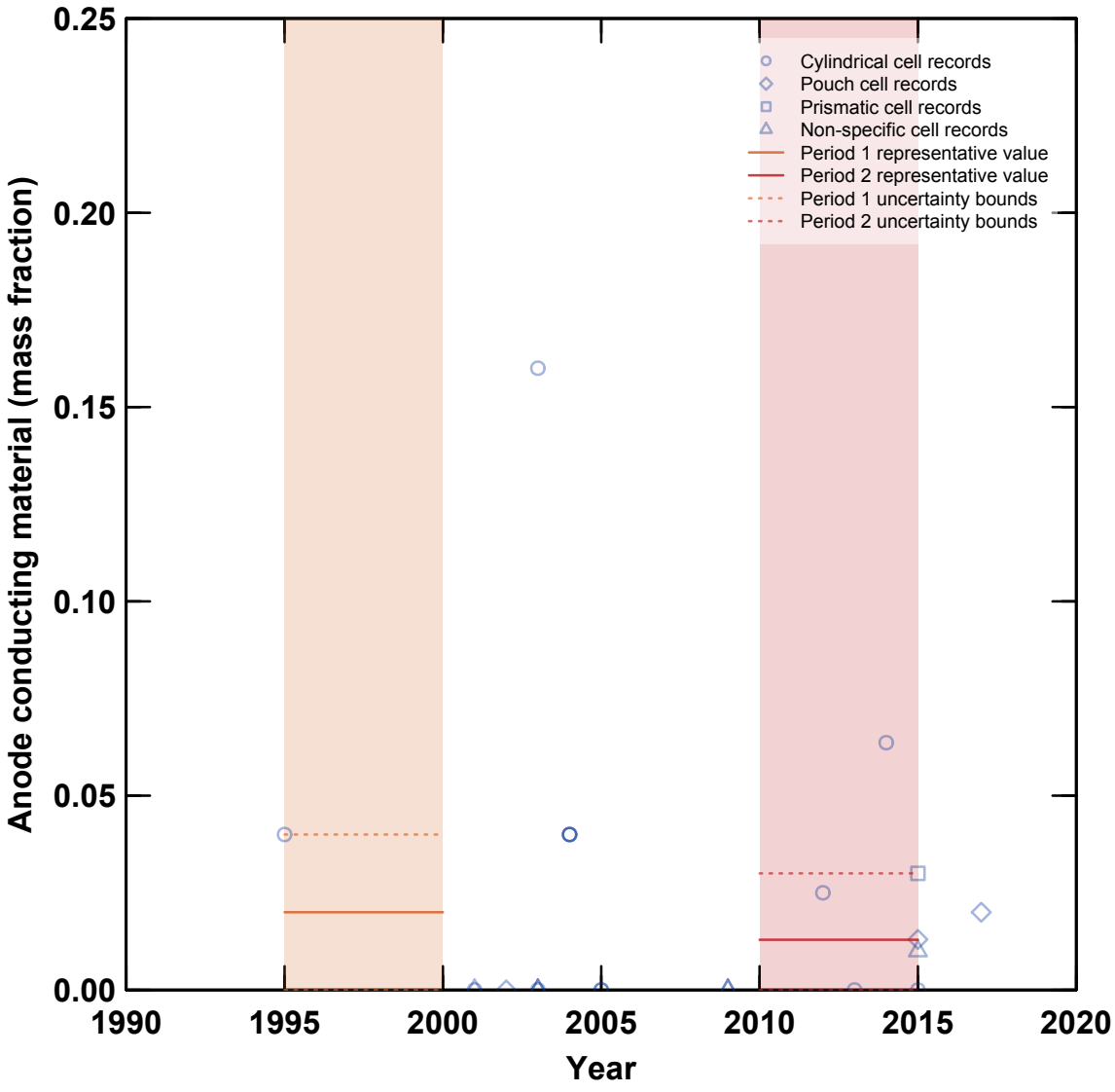

Figure S22: Mass fractions of conducting material in total anode material, by cell shape.

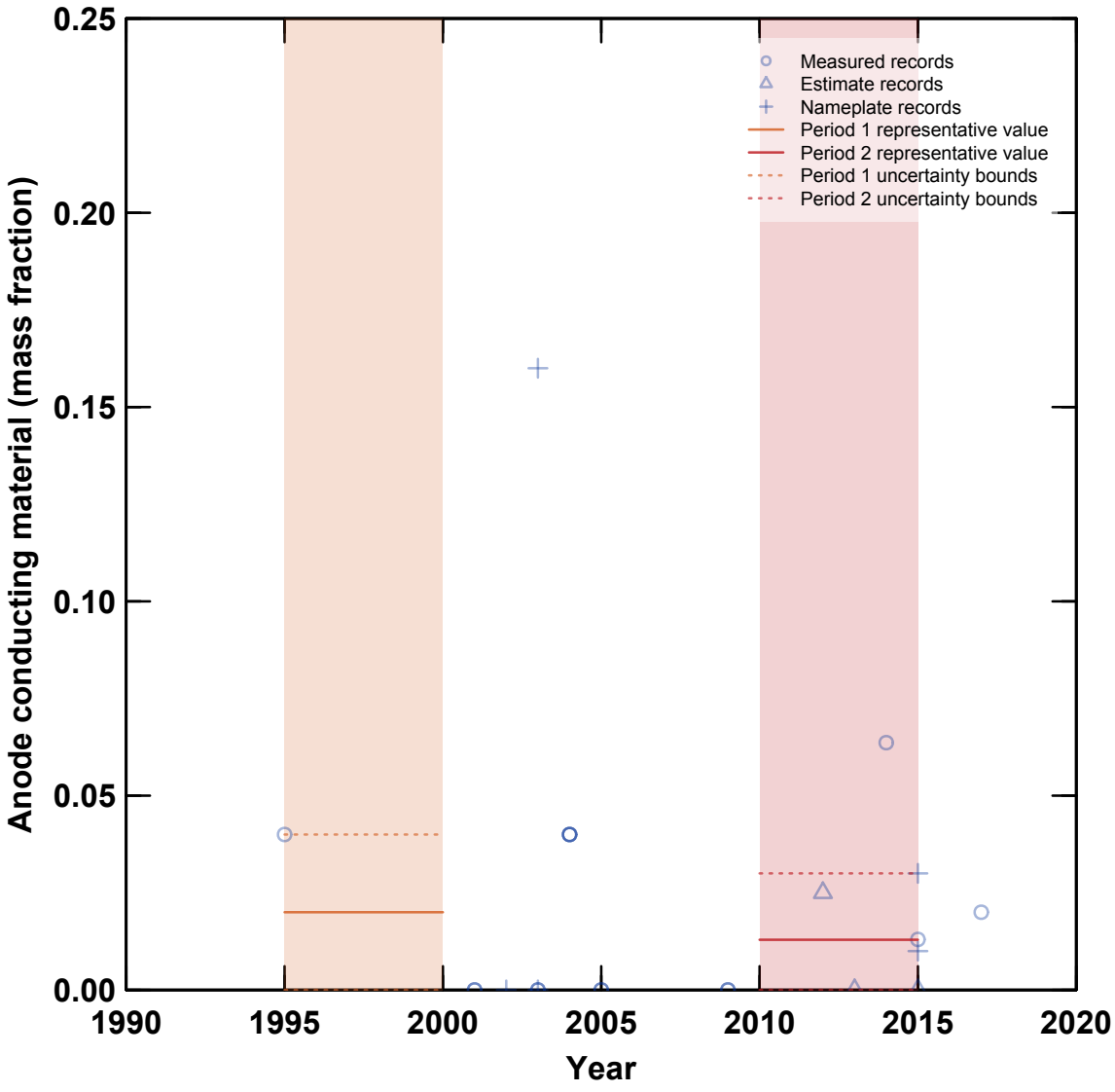

Figure S23: Mass fractions of conducting material in total anode material, by record type.

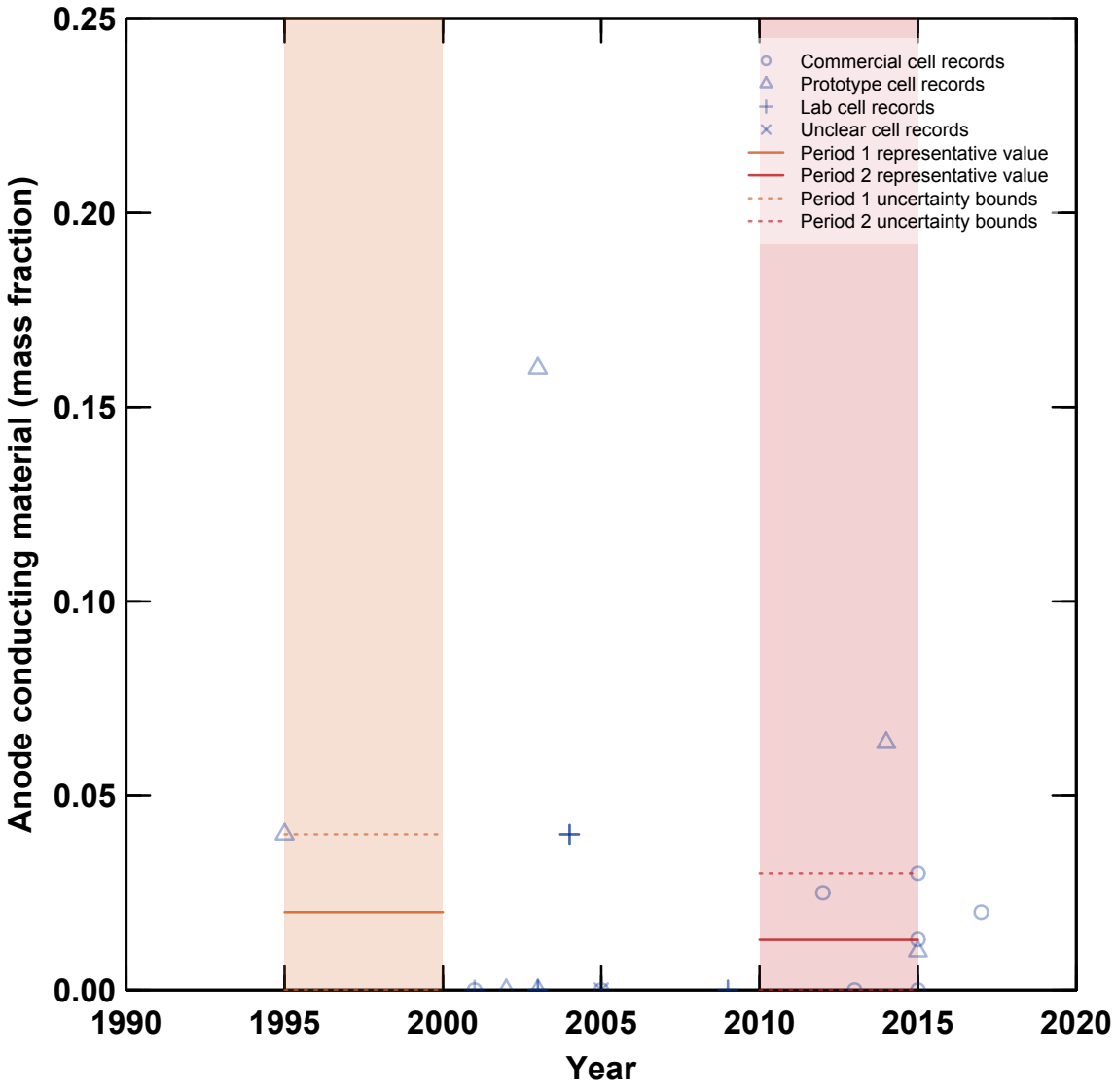

Figure S24: Mass fractions of conducting material in total anode material, by cell type.

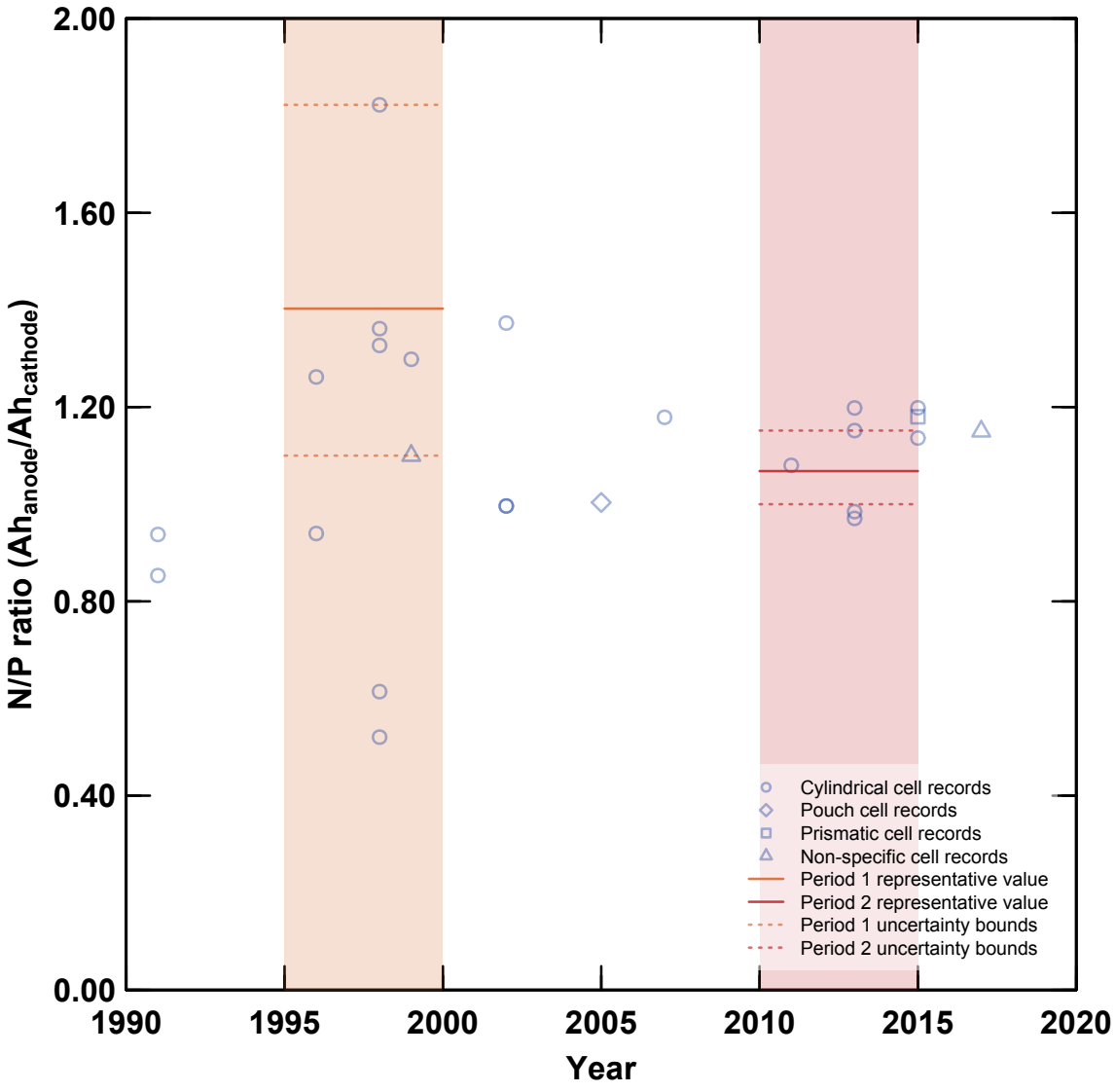

Figure S25: N/P ratios, categorized by cell shape.

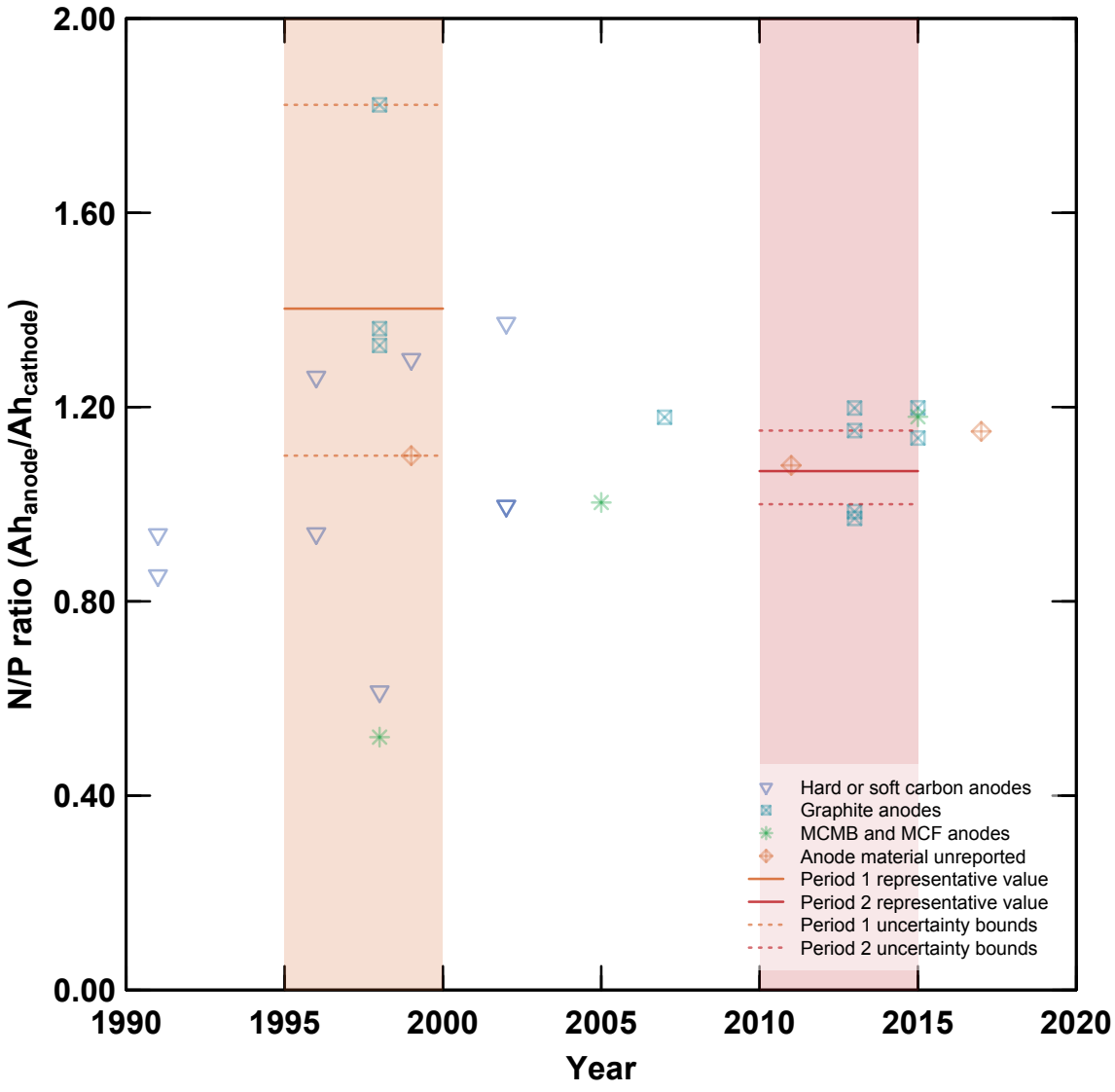

Figure S26: N/P ratios, categorized by anode material.

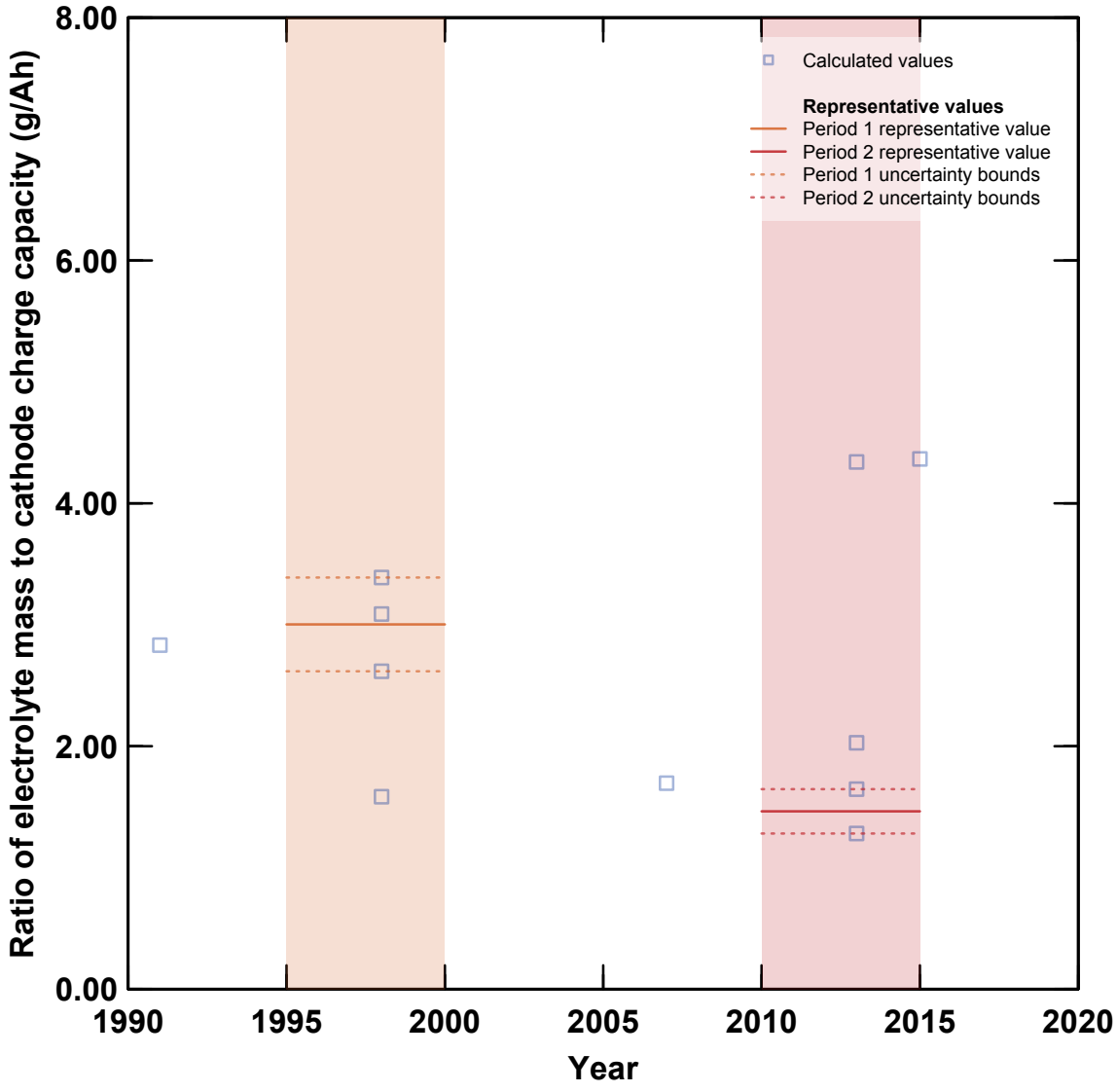

Figure S27: Ratios of electrolyte solution mass to cathode charge capacity for commercial 18650-sized cells, categorized by record type.

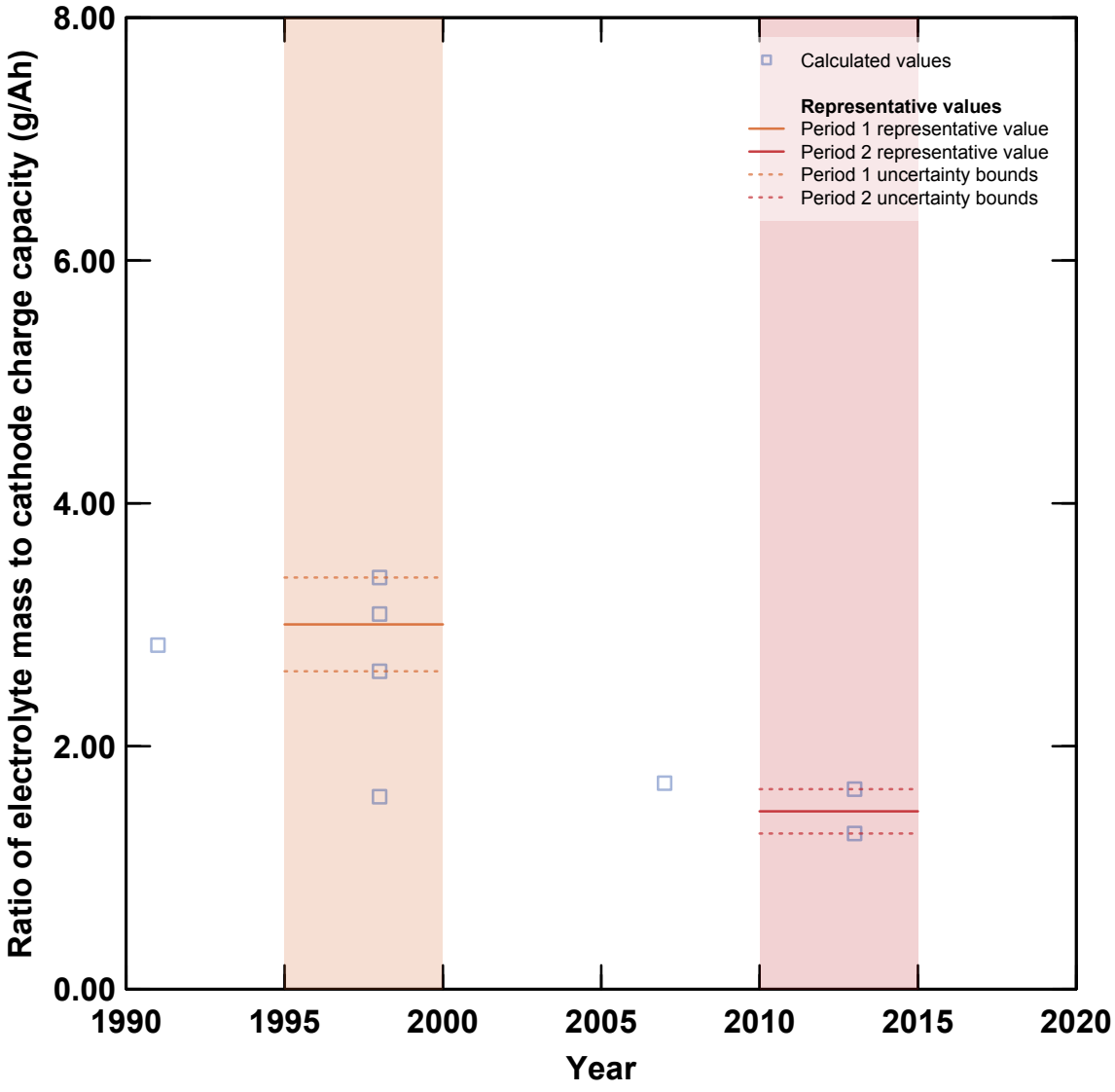

Figure S28: Ratios of electrolyte solution mass to cathode charge capacity for commercial 18650-sized cells, categorized by record type and limited to high energy density cells in the second period.

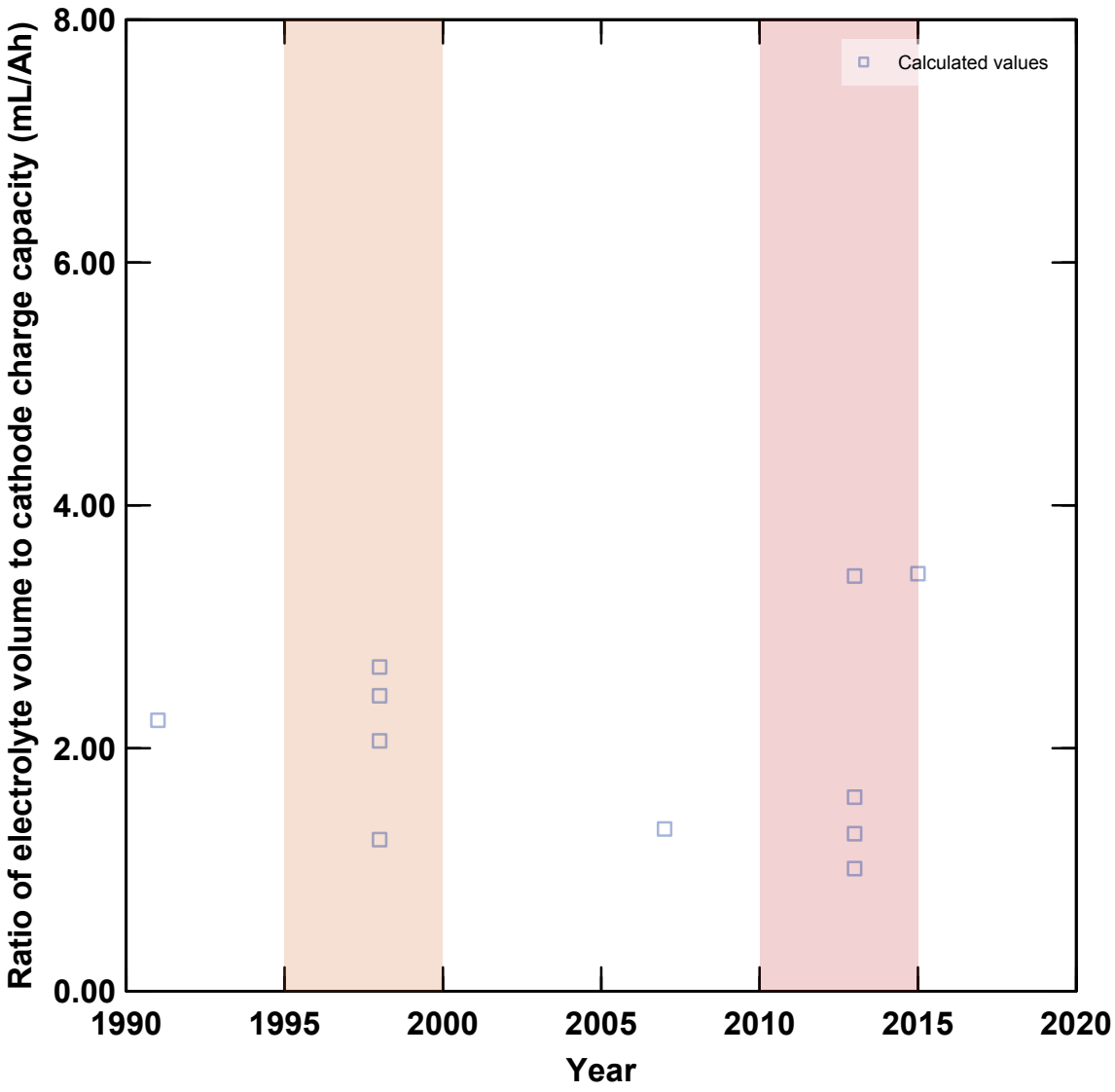

Figure S29: Ratios of electrolyte solution volume to cathode charge capacity for commercial 18650-sized cells, categorized by record type. When electrolyte solution density was not specified, electrolyte solution masses were converted to volumes assuming a density of 1.27 g/mL.

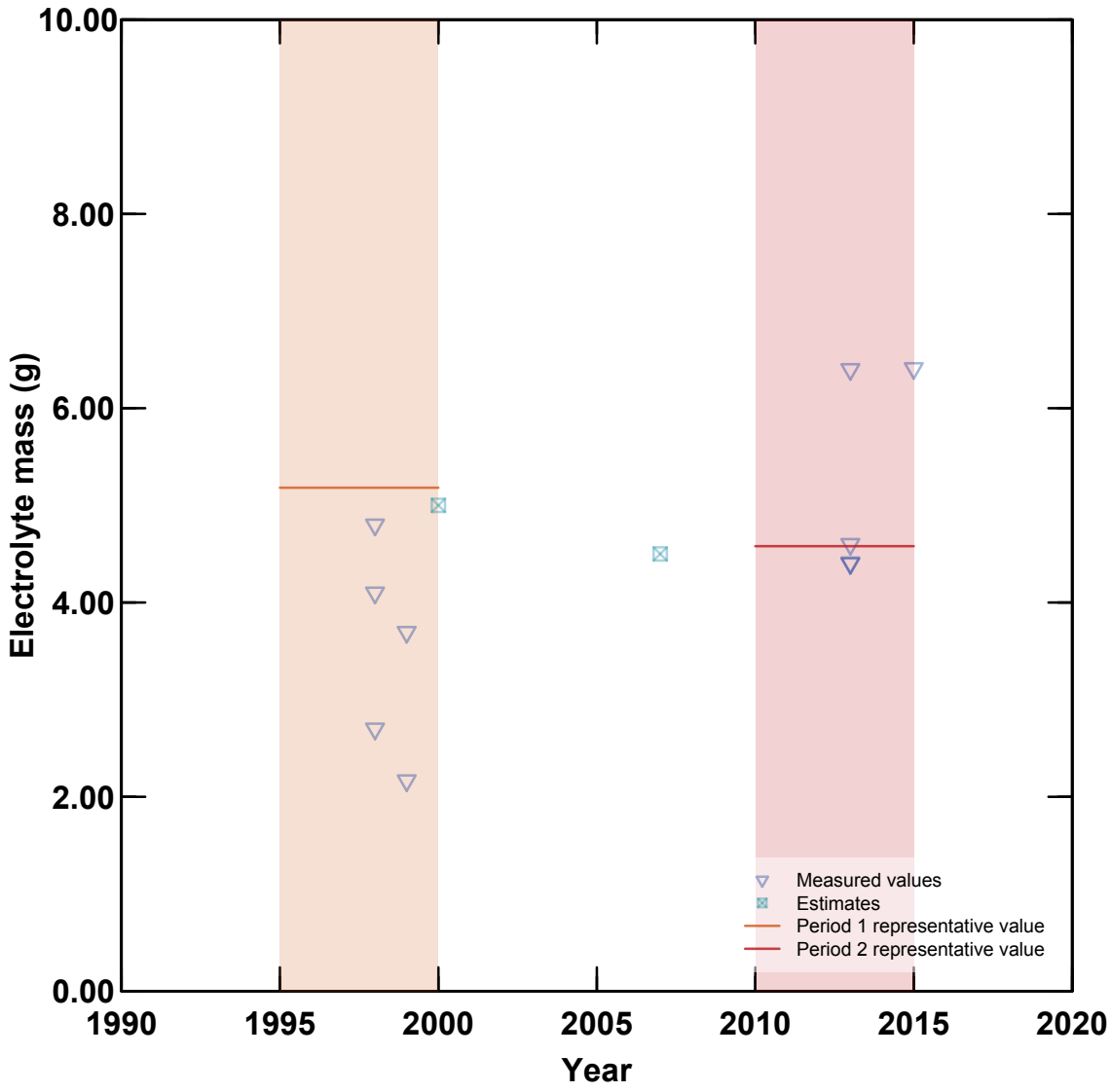

Figure S30: Electrolyte solution masses for 18650-sized cells, categorized by record type. "Representative" values displayed here are obtained by multiplying the representative electrolyte solution mass to cathode charge capacity ratios by the representative cathode charge capacities for a fixed volume for each period.

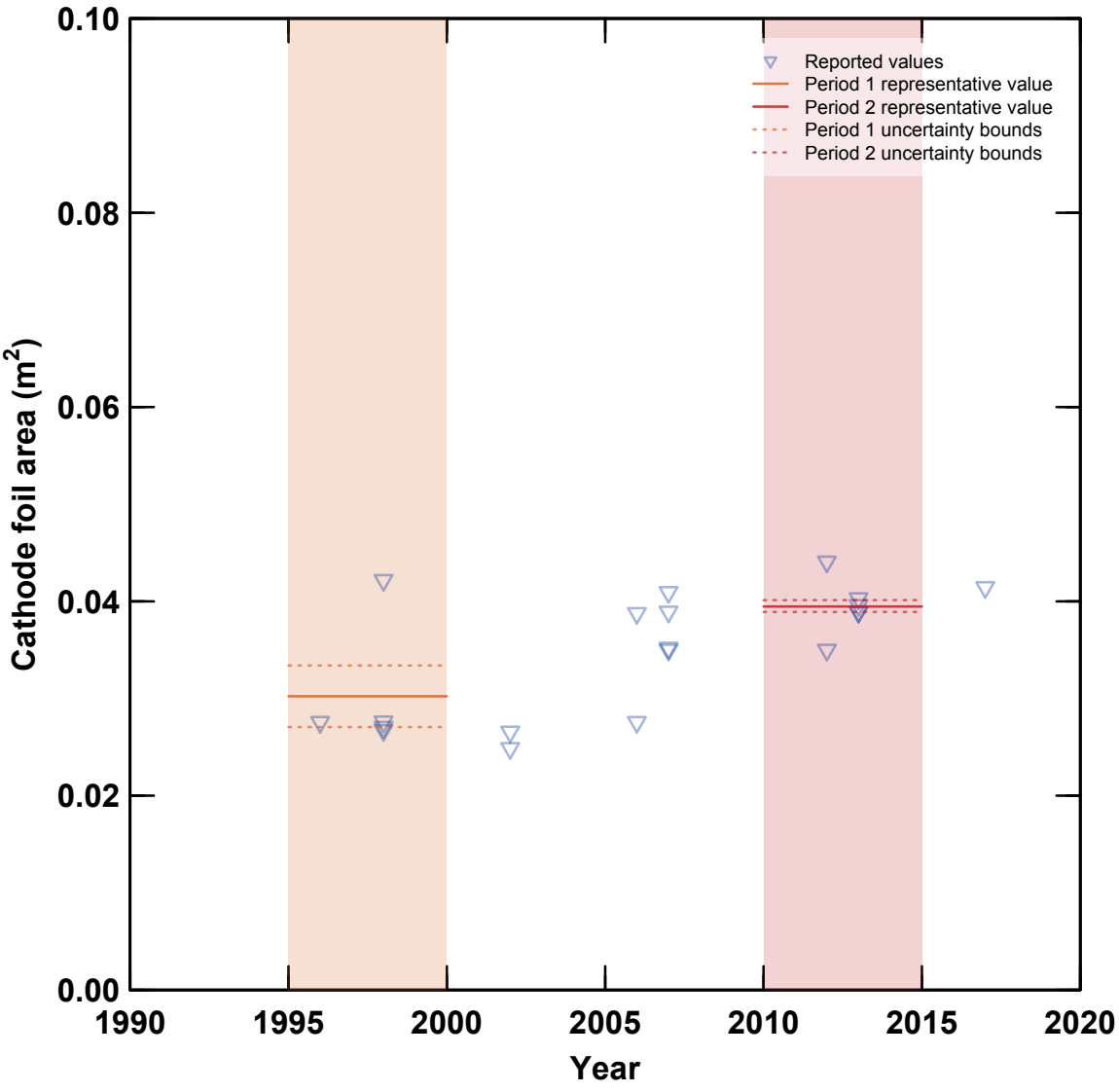

Figure S31: Reported values for cathode foil area for 18650-sized cells.

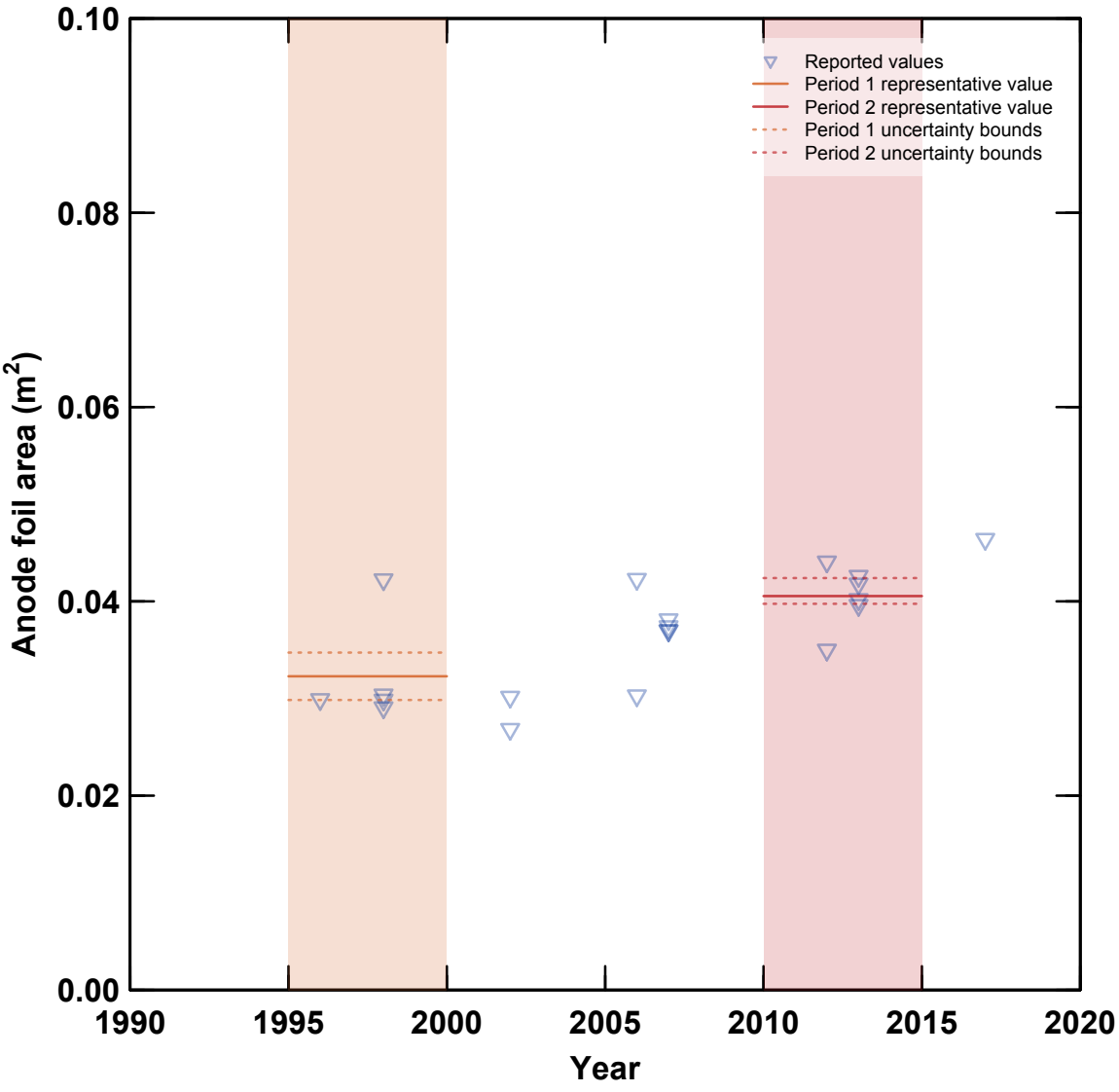

Figure S32: Reported values for anode foil area for 18650-sized cells.

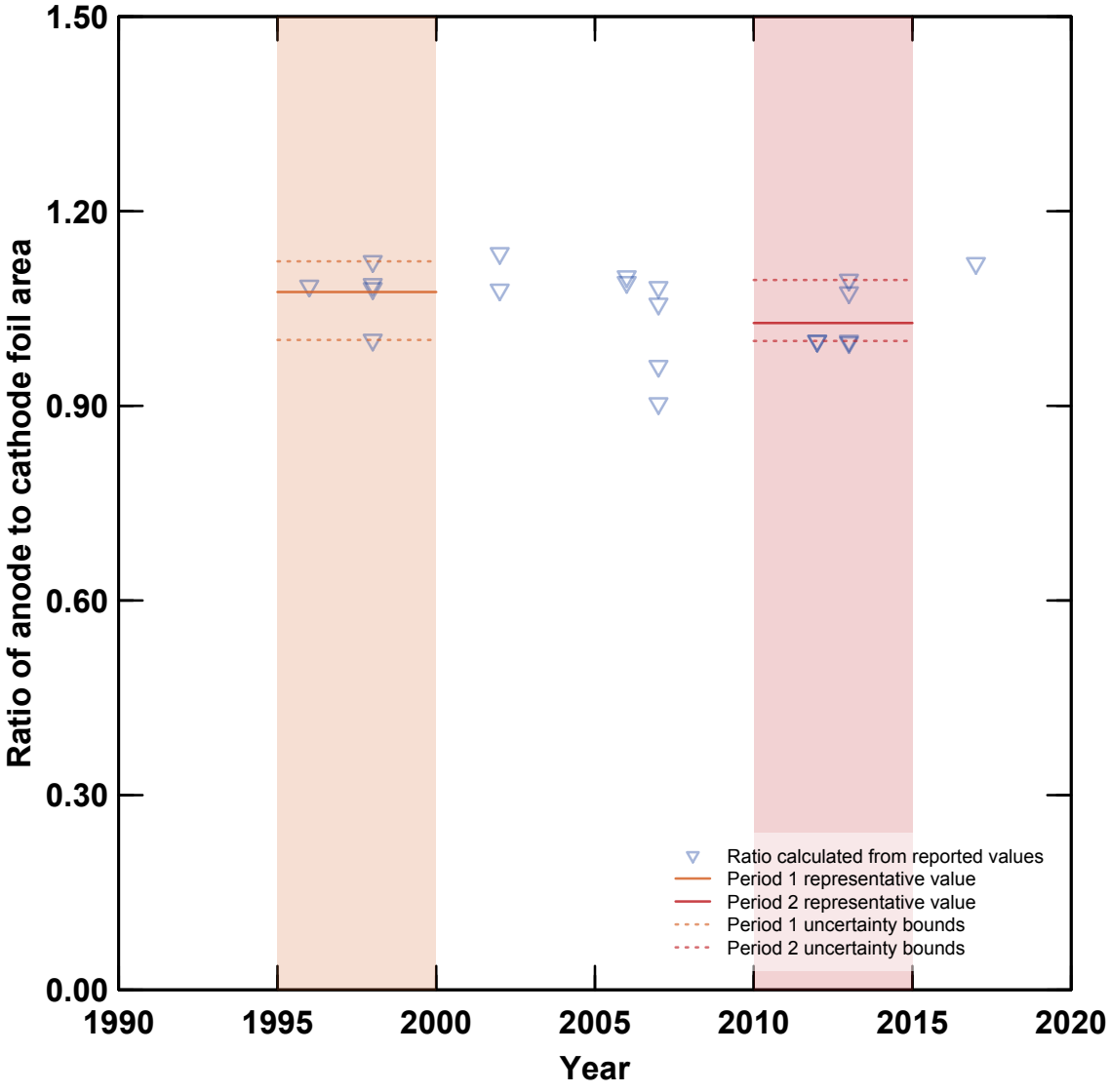

Figure S33: Ratios of reported anode and cathode foil areas for 18650-sized cells.

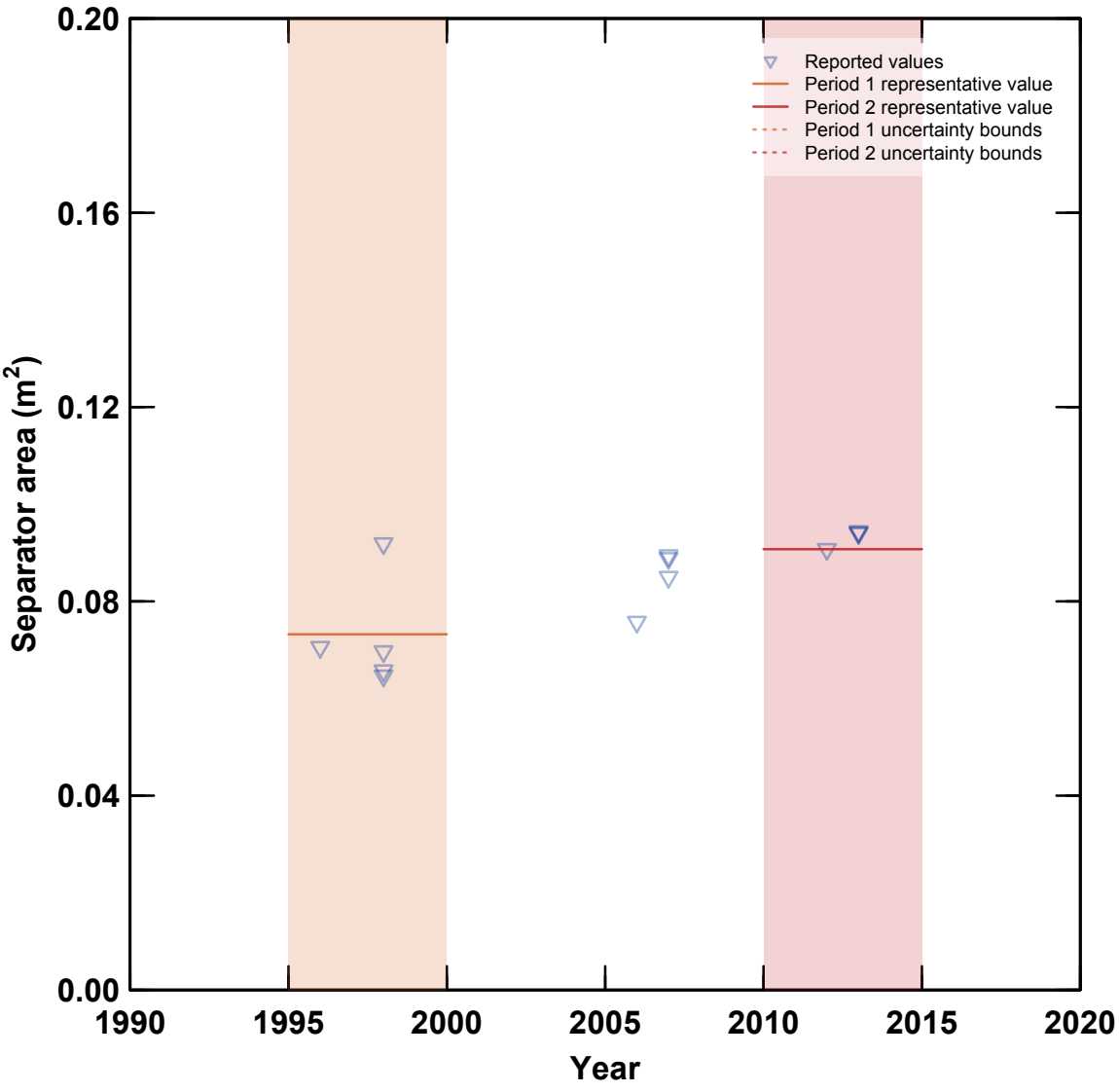

Figure S34: Reported values for separator area for 18650-sized cells.

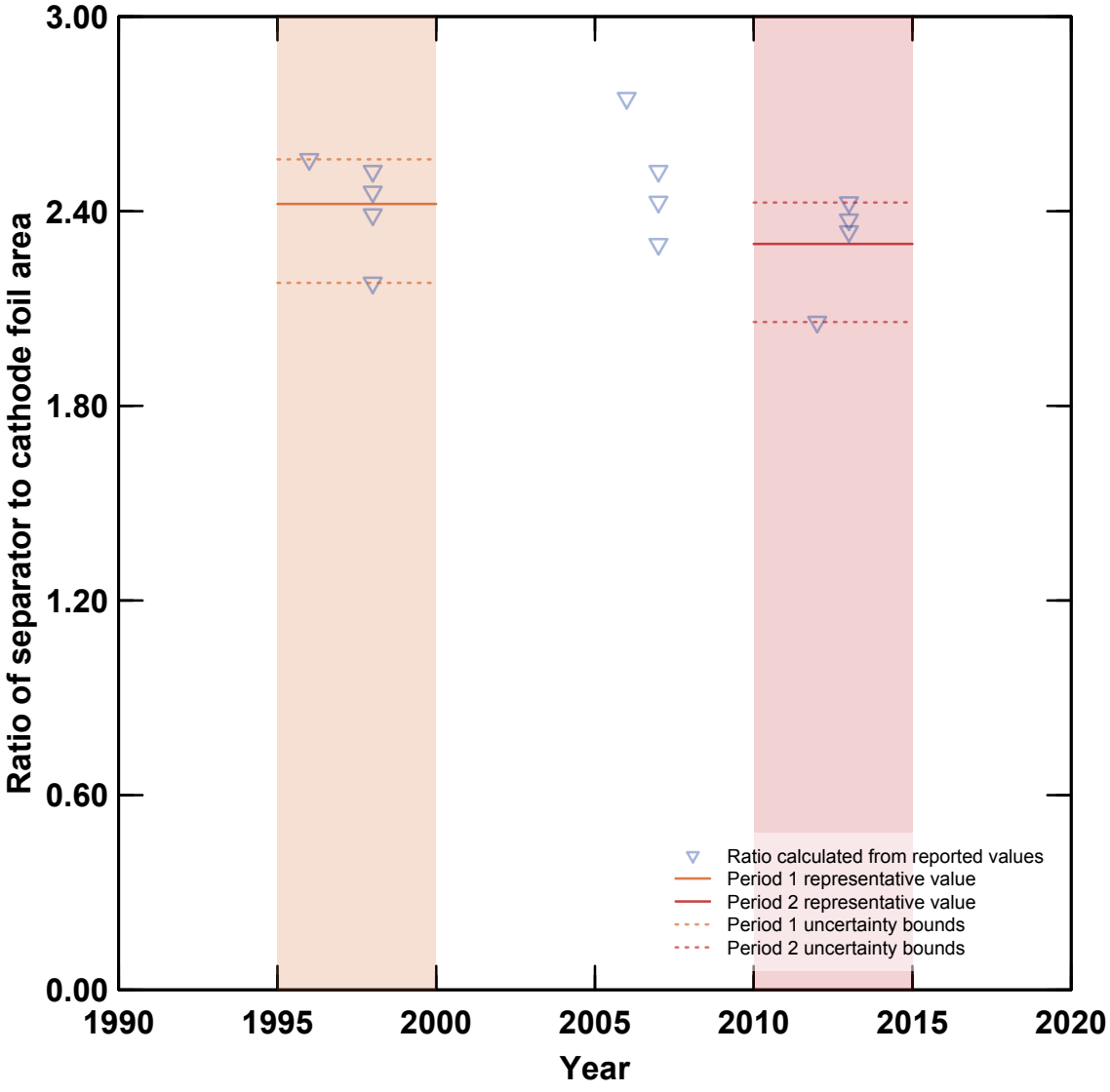

Figure S35: Ratios of reported separator and cathode foil areas for 18650-sized cells.

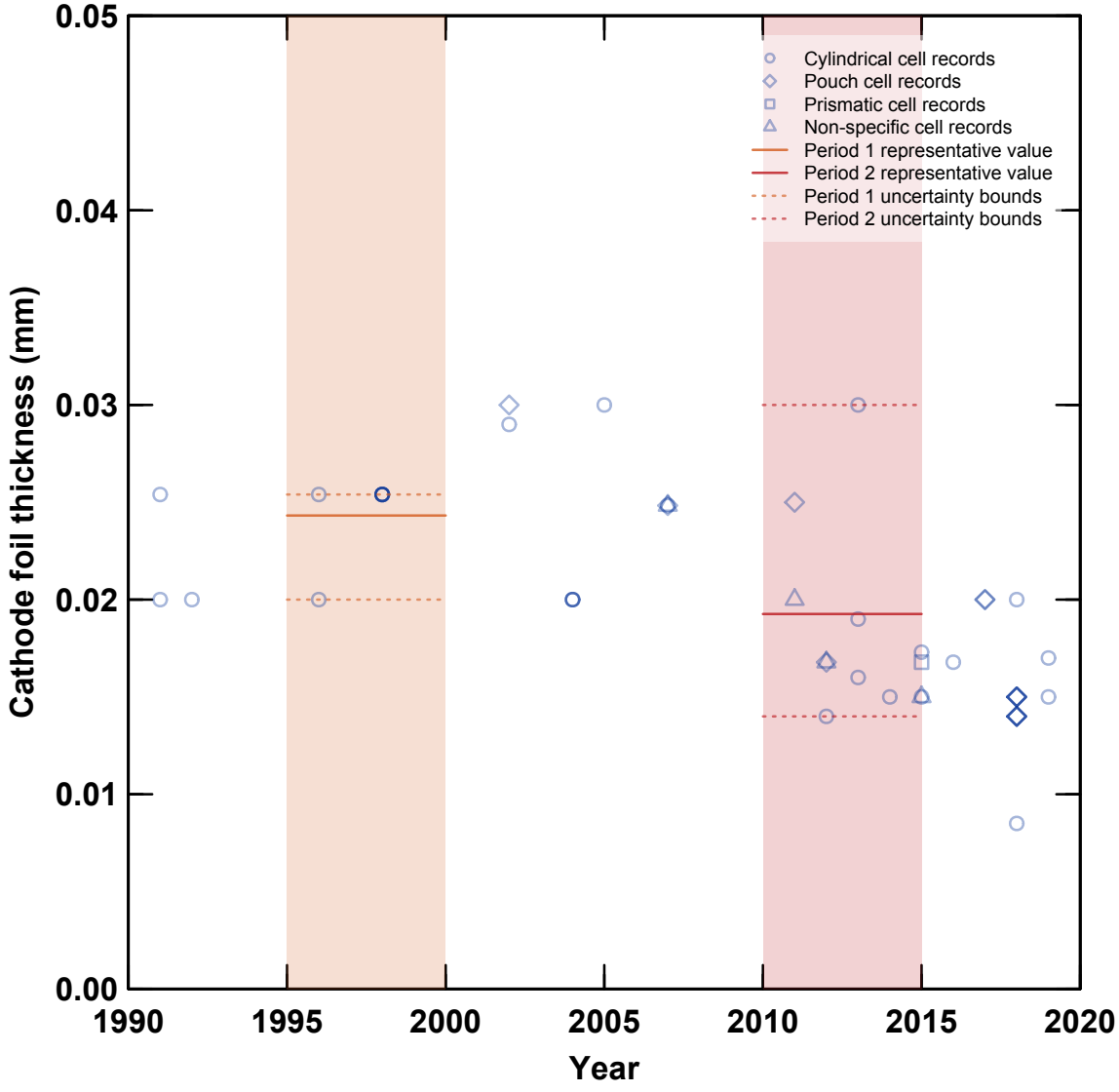

Figure S36: Reported thicknesses of cathode foils. Note that not all thicknesses plotted are for commercial, 18650-sized cells, which were those used to develop the representative values.

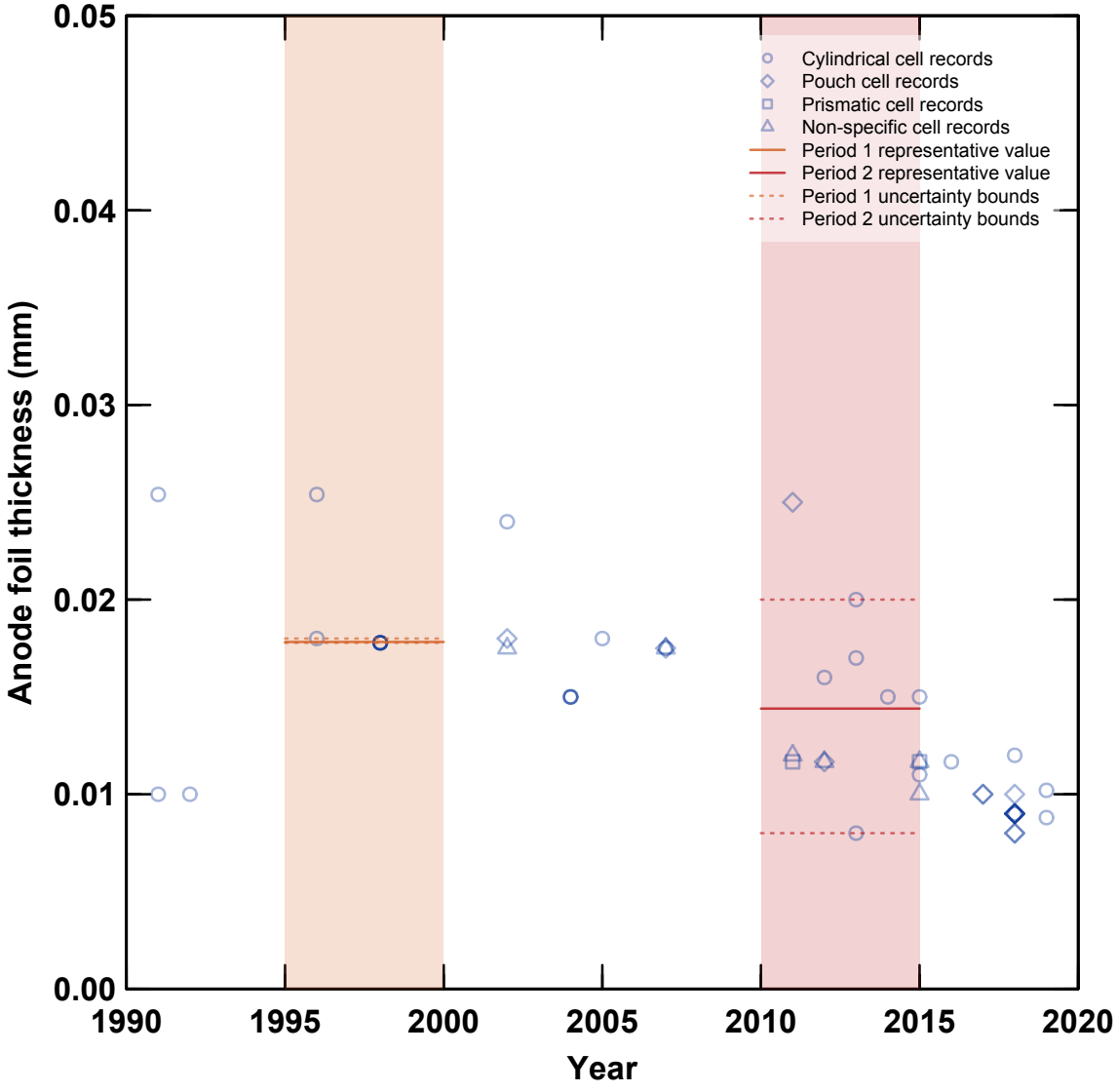

Figure S37: Reported thicknesses of anode foils. Note that not all thicknesses plotted are for commercial, 18650-sized cells, which were those used to develop the representative values.

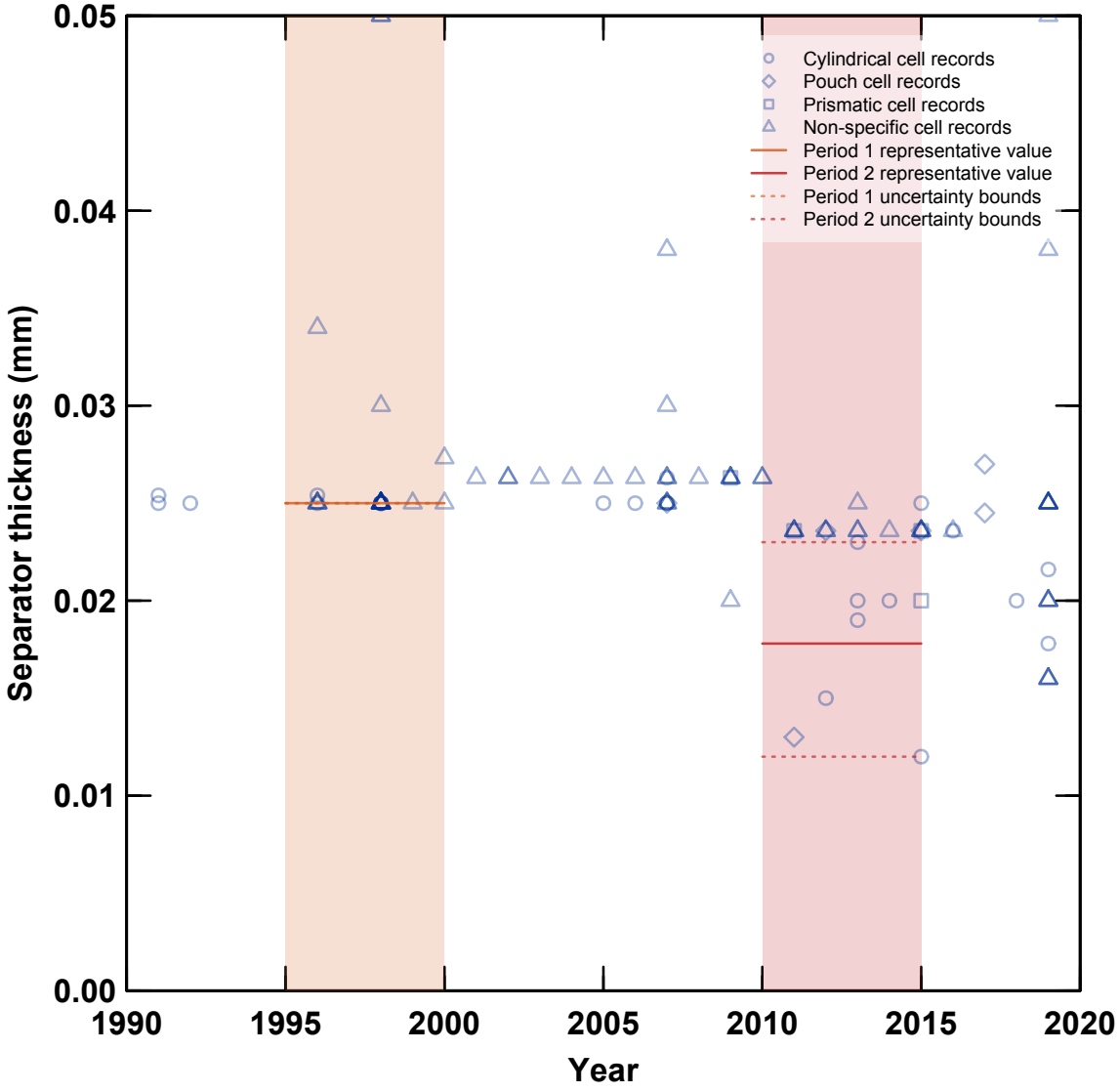

Figure S38: Reported thicknesses of separators. Note that not all thicknesses plotted are for commercial, 18650-sized cells, which were those used to develop the representative values.

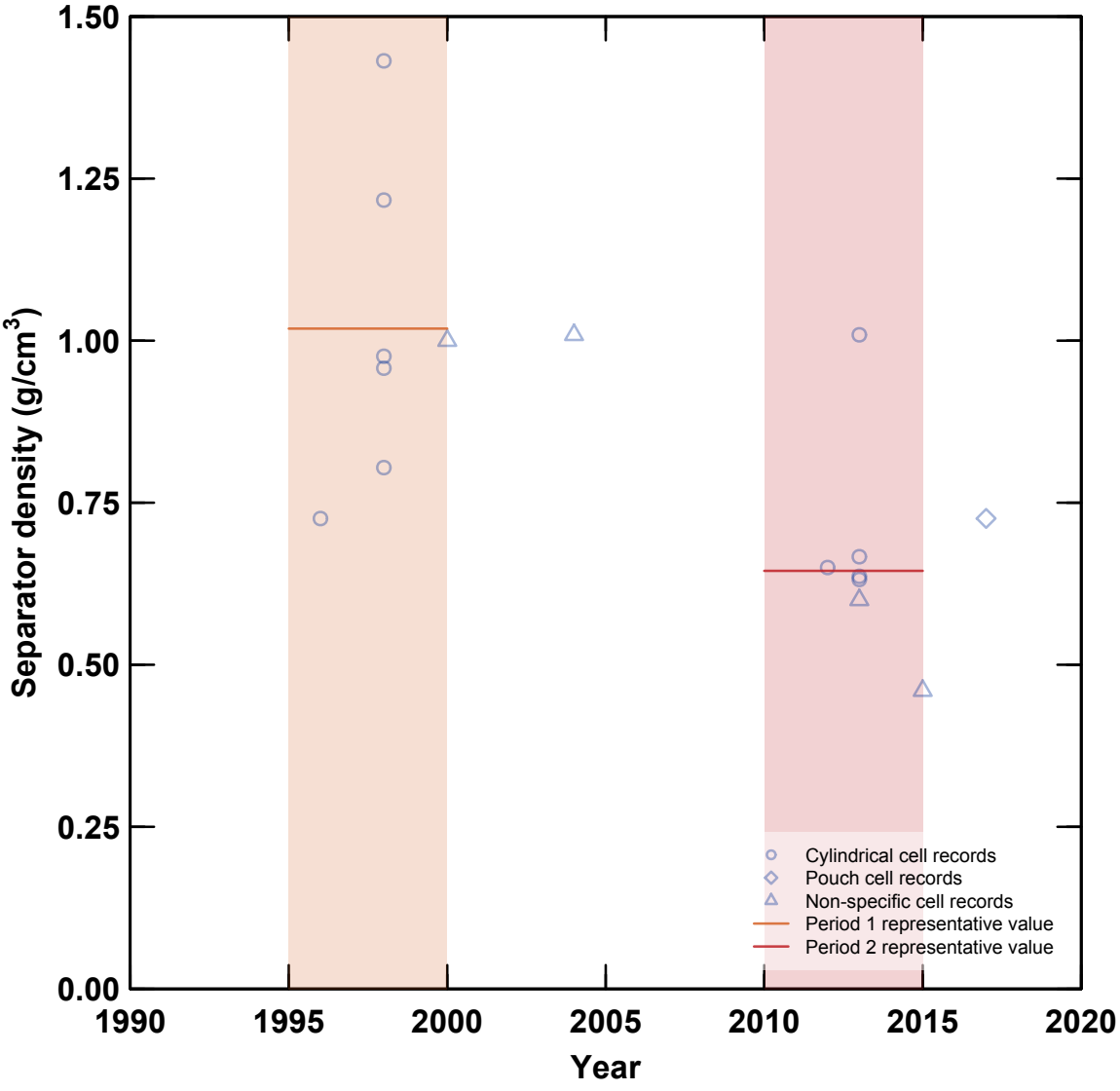

Figure S39: Densities of separators calculated from reported values, by cell shape.

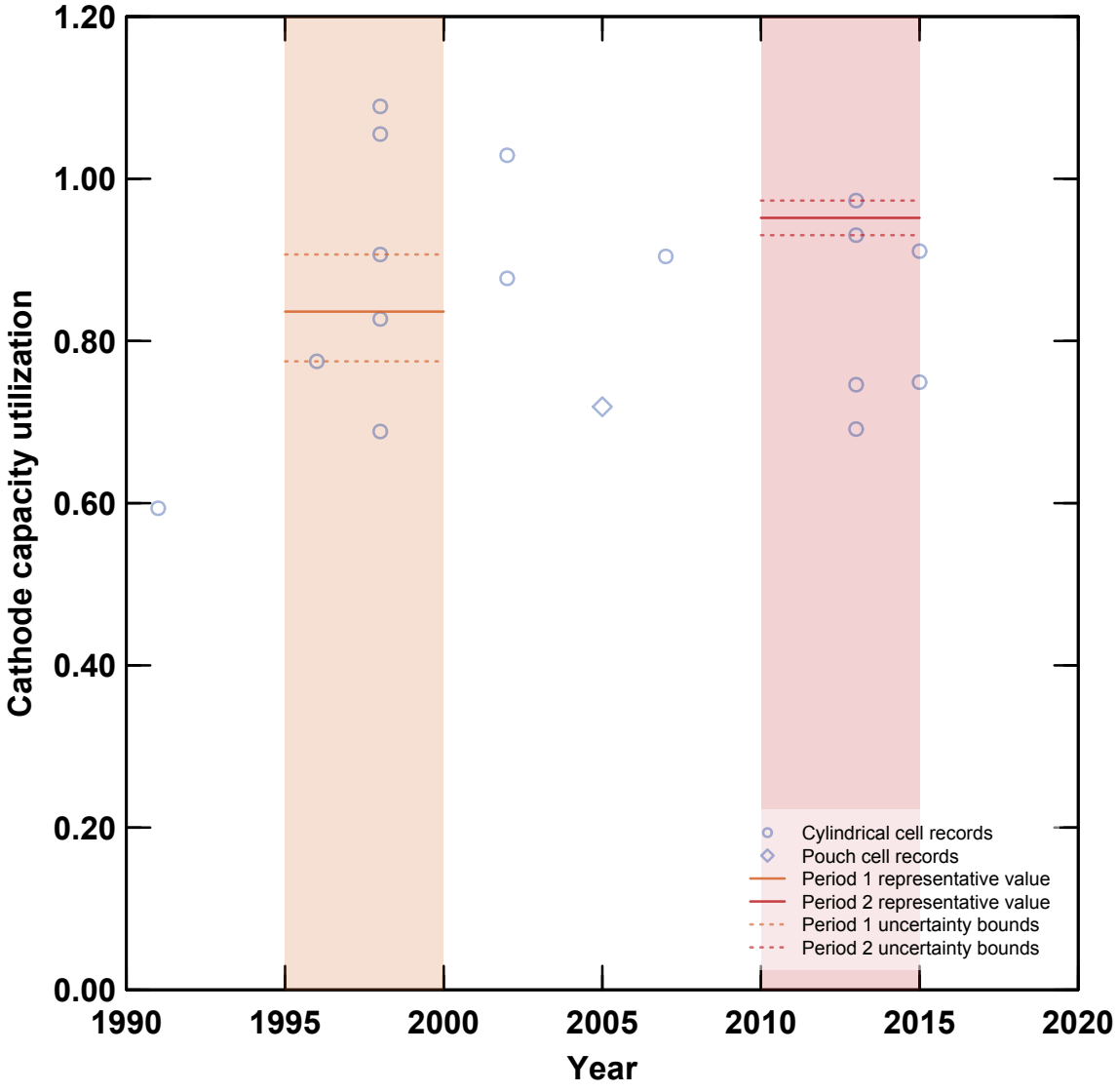

Figure S40: Calculated cathode charge capacity utilization ratios, by cell shape.

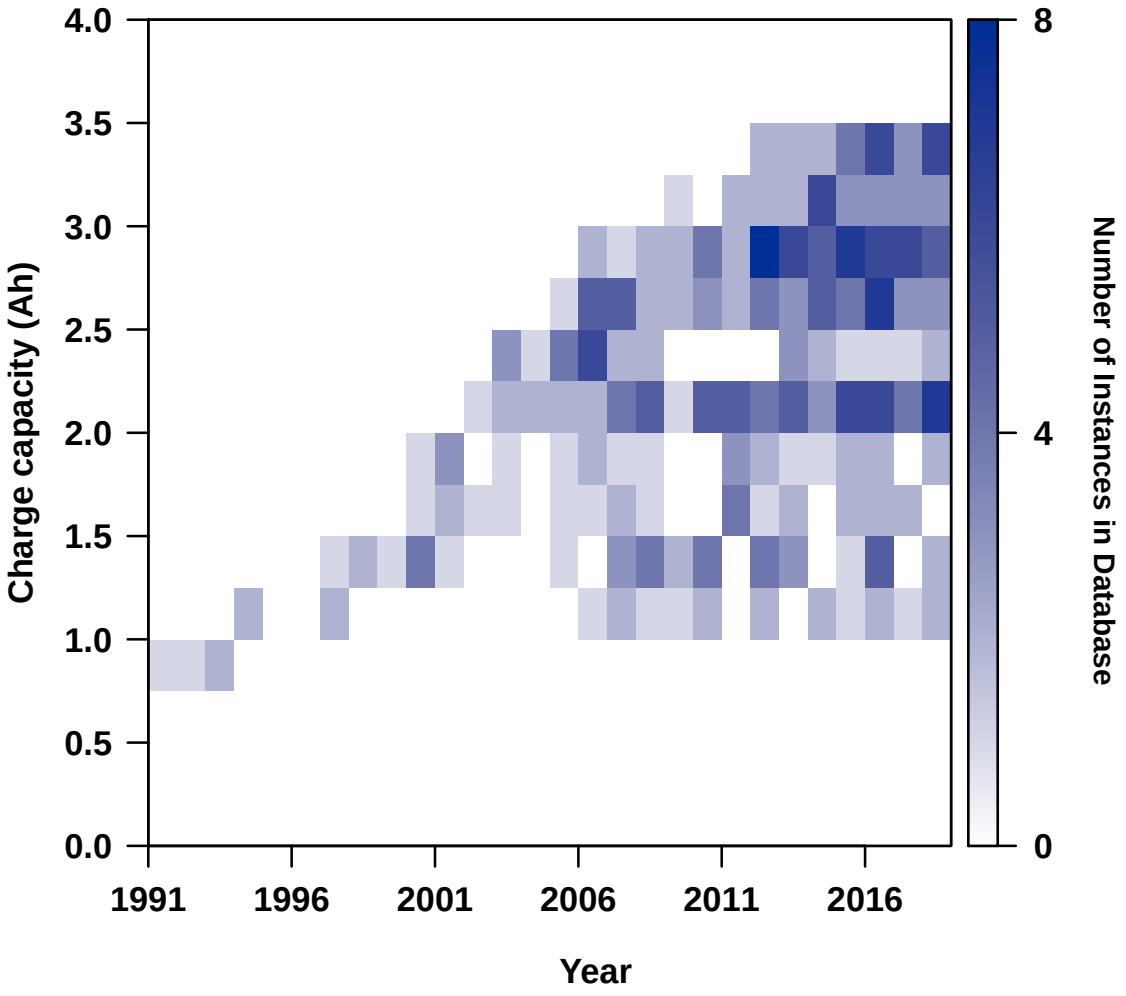

Figure S41: Nameplate charge capacities of commercial, 18650-sized lithium-ion cells between 1991 and 2018.

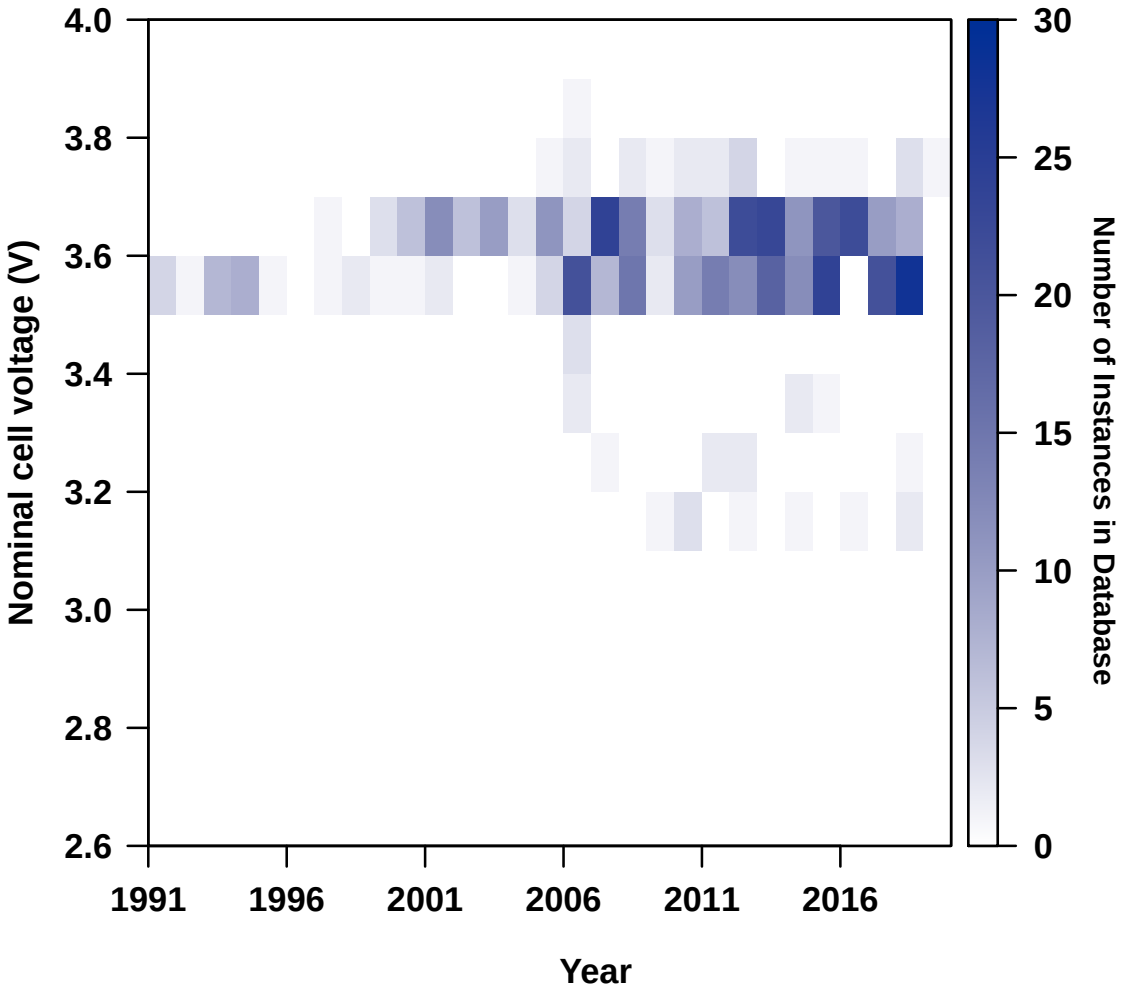

Figure S42: Nameplate nominal operating voltage of commercial, cylindrical lithium-ion cells between 1991 and 2018.

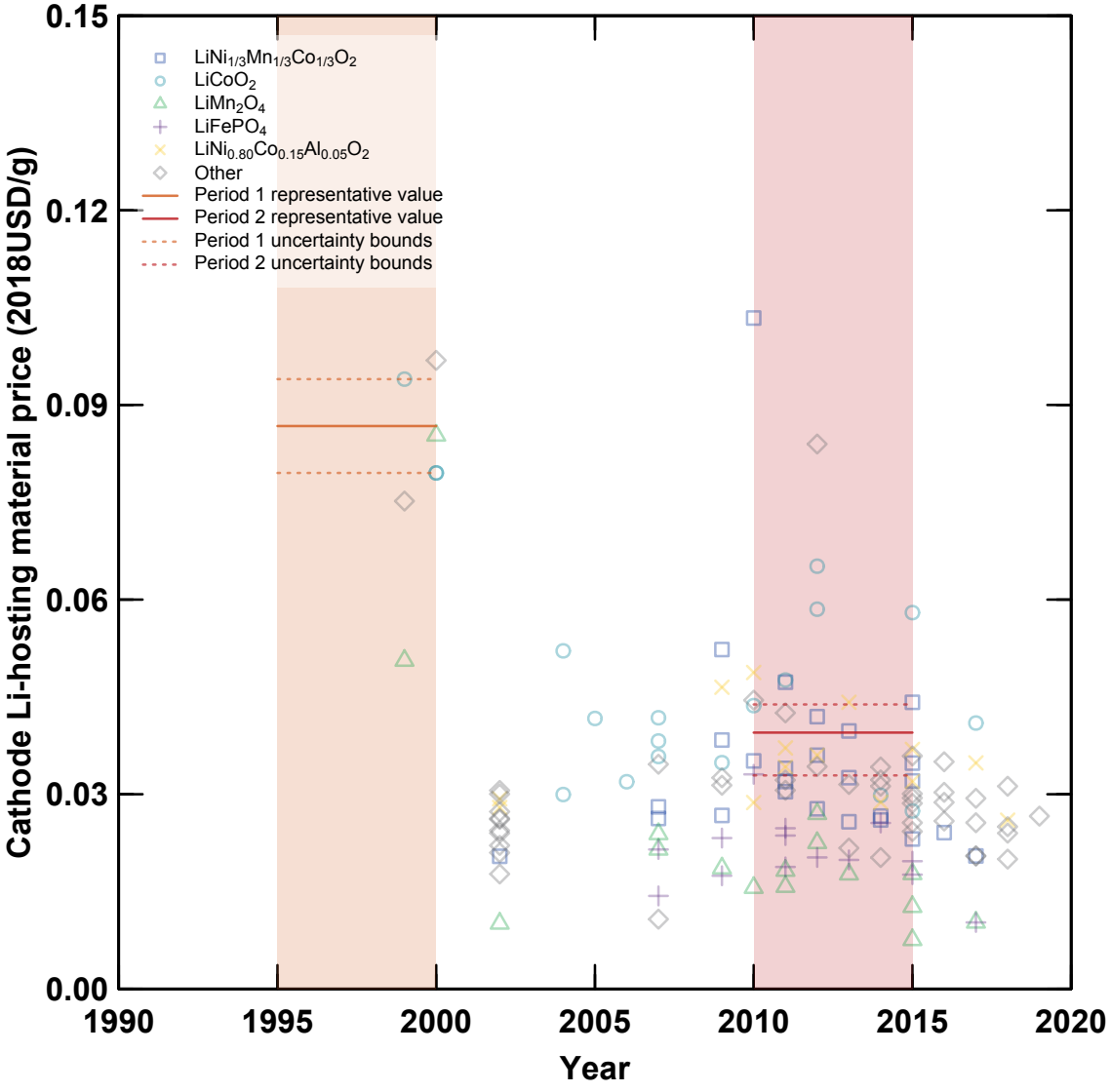

Figure S43: Specific prices of metal oxide materials considered for lithium-ion cell cathodes, by material composition.

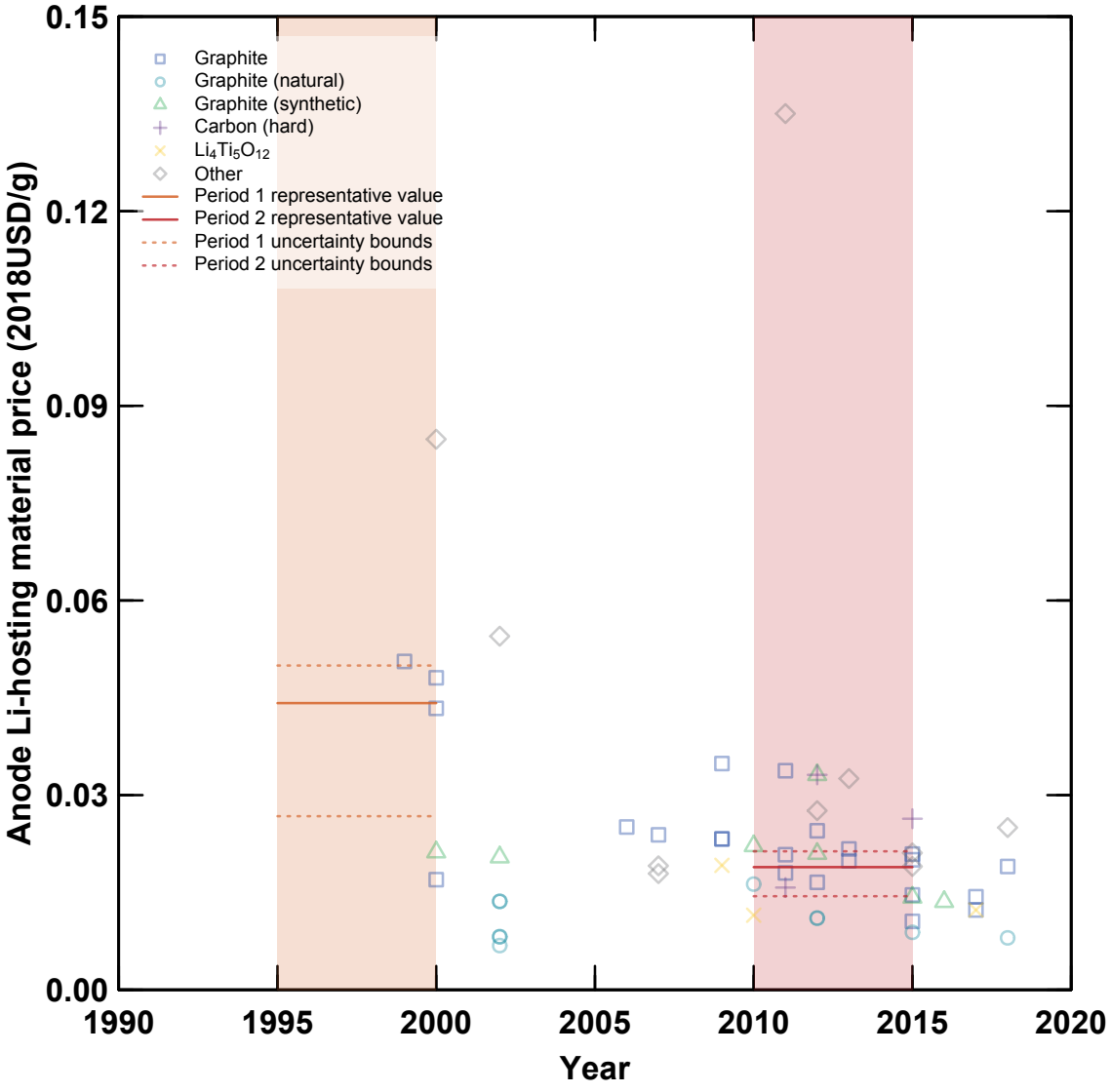

Figure S44: Specific prices of materials considered for lithium-ion cell anodes, by material type.

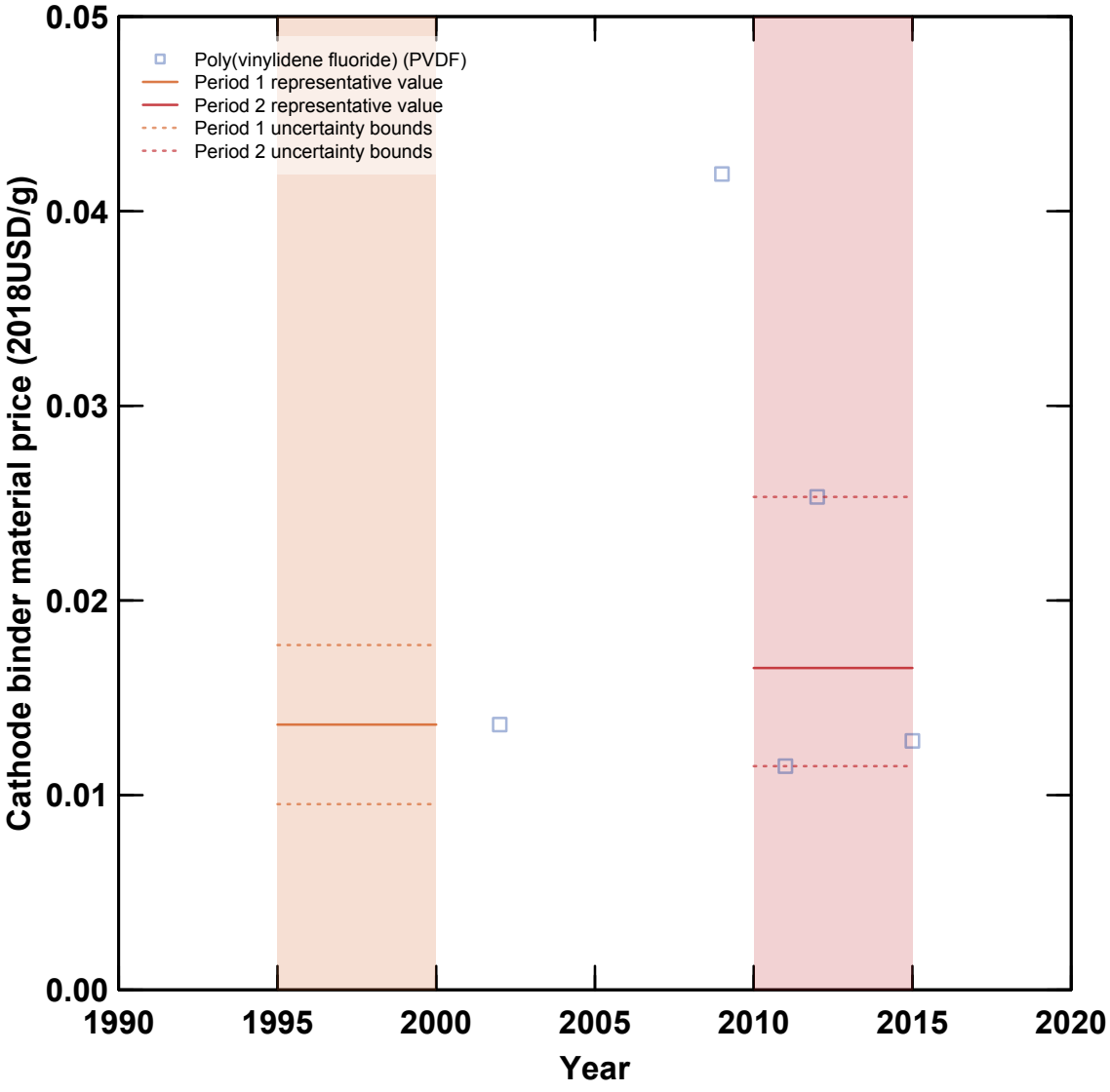

Figure S45: Specific prices of binder materials for lithium-ion cell cathodes, by material type.

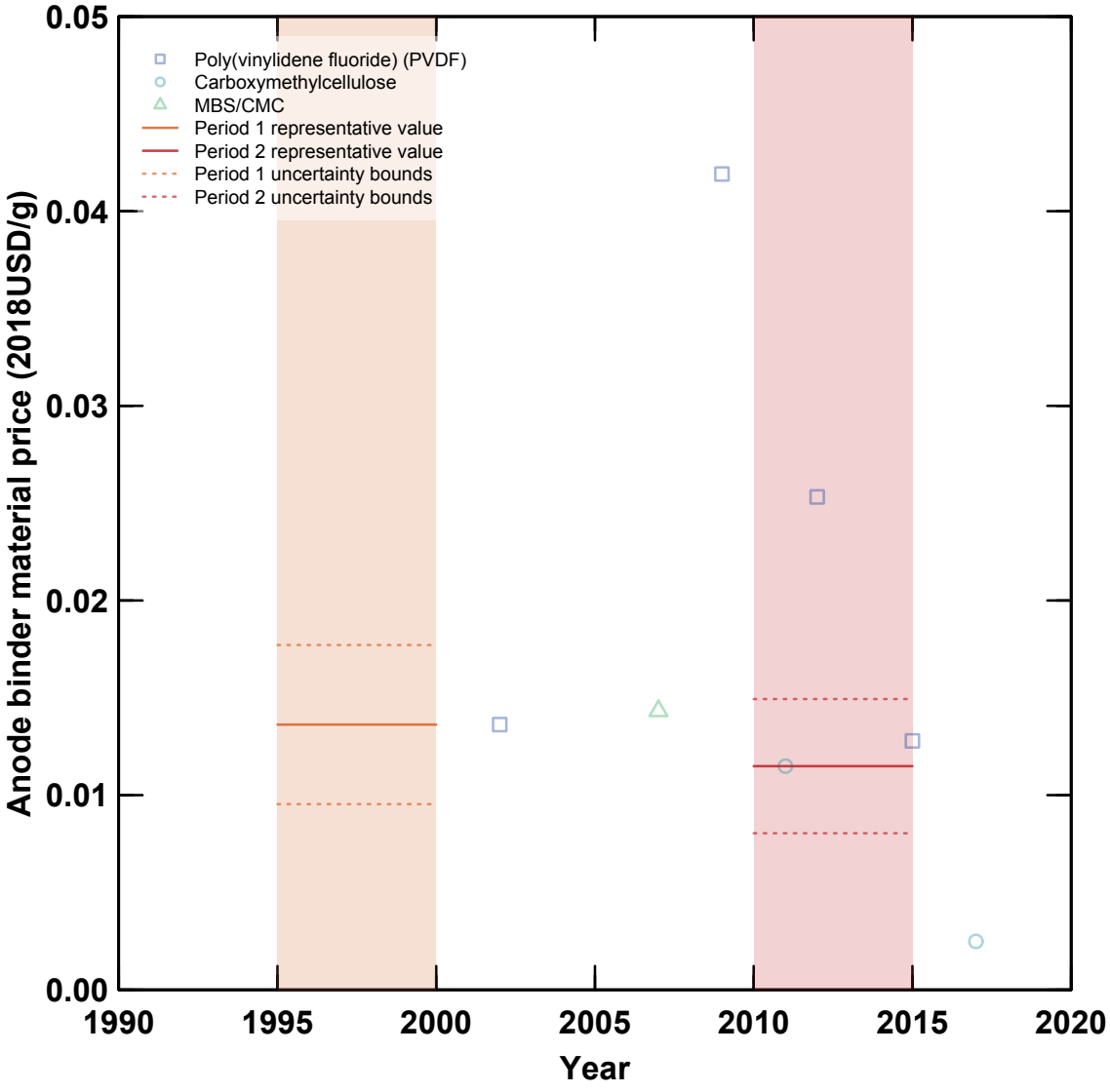

Figure S46: Specific prices of binder materials for lithium-ion cell anodes, by material type.

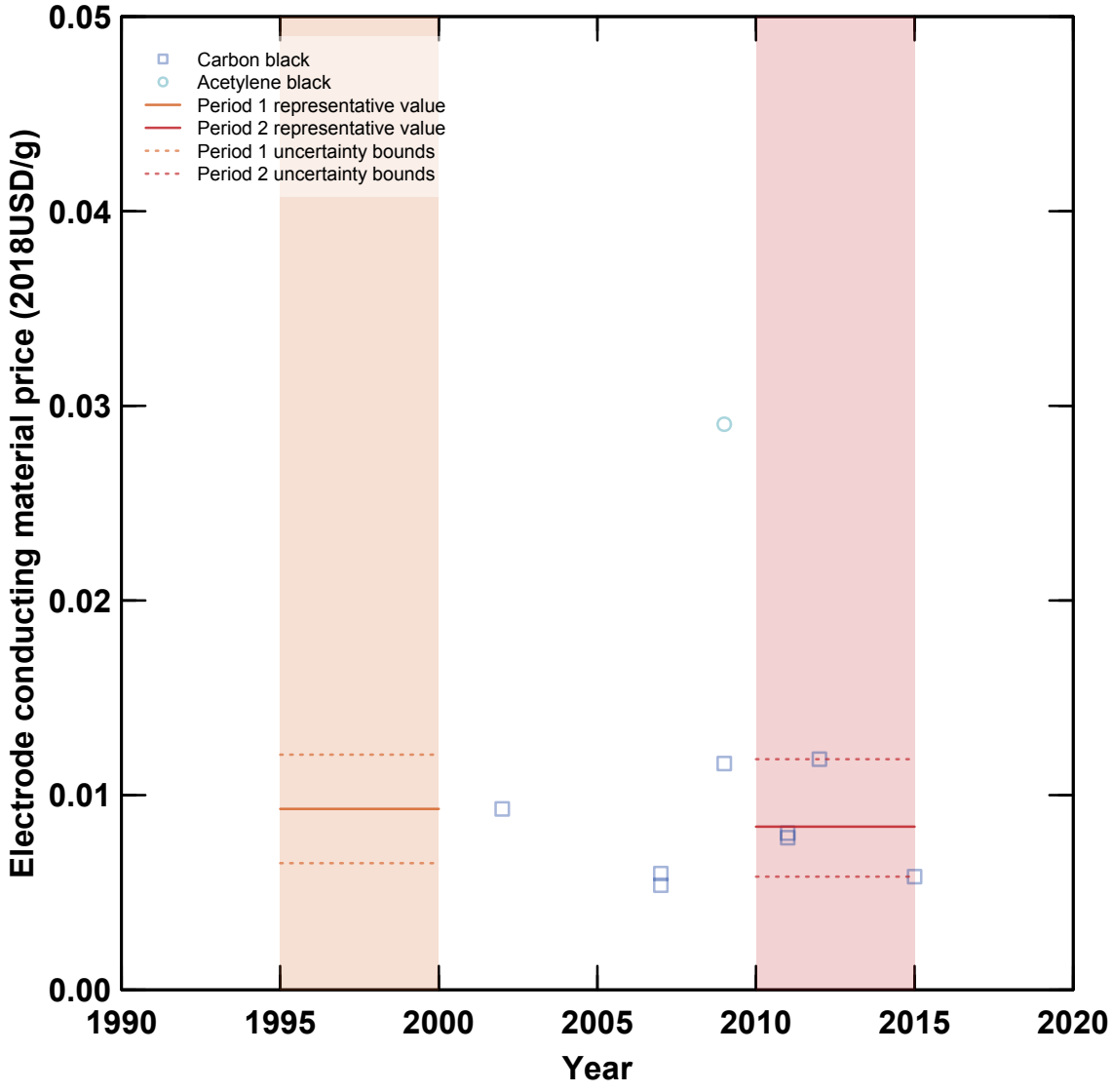

Figure S47: Specific prices of conducting materials for lithium-ion cell electrodes, by material type.

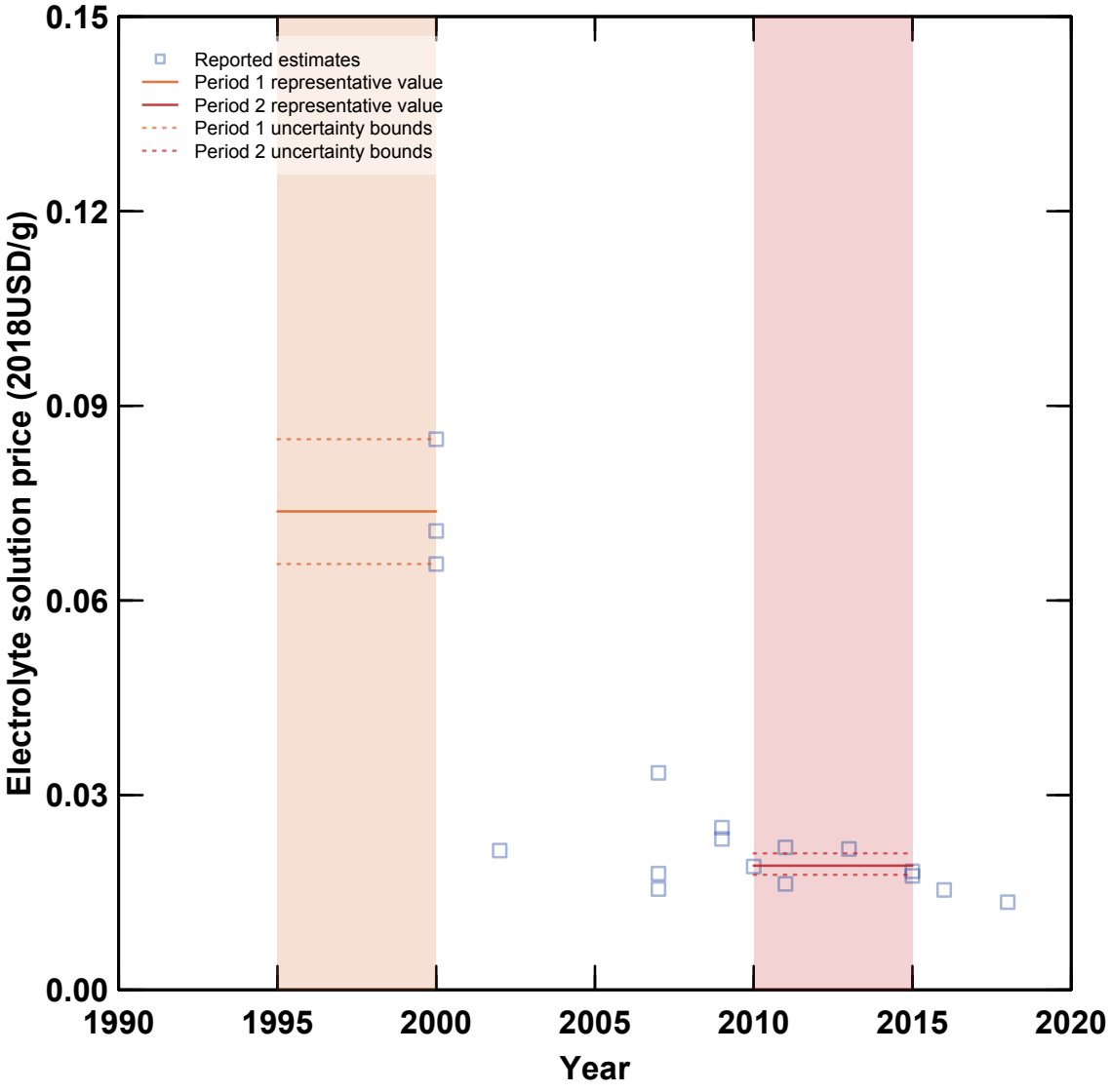

Figure S48: Specific prices of electrolyte solutions for lithium-ion cells.

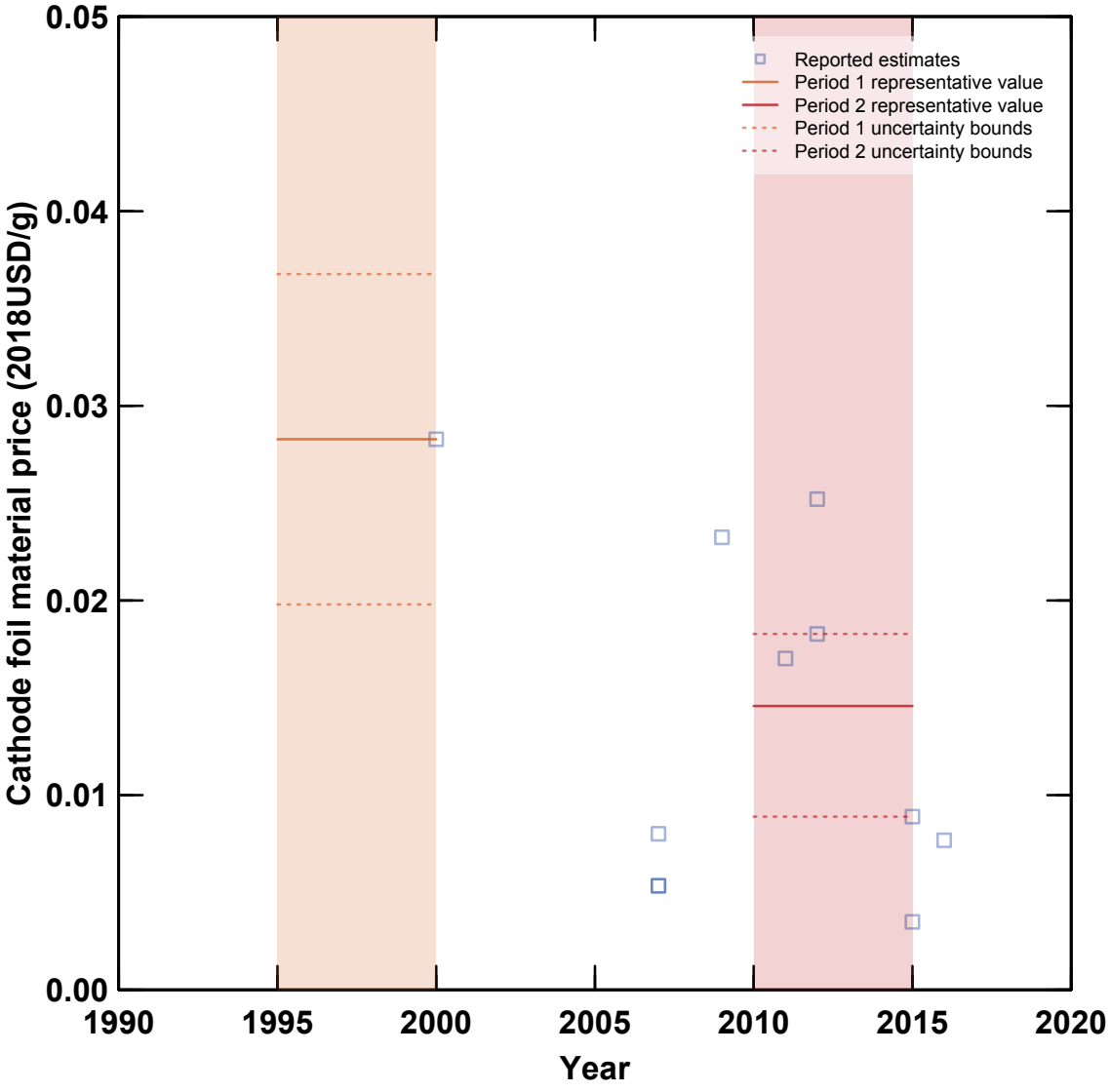

Figure S49: Specific prices of cathode current collector foils for lithium-ion cells.

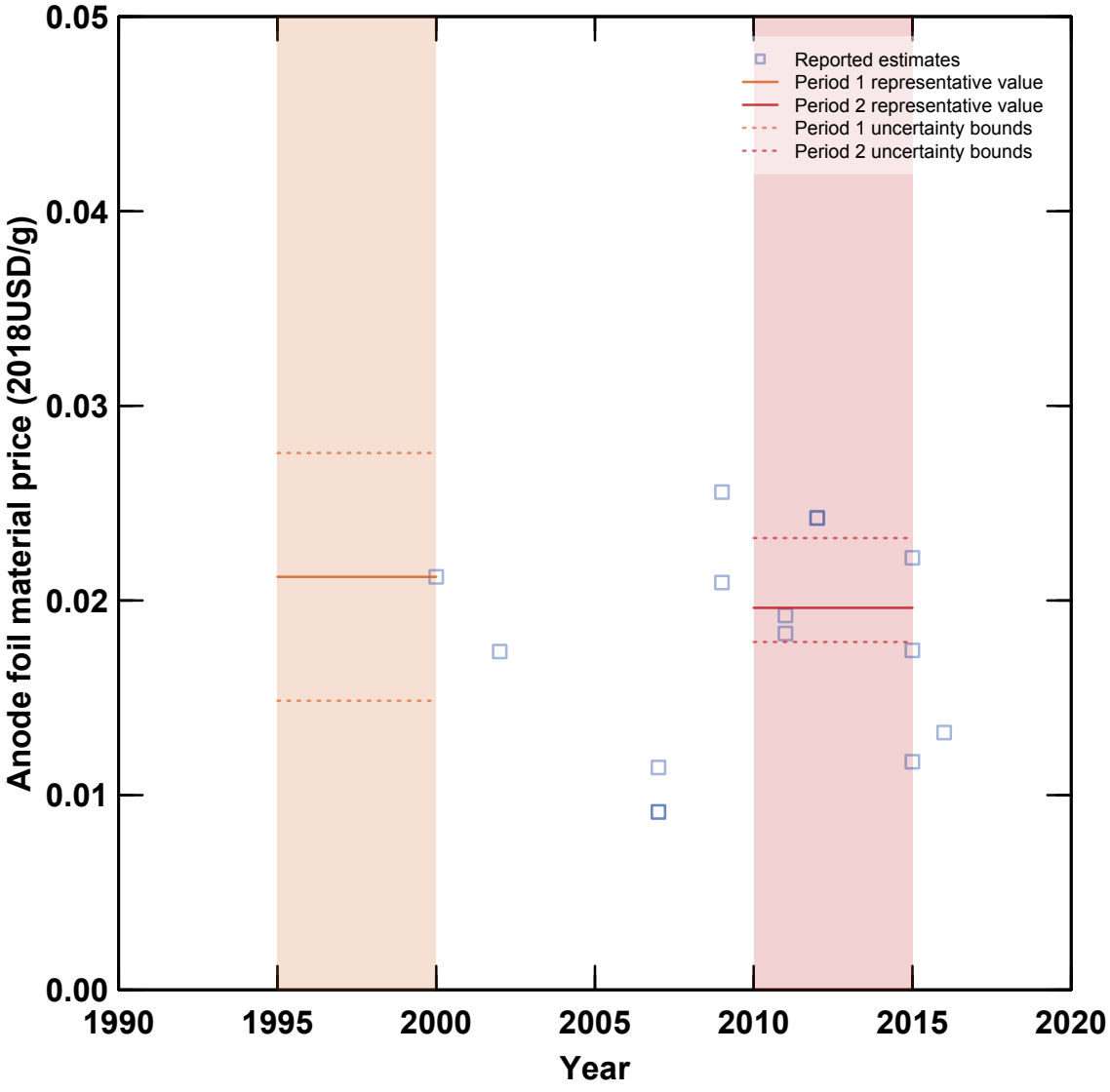

Figure S50: Specific prices of anode current collector foils for lithium-ion cells.

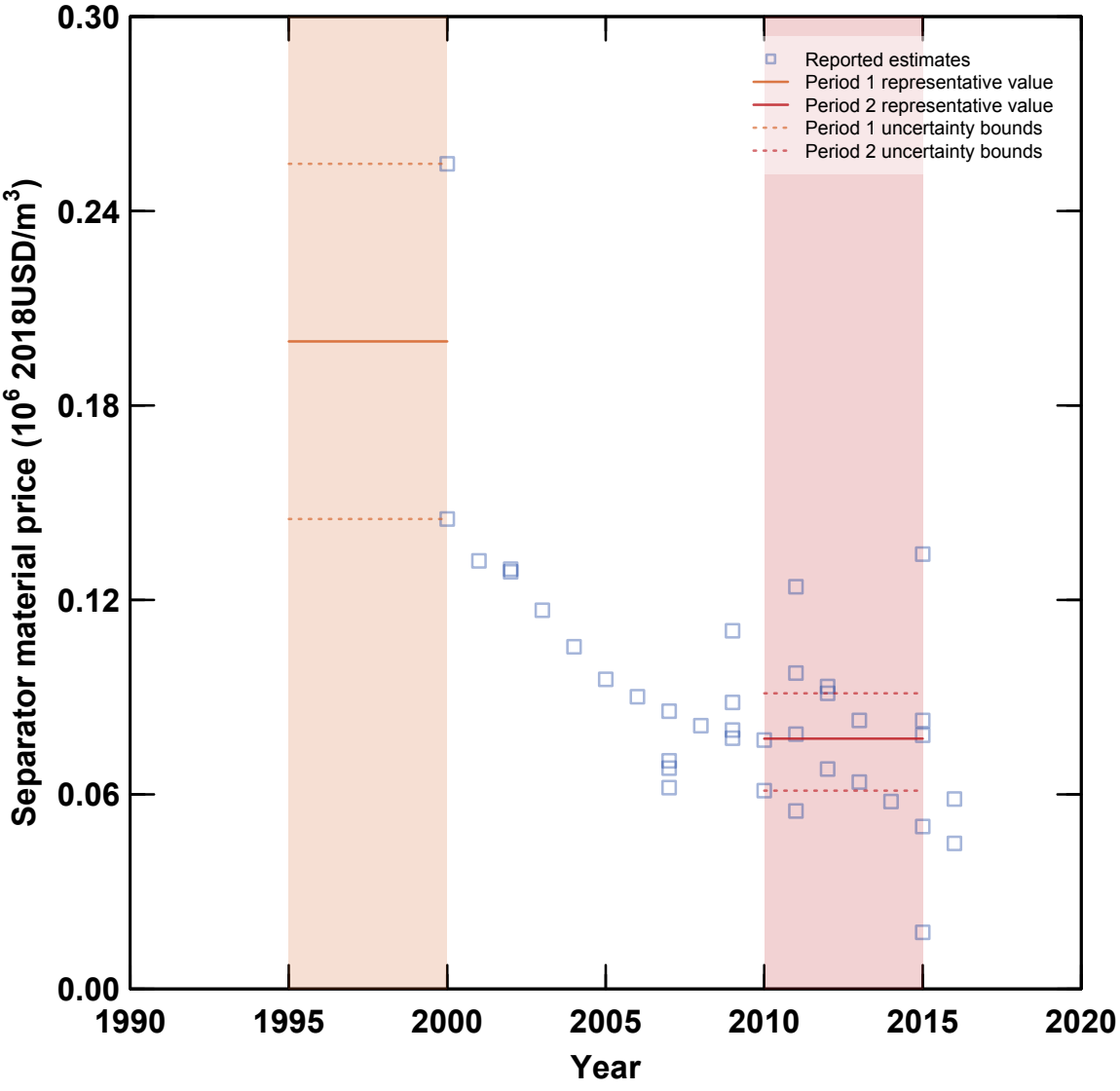

Figure S51: Price densities of separators for lithium-ion cells.

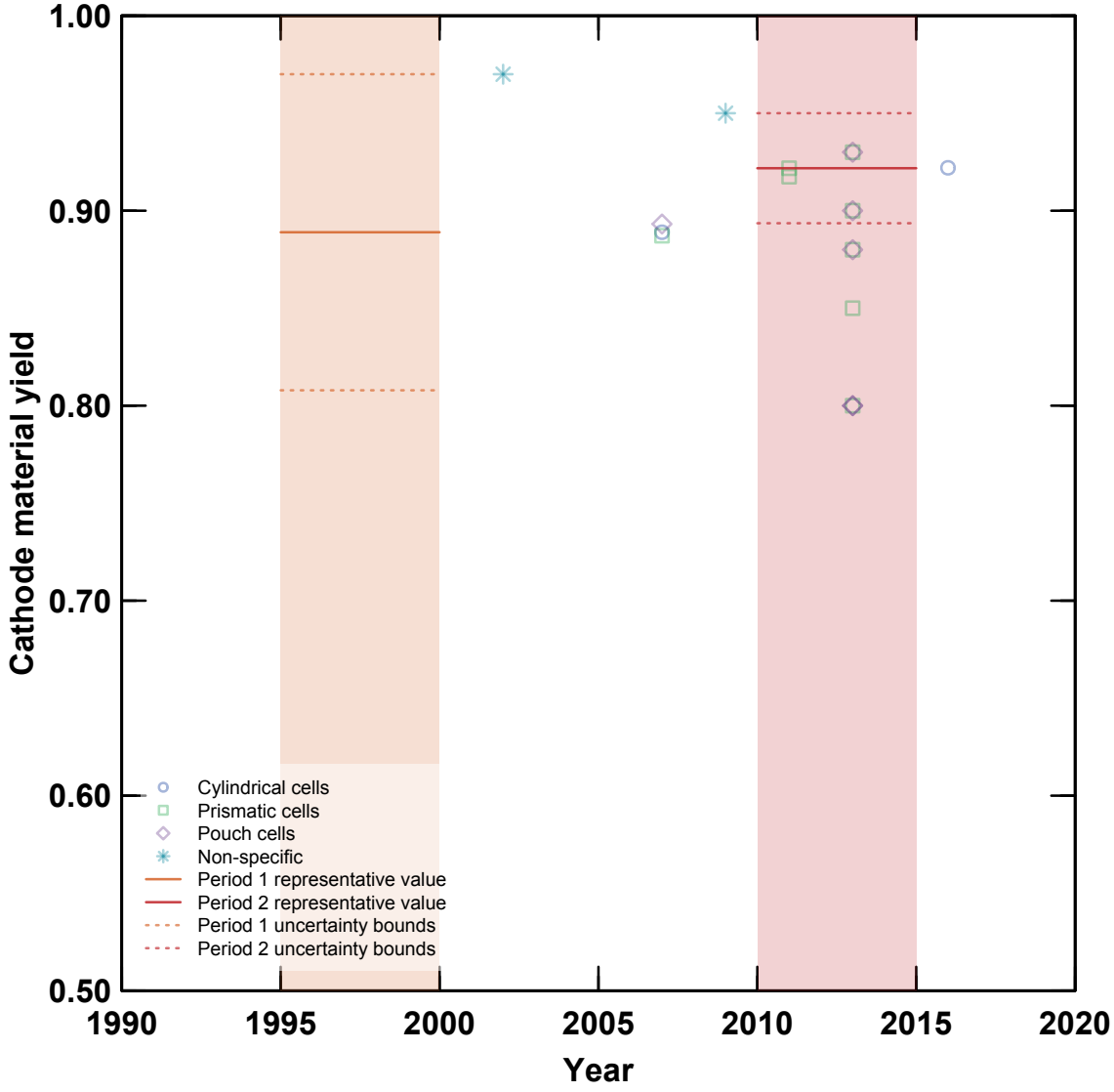

Figure S52: Yield estimates for cathode materials (*i.e.* the mixture of metal oxide, conducting material, and binder).

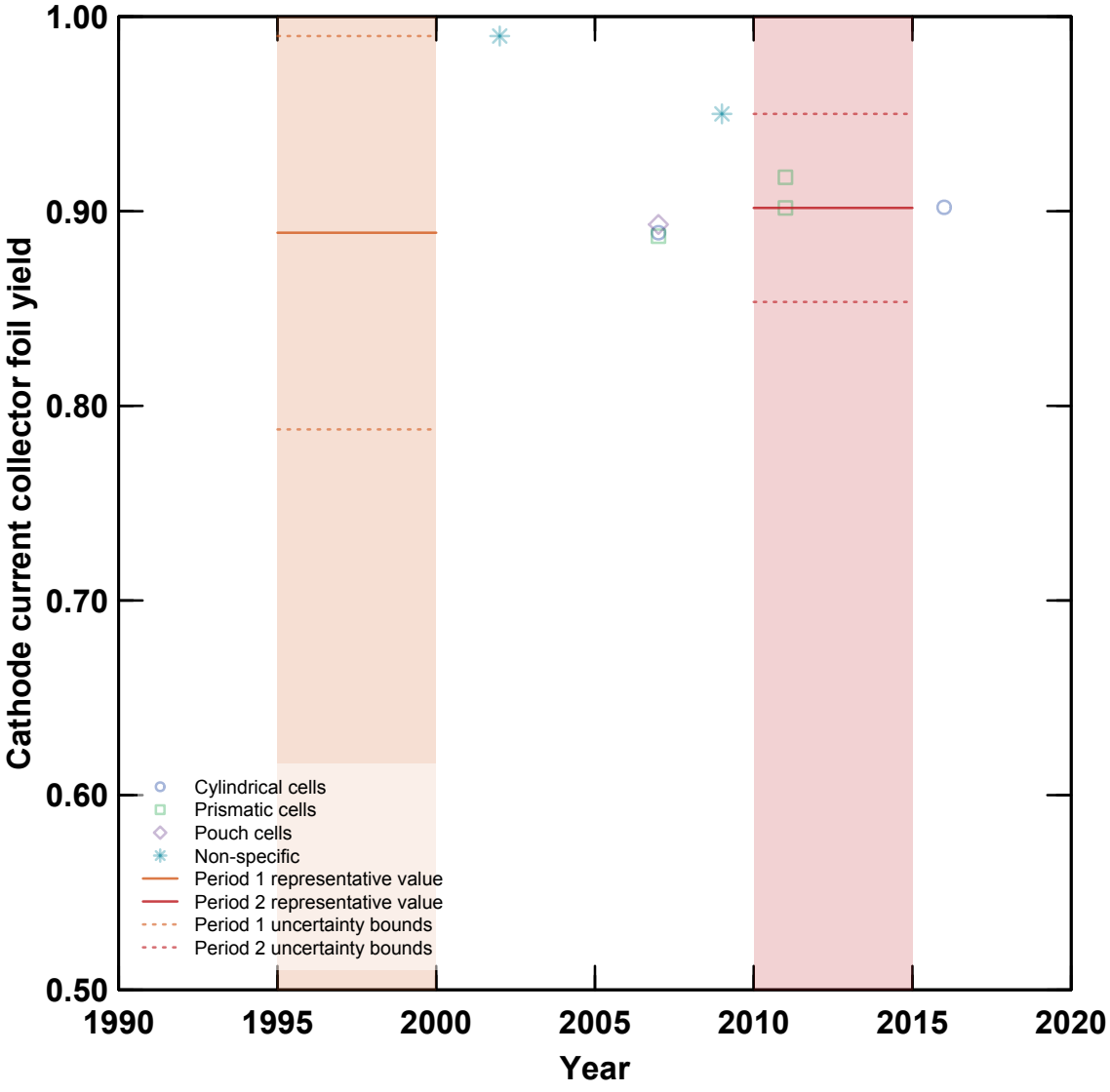

Figure S53: Yield estimates for cathode current collector foil.

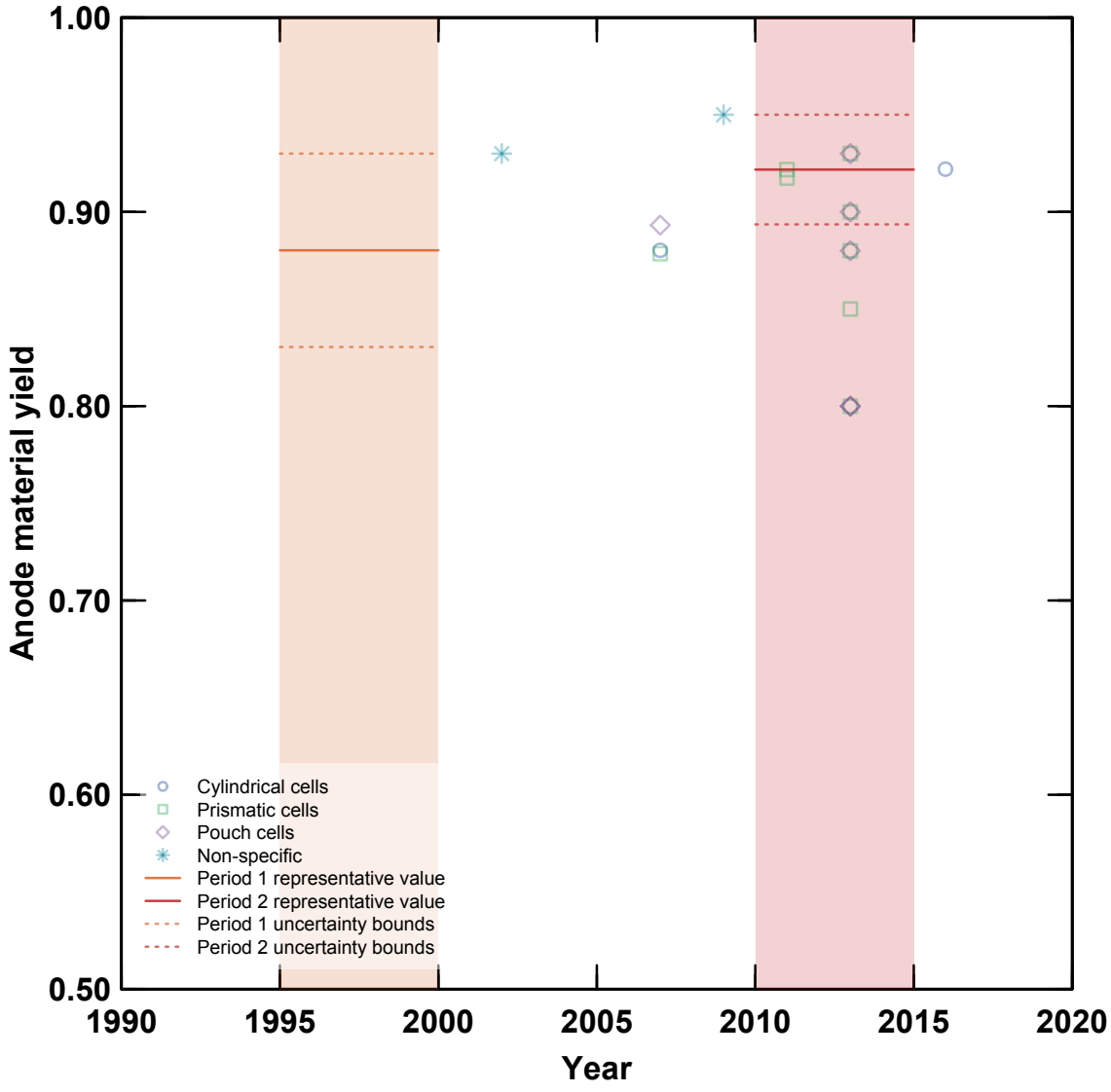

Figure S54: Yield estimates for anode materials (*i.e.* the mixture of graphite (typically), conducting material (if present), and binder).

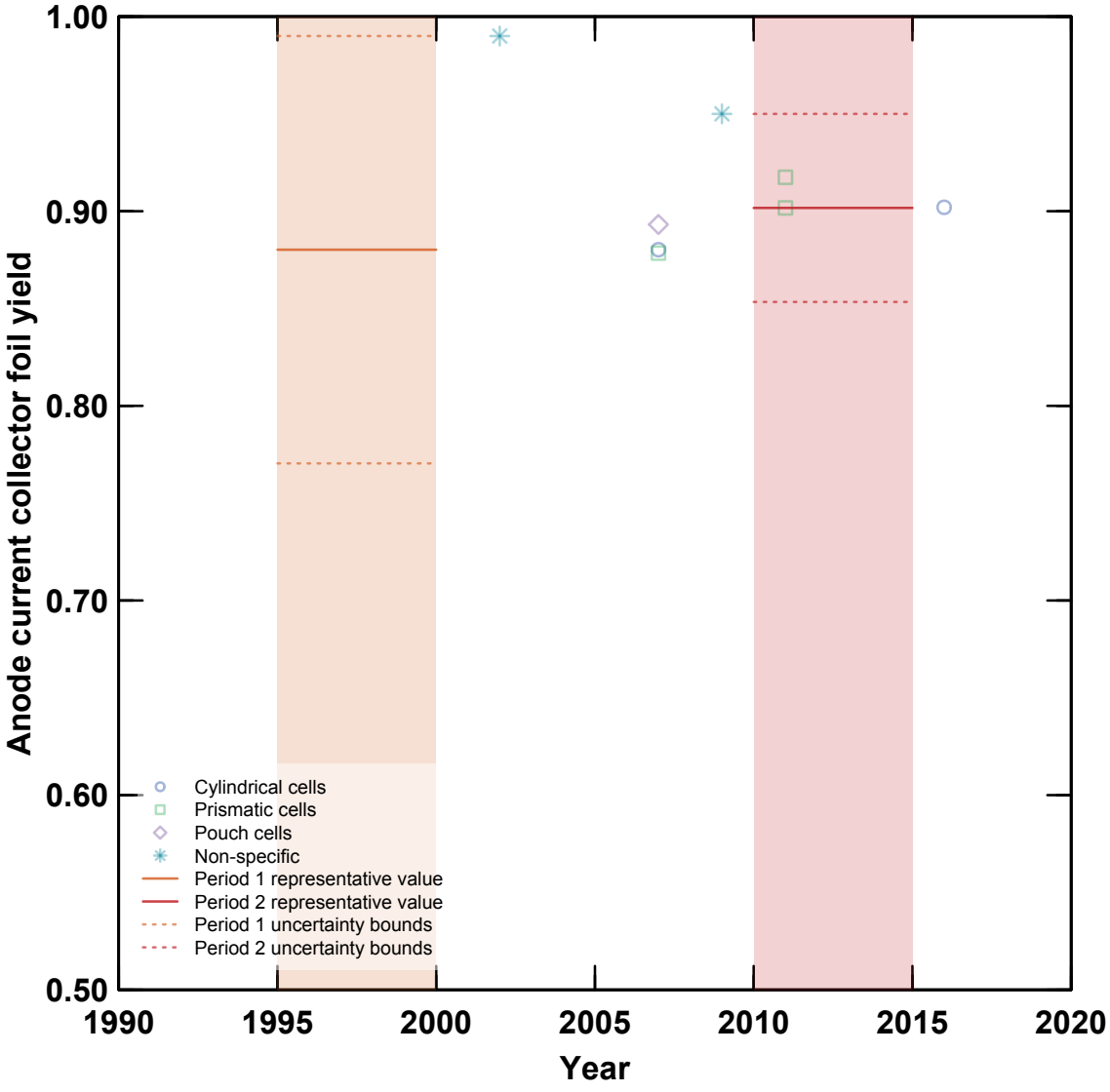

Figure S55: Yield estimates for anode current collector foil.

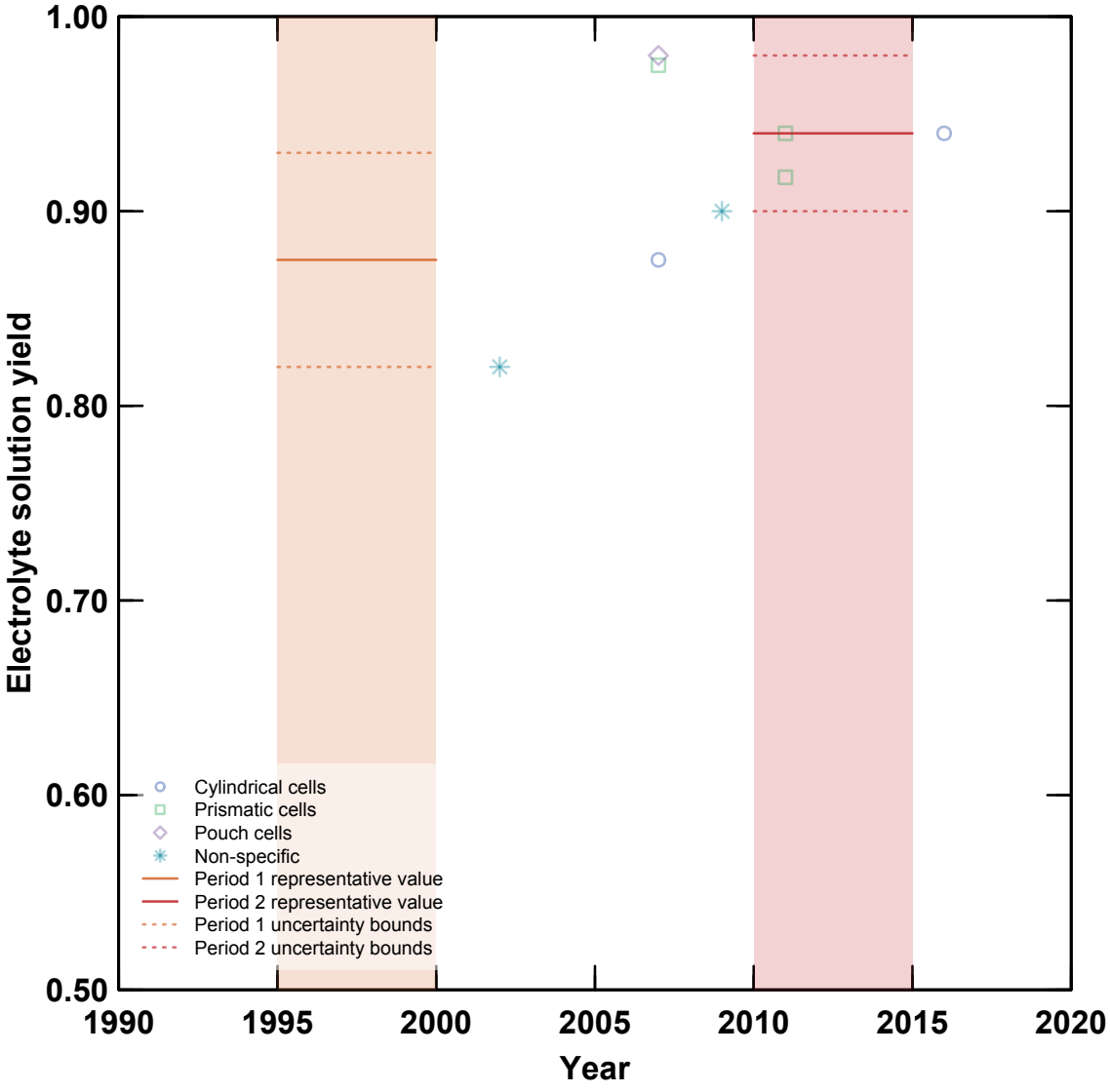

Figure S56: Yield estimates for electrolyte solution.

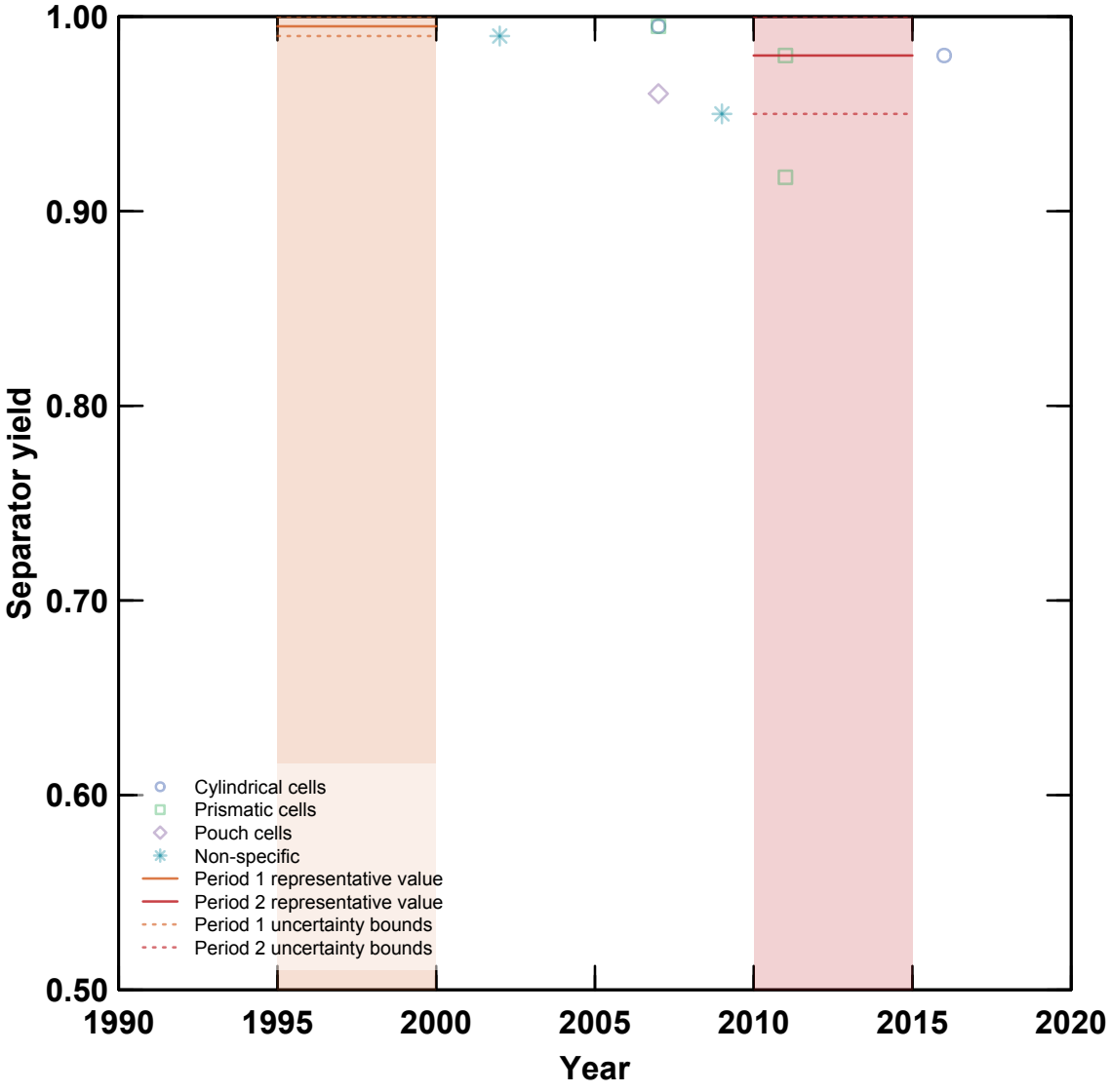

Figure S57: Yield estimates for separator material.

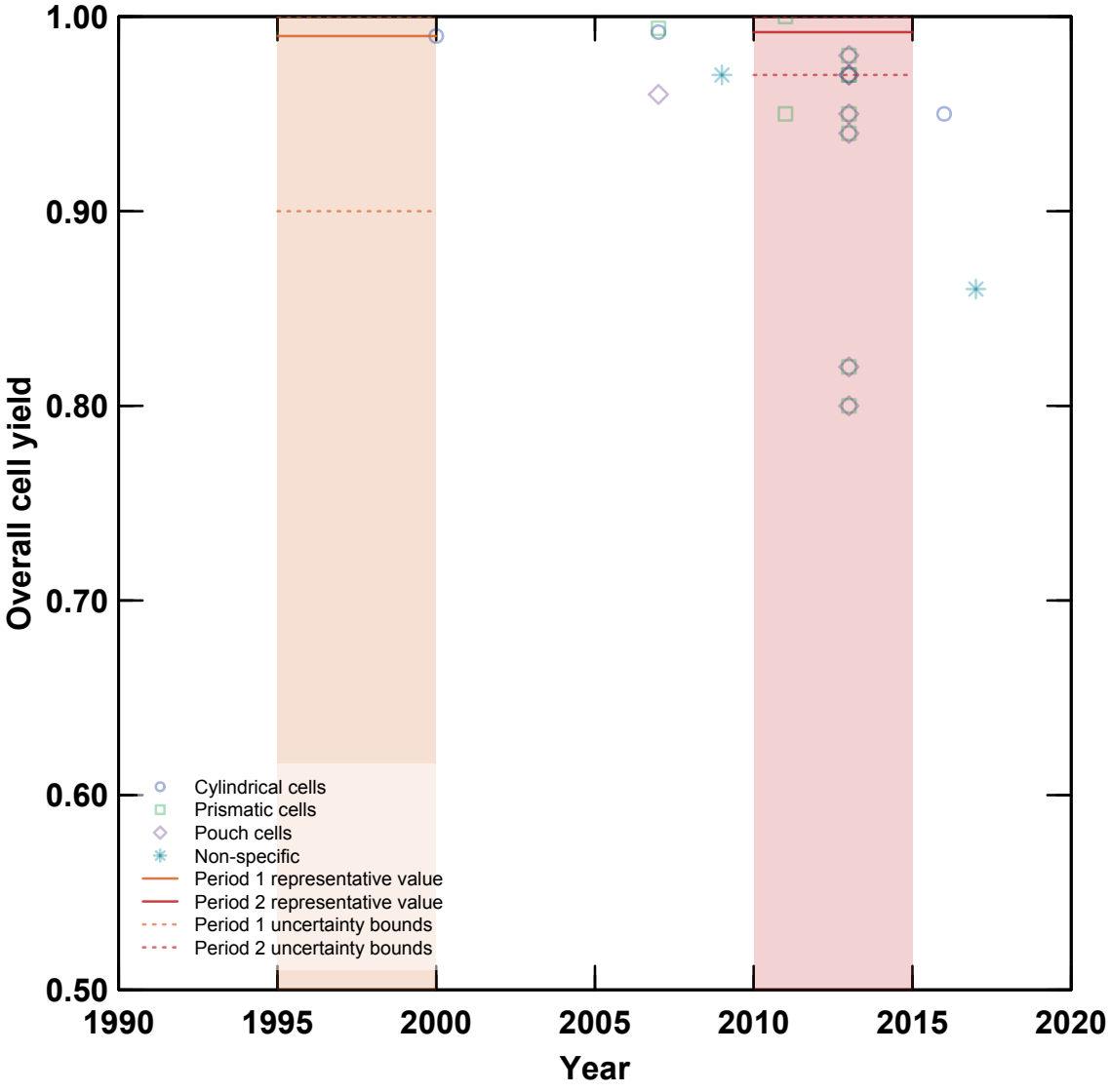

Figure S58: Yield estimates for overall cells.

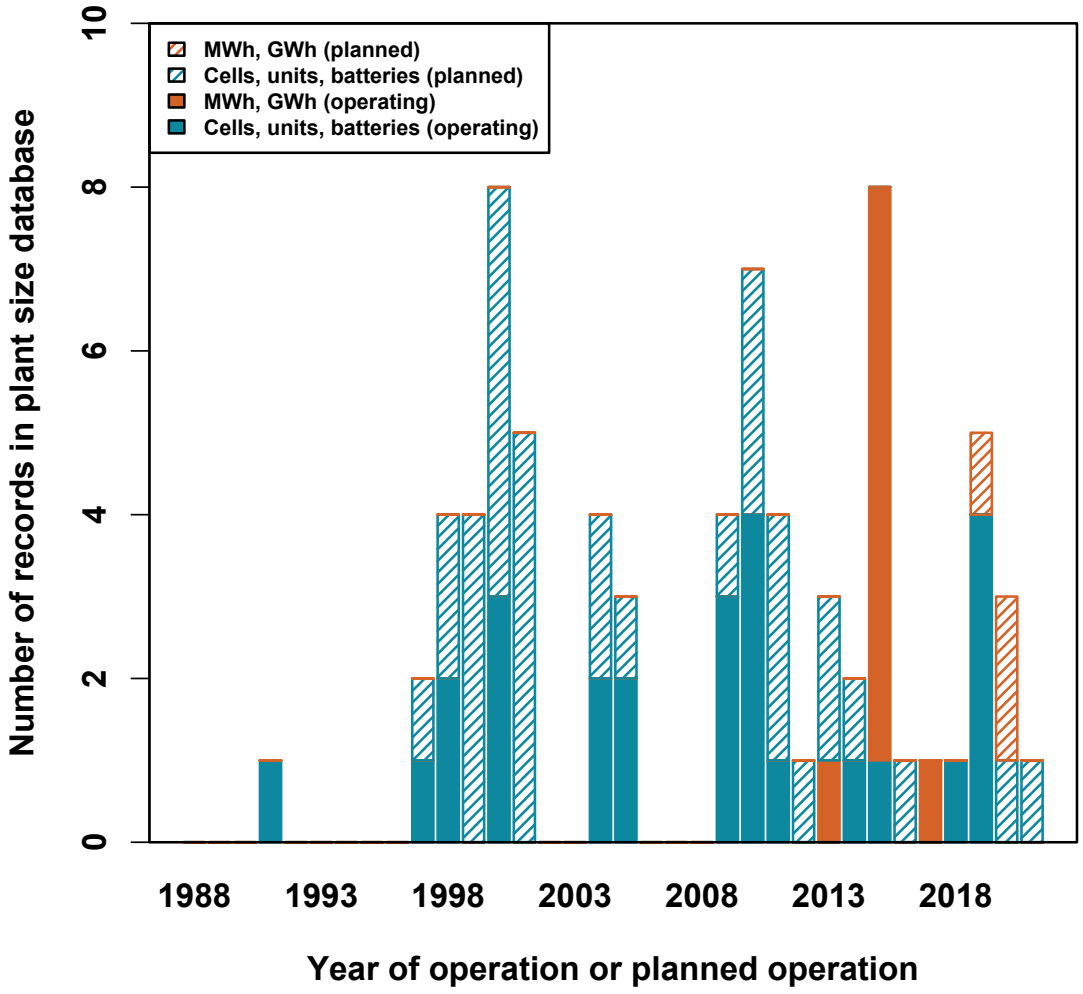

Figure S59: Units of reported yearly production capacities of lithium-ion cell manufacturing plants, by plant status (operating or planned).

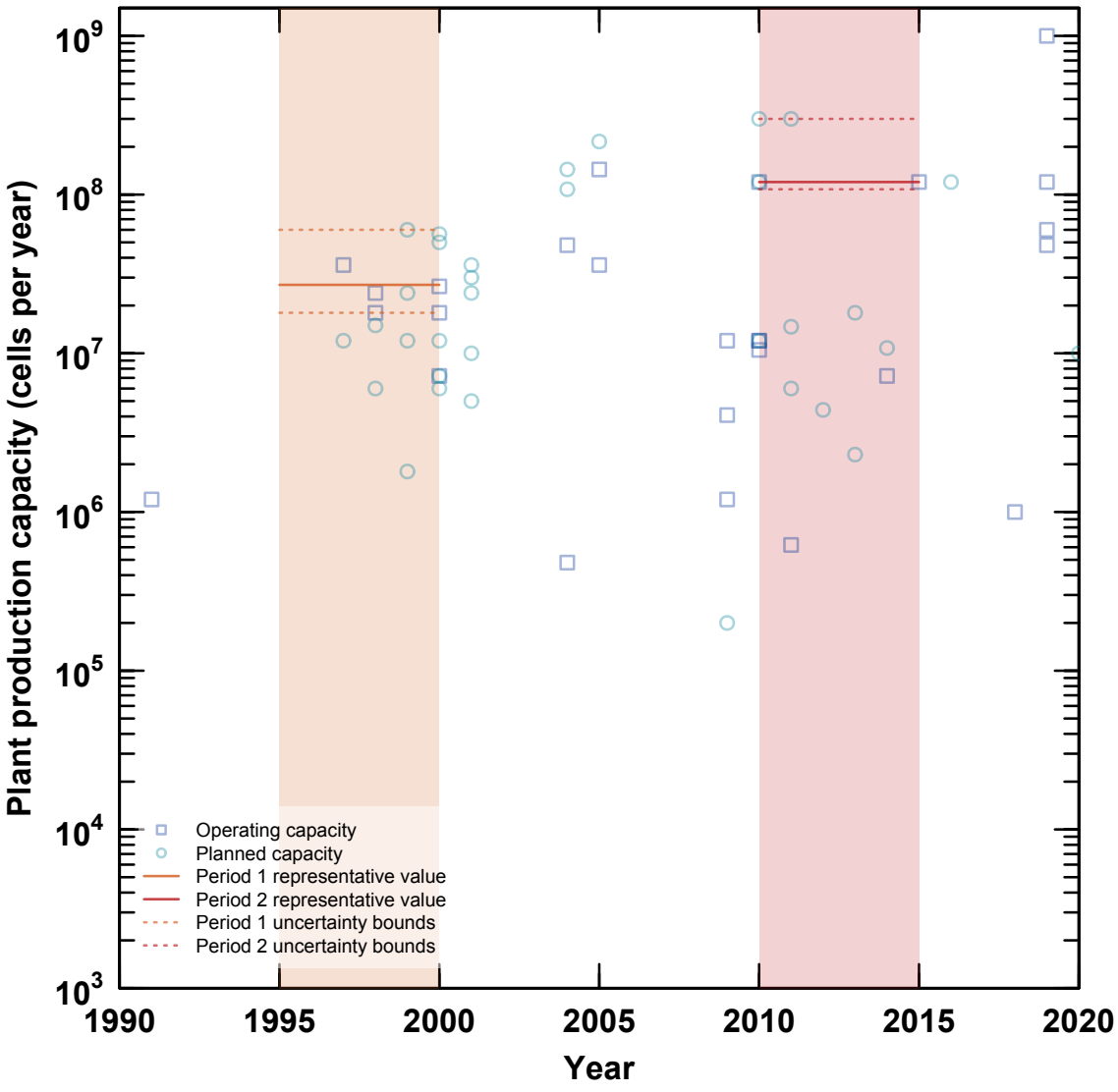

Figure S60: Reported yearly production capacities of lithium-ion cell manufacturing plants, by plant status (operating or planned).

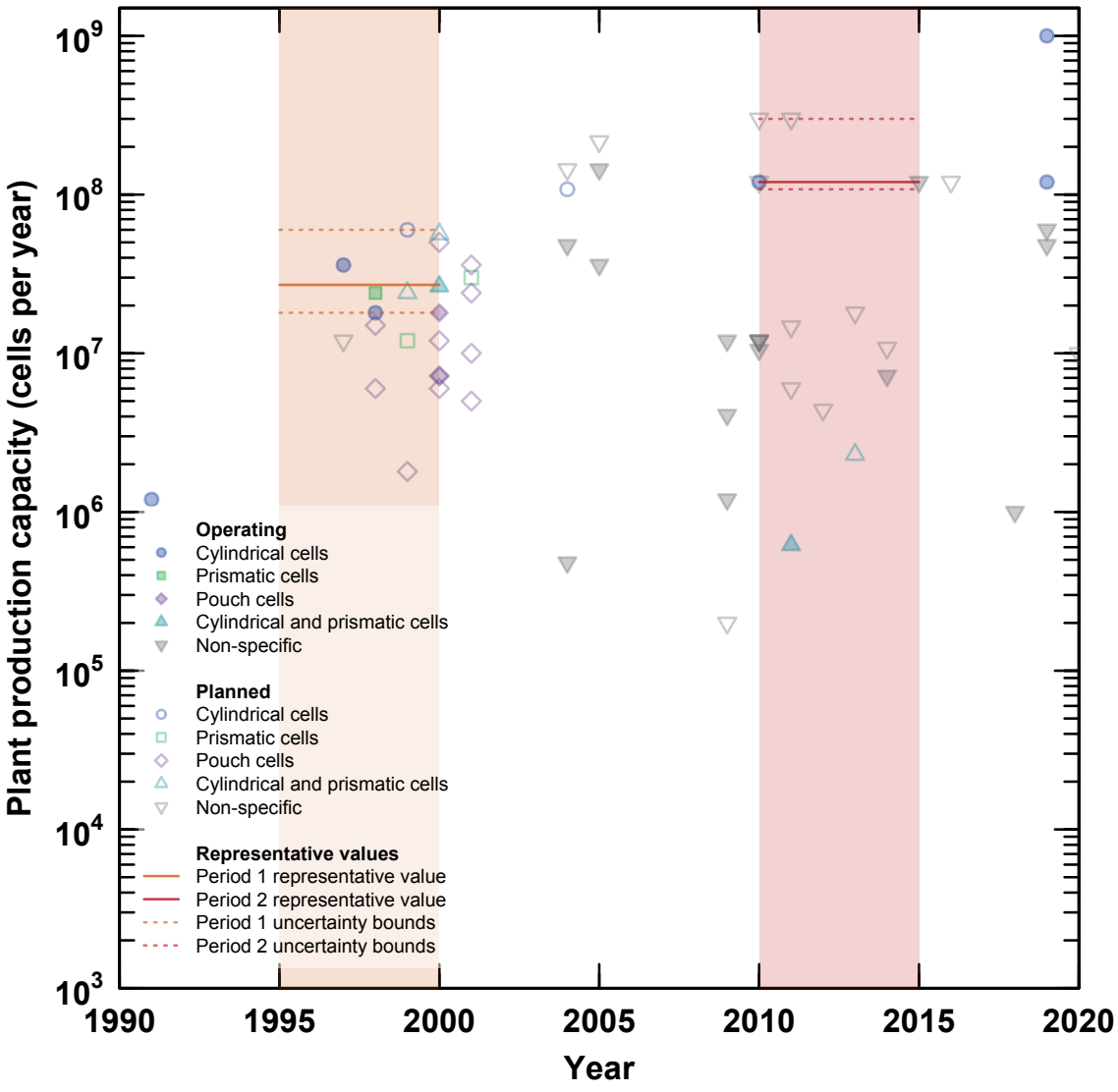

Figure S61: Reported yearly production capacities of lithium-ion cell manufacturing plants, by the shape of cells produced.

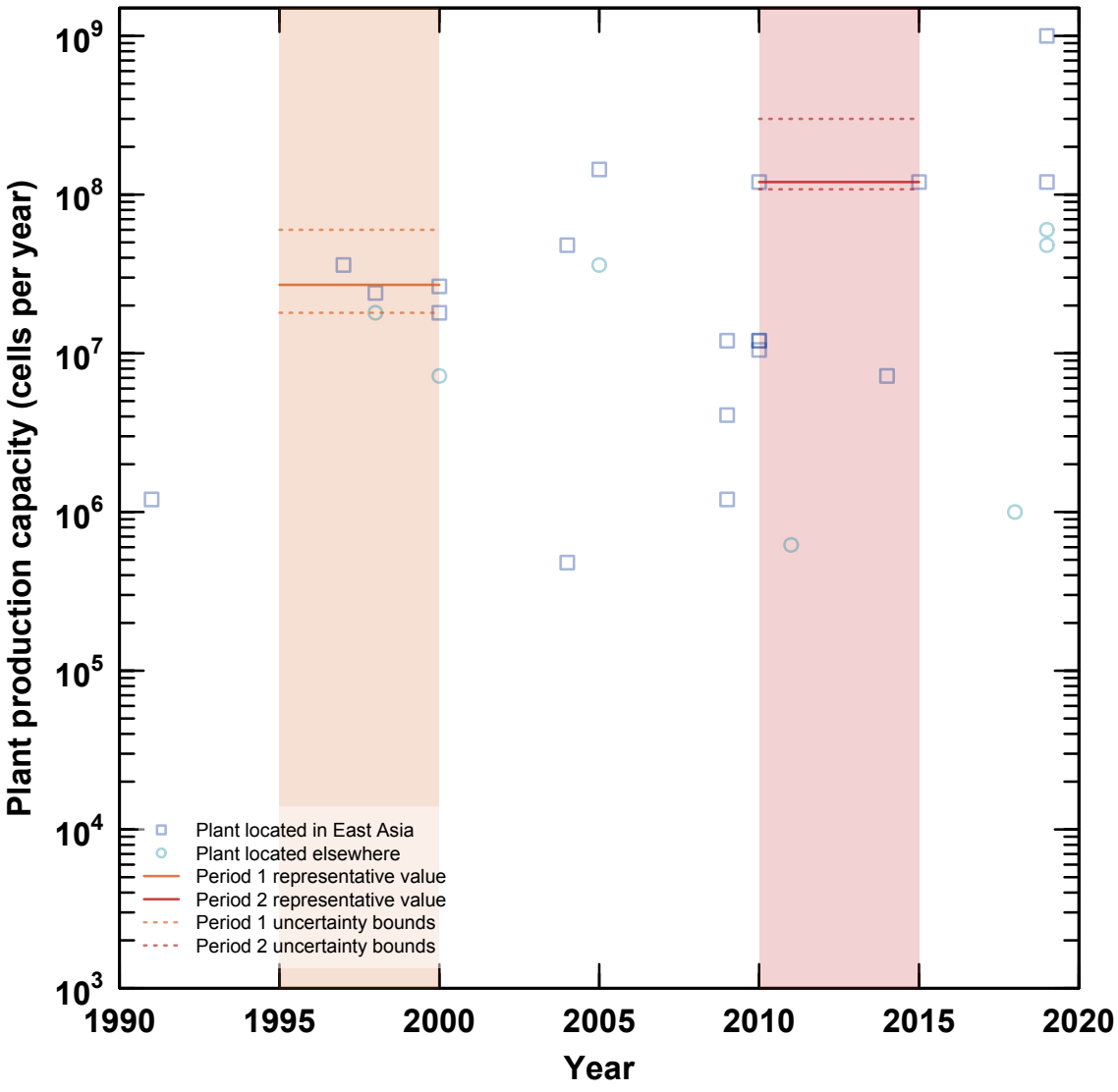

Figure S62: Reported yearly production capacities of lithium-ion cell manufacturing plants for existing plants, by location.

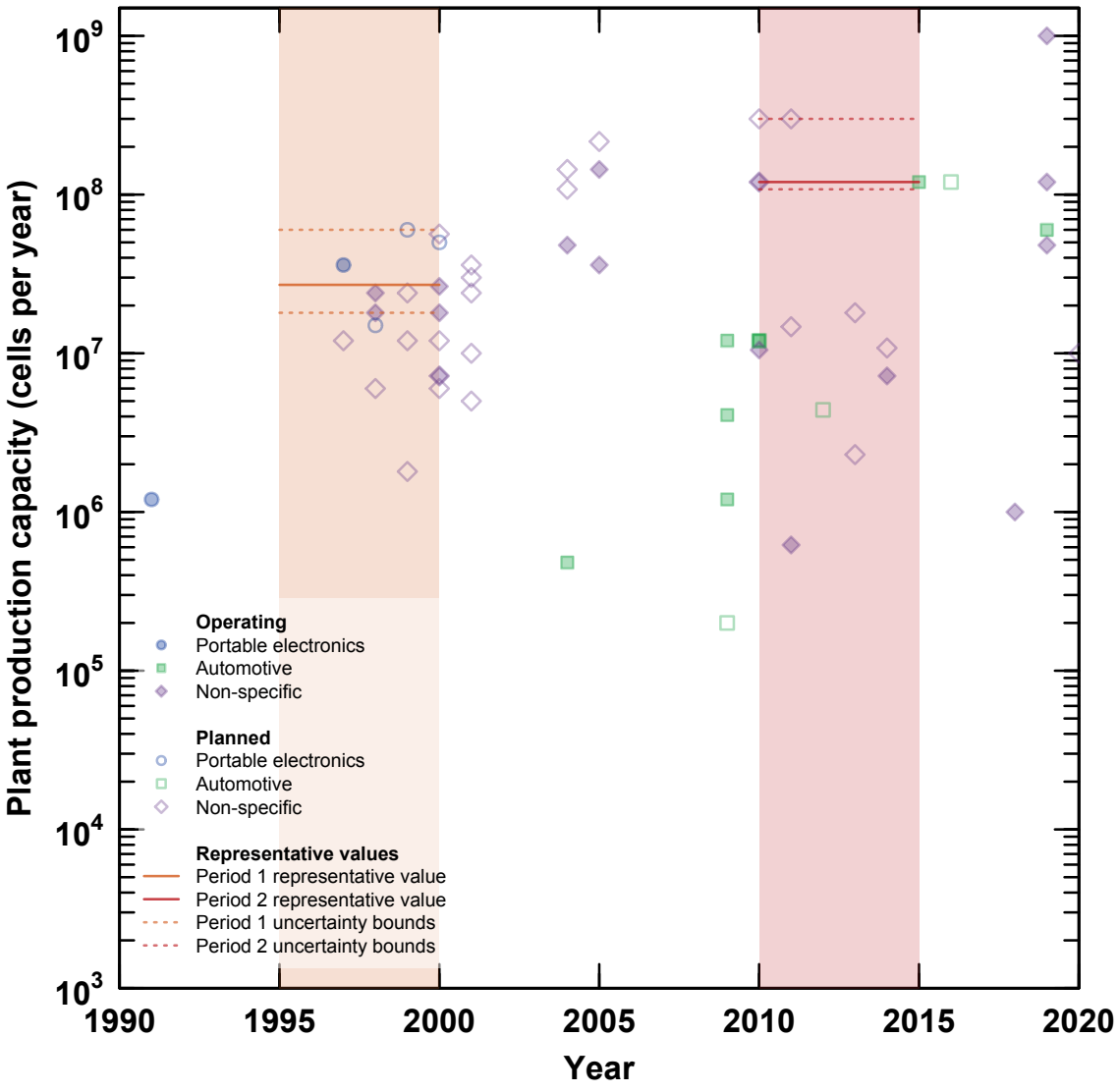

Figure S63: Reported yearly production capacities of lithium-ion cell manufacturing plants for existing plants, by application.

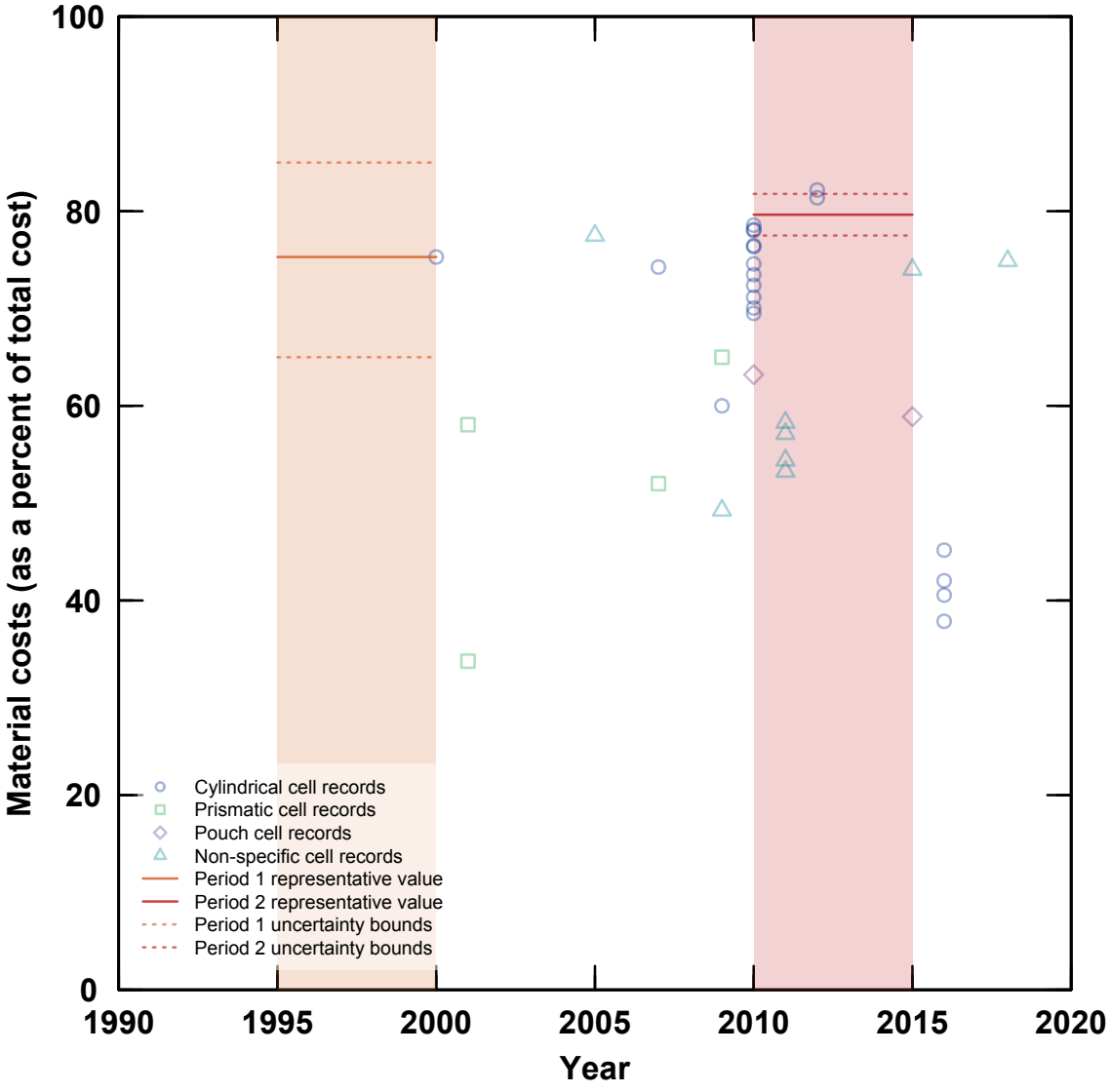

Figure S64: Reported estimates of material cost contributions to lithium-ion cells.

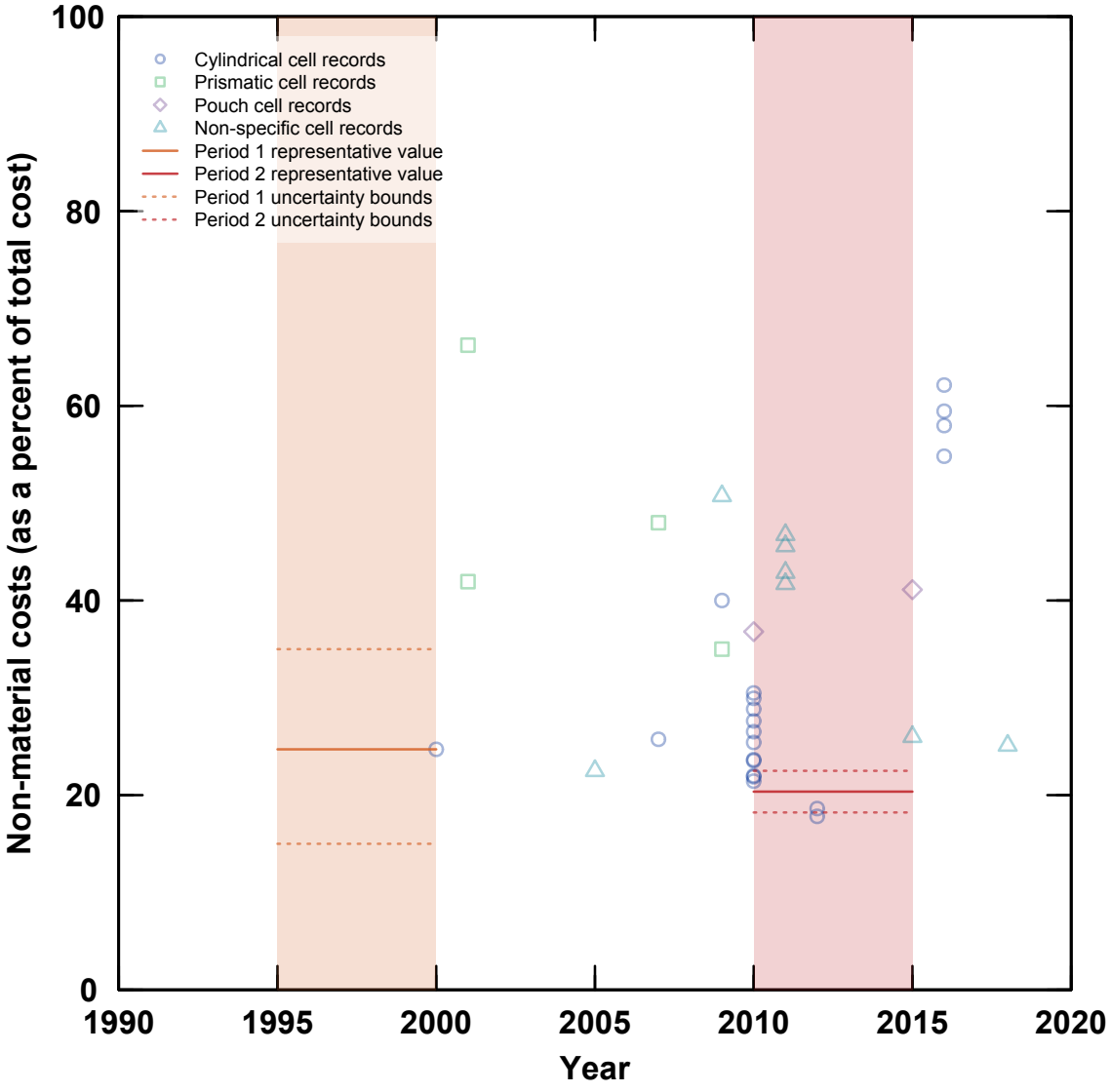

Figure S65: Reported estimates of non-material cost contributions to lithium-ion cells.

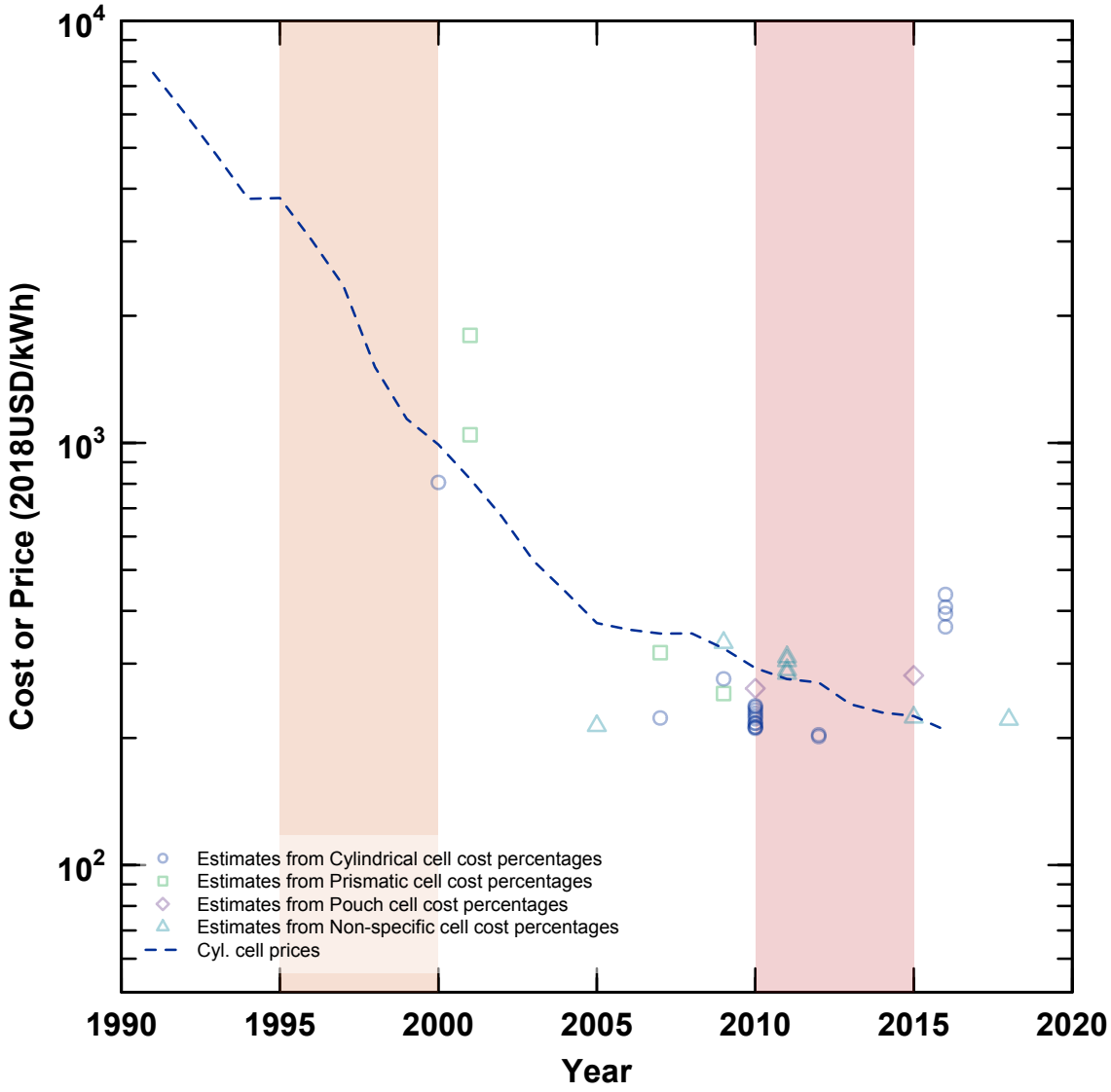

Figure S66: Estimated cell-level costs for 18650-sized lithium-ion cells using different estimates for the fraction of costs that are material costs. For values before 2005, the material costs are calculated using the representative values for period 1. For values after 2005, the material costs are calculated using the representative values for period 2.

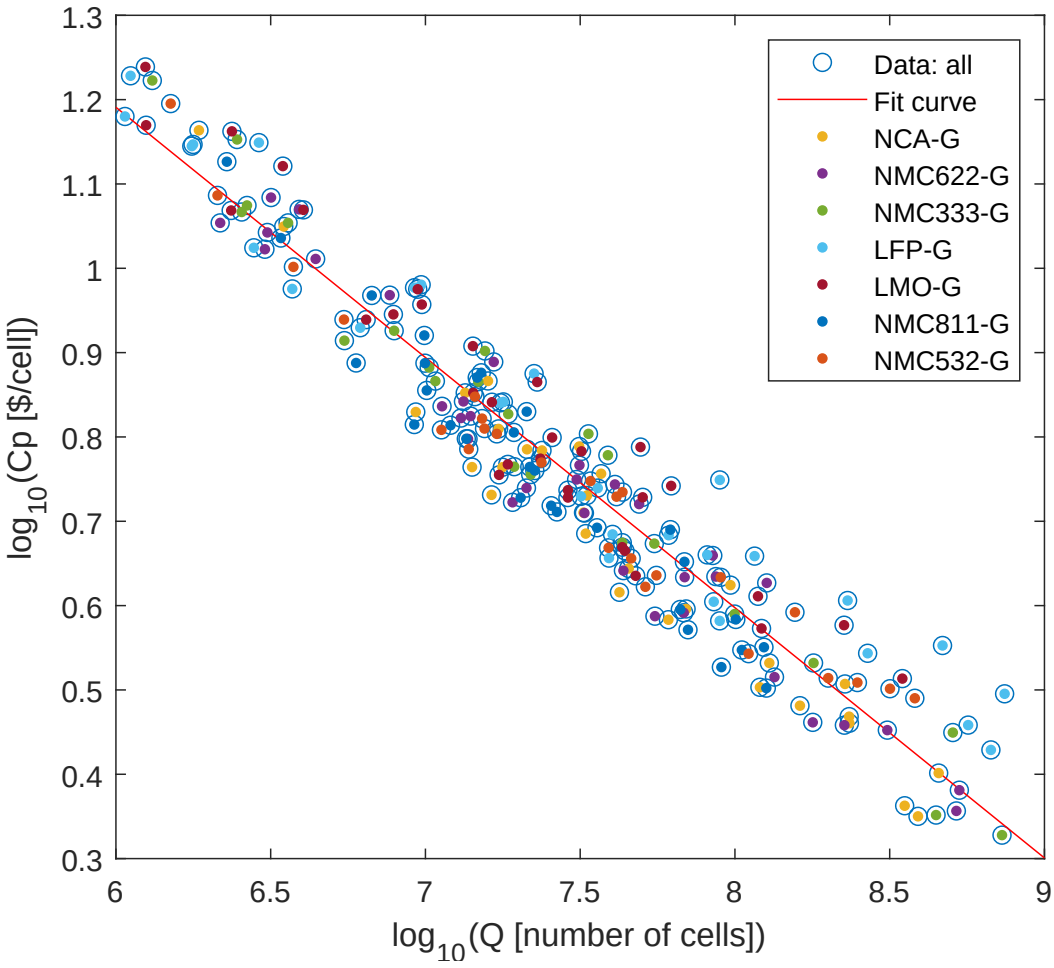

Figure S67: Non-material costs versus production scale for a random assortment of cells, as estimated by BatPaC.

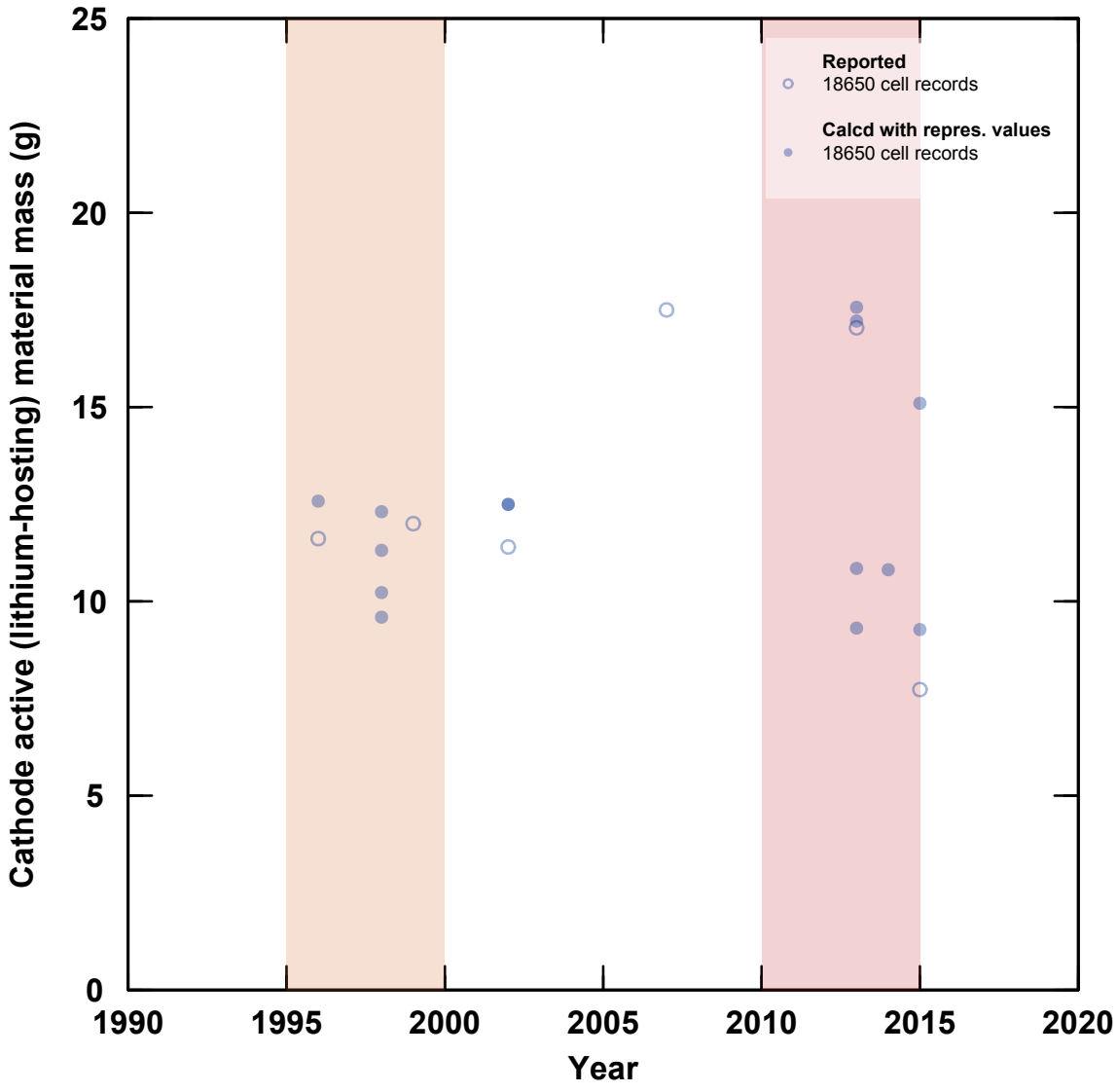

Figure S68: Reported and calculated cathode active material masses in 18650-sized lithium-ion cells.

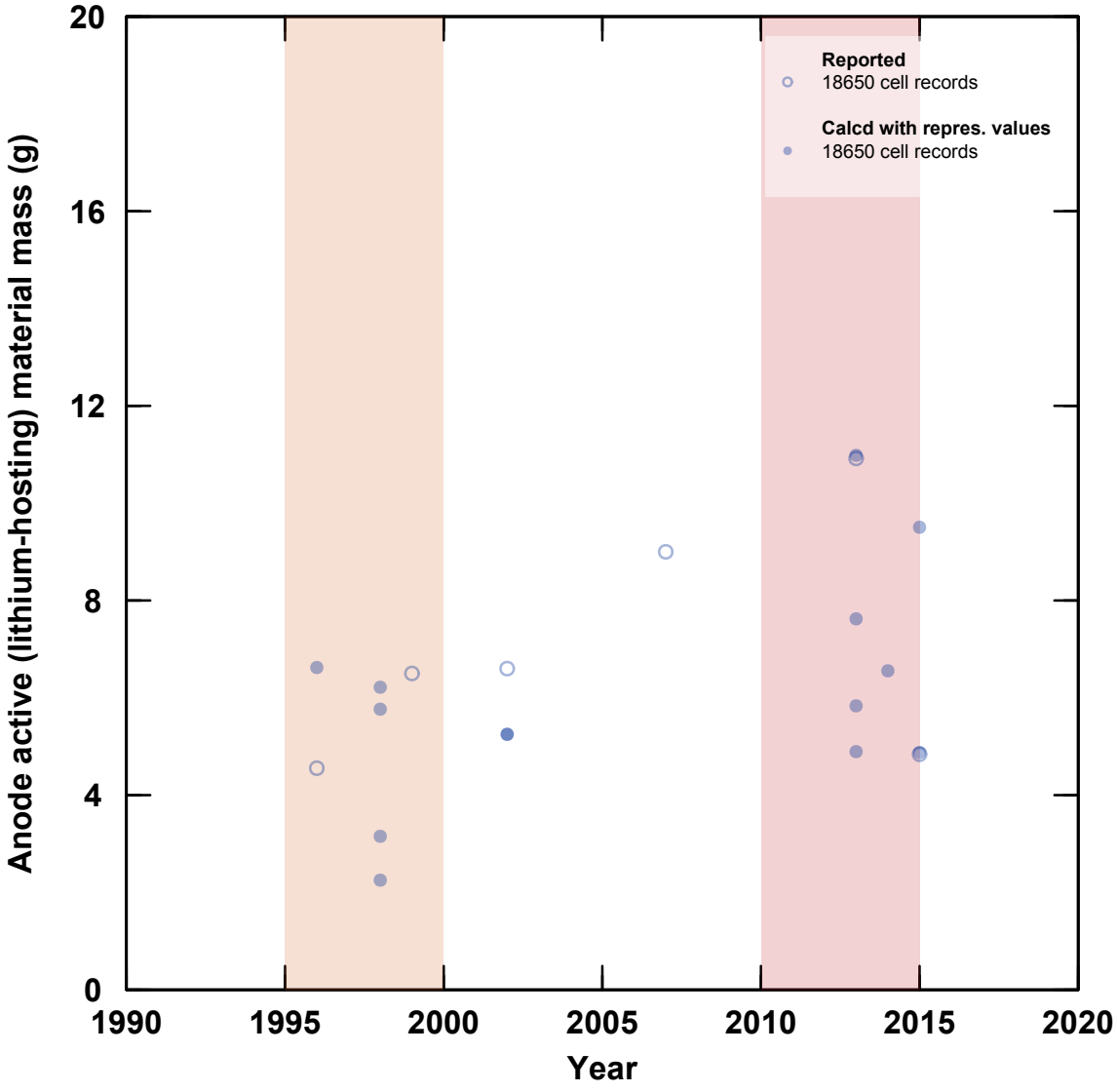

Figure S69: Reported and calculated anode active material masses in 18650-sized lithium-ion cells.

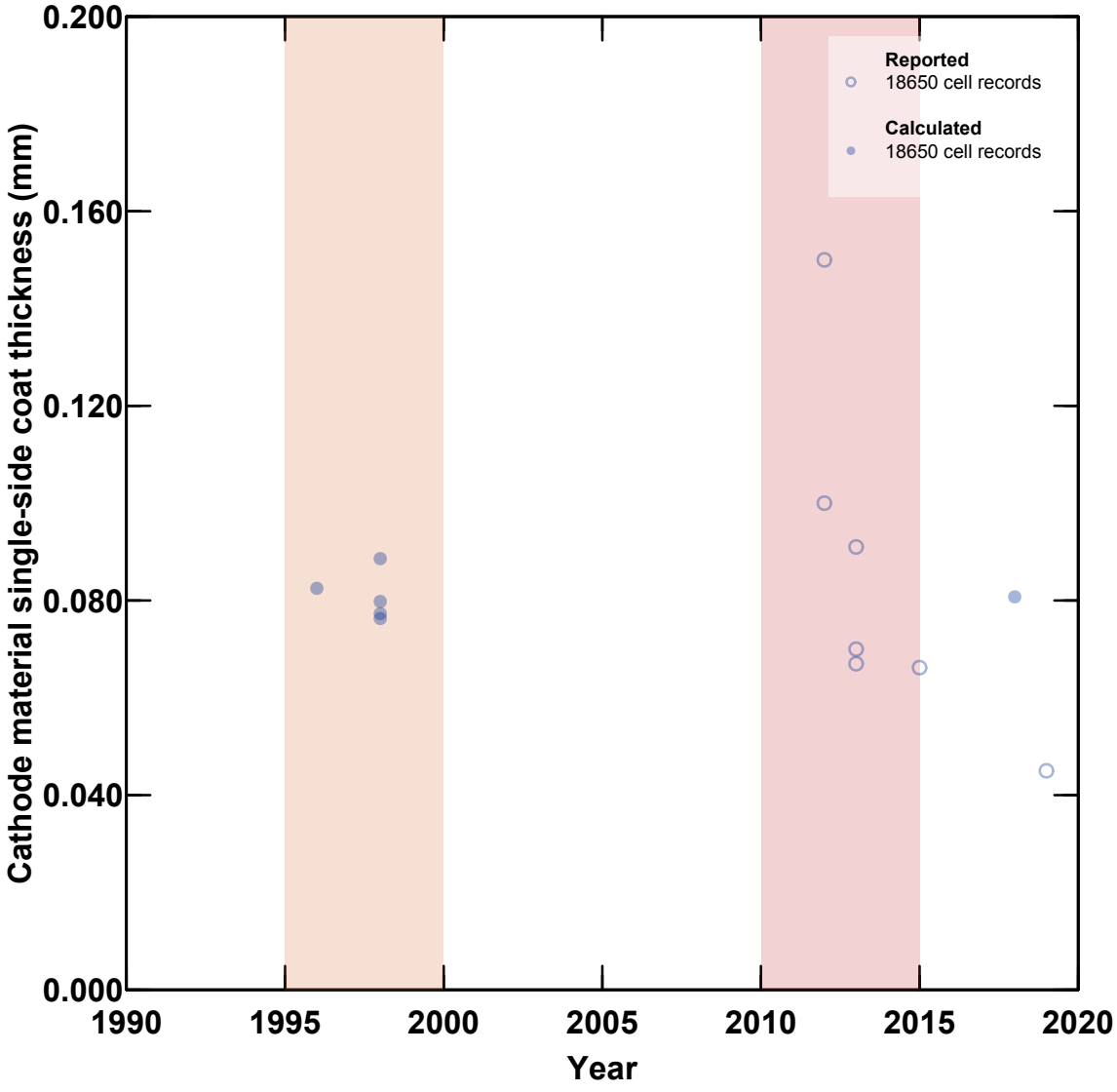

Figure S70: Reported and calculated cathode material thicknesses in 18650-sized lithium-ion cells.

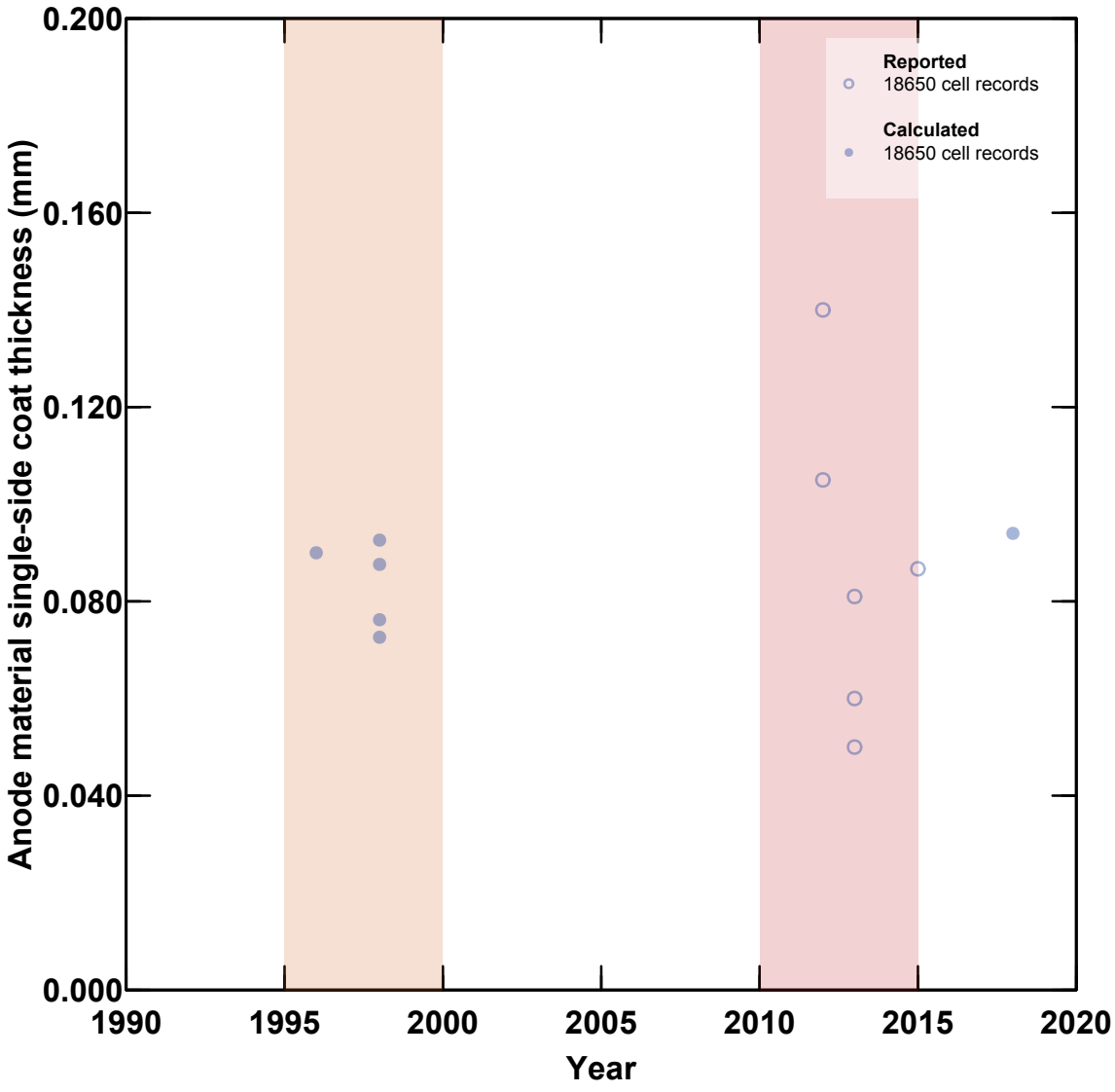

Figure S71: Reported and calculated anode material thicknesses in 18650-sized lithium-ion cells.

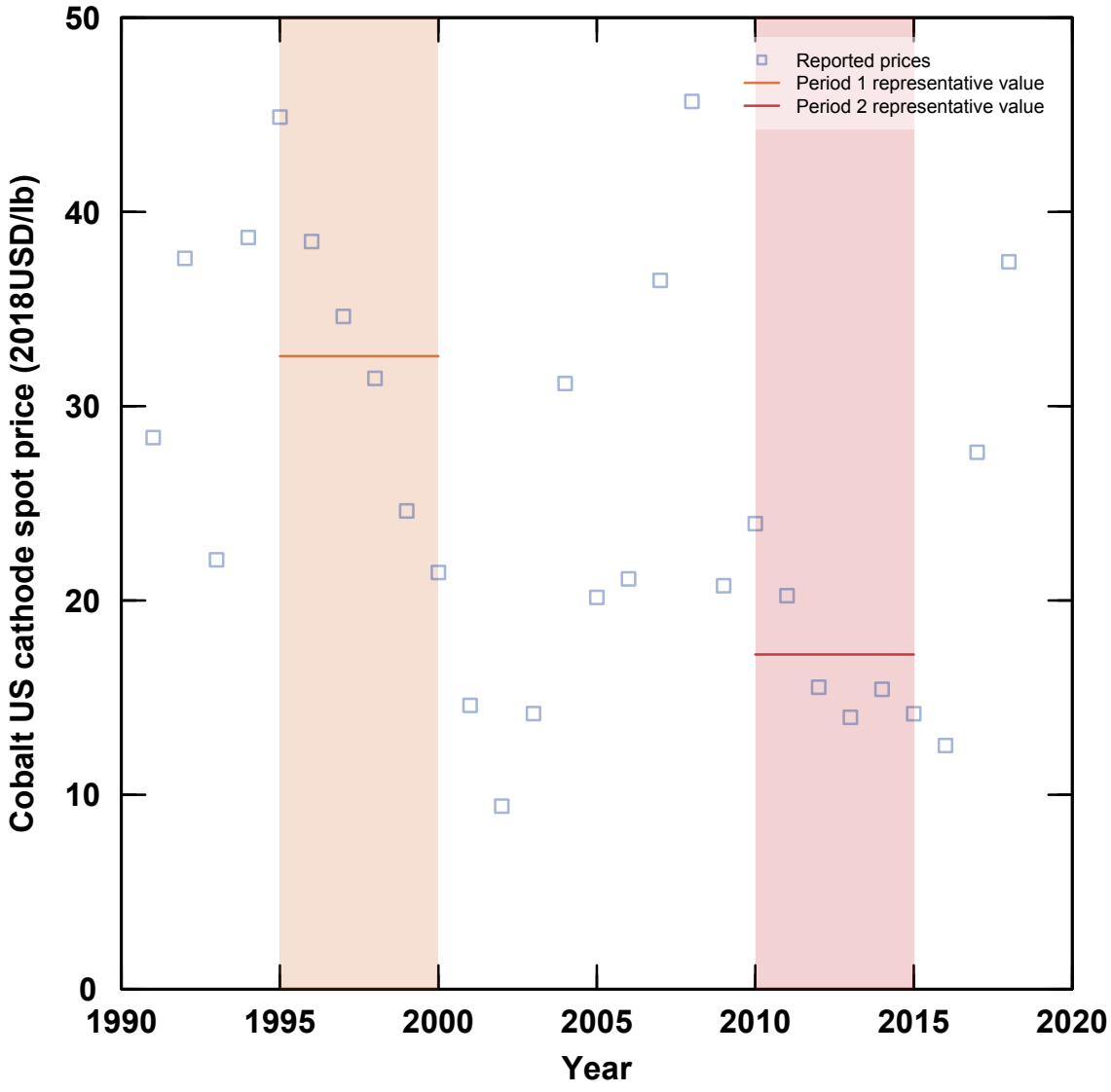

Figure S72: Reported cobalt cathode (metal) spot prices from USGS Mineral Commodity Summaries and average values for the two periods being examined.[52–76]

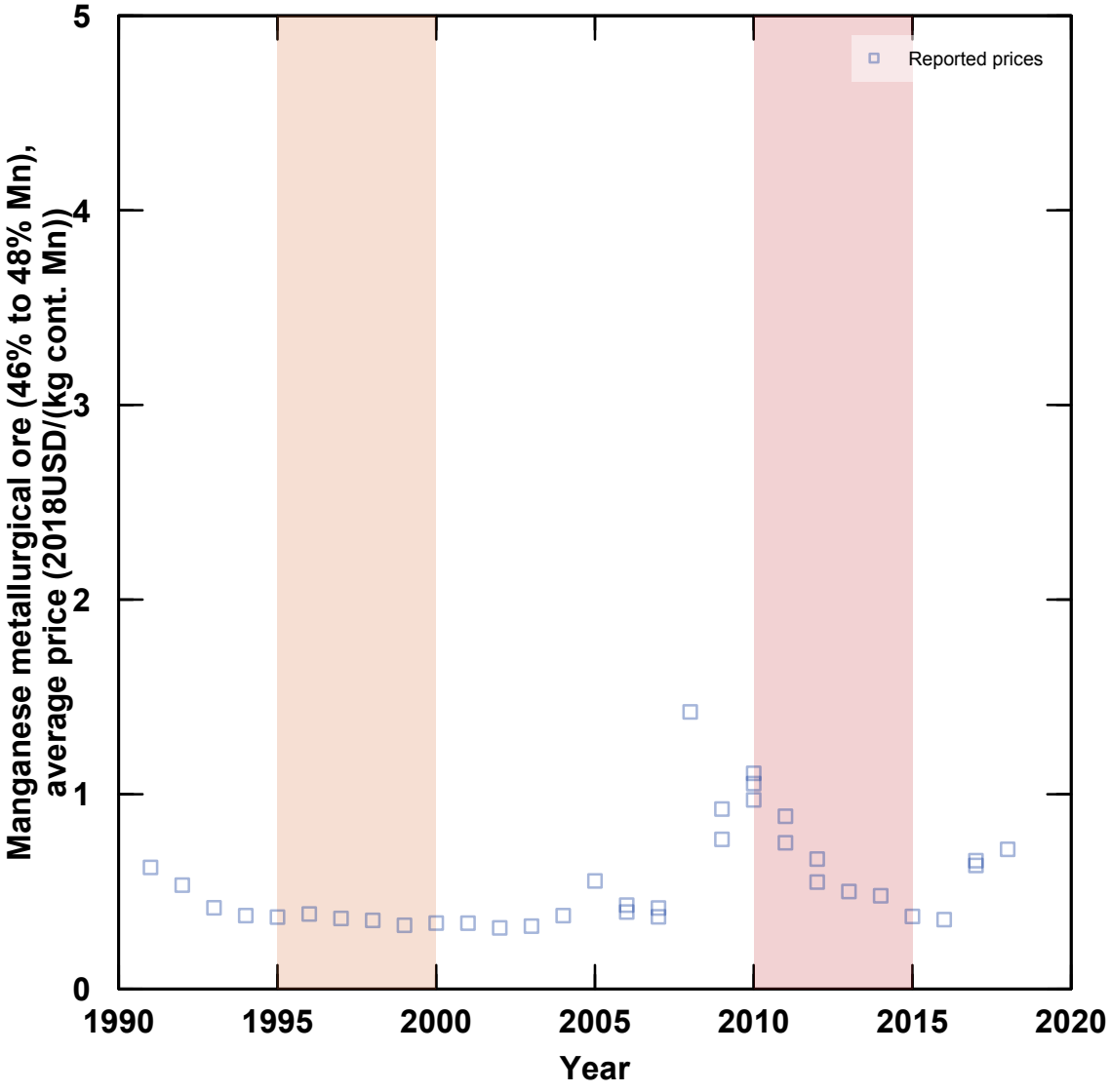

Figure S73: Reported manganese metallurgical ore price (cost, insurance, and freight, U.S. ports) from USGS Mineral Commodity Summaries.[52–76]

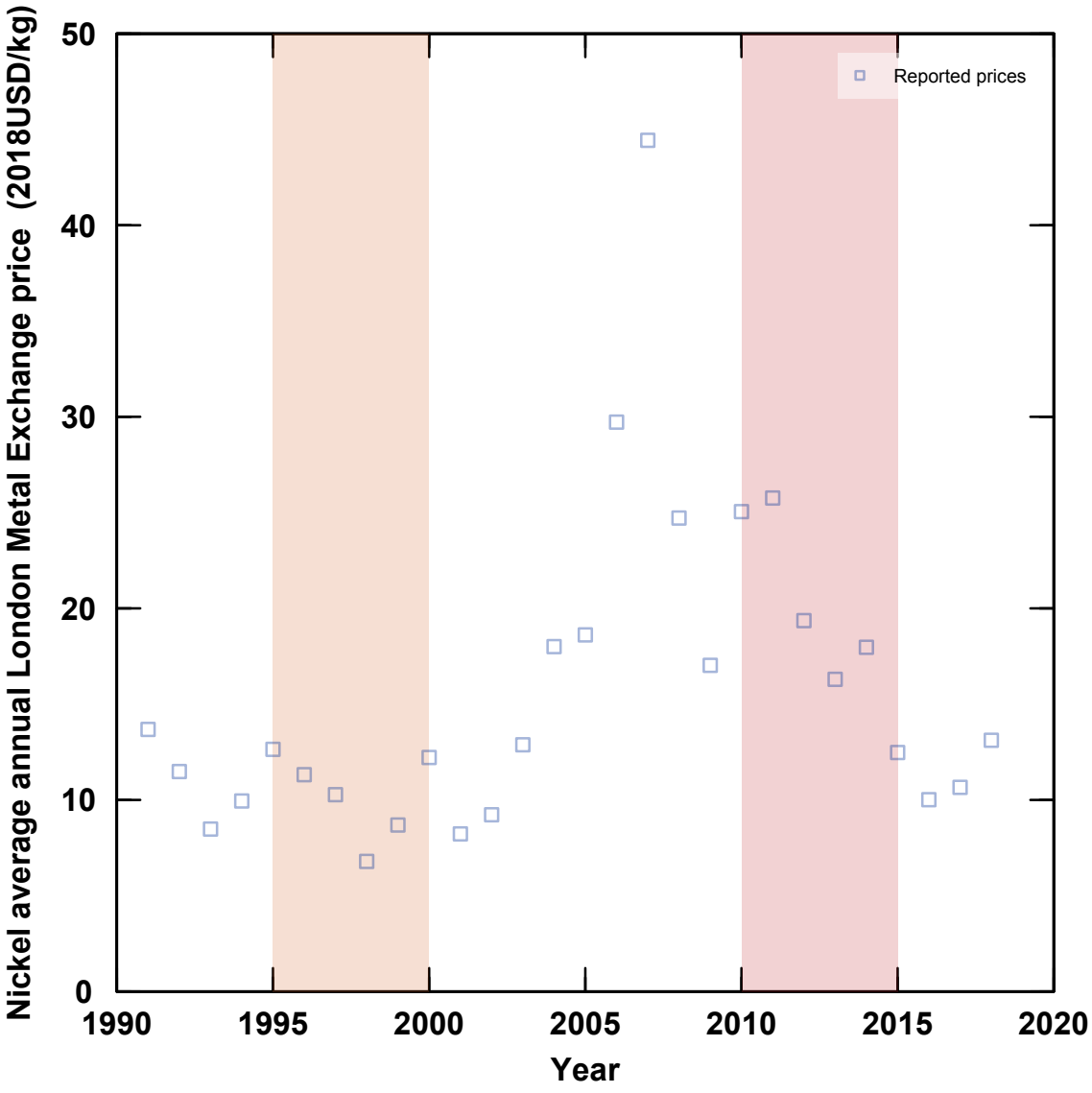

Figure S74: Reported average annual nickel metal prices on the London Metal Exchange from USGS Mineral Commodity Summaries.[52–76]

8 Aggregation and low-level to high-level mechanism assignment tables

Table S1: Assignments of mass-related cost contributors employed for aggregated low-level cost change analysis

Low-level mechanism	Variable symbol	Aggregated low-level cost change mechanisms											
		Cell charge density	**Charge capacity utilization**	**Cell voltage**	**Cathode foil area**	**Cathode materials prices**	**Anode materials prices**	**Electrolyte solution price**	**Current collectors prices**	**Separator price**	**Other hardware price**	**Materials and manufacturing yields**	**Plant size and p_0**
Cathode active material mass fraction	$w_{\mathrm{act,ca}}$	100%	0%	0%	0%	0%	0%	0%	0%	0%	0%	0%	0%
Cathode active material price	$p_{\mathrm{act,ca}}$	0%	0%	0%	0%	100%	0%	0%	0%	0%	0%	0%	0%
Cathode binder mass fraction	$w_{\mathrm{bin,ca}}$	100%	0%	0%	0%	0%	0%	0%	0%	0%	0%	0%	0%
Cathode binder price	$p_{\mathrm{bin,ca}}$	0%	0%	0%	0%	100%	0%	0%	0%	0%	0%	0%	0%
Cathode conductor mass fraction	$w_{\mathrm{con,ca}}$	100%	0%	0%	0%	0%	0%	0%	0%	0%	0%	0%	0%
Cathode conductor price	$p_{\mathrm{con,ca}}$	0%	0%	0%	0%	100%	0%	0%	0%	0%	0%	0%	0%
Cathode active material specific charge capacity	q_{ca}	100%	0%	0%	0%	0%	0%	0%	0%	0%	0%	0%	0%
Cathode material yield	y_{ca}	0%	0%	0%	0%	0%	0%	0%	0%	0%	0%	100%	0%
N/P ratio	$(\mathrm{N/P})_Q$	100%	0%	0%	0%	0%	0%	0%	0%	0%	0%	0%	0%
Anode active material mass fraction	$w_{\mathrm{act,an}}$	100%	0%	0%	0%	0%	0%	0%	0%	0%	0%	0%	0%
Anode active material price	$p_{\mathrm{act,an}}$	0%	0%	0%	0%	0%	100%	0%	0%	0%	0%	0%	0%
Anode binder mass fraction	$w_{\mathrm{bin,an}}$	100%	0%	0%	0%	0%	0%	0%	0%	0%	0%	0%	0%
Anode binder price	$p_{\mathrm{bin,an}}$	0%	0%	0%	0%	0%	100%	0%	0%	0%	0%	0%	0%
Anode conductor mass fraction	$w_{\mathrm{con,an}}$	100%	0%	0%	0%	0%	0%	0%	0%	0%	0%	0%	0%
Anode conductor price	$p_{\mathrm{con,an}}$	0%	0%	0%	0%	0%	100%	0%	0%	0%	0%	0%	0%
Anode active material specific charge capacity	q_{an}	100%	0%	0%	0%	0%	0%	0%	0%	0%	0%	0%	0%
Anode material yield	y_{an}	0%	0%	0%	0%	0%	0%	0%	0%	0%	0%	100%	0%
Electrolyte solution mass to cathode charge capacity ratio	D_{el}	100%	0%	0%	0%	0%	0%	0%	0%	0%	0%	0%	0%
Electrolyte solution price	p_{el}	0%	0%	0%	0%	0%	0%	100%	0%	0%	0%	0%	0%
Electrolyte solution yield	y_{el}	0%	0%	0%	0%	0%	0%	0%	0%	0%	0%	100%	0%

Table S2: Assignments of area-related cost contributors employed for aggregated low-level cost change analysis

Low-level mechanism	**Variable symbol**	**Aggregated low-level cost change mechanisms**										
		Cell charge density	**Charge capacity utilization**	**Cell voltage**	**Cathode foil area**	**Cathode materials prices**	**Anode materials prices**	**Electrolyte solution price**	**Current collectors prices**	**Separator price**	**Other hardware price**	**Materials and manufacturing yields**	**Plant size and p_0**
Cathode foil area	a_{Al}	0%	0%	0%	100%	0%	0%	0%	0%	0%	0%	0%	0%
Cathode foil thickness	t_{Al}	100%	0%	0%	0%	0%	0%	0%	0%	0%	0%	0%	0%
Cathode foil price	p_{Al}	0%	0%	0%	0%	0%	0%	0%	100%	0%	0%	0%	0%
Cathode foil yield	y_{Al}	0%	0%	0%	0%	0%	0%	0%	0%	0%	0%	100%	0%
Anode foil to cathode foil area ratio	$(\mathrm{an/ca})_A$	100%	0%	0%	0%	0%	0%	0%	0%	0%	0%	0%	0%
Anode foil thickness	t_{Cu}	100%	0%	0%	0%	0%	0%	0%	0%	0%	0%	0%	0%
Anode foil price	p_{Cu}	0%	0%	0%	0%	0%	0%	0%	100%	0%	0%	0%	0%
Anode foil yield	y_{Cu}	0%	0%	0%	0%	0%	0%	0%	0%	0%	0%	100%	0%
Separator to cathode foil area ratio	$(\mathrm{se/ca})_A$	100%	0%	0%	0%	0%	0%	0%	0%	0%	0%	0%	0%
Separator thickness	t_{se}	100%	0%	0%	0%	0%	0%	0%	0%	0%	0%	0%	0%
Separator price	$p_{\mathrm{V,se}}$	0%	0%	0%	0%	0%	0%	0%	0%	100%	0%	0%	0%
Separator yield	y_{se}	0%	0%	0%	0%	0%	0%	0%	0%	0%	0%	100%	0%

Table S3: Assignments of other cell cost contributors and cell-level characteristics employed for aggregated low-level cost change analysis

Low-level mechanism	**Variable symbol**	**Aggregated low-level cost change mechanisms**											
		Cell charge density	**Charge capacity utilization**	**Cell voltage**	**Cathode foil area**	**Cathode materials prices**	**Anode materials prices**	**Electrolyte solution price**	**Current collectors prices**	**Separator price**	**Other hardware price**	**Materials and manufacturing yields**	**Plant size and p_0**
Cell-level characteristics													
Charge capacity utilization	η_{util}	0%	100%	0%	0%	0%	0%	0%	0%	0%	0%	0%	0%
Cathode charge capacity for a fixed volume	Q_{ca}	100%	0%	0%	0%	0%	0%	0%	0%	0%	0%	0%	0%
Cell voltage	V	0%	0%	100%	0%	0%	0%	0%	0%	0%	0%	0%	0%
Cell-level yield	y_{cell}	0%	0%	0%	0%	0%	0%	0%	0%	0%	0%	100%	0%
Hardware cost component													
Other hardware price	p_{can}	0%	0%	0%	0%	0%	0%	0%	0%	0%	100%	0%	0%
Other hardware yield	y_{can}	0%	0%	0%	0%	0%	0%	0%	0%	0%	0%	100%	0%
Plant size–dependent characteristics													
p_0	p_0	0%	0%	0%	0%	0%	0%	0%	0%	0%	0%	0%	100%
Plant size	K	0%	0%	0%	0%	0%	0%	0%	0%	0%	0%	0%	100%

Table S4: Assignments of mass-related cost contributors employed for estimating high-level mechanisms of cost change

Low-level mechanism	**Variable symbol**	**High-level cost change mechanisms**			
		Public and private research and development	**Learning-by-doing**	**Economies of scale**	**Other**
Cathode active material mass fraction	$w_{\mathrm{act,ca}}$	100%	0%	0%	0%
Cathode active material price	$p_{\mathrm{act,ca}}$	33.33%	0.00%	33.33%	33.33%
Cathode binder mass fraction	$w_{\mathrm{bin,ca}}$	100%	0%	0%	0%
Cathode binder price	$p_{\mathrm{bin,ca}}$	0%	0%	100%	0%
Cathode conductor mass fraction	$w_{\mathrm{con,ca}}$	100%	0%	0%	0%
Cathode conductor price	$p_{\mathrm{con,ca}}$	0%	0%	100%	0%
Cathode active material specific charge capacity	q_{ca}	100%	0%	0%	0%
Cathode material yield	y_{ca}	0%	100%	0%	0%
N/P ratio	$(\mathrm{N/P})_Q$	100%	0%	0%	0%
Anode active material mass fraction	$w_{\mathrm{act,an}}$	100%	0%	0%	0%
Anode active material price	$p_{\mathrm{act,an}}$	33.33%	0.00%	33.33%	33.33%
Anode binder mass fraction	$w_{\mathrm{bin,an}}$	100%	0%	0%	0%
Anode binder price	$p_{\mathrm{bin,an}}$	50%	0%	50%	0%
Anode conductor mass fraction	$w_{\mathrm{con,an}}$	100%	0%	0%	0%
Anode conductor price	$p_{\mathrm{con,an}}$	0%	0%	100%	0%
Anode active material specific charge capacity	q_{an}	100%	0%	0%	0%
Anode material yield	y_{an}	0%	100%	0%	0%
Electrolyte solution mass to cathode charge capacity ratio	D_{el}	100%	0%	0%	0%
Electrolyte solution price	p_{el}	0%	0%	100%	0%
Electrolyte solution yield	y_{el}	0%	100%	0%	0%

Table S5: Assignments of area-related cost contributors employed for estimating high-level mechanisms of cost change

Low-level mechanism	**Variable symbol**	**High-level cost change mechanisms**			
		Public and private research and development	**Learning-by-doing**	**Economies of scale**	**Other**
Cathode foil area	a_{Al}	100%	0%	0%	0%
Cathode foil thickness	t_{Al}	100%	0%	0%	0%
Cathode foil price	p_{Al}	0%	0%	50%	50%
Cathode foil yield	y_{Al}	0%	100%	0%	0%
Anode foil to cathode foil area ratio	$(\mathrm{an/ca})_A$	100%	0%	0%	0%
Anode foil thickness	t_{Cu}	100%	0%	0%	0%
Anode foil price	p_{Cu}	0%	0%	50%	50%
Anode foil yield	y_{Cu}	0%	100%	0%	0%
Separator to cathode foil area ratio	$(\mathrm{se/ca})_A$	100%	0%	0%	0%
Separator thickness	t_{se}	100%	0%	0%	0%
Separator price	$p_{\mathrm{V,se}}$	0%	0%	100%	0%
Separator yield	y_{se}	0%	100%	0%	0%

Table S6: Assignments of other cell cost contributors and cell-level characteristics employed for estimating high-level mechanisms of cost change

Low-level mechanism	Variable symbol	High-level cost change mechanisms			
		Public and private research and development	Learning-by-doing	Economies of scale	Other
Cell-level characteristics					
Charge capacity utilization	η_{util}	100%	0%	0%	0%
Cathode charge capacity for a fixed volume	Q_{ca}	100%	0%	0%	0%
Cell voltage	V	100%	0%	0%	0%
Cell-level yield	y_{cell}	0%	100%	0%	0%
Hardware cost component					
Other hardware price	p_{can}	25%	0%	75%	0%
Other hardware yield	y_{can}	0%	100%	0%	0%
Plant size–dependent characteristics					
p_0	p_0	0%	0%	0%	100%
Plant size	K	0%	0%	100%	0%

9 Sensitivity analysis for low-level mechanisms

9.1 Model sensitivity analysis

To explore the sensitivity of the model to the variables presented in Tables 1–3, we vary each by ±15%. As this variation can result in unrealistic scenarios, we bound some of the values. Notably, we restrict the charge capacity utilization fraction, yields, mass fractions, and the material cost fraction to less than or equal to 1.0. Similarly, as this study focuses on cathode-limited cells, the N/P ratio and anode foil to cathode foil area ratio are required to be greater than or equal to 1.0 while the separator to cathode foil area ratio is required to be greater than or equal to 2. When varying the mass fractions of the cathode and anode component materials, some unrealistic sums are encountered as the sensitivity analysis treats these values independently. However, these variables were found to have very small impacts overall, mitigating the impact these unrealistic sums have on our sensitivity analysis results.

The model sensitivity analysis results are presented in Figures S75–S116.

9.1.1 Model sensitivity analysis figures for mass-related variables

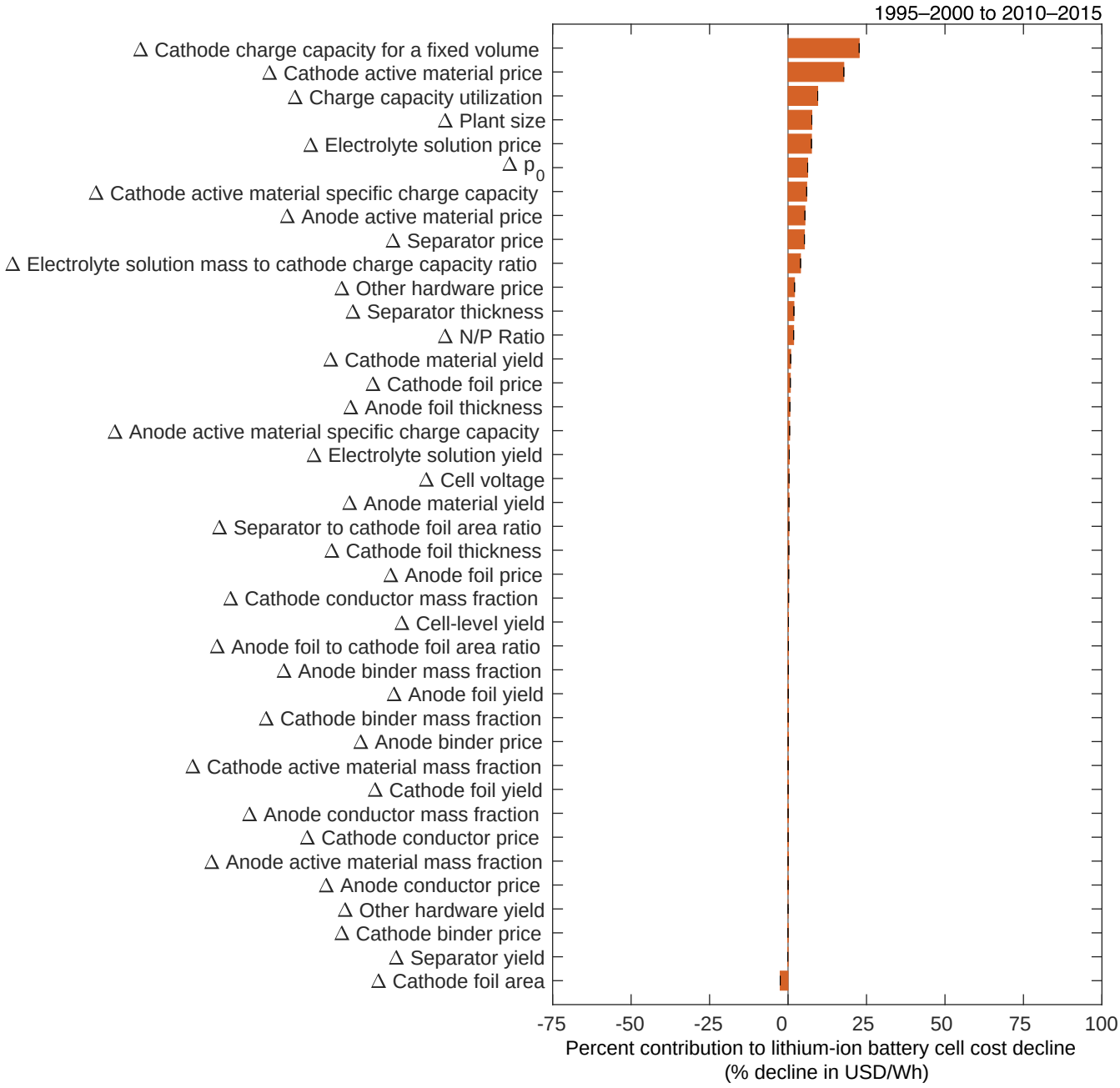

Figure S75: Sensitivity analysis for cathode active material mass fraction ($w_{\text{act,ca}}$). The value is varied in both periods, and for each combination, we recompute the low-level mechanisms' contributions to cost change. The error bars show the minimum and maximum values of the low-level mechanisms' contributions to cost reduction.

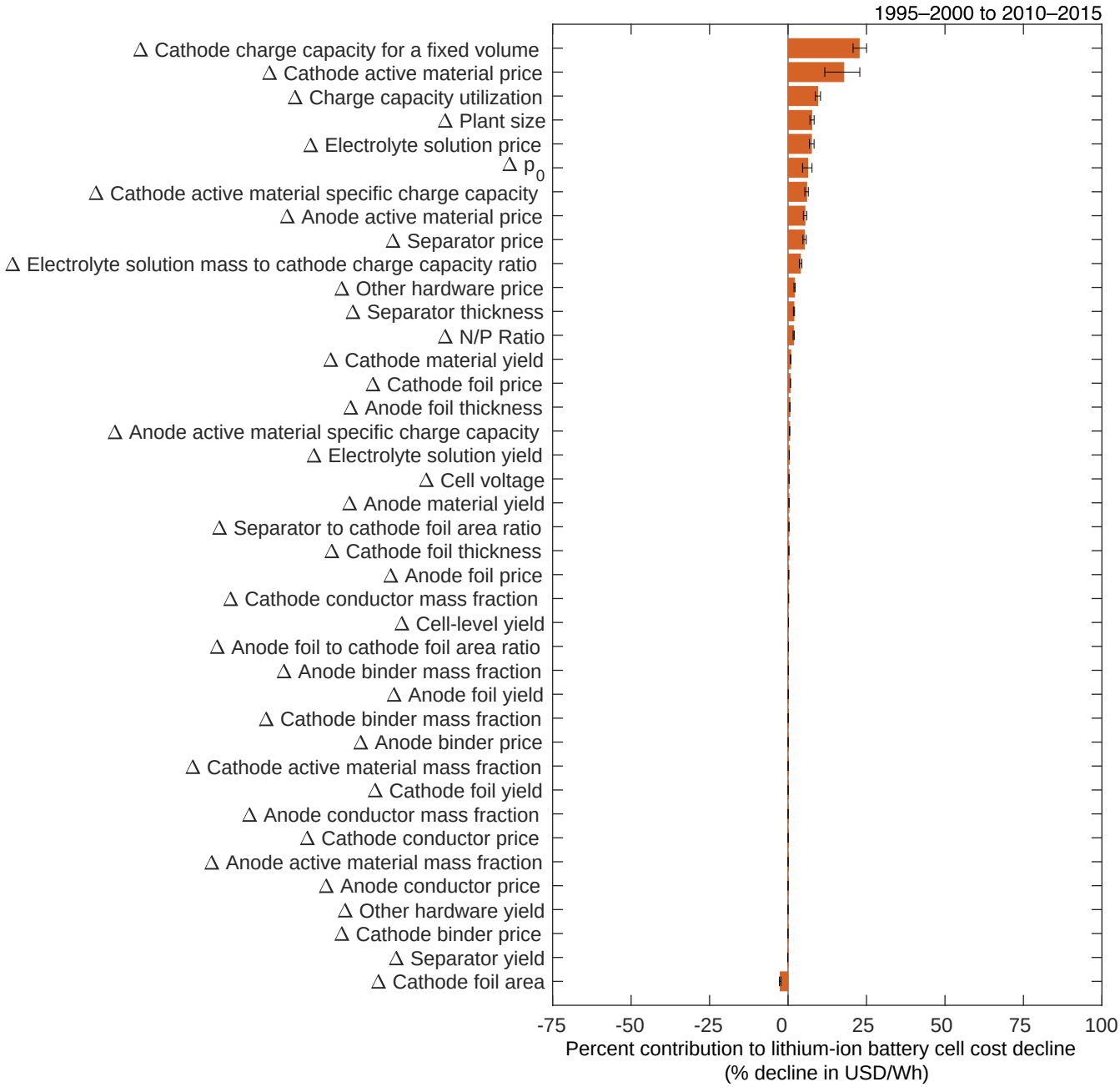

Figure S76: Sensitivity analysis for cathode active material price ($p_{\mathrm{act,ca}}$). The value is varied in both periods, and for each combination, we recompute the low-level mechanisms' contributions to cost change. The error bars show the minimum and maximum values of the low-level mechanisms' contributions to cost reduction.

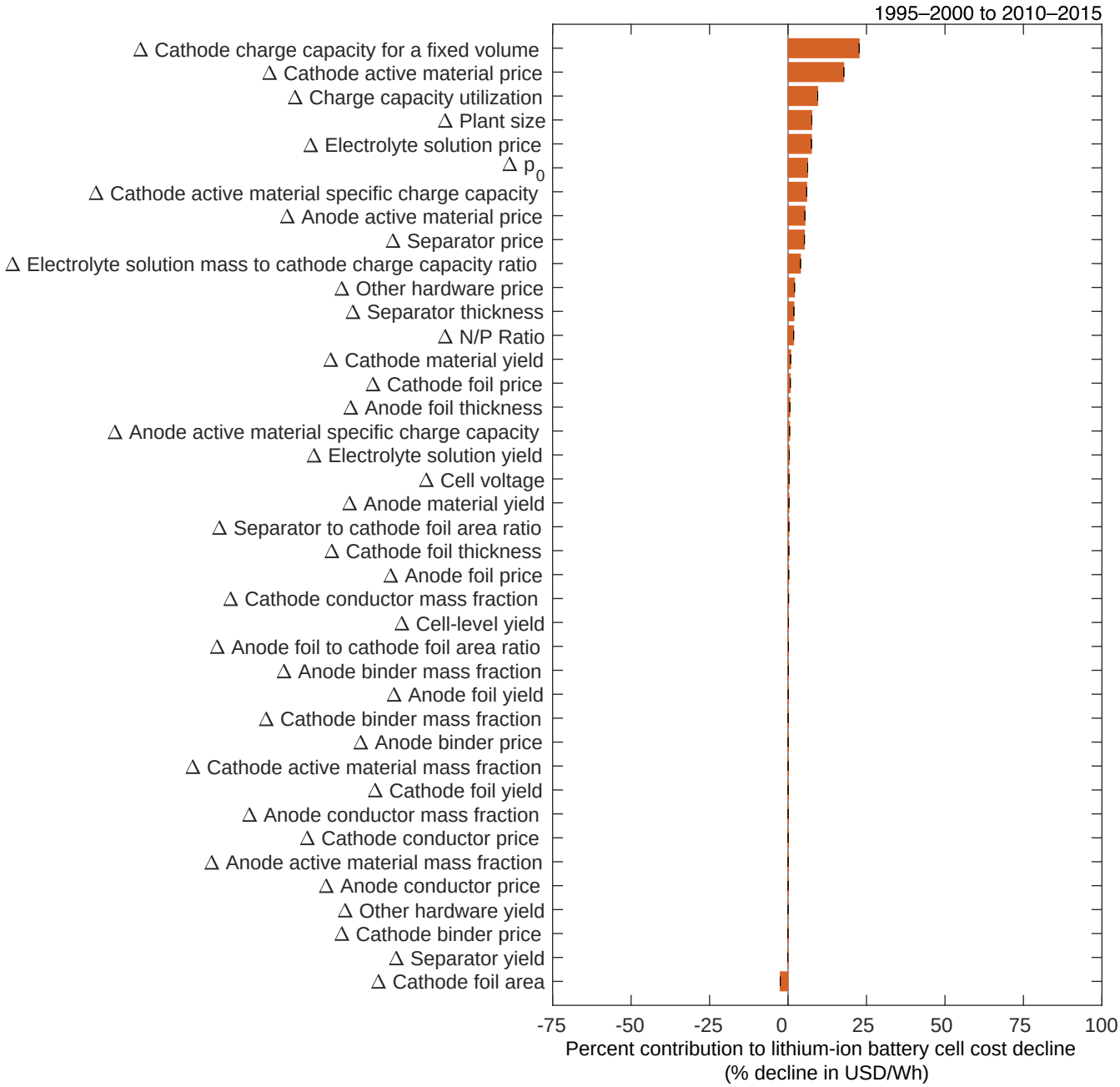

Figure S77: Sensitivity analysis for cathode binder mass fraction ($w_{\text{bin,ca}}$). The value is varied in both periods, and for each combination, we recompute the low-level mechanisms' contributions to cost change. The error bars show the minimum and maximum values of the low-level mechanisms' contributions to cost reduction.

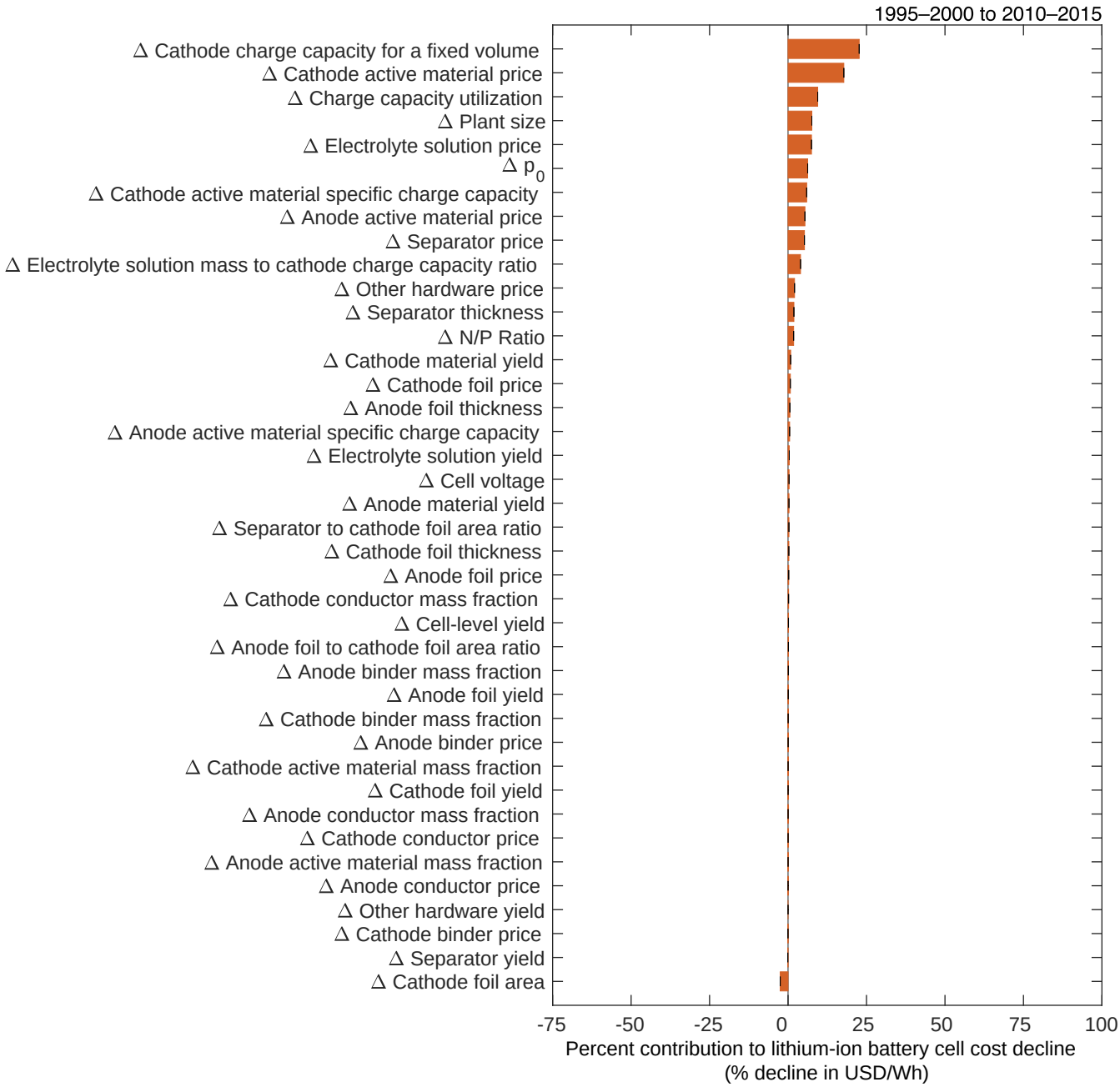

Figure S78: Sensitivity analysis for cathode binder price ($p_{\text{bin,ca}}$). The value is varied in both periods, and for each combination, we recompute the low-level mechanisms' contributions to cost change. The error bars show the minimum and maximum values of the low-level mechanisms' contributions to cost reduction.

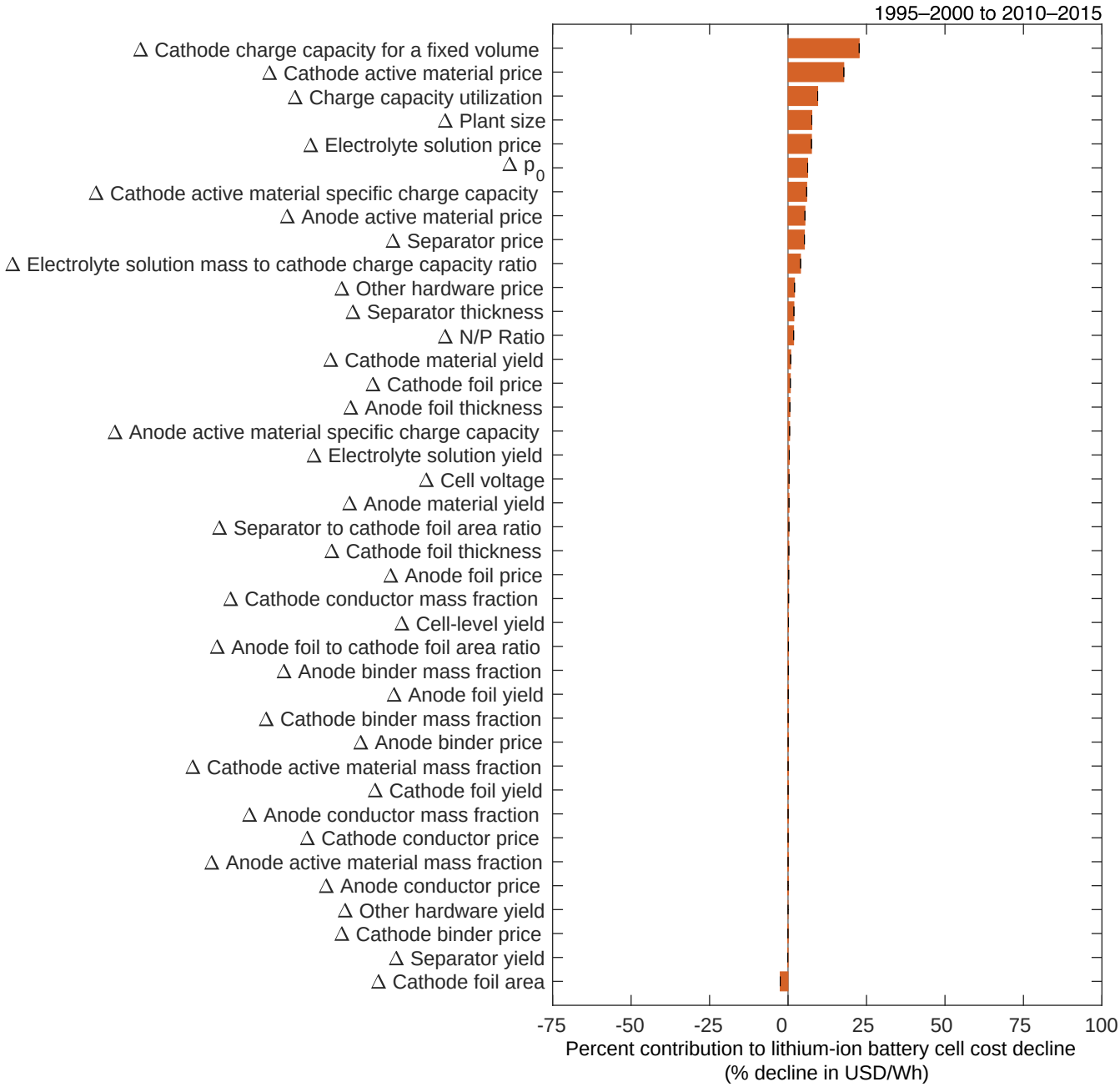

Figure S79: Sensitivity analysis for cathode conductor mass fraction ($w_{\text{con,ca}}$). The value is varied in both periods, and for each combination, we recompute the low-level mechanisms' contributions to cost change. The error bars show the minimum and maximum values of the low-level mechanisms' contributions to cost reduction.

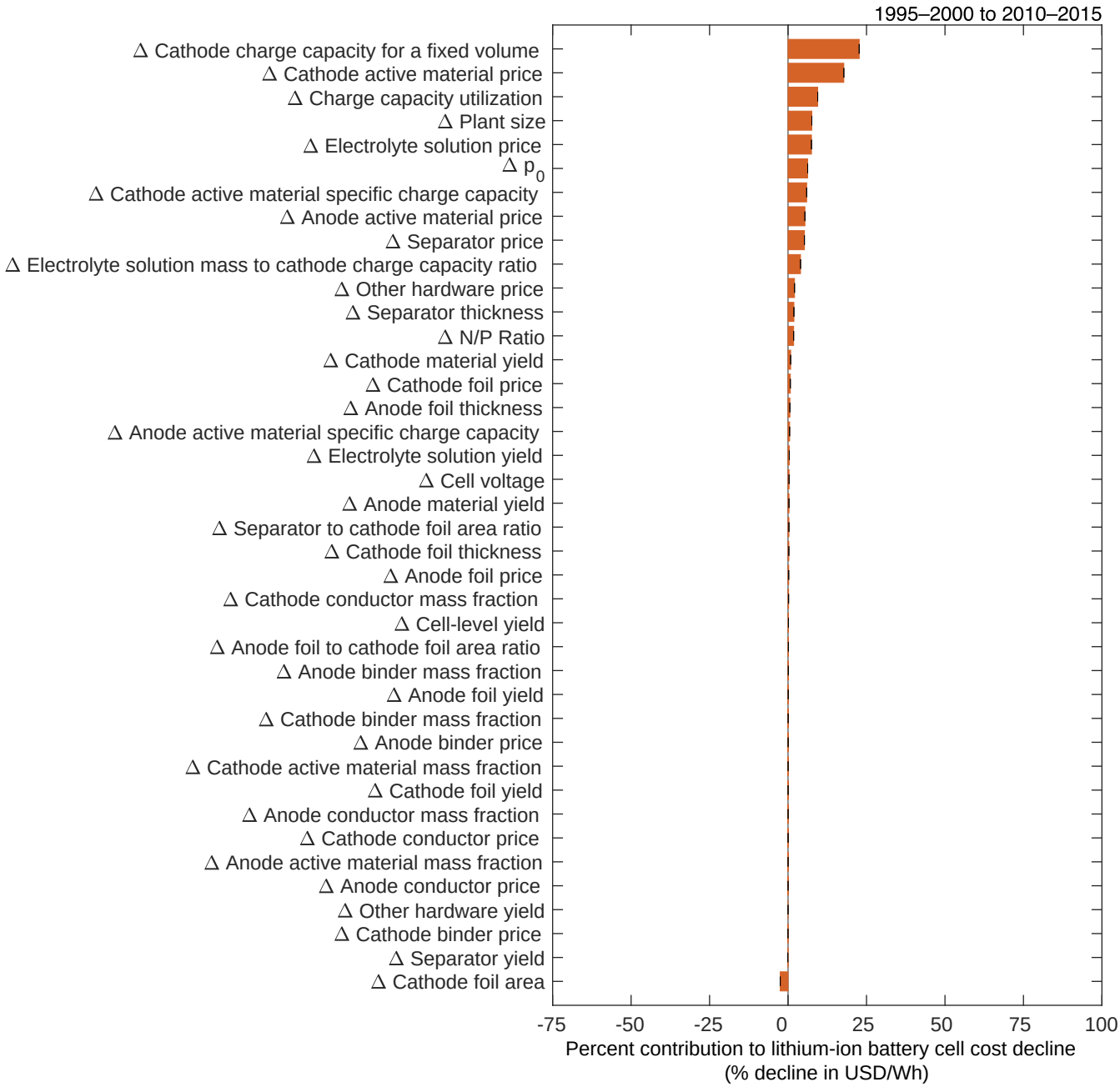

Figure S80: Sensitivity analysis for cathode conductor price ($p_{\text{con,ca}}$). The value is varied in both periods, and for each combination, we recompute the low-level mechanisms' contributions to cost change. The error bars show the minimum and maximum values of the low-level mechanisms' contributions to cost reduction.

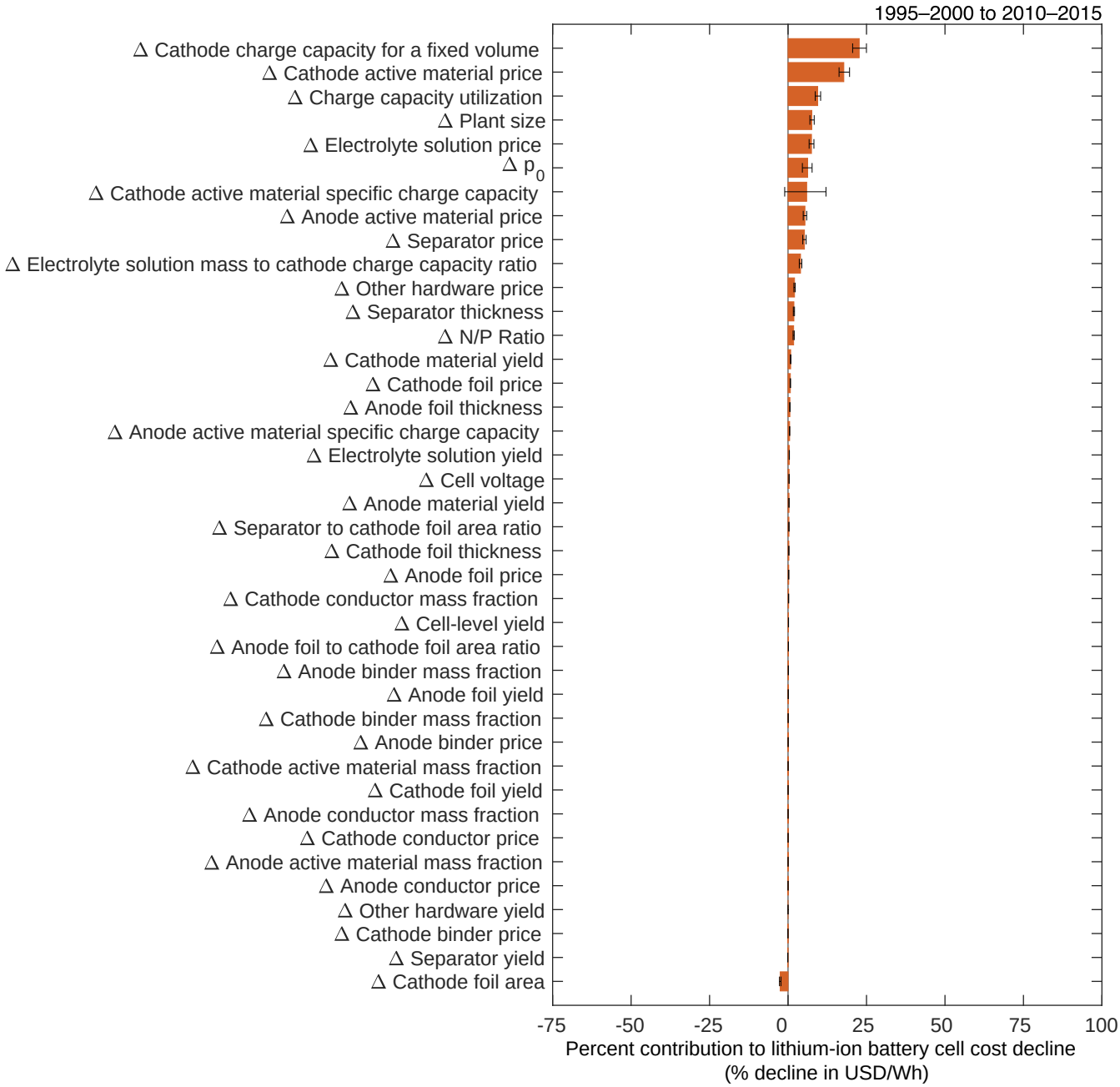

Figure S81: Sensitivity analysis for cathode active material specific charge capacity (q_{ca}). The value is varied in both periods, and for each combination, we recompute the low-level mechanisms' contributions to cost change. The error bars show the minimum and maximum values of the low-level mechanisms' contributions to cost reduction.

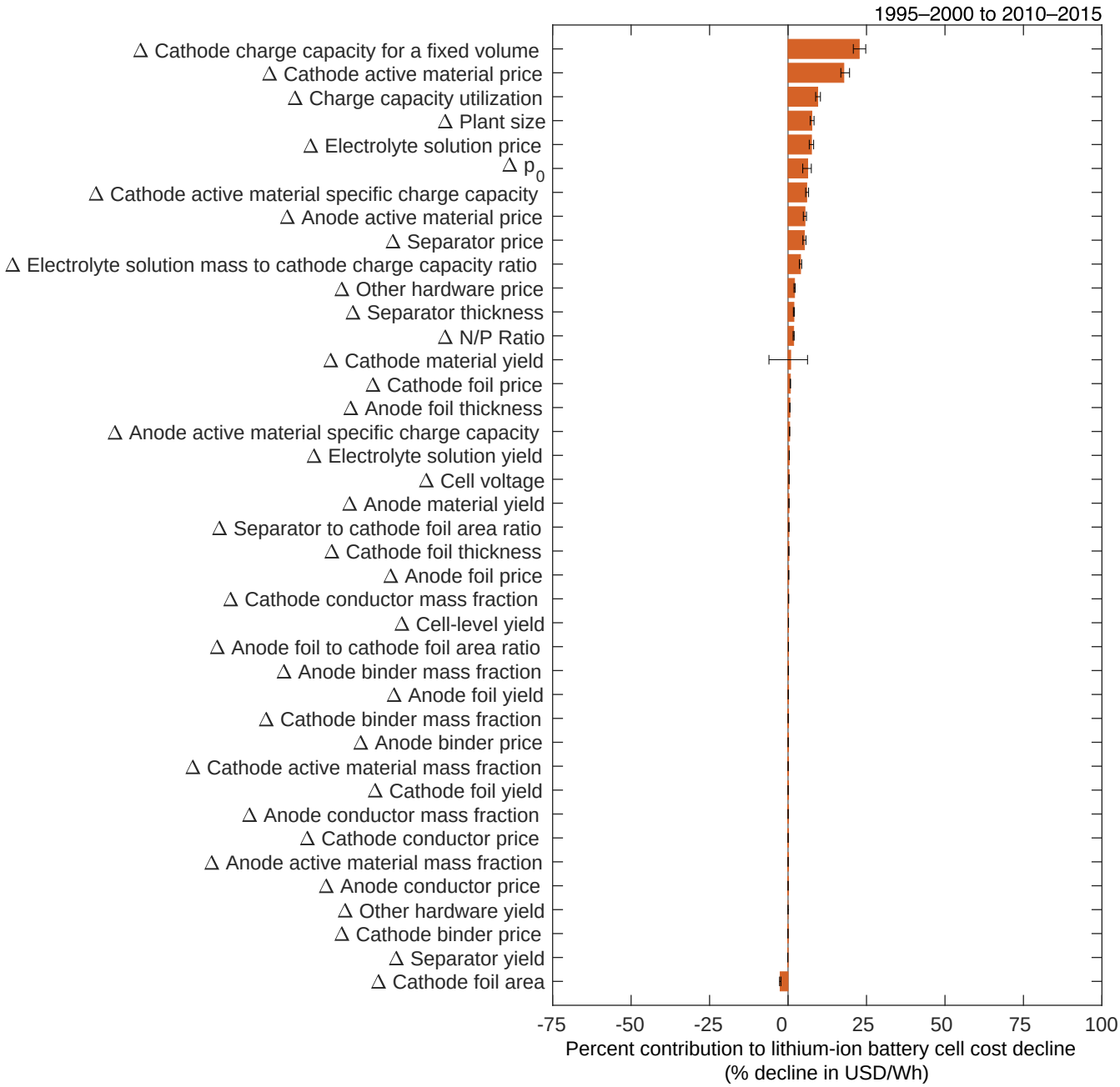

Figure S82: Sensitivity analysis for cathode material yield (y_{ca}). The value is varied in both periods, and for each combination, we recompute the low-level mechanisms' contributions to cost change. The error bars show the minimum and maximum values of the low-level mechanisms' contributions to cost reduction.

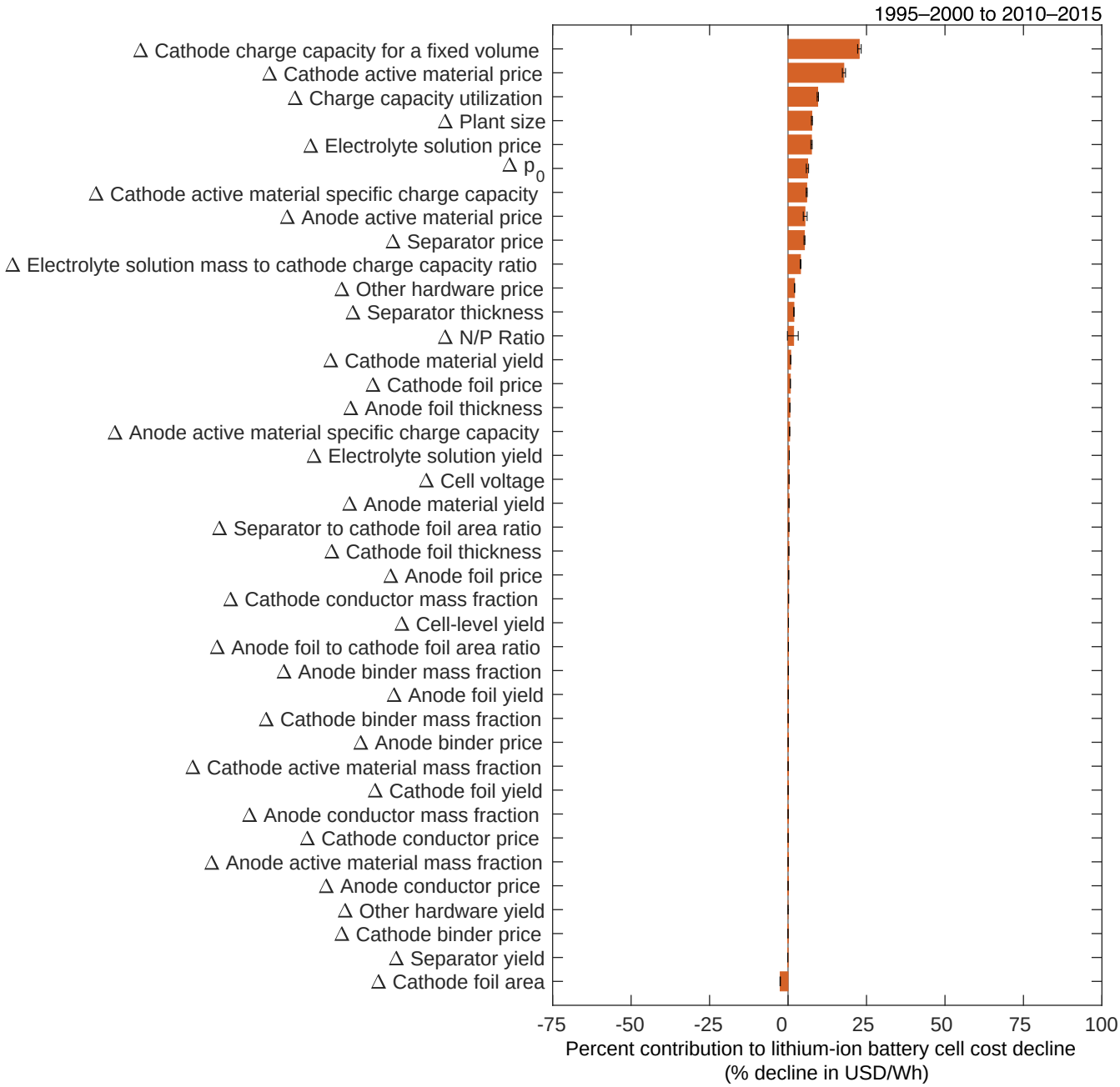

Figure S83: Sensitivity analysis for the N/P ratio ($(\mathrm{N/P})_Q$). The value is varied in both periods, and for each combination, we recompute the low-level mechanisms' contributions to cost change. The error bars show the minimum and maximum values of the low-level mechanisms' contributions to cost reduction.

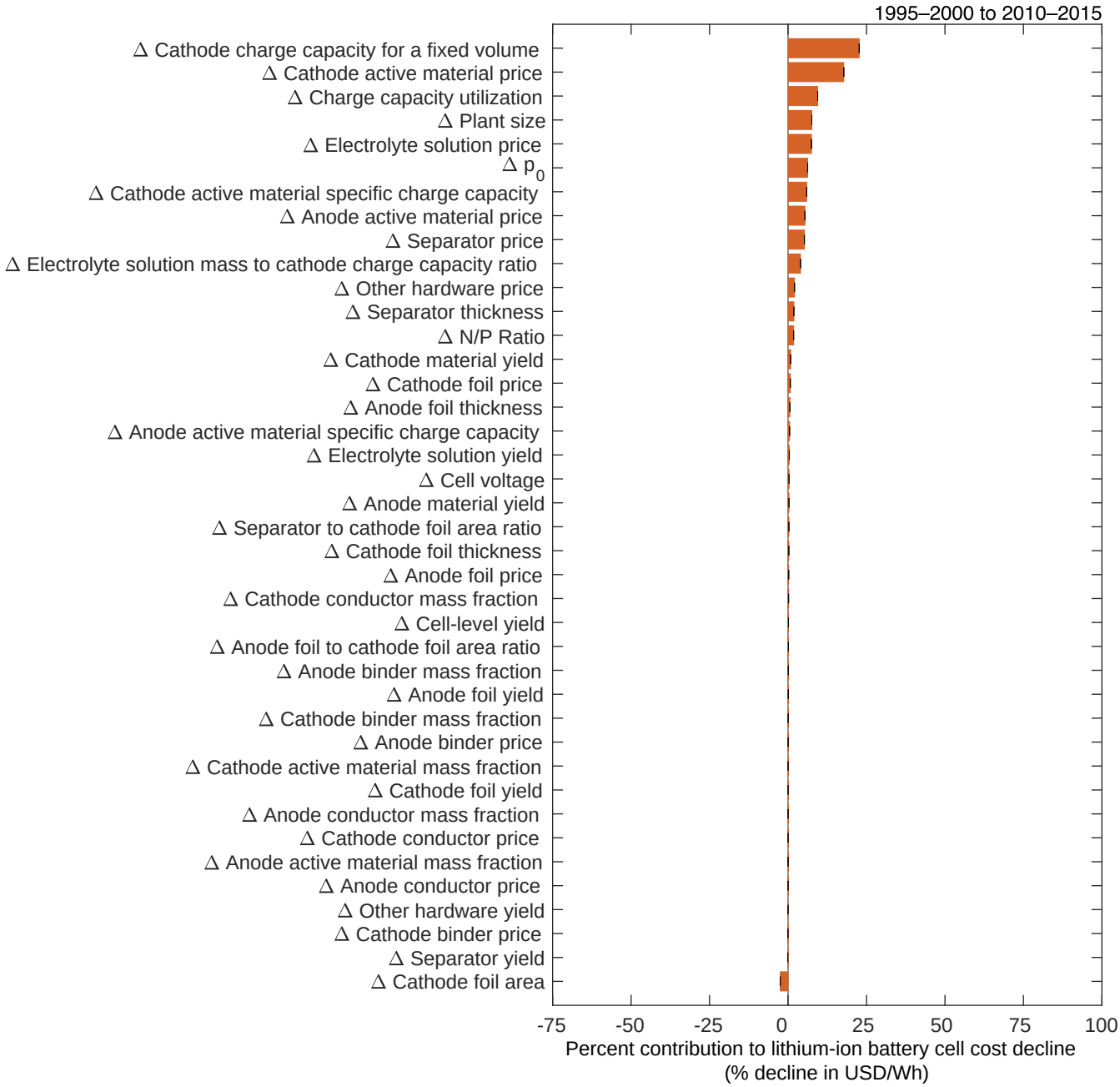

Figure S84: Sensitivity analysis for anode active material mass fraction ($w_{\text{act,an}}$). The value is varied in both periods, and for each combination, we recompute the low-level mechanisms' contributions to cost change. The error bars show the minimum and maximum values of the low-level mechanisms' contributions to cost reduction.

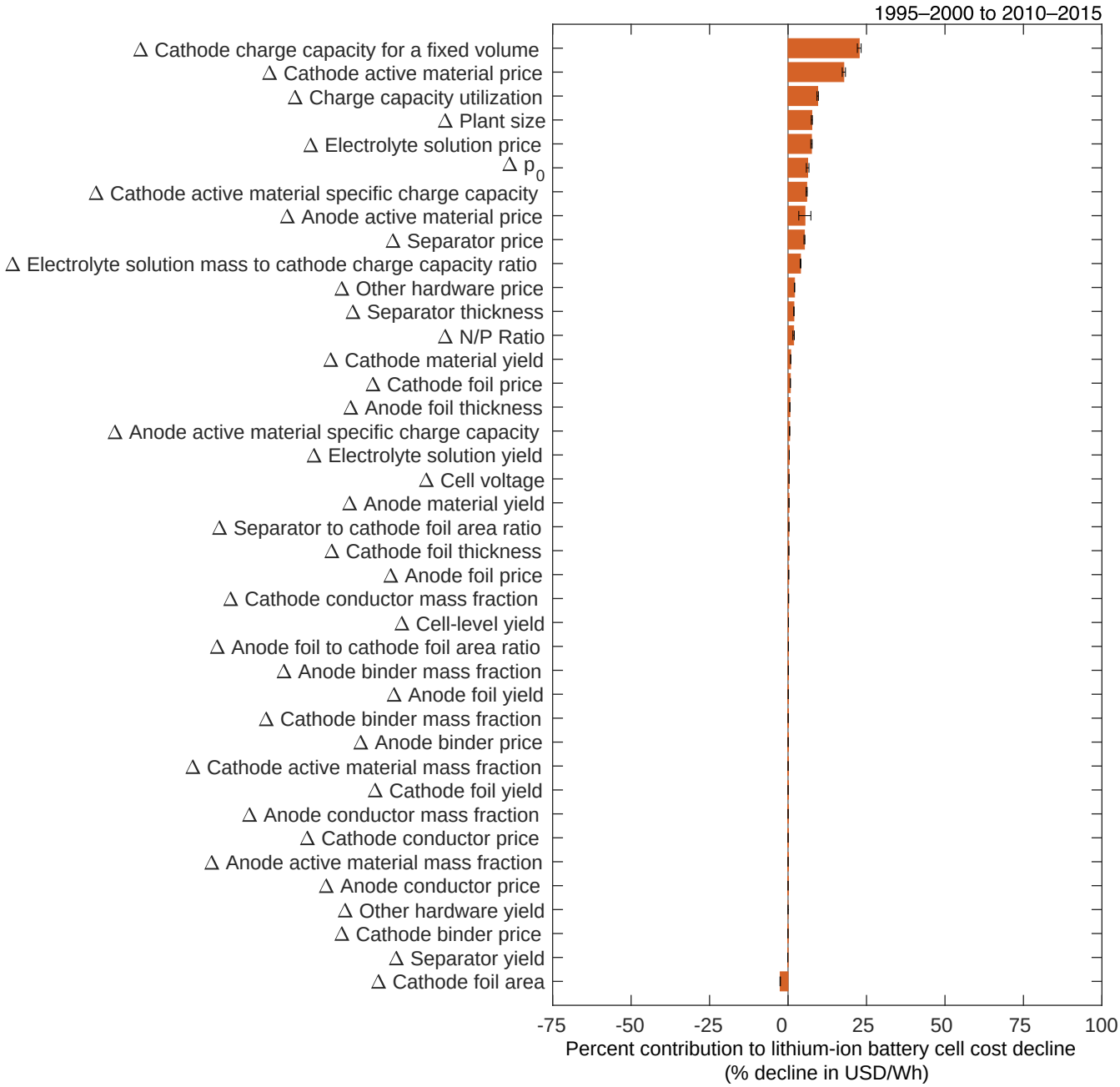

Figure S85: Sensitivity analysis for anode active material price ($p_{\text{act,an}}$). The value is varied in both periods, and for each combination, we recompute the low-level mechanisms' contributions to cost change. The error bars show the minimum and maximum values of the low-level mechanisms' contributions to cost reduction.

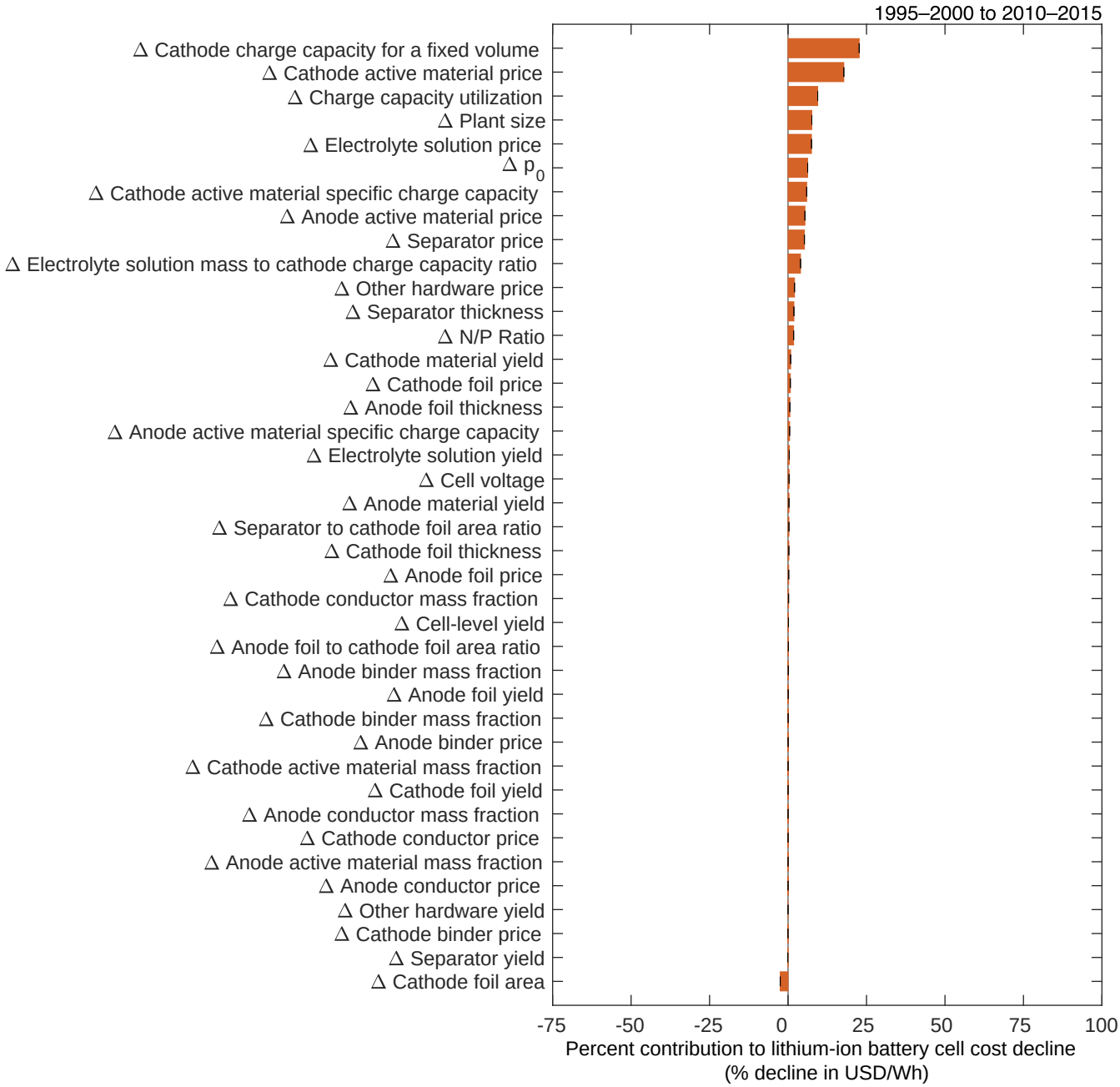

Figure S86: Sensitivity analysis for anode binder mass fraction ($w_{\text{bin,an}}$). The value is varied in both periods, and for each combination, we recompute the low-level mechanisms' contributions to cost change. The error bars show the minimum and maximum values of the low-level mechanisms' contributions to cost reduction.

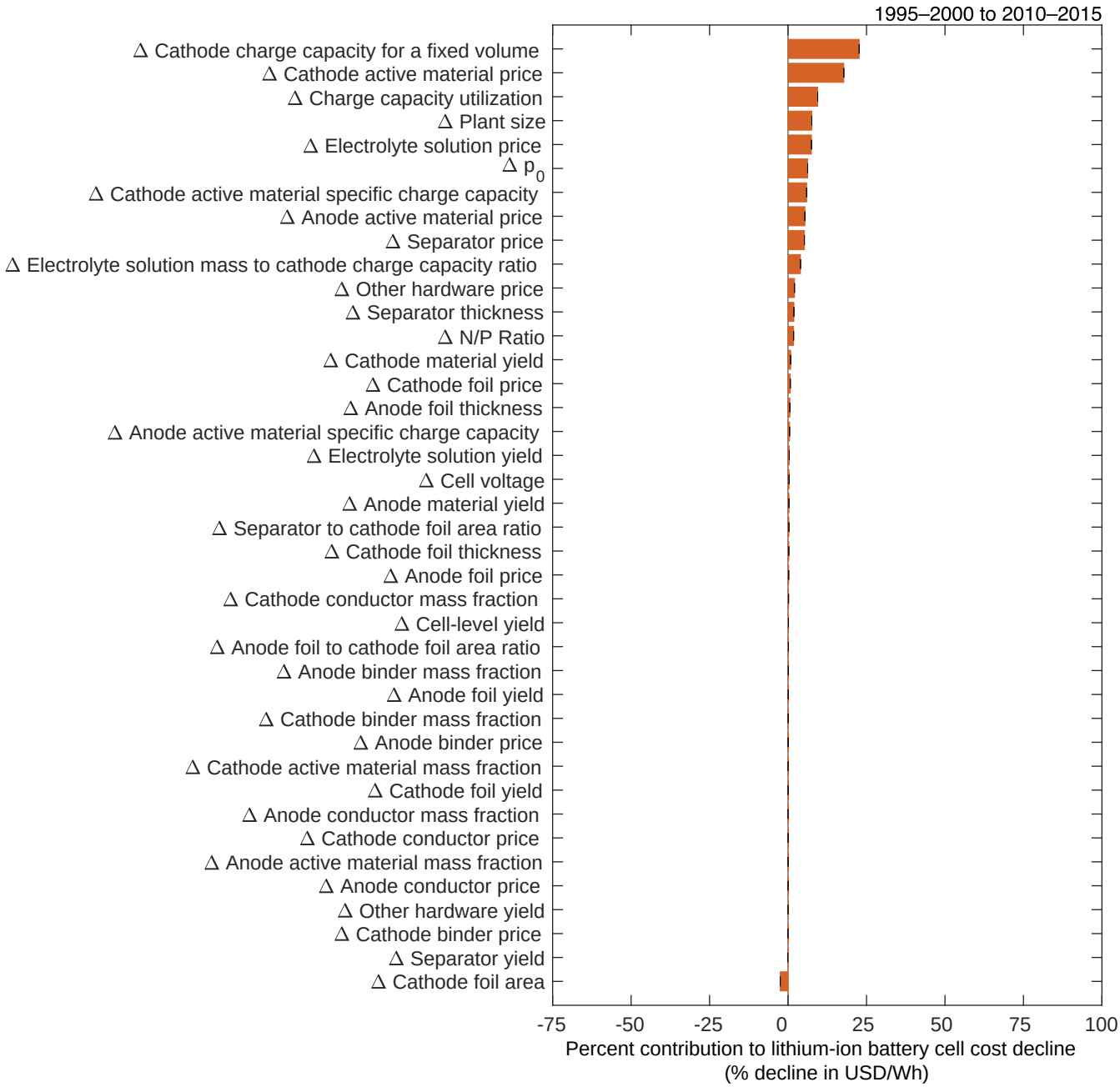

Figure S87: Sensitivity analysis for anode binder price ($p_{\text{bin,an}}$). The value is varied in both periods, and for each combination, we recompute the low-level mechanisms' contributions to cost change. The error bars show the minimum and maximum values of the low-level mechanisms' contributions to cost reduction.

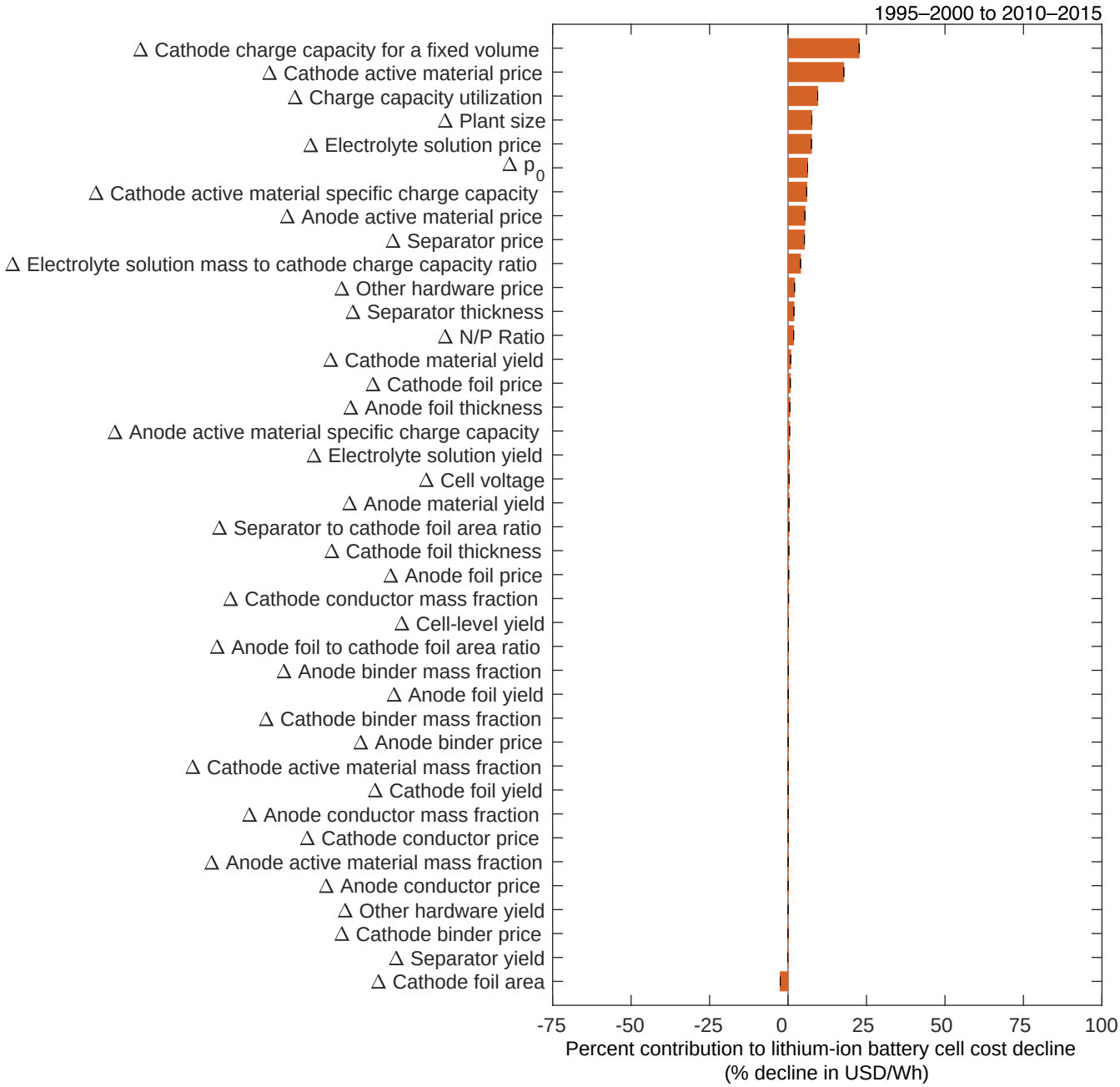

Figure S88: Sensitivity analysis for anode conductor mass fraction ($w_{\text{con,an}}$). The value is varied in both periods, and for each combination, we recompute the low-level mechanisms' contributions to cost change. The error bars show the minimum and maximum values of the low-level mechanisms' contributions to cost reduction.

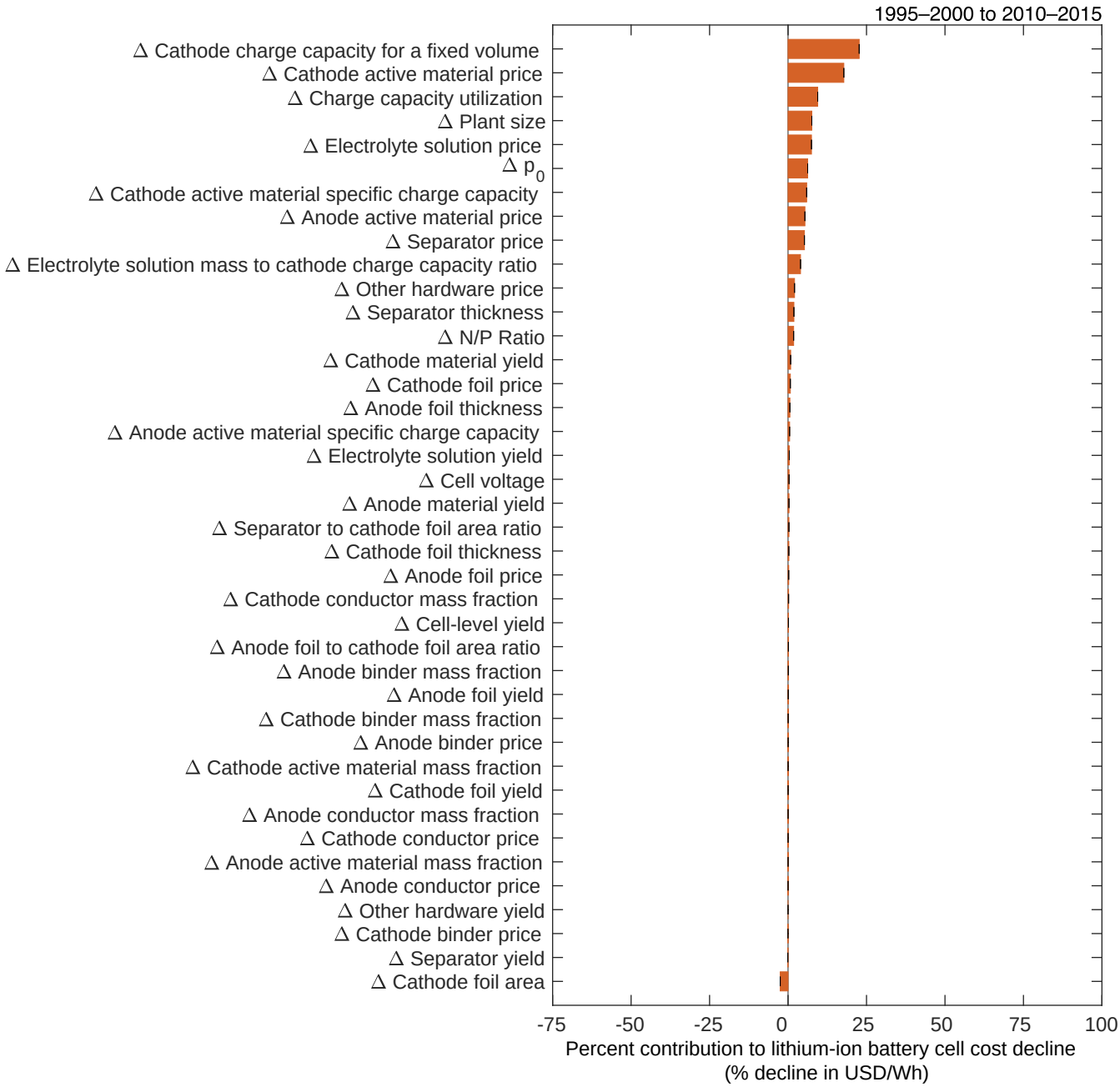

Figure S89: Sensitivity analysis for anode conductor price ($p_{\text{con,an}}$). The value is varied in both periods, and for each combination, we recompute the low-level mechanisms' contributions to cost change. The error bars show the minimum and maximum values of the low-level mechanisms' contributions to cost reduction.

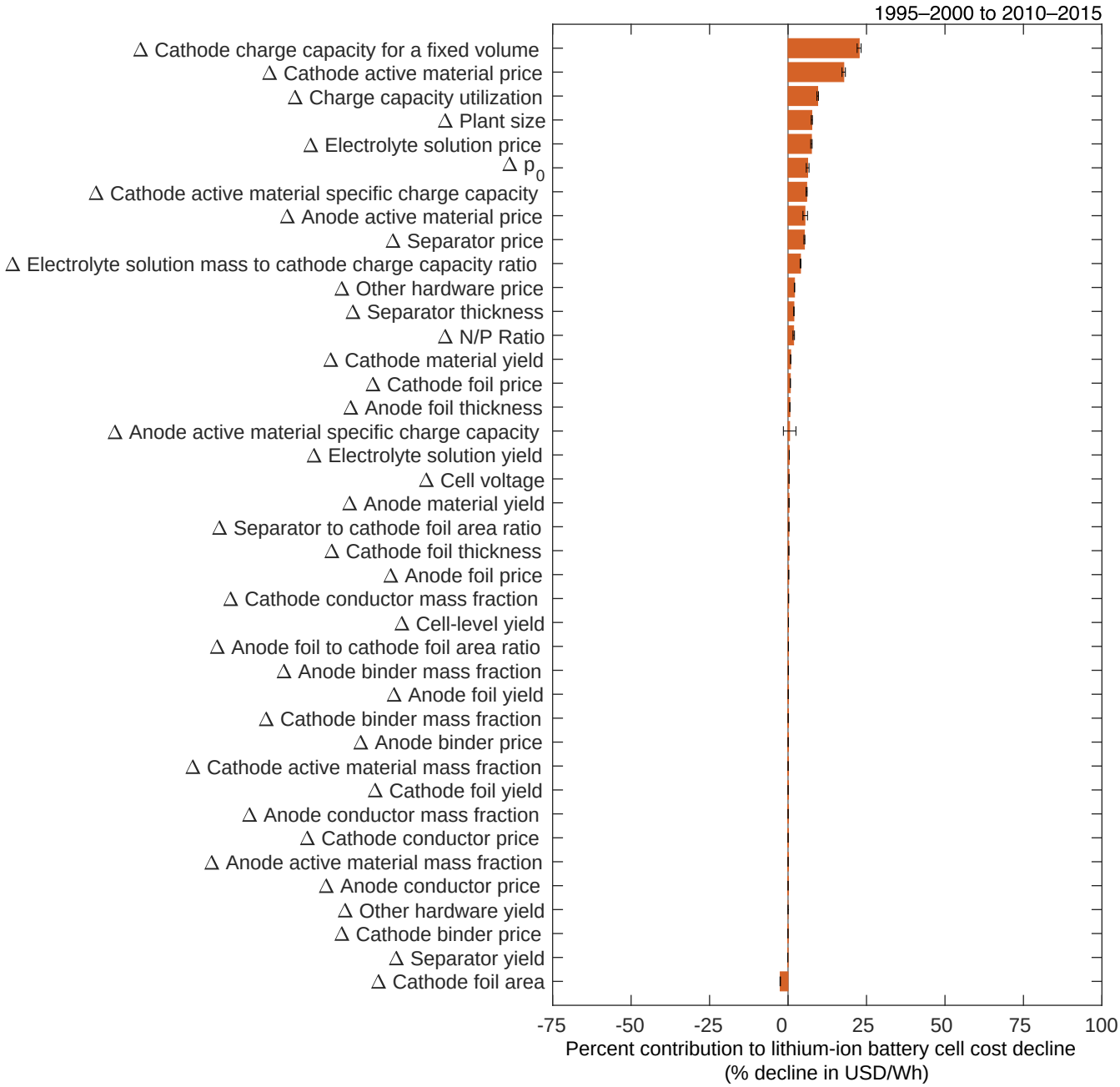

Figure S90: Sensitivity analysis for anode active material specific charge capacity (q_{an}). The value is varied in both periods, and for each combination, we recompute the low-level mechanisms' contributions to cost change. The error bars show the minimum and maximum values of the low-level mechanisms' contributions to cost reduction.

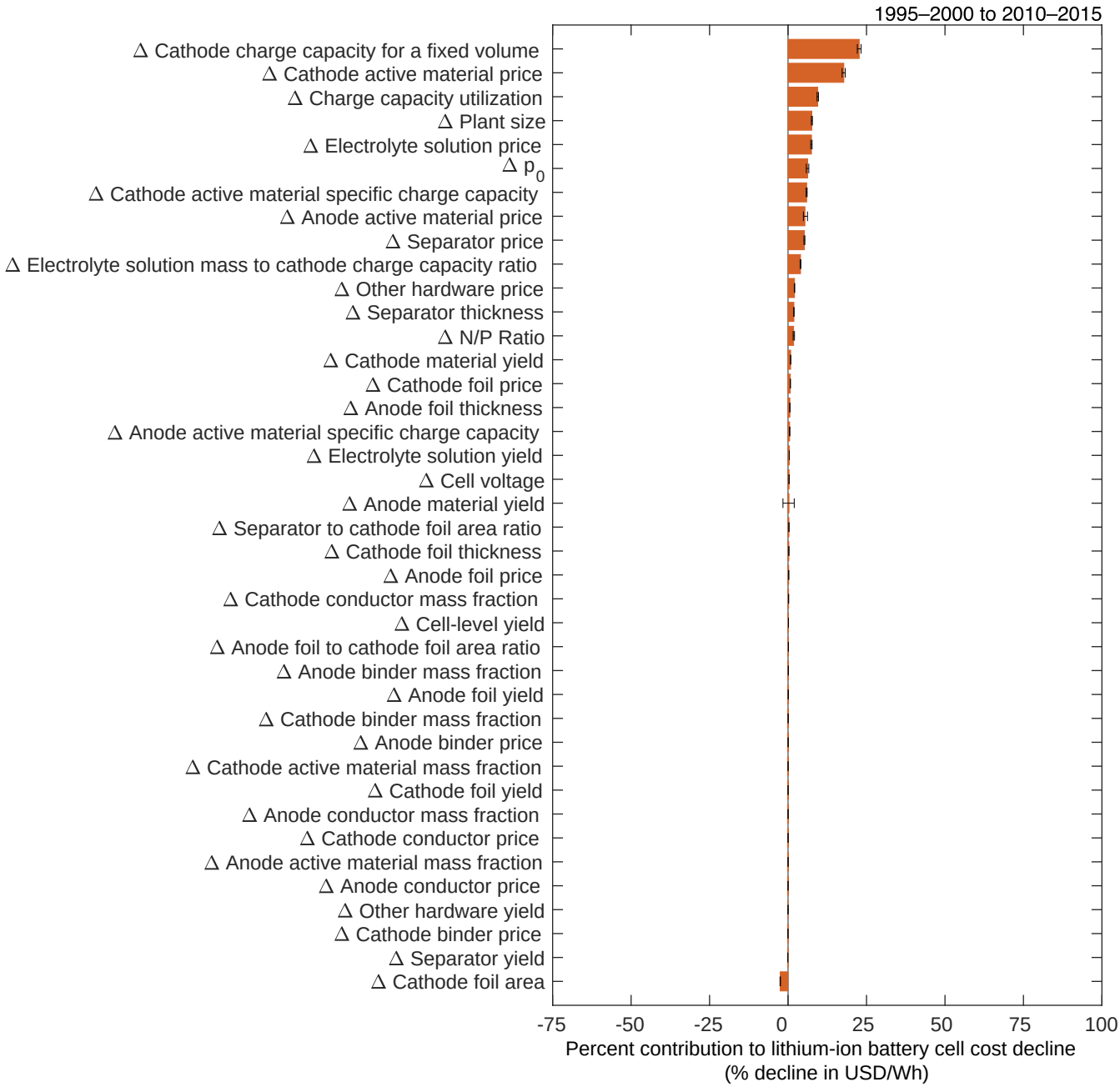

Figure S91: Sensitivity analysis for anode material yield (y_{an}). The value is varied in both periods, and for each combination, we recompute the low-level mechanisms' contributions to cost change. The error bars show the minimum and maximum values of the low-level mechanisms' contributions to cost reduction.

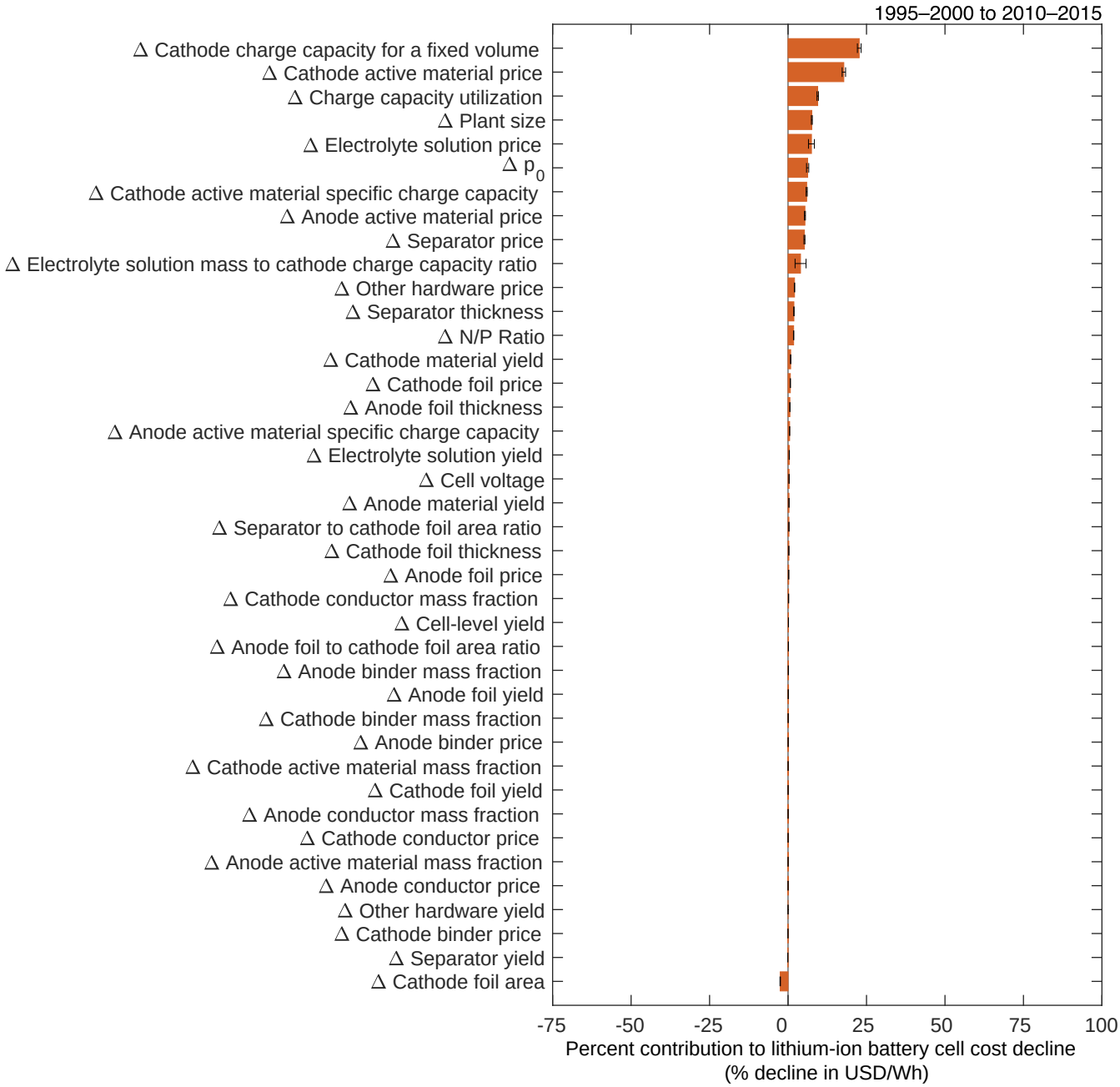

Figure S92: Sensitivity analysis for the ratio of electrolyte solution mass to cathode charge capacity (D_{el}). The value is varied in both periods, and for each combination, we recompute the low-level mechanisms' contributions to cost change. The error bars show the minimum and maximum values of the low-level mechanisms' contributions to cost reduction.

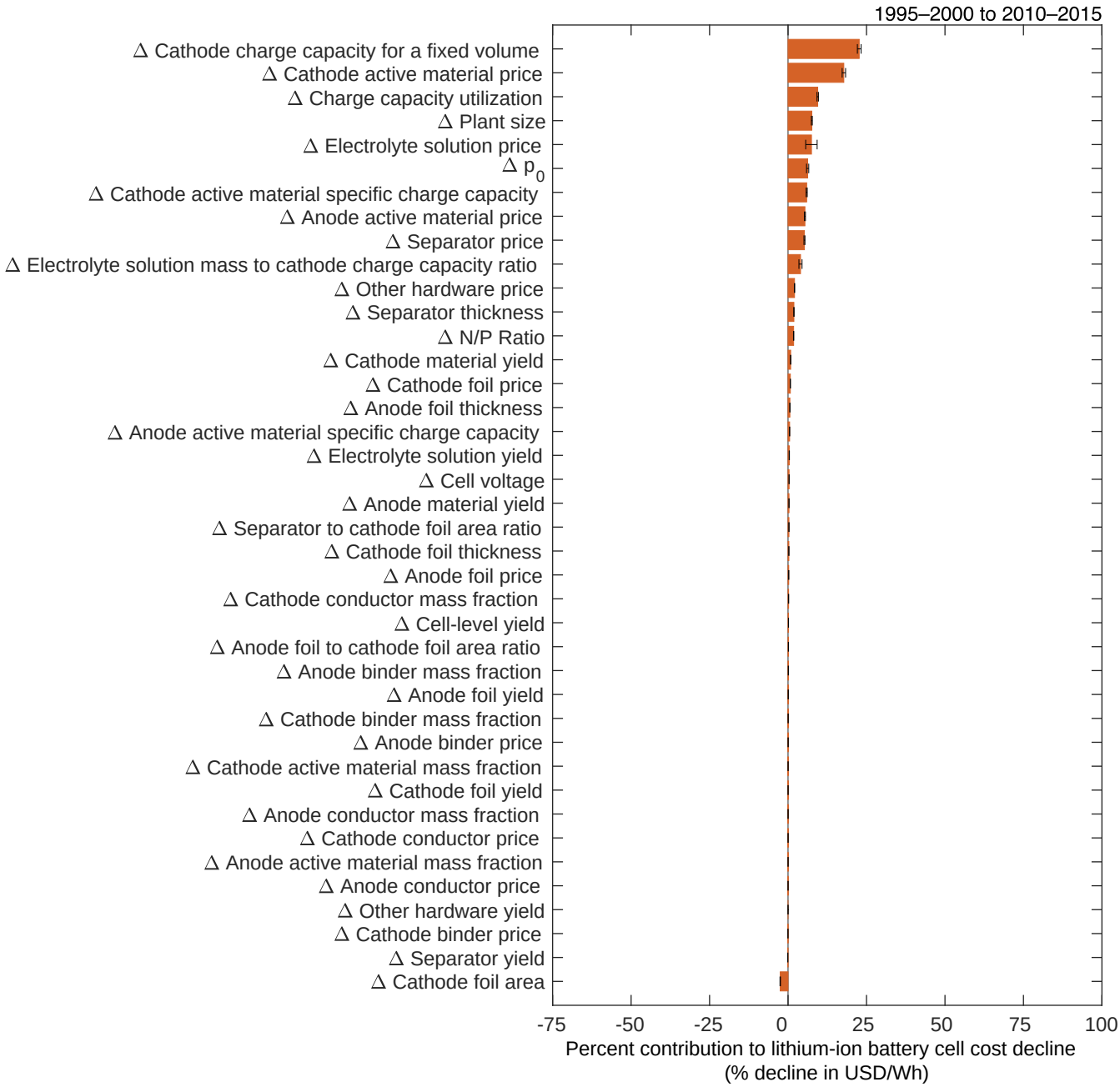

Figure S93: Sensitivity analysis for electrolyte solution price (p_{el}). The value is varied in both periods, and for each combination, we recompute the low-level mechanisms' contributions to cost change. The error bars show the minimum and maximum values of the low-level mechanisms' contributions to cost reduction.

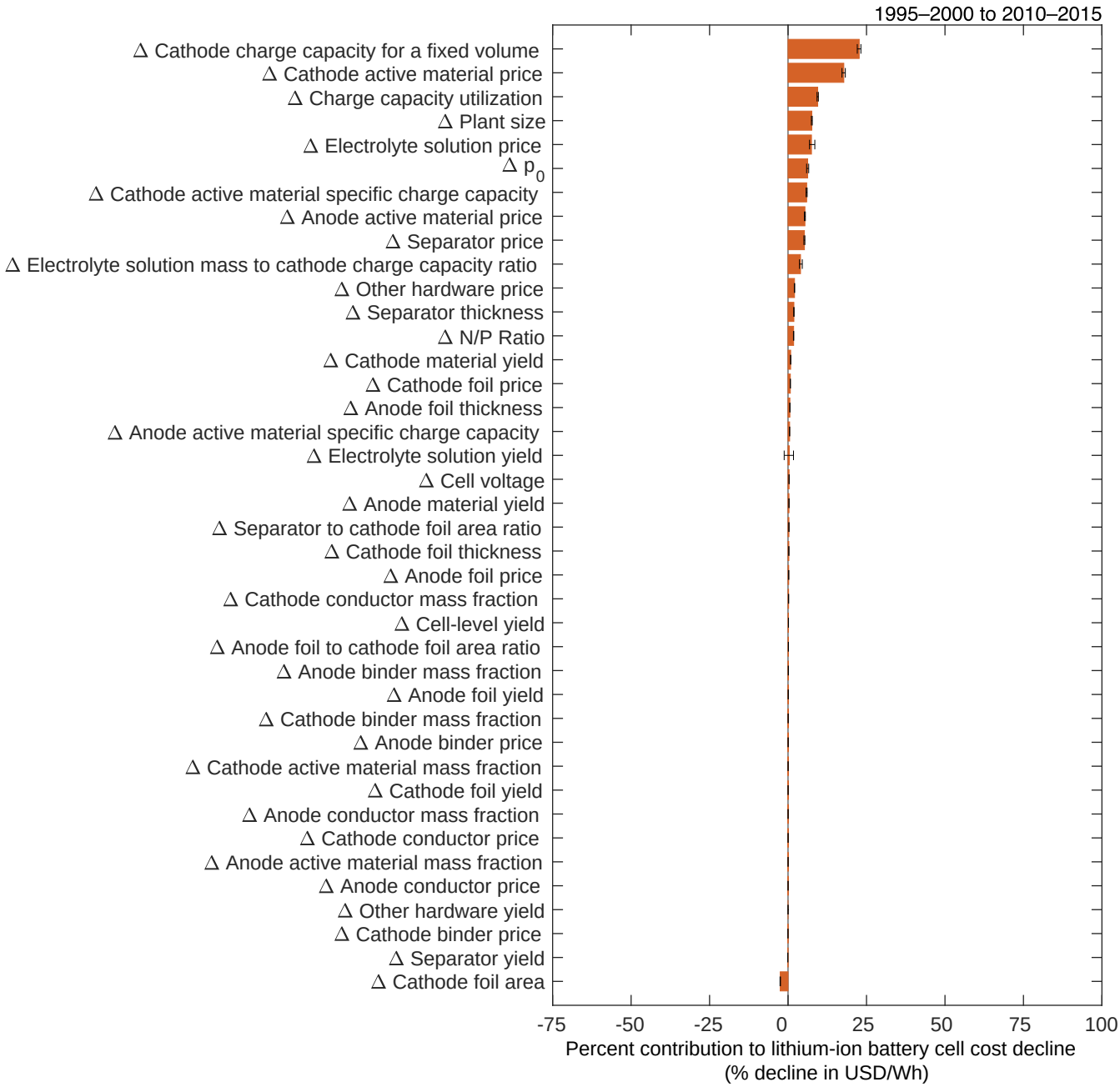

Figure S94: Sensitivity analysis for electrolyte solution yield (y_{el}). The value is varied in both periods, and for each combination, we recompute the low-level mechanisms' contributions to cost change. The error bars show the minimum and maximum values of the low-level mechanisms' contributions to cost reduction.

9.1.2 Model sensitivity analysis figures for area-related variables

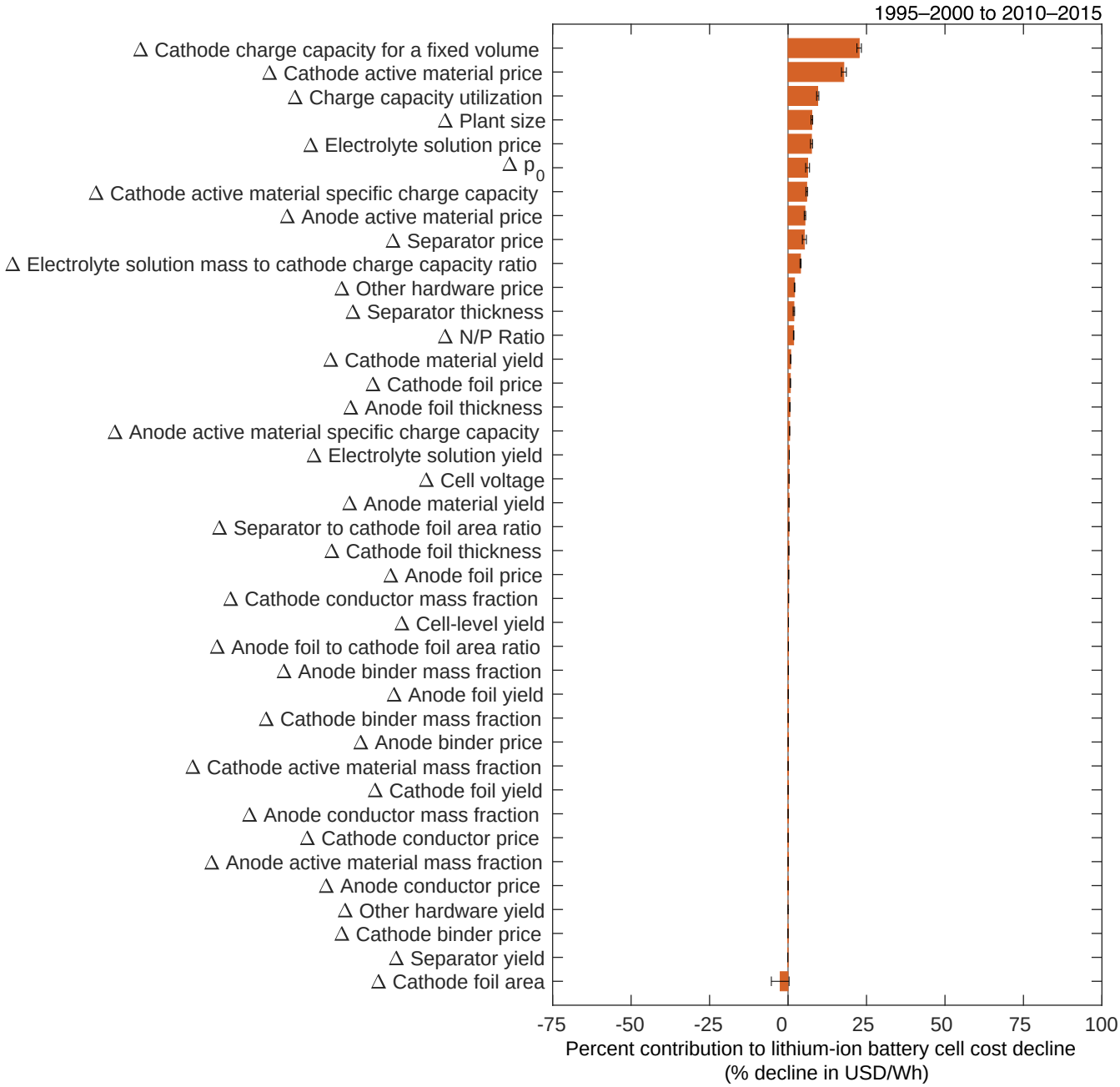

Figure S95: Sensitivity analysis for cathode foil area (a_{Al}). The value is varied in both periods, and for each combination, we recompute the low-level mechanisms' contributions to cost change. The error bars show the minimum and maximum values of the low-level mechanisms' contributions to cost reduction.

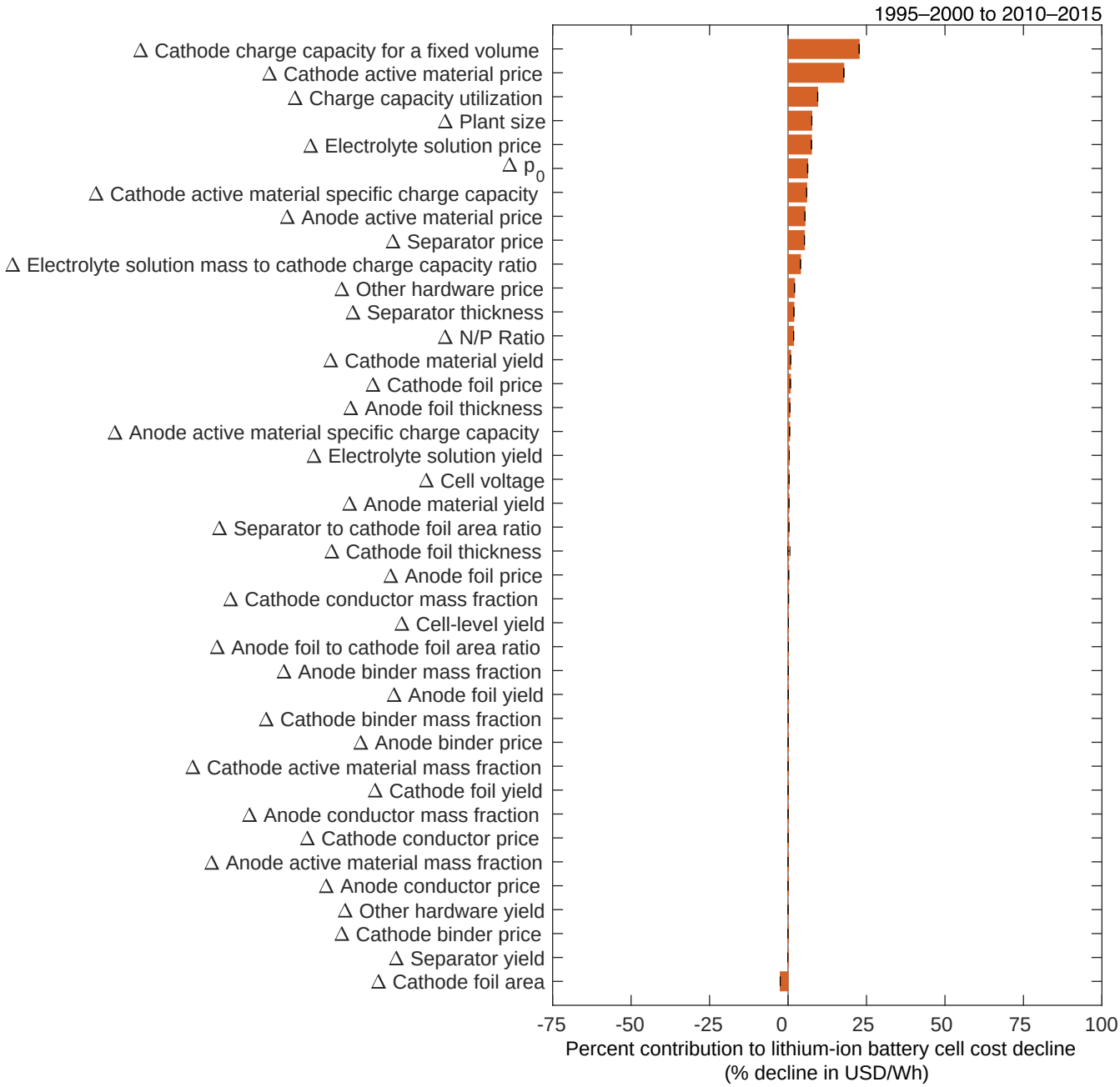

Figure S96: Sensitivity analysis for cathode foil thickness (t_{Al}). The value is varied in both periods, and for each combination, we recompute the low-level mechanisms' contributions to cost change. The error bars show the minimum and maximum values of the low-level mechanisms' contributions to cost reduction.

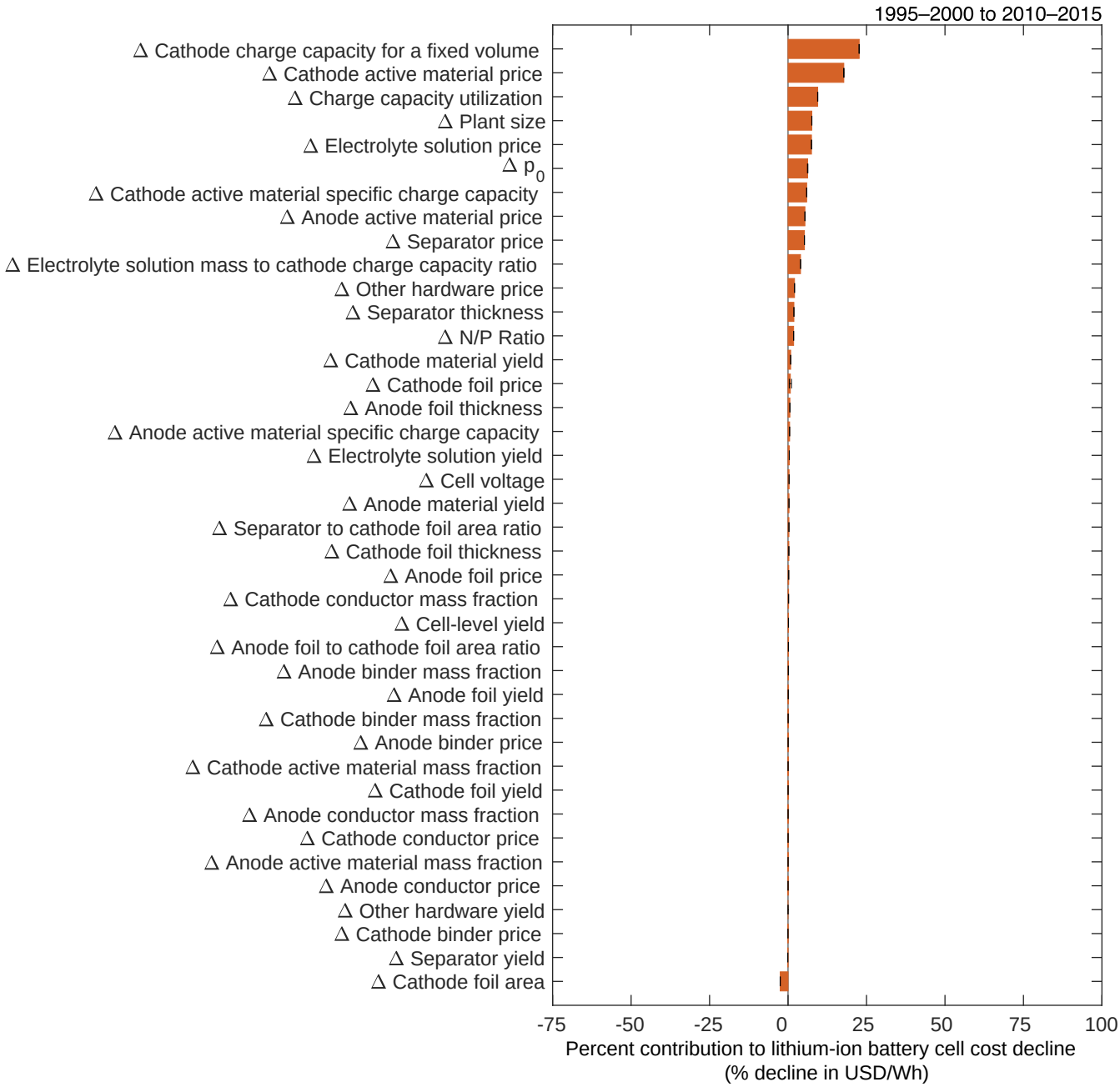

Figure S97: Sensitivity analysis for cathode foil price (p_{Al}). The value is varied in both periods, and for each combination, we recompute the low-level mechanisms' contributions to cost change. The error bars show the minimum and maximum values of the low-level mechanisms' contributions to cost reduction.

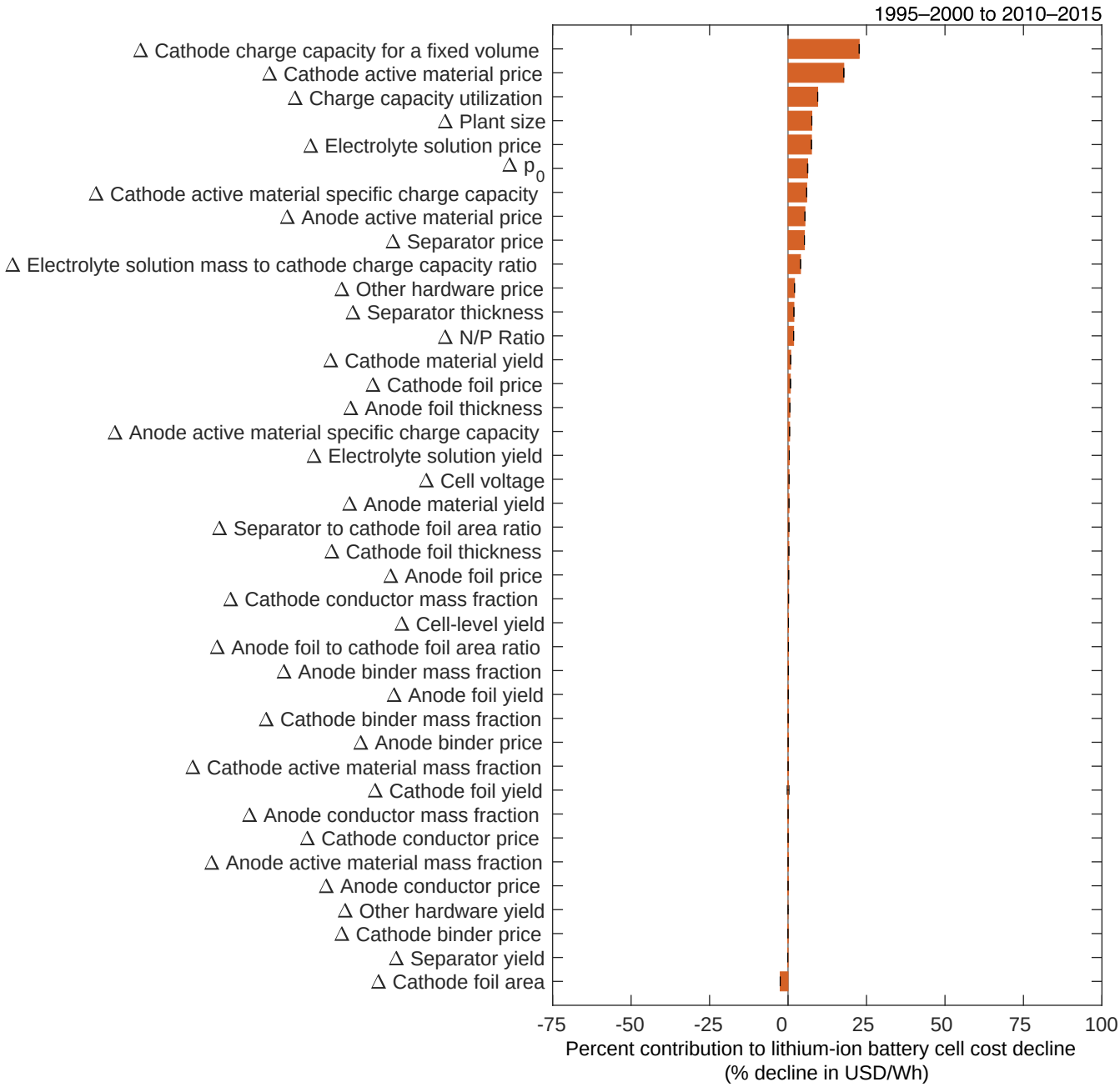

Figure S98: Sensitivity analysis for cathode foil yield (y_{Al}). The value is varied in both periods, and for each combination, we recompute the low-level mechanisms' contributions to cost change. The error bars show the minimum and maximum values of the low-level mechanisms' contributions to cost reduction.

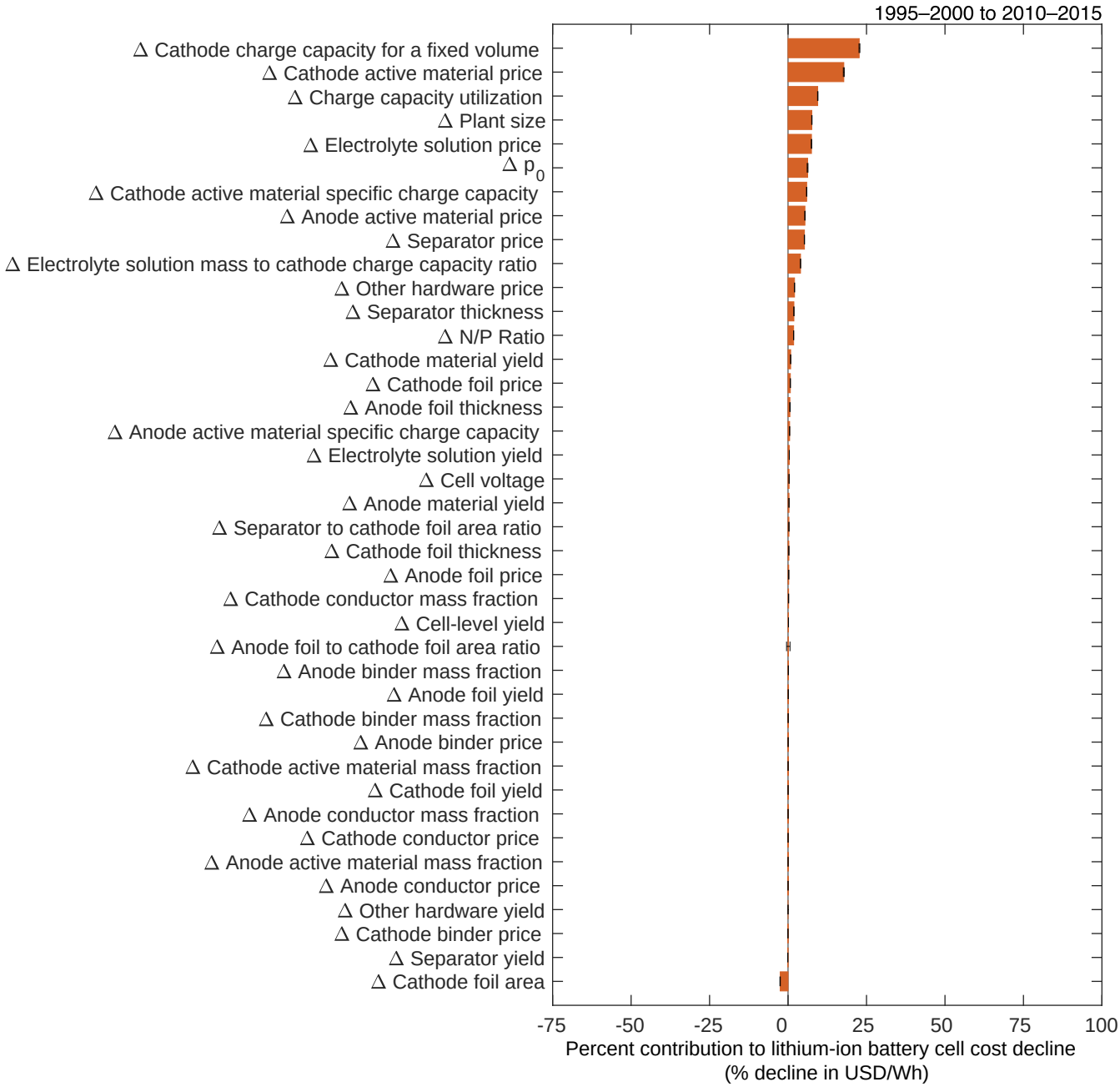

Figure S99: Sensitivity analysis for anode foil to cathode foil area ratio ($(\text{an/ca})_A$). The value is varied in both periods, and for each combination, we recompute the low-level mechanisms' contributions to cost change. The error bars show the minimum and maximum values of the low-level mechanisms' contributions to cost reduction.

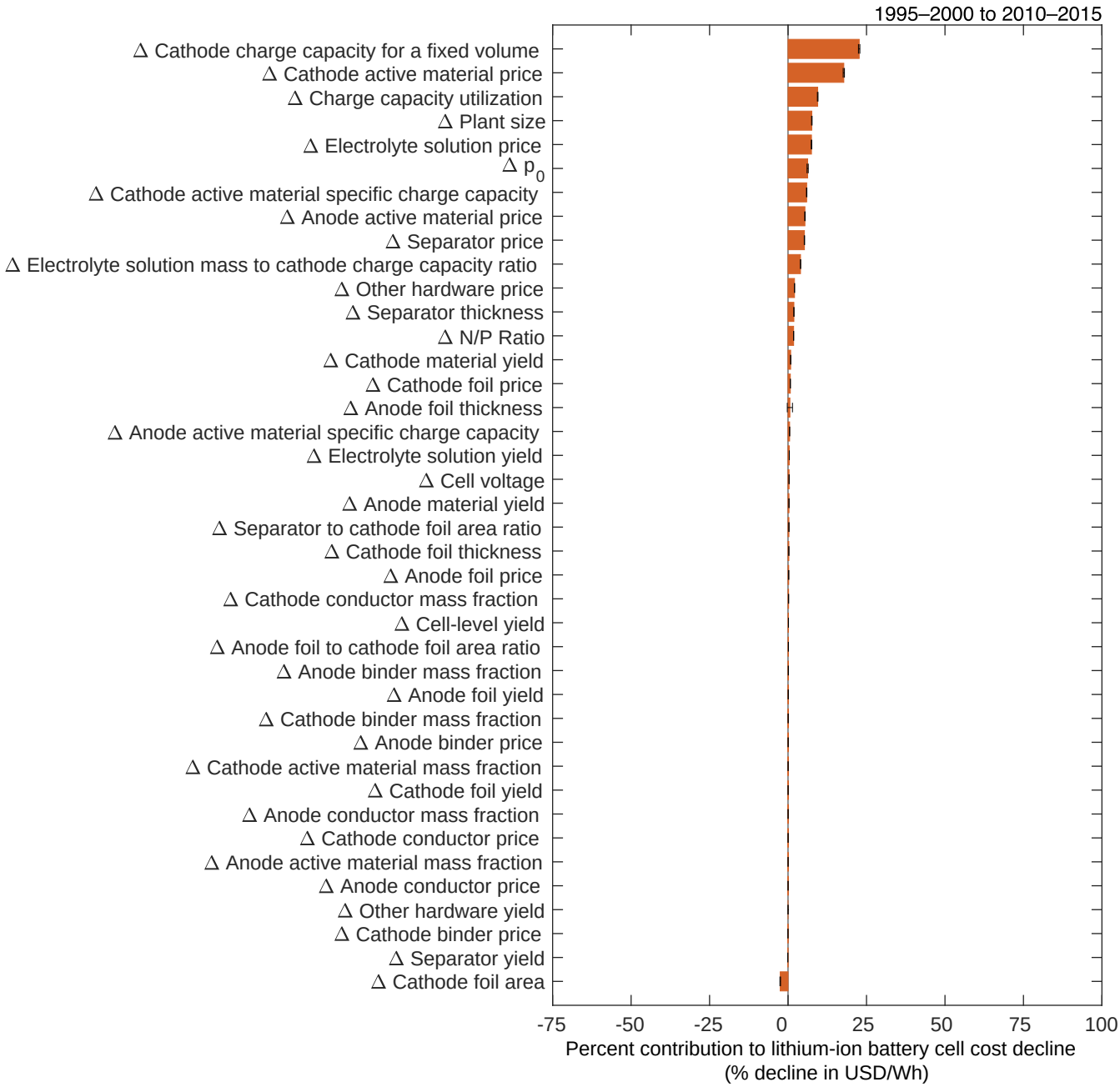

Figure S100: Sensitivity analysis for anode foil thickness (t_{Cu}). The value is varied in both periods, and for each combination, we recompute the low-level mechanisms' contributions to cost change. The error bars show the minimum and maximum values of the low-level mechanisms' contributions to cost reduction.

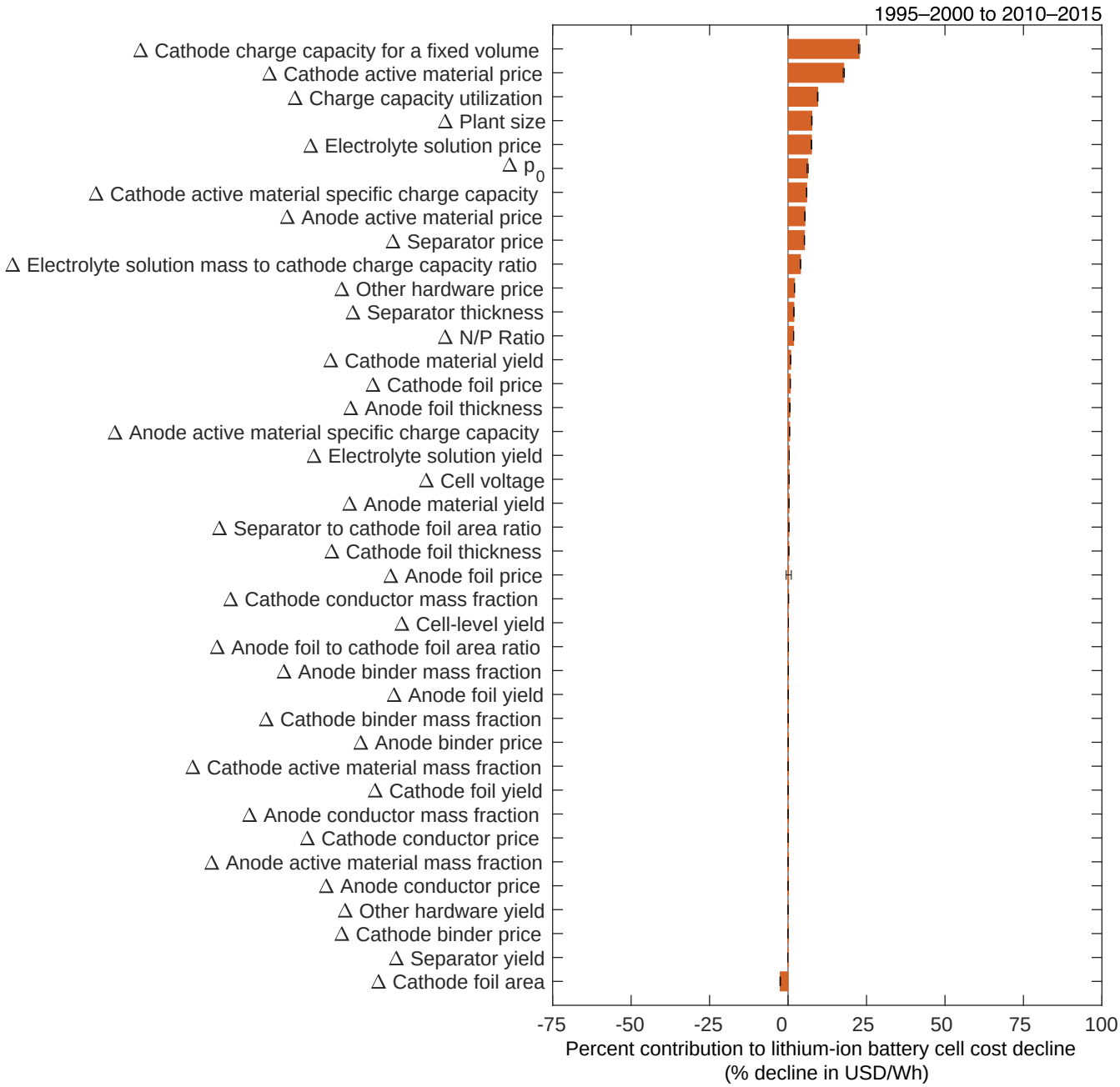

Figure S101: Sensitivity analysis for anode foil price (p_{Cu}). The value is varied in both periods, and for each combination, we recompute the low-level mechanisms' contributions to cost change. The error bars show the minimum and maximum values of the low-level mechanisms' contributions to cost reduction.

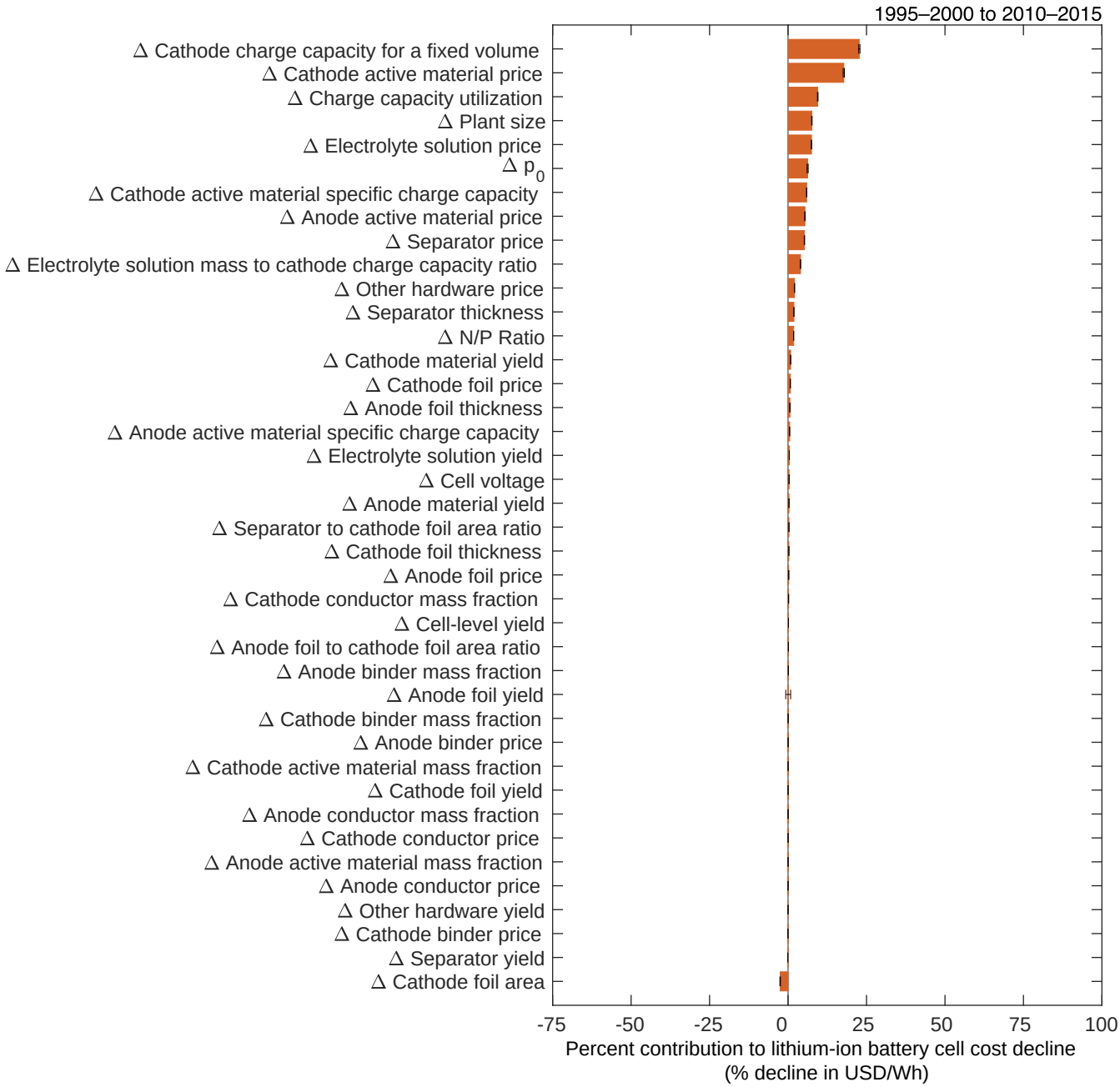

Figure S102: Sensitivity analysis for anode foil yield (y_{Cu}). The value is varied in both periods, and for each combination, we recompute the low-level mechanisms' contributions to cost change. The error bars show the minimum and maximum values of the low-level mechanisms' contributions to cost reduction.

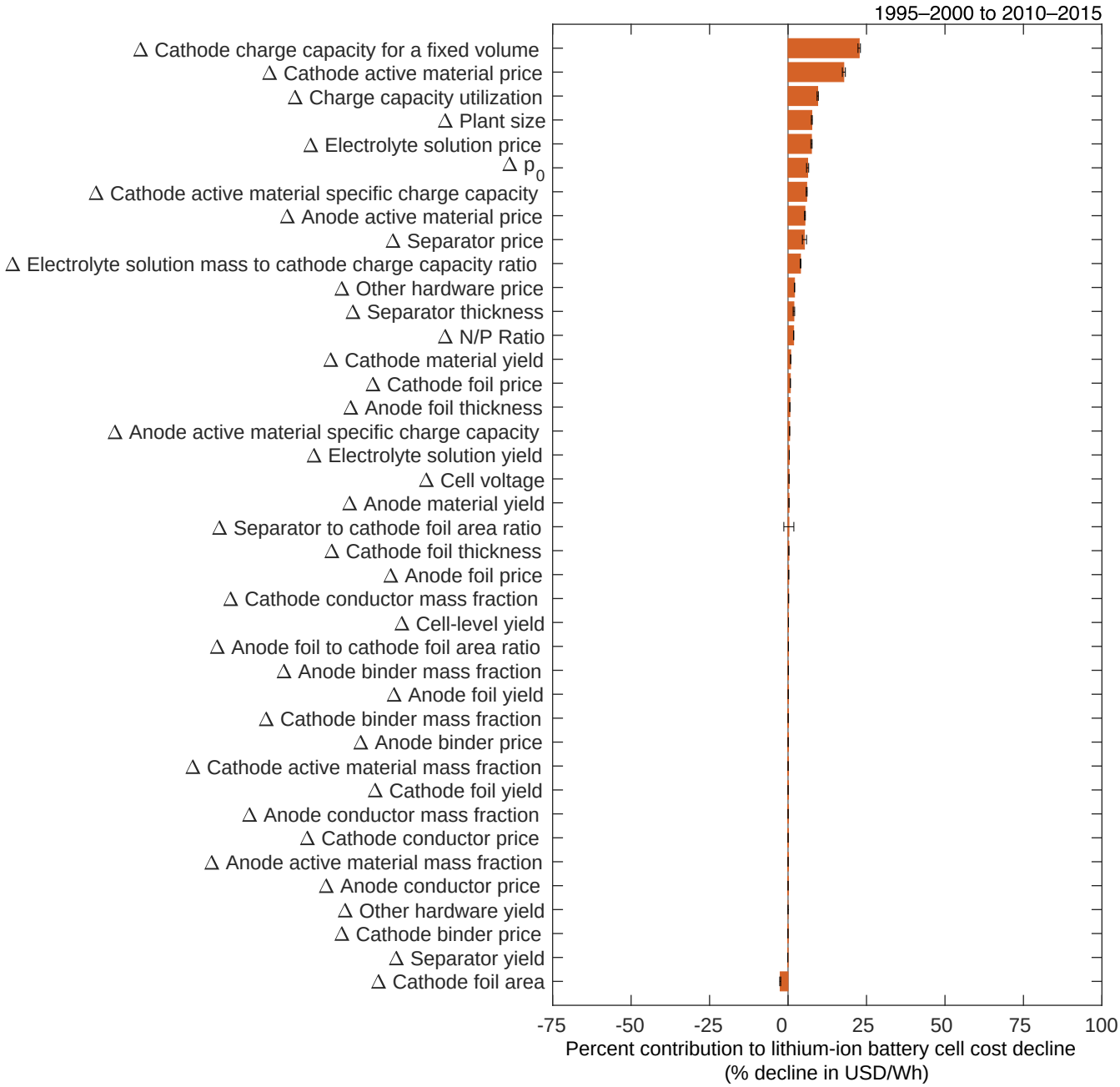

Figure S103: Sensitivity analysis for separator to cathode foil area ratio ($(\text{se/ca})_A$). The value is varied in both periods, and for each combination, we recompute the low-level mechanisms' contributions to cost change. The error bars show the minimum and maximum values of the low-level mechanisms' contributions to cost reduction.

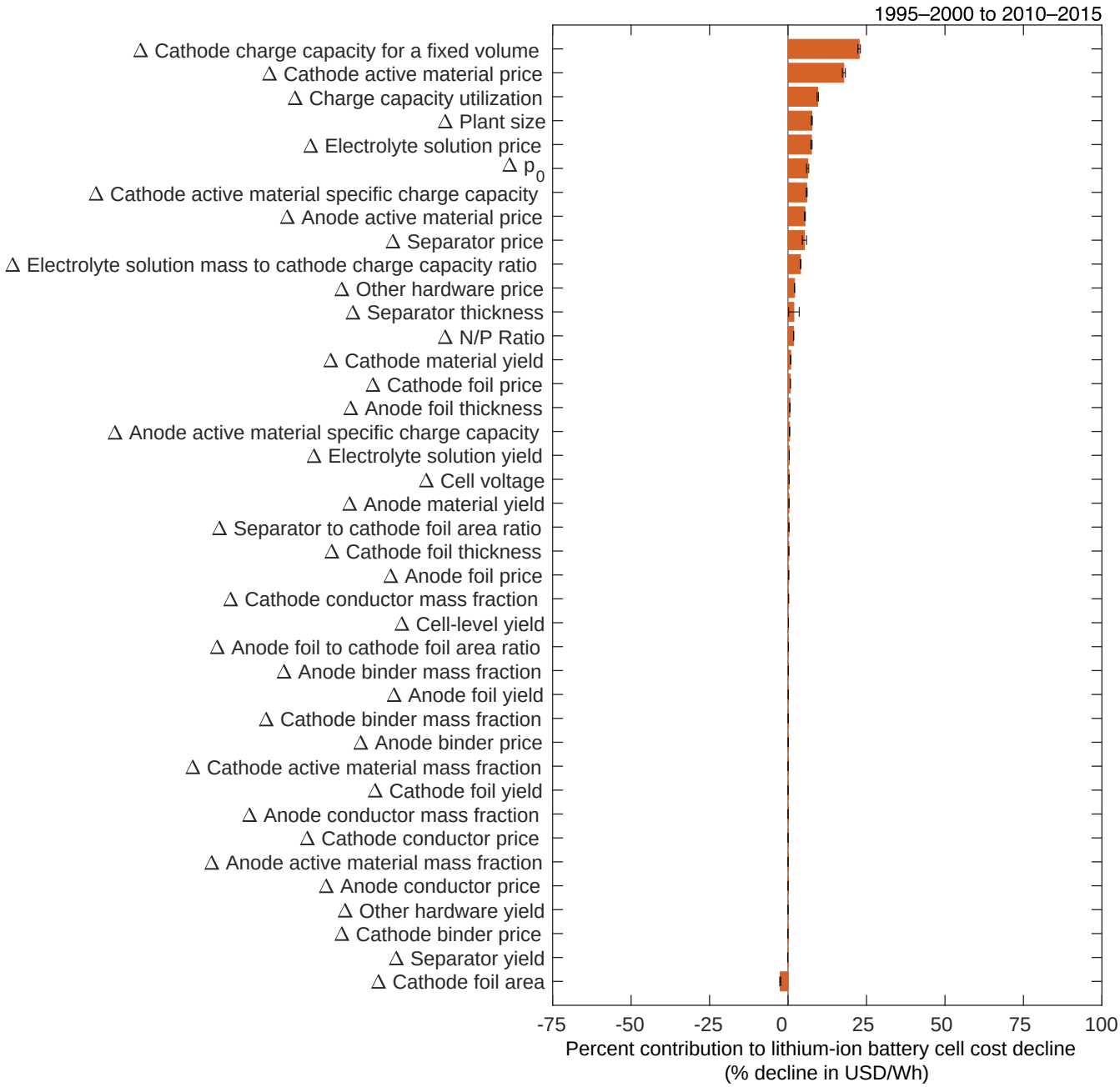

Figure S104: Sensitivity analysis for separator thickness (t_{se}). The value is varied in both periods, and for each combination, we recompute the low-level mechanisms' contributions to cost change. The error bars show the minimum and maximum values of the low-level mechanisms' contributions to cost reduction.

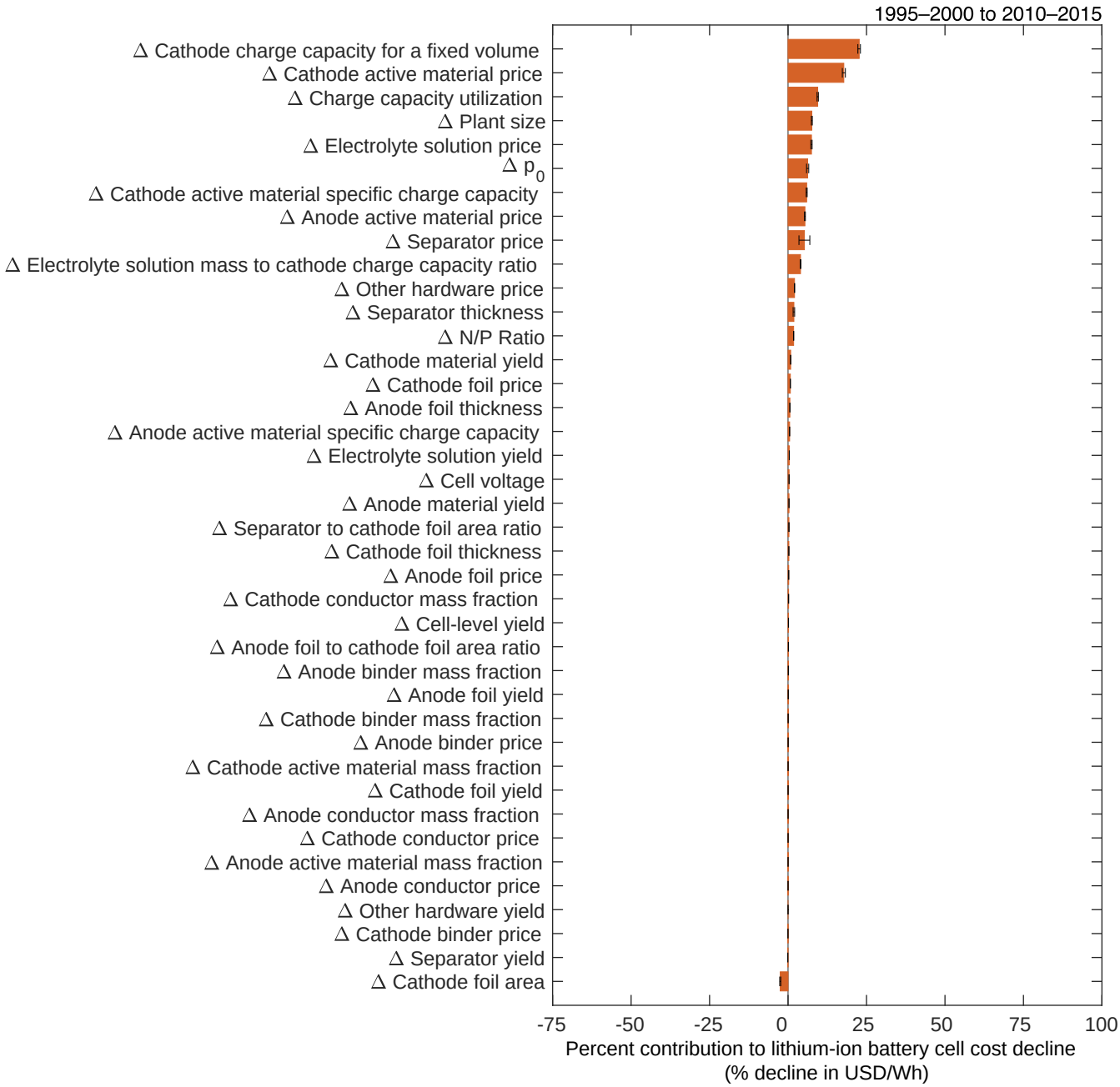

Figure S105: Sensitivity analysis for separator price ($p_{\mathrm{V,se}}$). The value is varied in both periods, and for each combination, we recompute the low-level mechanisms' contributions to cost change. The error bars show the minimum and maximum values of the low-level mechanisms' contributions to cost reduction.

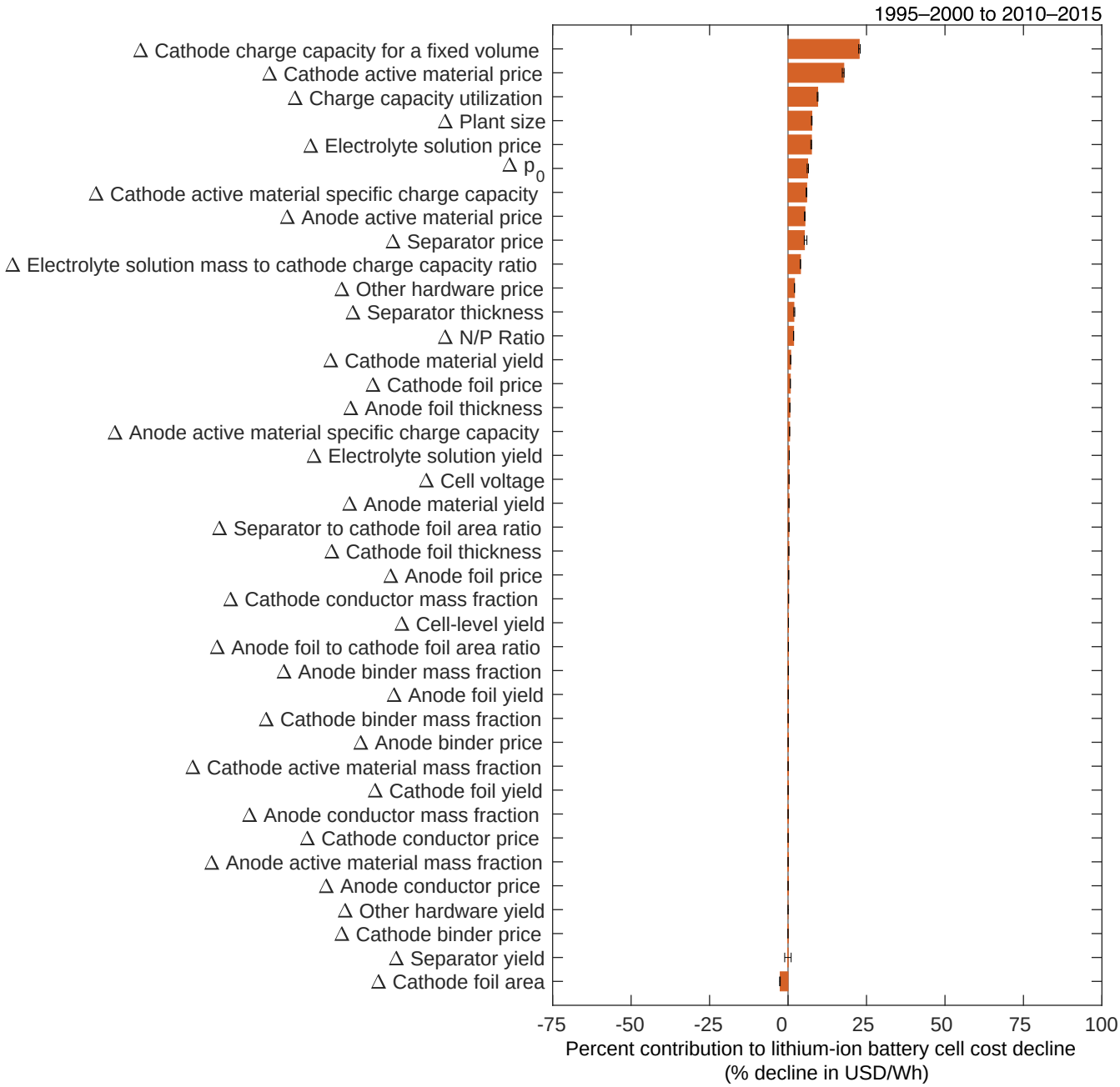

Figure S106: Sensitivity analysis for separator yield (y_{se}). The value is varied in both periods, and for each combination, we recompute the low-level mechanisms' contributions to cost change. The error bars show the minimum and maximum values of the low-level mechanisms' contributions to cost reduction.

9.1.3 Model sensitivity analysis figures for other cell cost components and cell-level variables

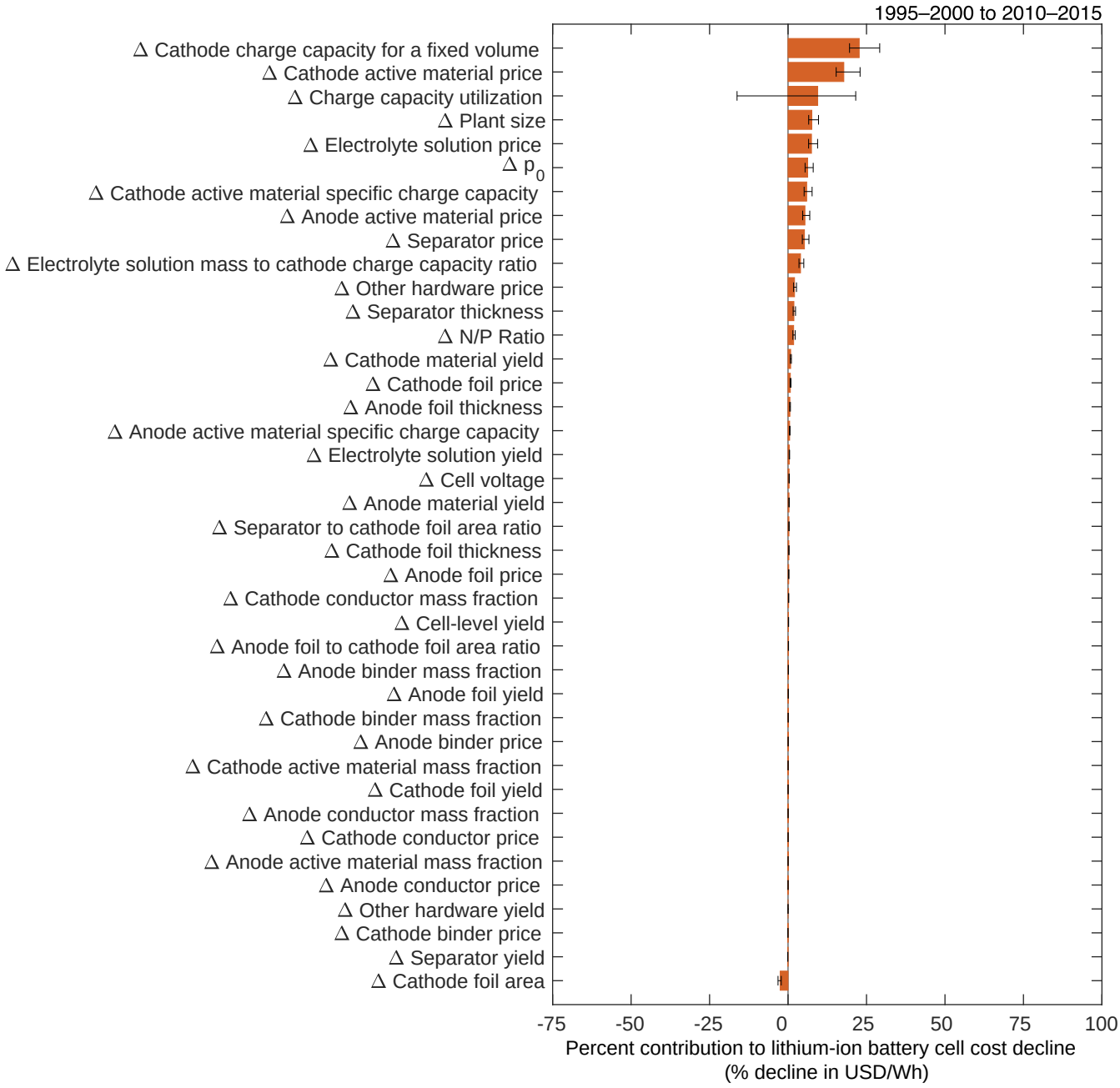

Figure S107: Sensitivity analysis for charge capacity utilization (η_{util}). The value is varied in both periods, and for each combination, we recompute the low-level mechanisms' contributions to cost change. The error bars show the minimum and maximum values of the low-level mechanisms' contributions to cost reduction.

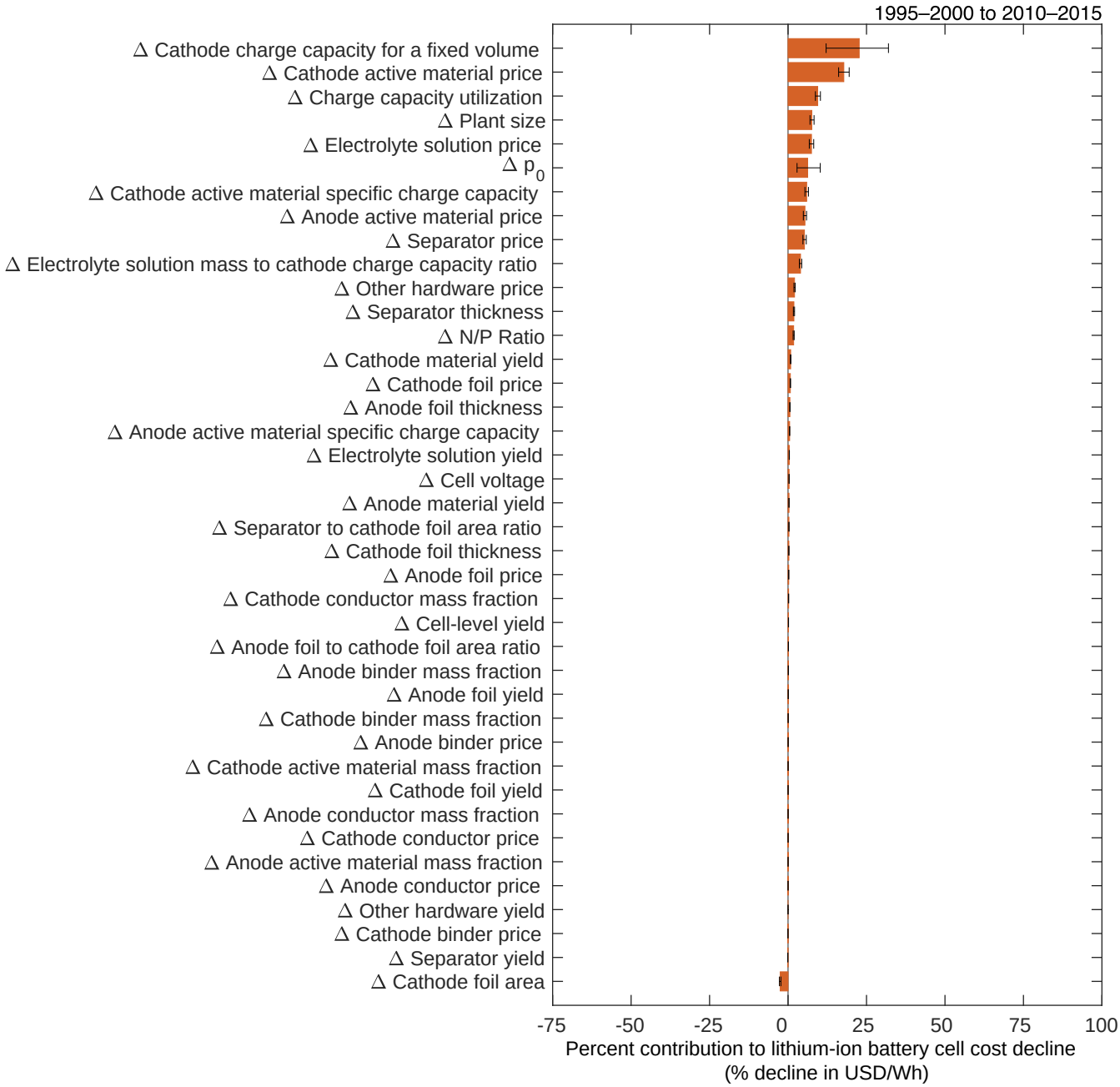

Figure S108: Sensitivity analysis for cathode charge capacity for a fixed volume (Q_{ca}). The value is varied in both periods, and for each combination, we recompute the low-level mechanisms' contributions to cost change. The error bars show the minimum and maximum values of the low-level mechanisms' contributions to cost reduction.

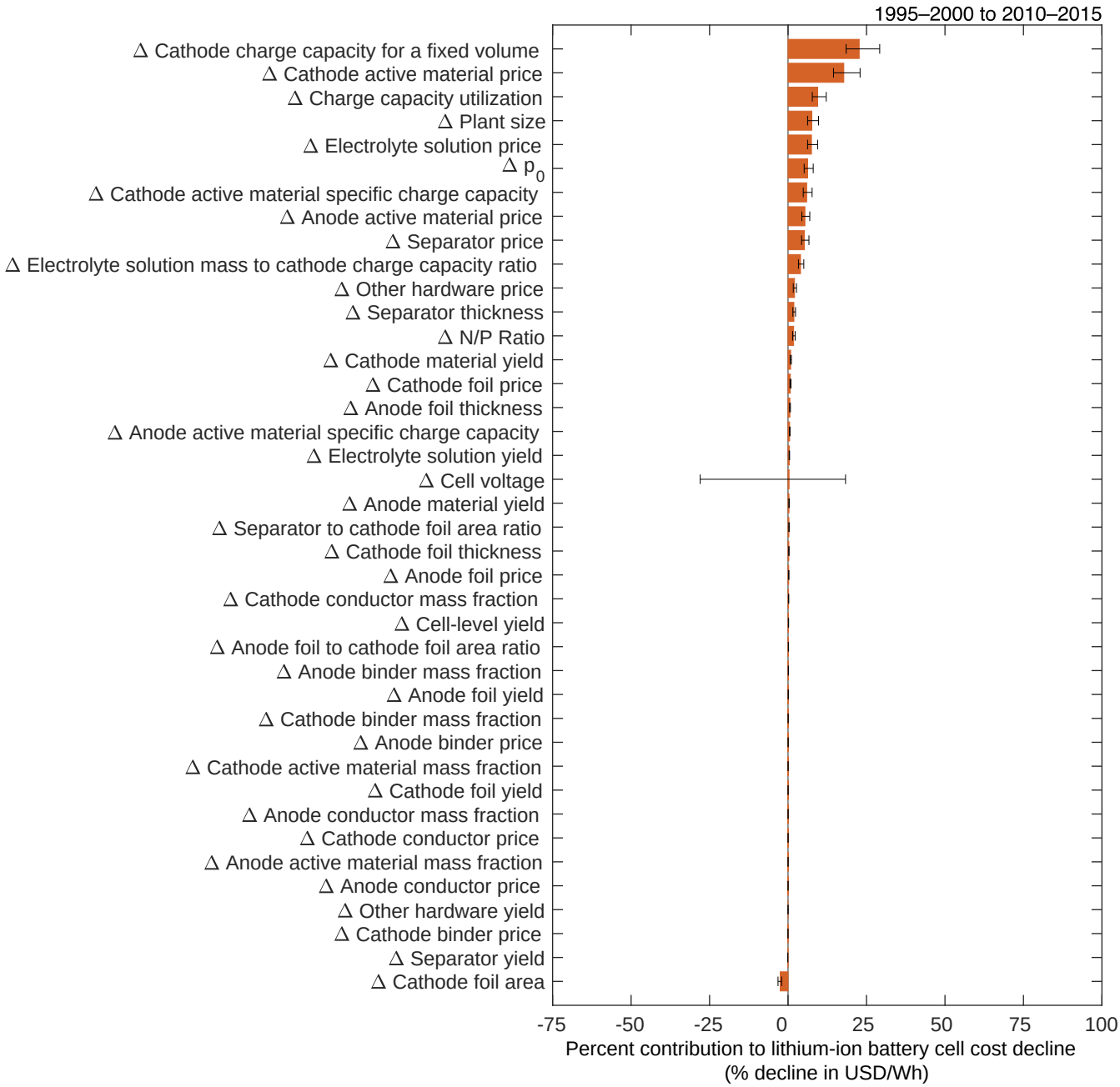

Figure S109: Sensitivity analysis for cell voltage (V). The value is varied in both periods, and for each combination, we recompute the low-level mechanisms' contributions to cost change. The error bars show the minimum and maximum values of the low-level mechanisms' contributions to cost reduction.

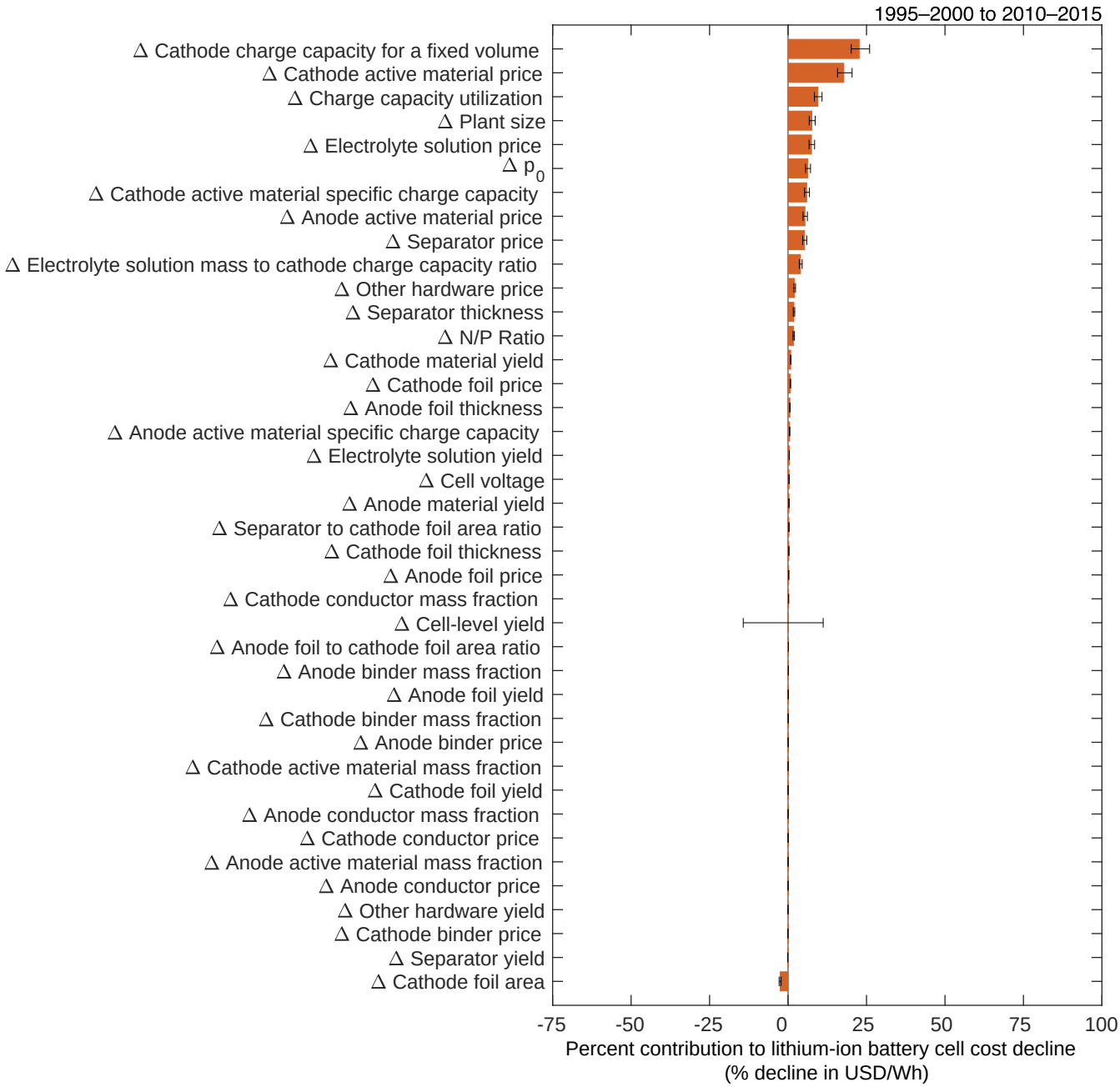

Figure S110: Sensitivity analysis for cell-level yield (y_{cell}). The value is varied in both periods, and for each combination, we recompute the low-level mechanisms' contributions to cost change. The error bars show the minimum and maximum values of the low-level mechanisms' contributions to cost reduction.

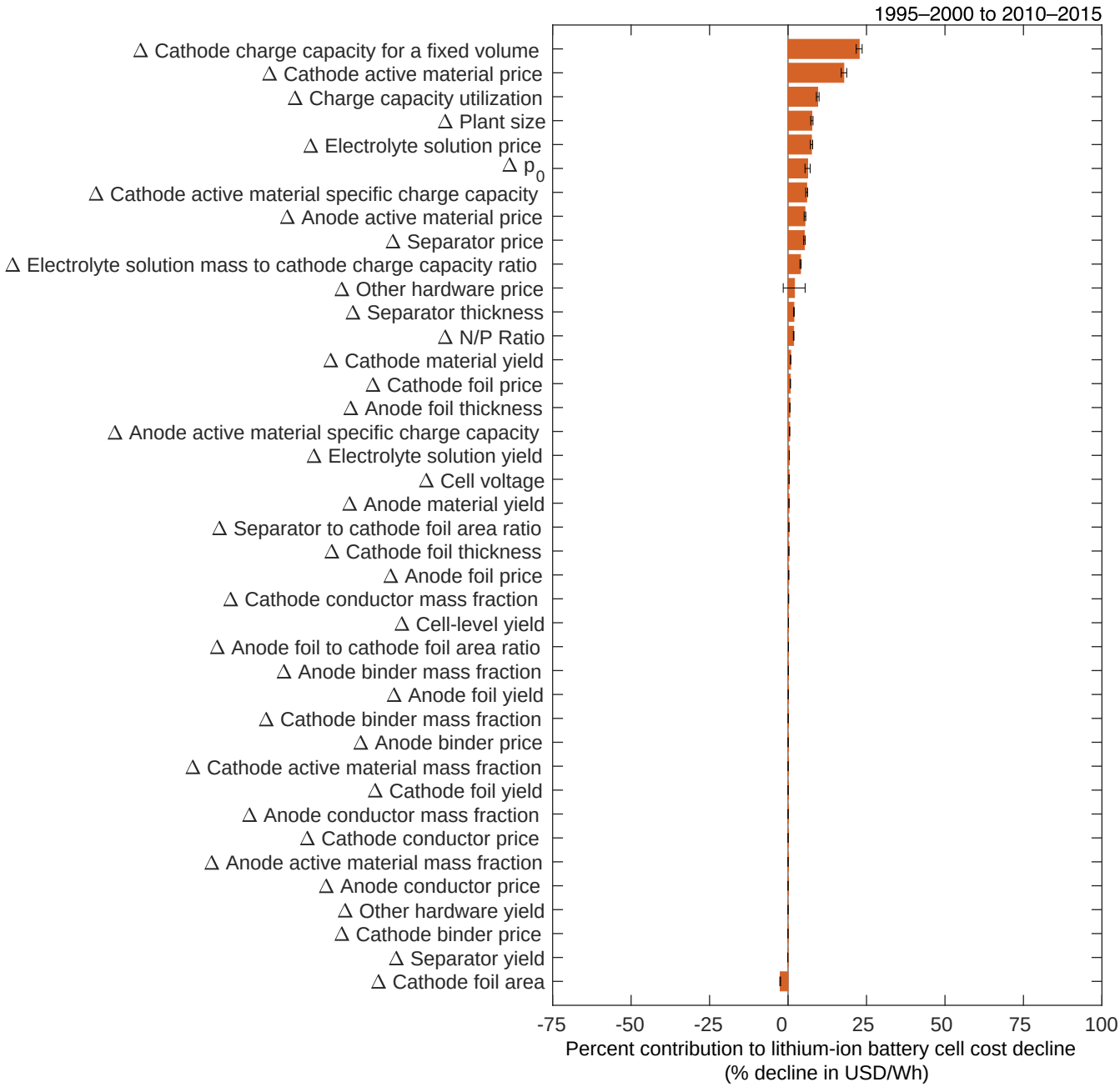

Figure S111: Sensitivity analysis for other hardware price (p_{can}). The value is varied in both periods, and for each combination, we recompute the low-level mechanisms' contributions to cost change. The error bars show the minimum and maximum values of the low-level mechanisms' contributions to cost reduction.

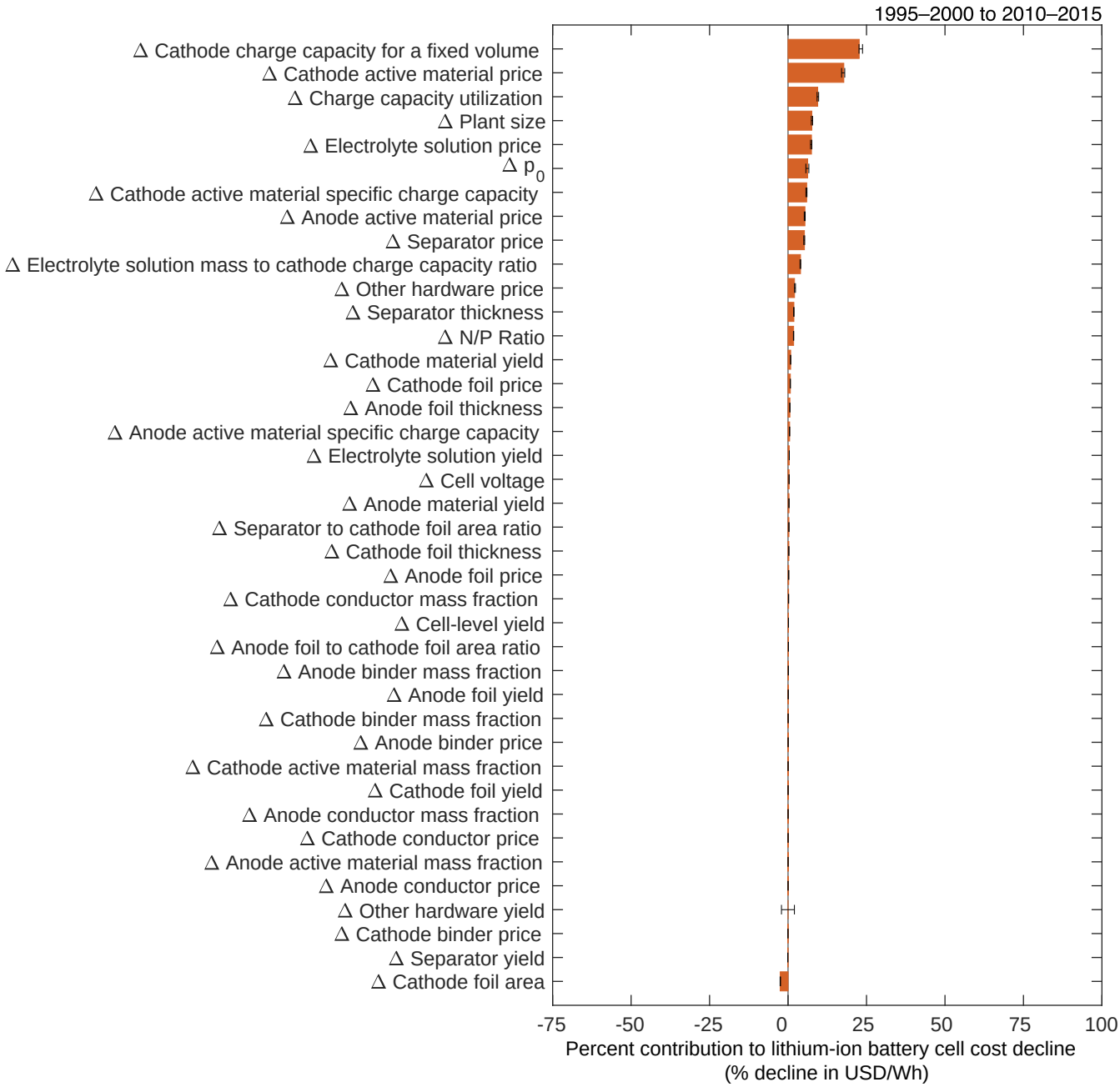

Figure S112: Sensitivity analysis for other hardware yield (y_{can}). The value is varied in both periods, and for each combination, we recompute the low-level mechanisms' contributions to cost change. The error bars show the minimum and maximum values of the low-level mechanisms' contributions to cost reduction.

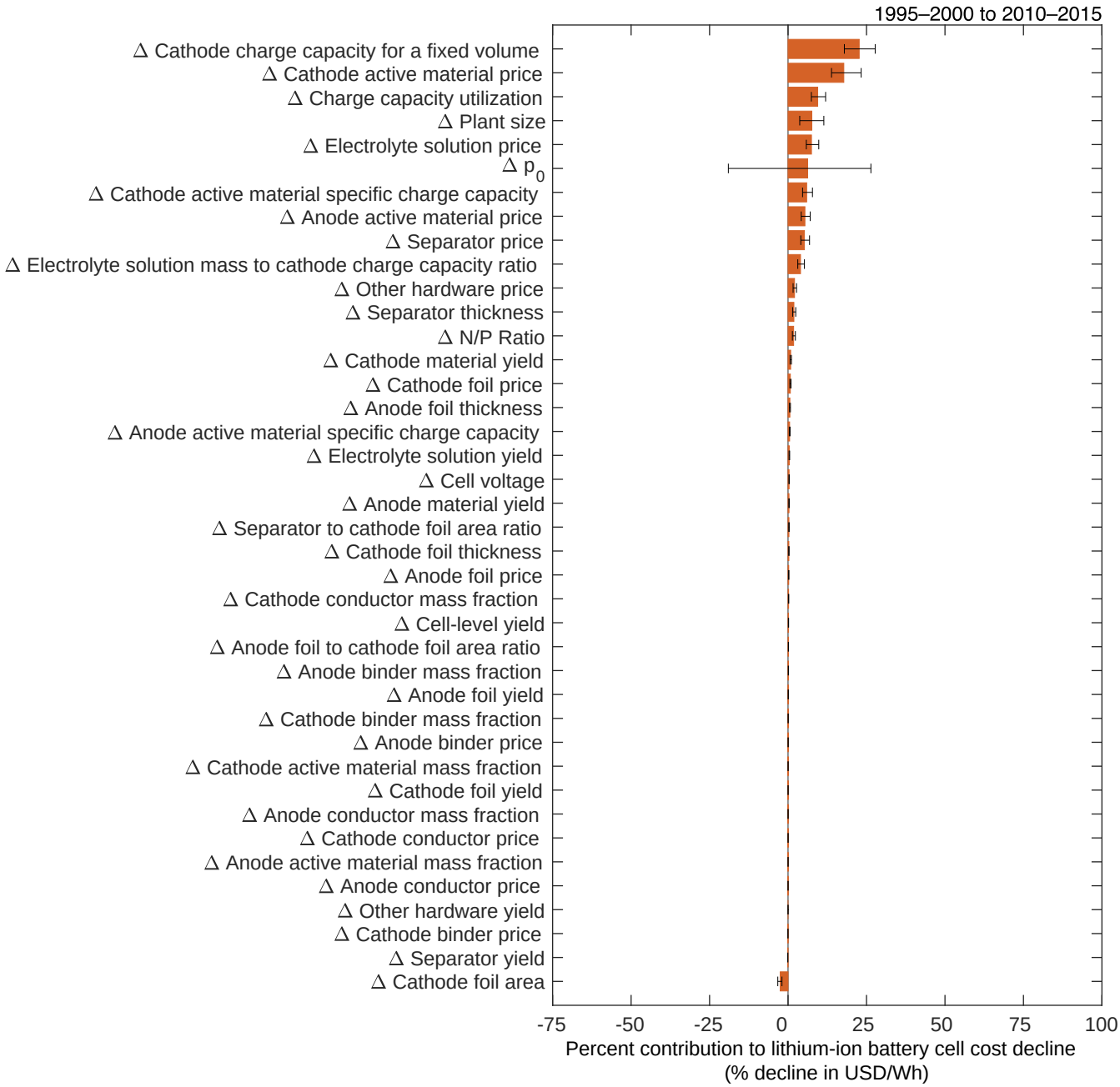

Figure S113: Sensitivity analysis for the material cost fraction (θ). The value is varied in both periods, and for each combination, we recompute the low-level mechanisms' contributions to cost change. The error bars show the minimum and maximum values of the low-level mechanisms' contributions to cost reduction.

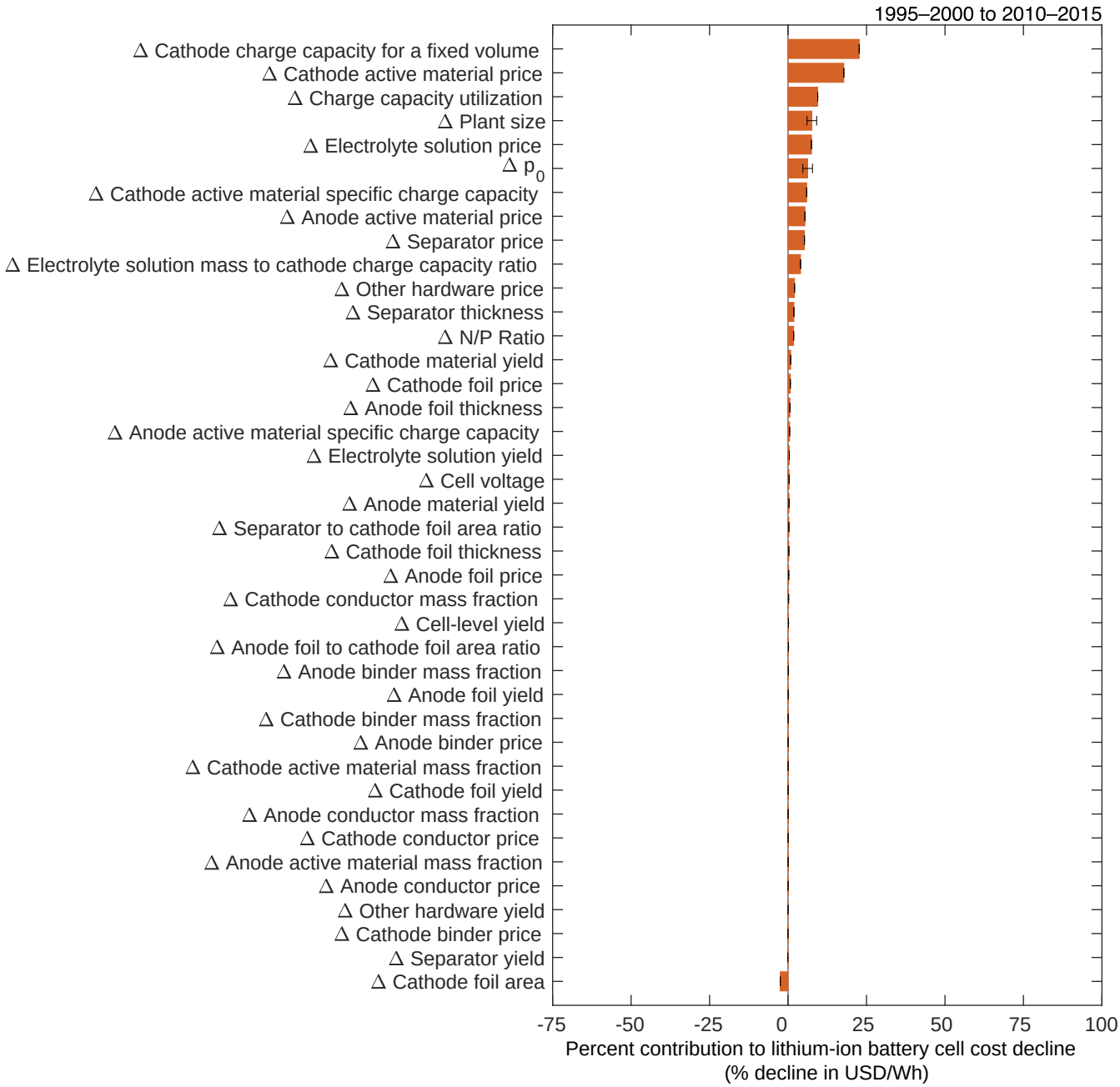

Figure S114: Sensitivity analysis for plant size (K). The value is varied in both periods, and for each combination, we recompute the low-level mechanisms' contributions to cost change. The error bars show the minimum and maximum values of the low-level mechanisms' contributions to cost reduction.

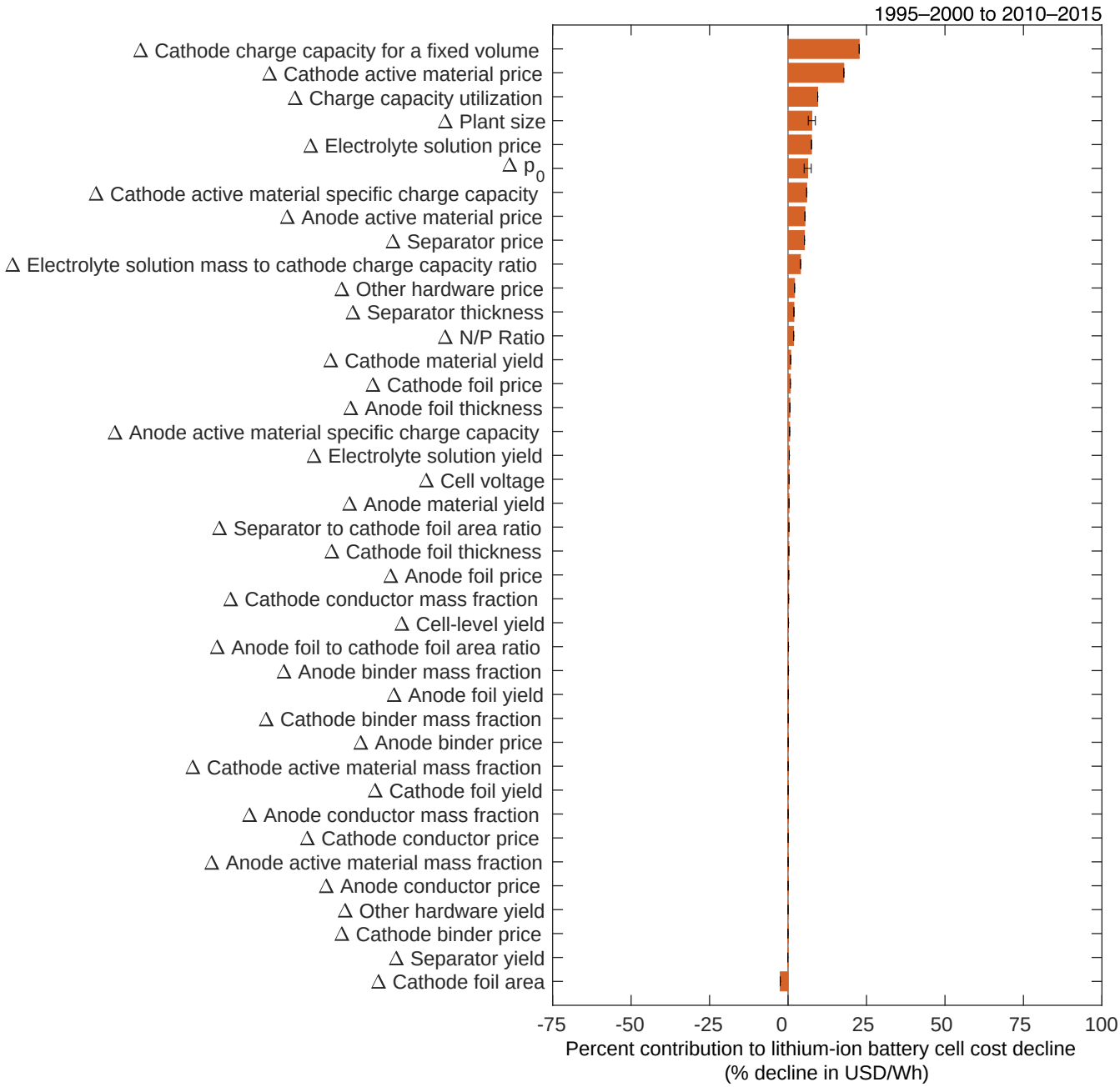

Figure S115: Sensitivity analysis for the scaling factor (b). The value is varied in both periods, and for each combination, we recompute the low-level mechanisms' contributions to cost change. The error bars show the minimum and maximum values of the low-level mechanisms' contributions to cost reduction.

9.1.4 Model sensitivity analysis for all variables

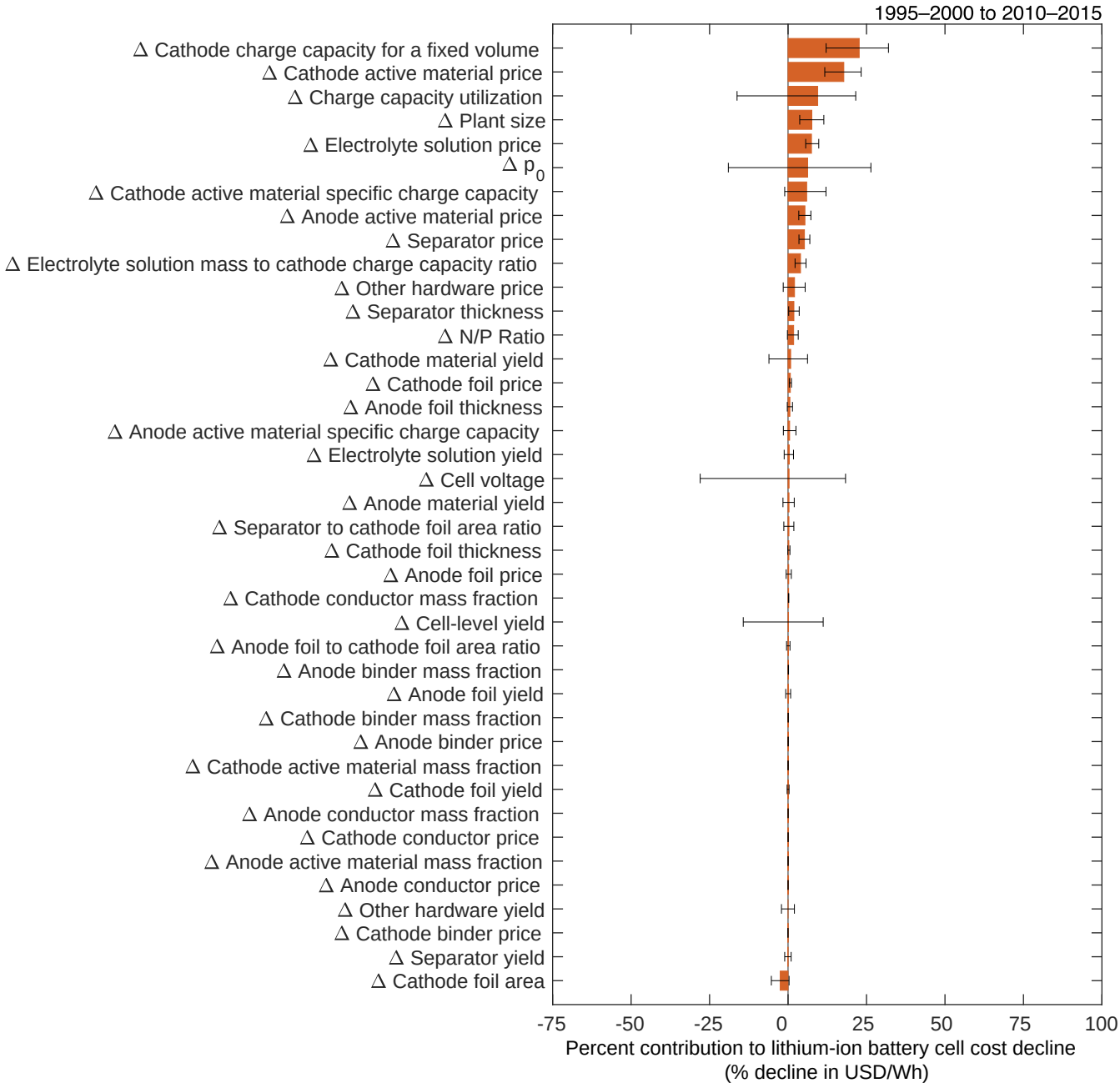

Figure S116: Cost reduction contributions with error bars representing the minimum and maximum values from all scenarios in which variables are varied ±15% relative to their central representative values, with the aforementioned limitations.

9.2 Data-informed sensitivity analysis

To explore the sensitivity of the cost change results to uncertainty in the representative values presented in Tables 1–3, we used the collected data to develop lower and upper bounds for each value (see Tables S7–S9), as described above. In many cases, the uncertainty bounds comprise the minima and maxima observed for a variable during a given period. When more data were available, often the 25^{th} and 75^{th} percentiles are employed as the lower and upper bounds respectively. When no other applicable, reliable estimates were available, large uncertainty ranges, typically ±30% are employed. Details describing the development of these ranges accompany the descriptions of the estimation of the representative values. The data-informed sensitivity analysis results are presented in Figures S117–S159.

As with the model sensitivity analysis, this sensitivity analysis also varies the mass fractions of the cathode and anode component materials independently, which can lead to some unrealistic sums. However, as these variables contribute little to overall cost change, the impacts of the unrealistic sums on the results of our sensitivity analysis are minimal.

Table S7: Data employed to calculate mass-related cell cost components with bounds

Variable	Symbol	Units	Period 1: 1995–2000			Period 2: 2010–2015		
			Mid	Low	High	Mid	Low	High
Cathode active material mass fraction	$w_{\text{act,ca}}$	unitless (fraction out of 1)	0.905	0.850	0.950	0.960	0.950	0.970
Cathode active material price	$p_{\text{act,ca}}$	USD/g	0.0868	0.0795	0.0940	0.0395	0.0329	0.0438
Cathode binder mass fraction	$w_{\text{bin,ca}}$	unitless (fraction out of 1)	0.0284	0.0149	0.0448	0.0217	0.0163	0.0271
Cathode binder price	$p_{\text{bin,ca}}$	USD/g	0.0136	0.0095	0.0177	0.0165	0.0115	0.0253
Cathode conductor mass fraction	$w_{\text{con,ca}}$	unitless (fraction out of 1)	0.0666	0.0351	0.1052	0.0183	0.0137	0.0229
Cathode conductor price	$p_{\text{con,ca}}$	USD/g	0.0093	0.0065	0.0121	0.0084	0.0058	0.0118
Cathode active material specific charge capacity	q_{ca}	ampere hour per gram	0.139	0.137	0.140	0.180	0.152	0.188
Cathode material yield	y_{ca}	unitless (fraction out of 1)	0.889	0.808	0.970	0.922	0.894	0.950
N/P ratio	$(\text{N/P})_Q$	unitless (ratio of capacities)	1.403	1.100	1.822	1.068	1.000	1.152
Anode active material mass fraction	$w_{\text{act,an}}$	unitless (fraction out of 1)	0.901	0.860	0.940	0.941	0.920	0.954
Anode active material price	$p_{\text{act,an}}$	USD/g	0.0442	0.0268	0.0500	0.0189	0.0144	0.0213
Anode binder mass fraction	$w_{\text{bin,an}}$	unitless (fraction out of 1)	0.0790	0.0490	0.1090	0.0460	0.0330	0.0508
Anode binder price	$p_{\text{bin,an}}$	USD/g	0.0136	0.0095	0.0177	0.0115	0.0080	0.0149
Anode conductor mass fraction	$w_{\text{con,an}}$	unitless (fraction out of 1)	0.0200	0.0000	0.0400	0.0129	0.0000	0.0300
Anode conductor price	$p_{\text{con,an}}$	USD/g	0.0093	0.0065	0.0121	0.0084	0.0058	0.0118
Anode active material specific charge capacity	q_{an}	ampere hour per gram	0.334	0.314	0.357	0.361	0.357	0.362
Anode material yield	y_{an}	unitless (fraction out of 1)	0.880	0.830	0.930	0.922	0.894	0.950
Electrolyte solution mass to cathode charge capacity ratio	D_{el}	g/Ah	3.003	2.617	3.389	1.464	1.281	1.646
Electrolyte solution price	p_{el}	USD/g	0.0737	0.0656	0.0849	0.0191	0.0177	0.0210
Electrolyte solution yield	y_{el}	unitless (fraction out of 1)	0.875	0.820	0.930	0.940	0.900	0.980

Table S8: Data employed to calculate area-related cell cost components with bounds

Variable	Symbol	Units	Period 1: 1995–2000			Period 2: 2010–2015		
			Mid	Low	High	Mid	Low	High
Cathode foil area	a_{Al}	meters^2	0.0302	0.0271	0.0334	0.0395	0.0389	0.0401
Cathode foil thickness	t_{Al}	μm	24.32	20.00	25.40	19.26	14.00	30.00
Cathode foil price	p_{Al}	USD/g	0.0283	0.0198	0.0368	0.0146	0.0089	0.0183
Cathode foil yield	y_{Al}	unitless (fraction out of 1)	0.889	0.788	0.990	0.902	0.853	0.950
Anode foil to cathode foil area ratio	$(\mathrm{an/ca})_A$	unitless (ratio of areas)	1.075	1.002	1.123	1.028	1.000	1.094
Anode foil thickness	t_{Cu}	μm	17.82	17.78	18.00	14.40	8.00	20.00
Anode foil price	p_{Cu}	USD/g	0.0212	0.0148	0.0276	0.0196	0.0179	0.0232
Anode foil yield	y_{Cu}	unitless (fraction out of 1)	0.880	0.770	0.990	0.902	0.853	0.950
Separator to cathode foil area ratio	$(\mathrm{se/ca})_A$	unitless (ratio of areas)	2.422	2.179	2.560	2.299	2.058	2.427
Separator thickness	t_{se}	μm	25	25	25	18	12	23
Separator price	$p_{\mathrm{V,se}}$	10^6 USD/meters^3	0.200	0.145	0.255	0.077	0.061	0.091
Separator yield	y_{se}	unitless (fraction out of 1)	0.995	0.990	1.000	0.980	0.950	1.000

Table S9: Data employed to calculate other cell cost components and cell-level characteristics with bounds

Variable	Symbol	Units	Period 1: 1995–2000			Period 2: 2010–2015		
			Mid	Low	High	Mid	Low	High
Cell-level characteristics								
Charge capacity utilization	η_{util}	unitless (fraction out of 1)	0.836	0.775	0.907	0.952	0.930	0.973
Cathode charge capacity for a fixed volume	Q_{ca}	ampere hour per cell	1.726	1.614	1.883	3.129	2.992	3.255
Cell voltage	V	volts	3.642	3.600	3.660	3.659	3.617	3.703
Cell-level yield	y_{cell}	unitless (fraction out of 1)	0.990	0.900	1.000	0.992	0.970	1.000
Hardware cost component								
Other hardware price	p_{can}	USD/cell	0.559	0.464	0.653	0.469	0.390	0.548
Other hardware yield	y_{can}	unitless (fraction out of 1)	1.00	0.95	1.00	1.00	0.95	1.00
Plant size–dependent characteristics								
Material cost fraction	θ	unitless (fraction out of 1)	0.753	0.650	0.850	0.796	0.775	0.818
Plant size	K	10^6 cells per year	27	18	60	120	108	300
Scaling factor	b	unitless	0.30	0.21	0.39	0.30	0.21	0.39

9.2.1 Data-informed sensitivity analysis figures for mass-related variables

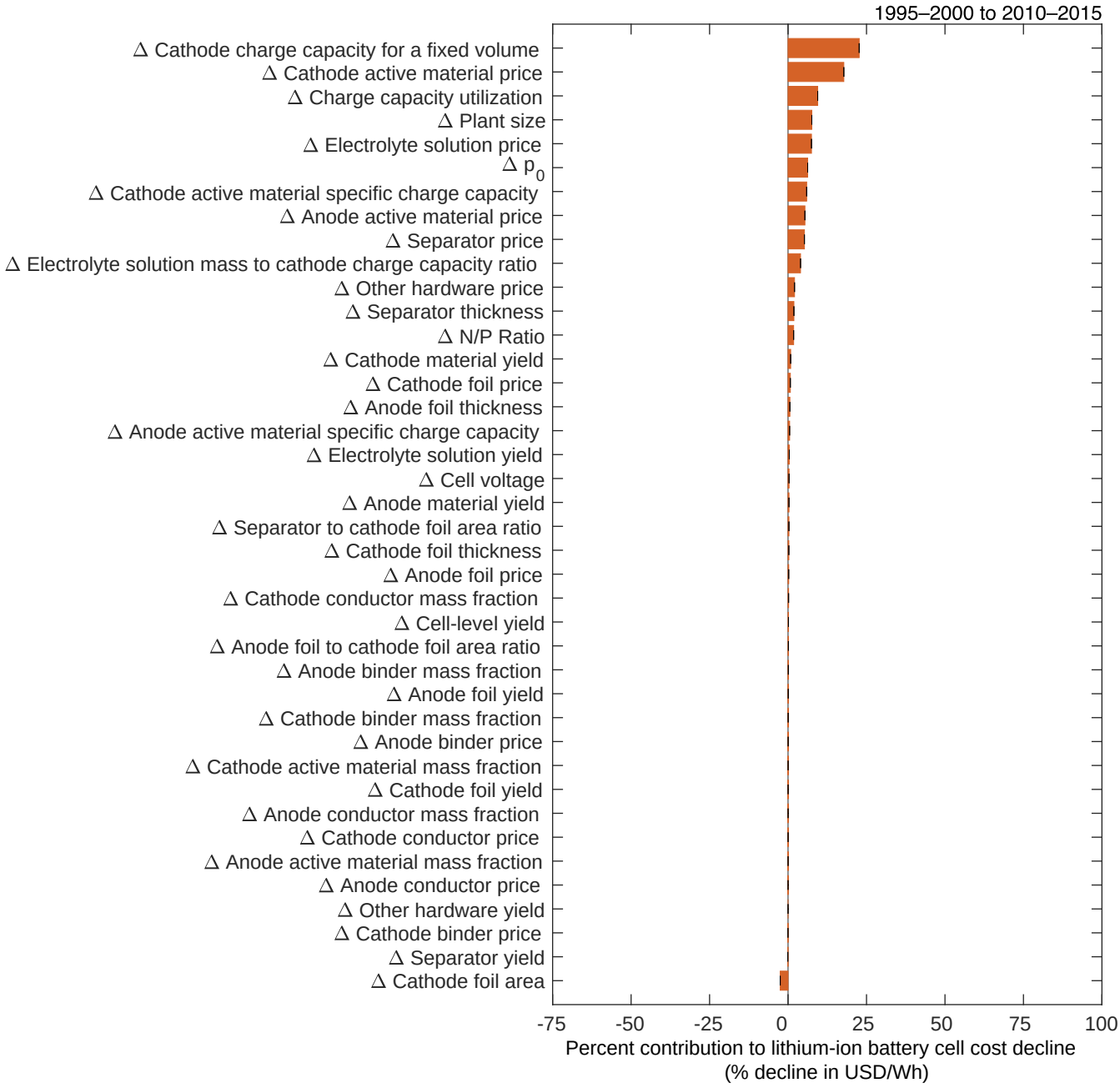

Figure S117: Sensitivity analysis for cathode active material mass fraction ($w_{\text{act,ca}}$). The value is varied in both periods to the lower and upper bounds given in Table S7, and for each combination, we recompute the contributions of the low-level mechanisms to cost change. The error bars show the minimum and maximum values of the low-level mechanisms' contributions to cost reduction.

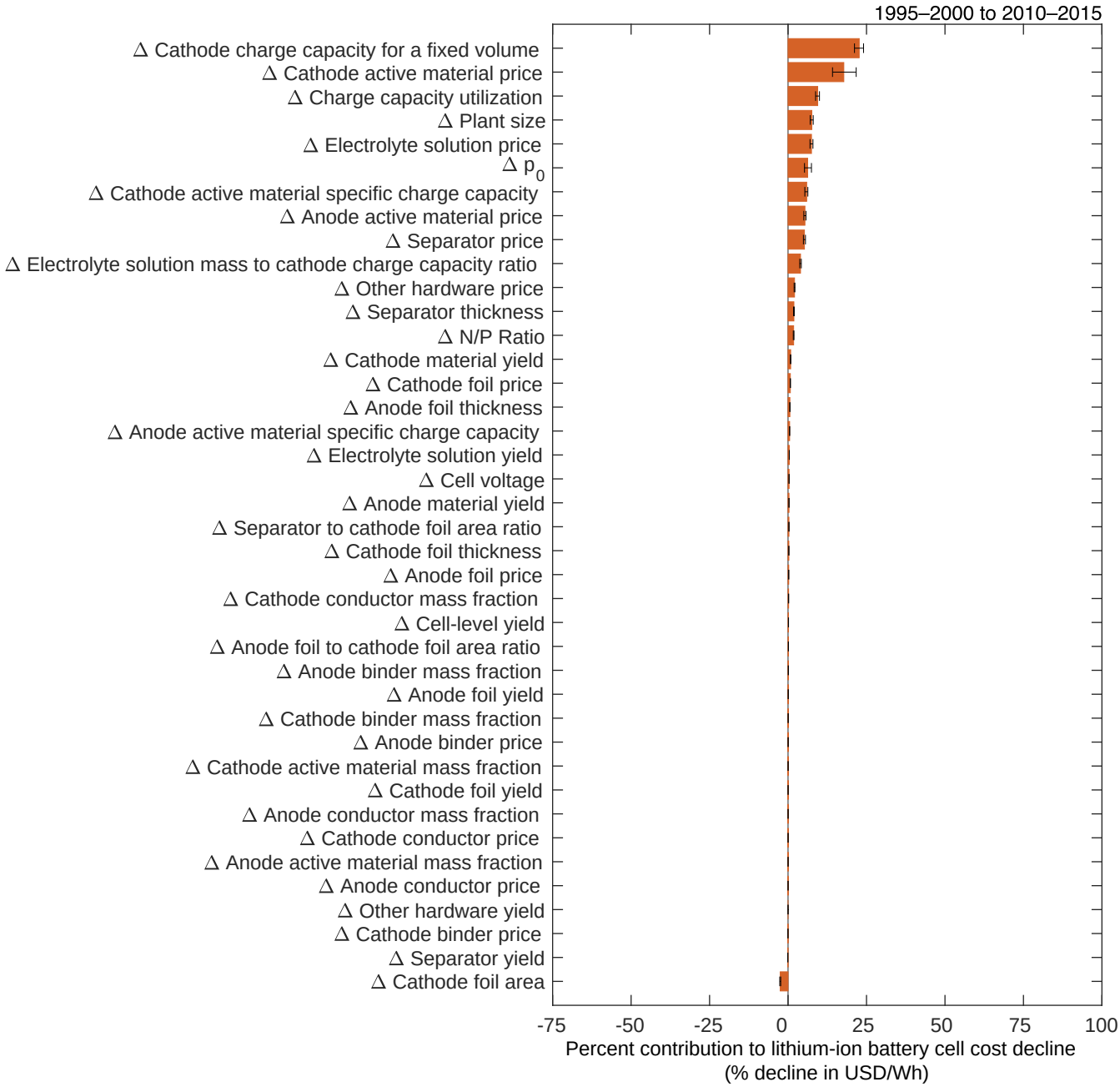

Figure S118: Sensitivity analysis for cathode active material price ($p_{\text{act,ca}}$). The value is varied in both periods to the lower and upper bounds given in Table S7, and for each combination, we recompute the contributions of the low-level mechanisms to cost change. The error bars show the minimum and maximum values of the low-level mechanisms' contributions to cost reduction.

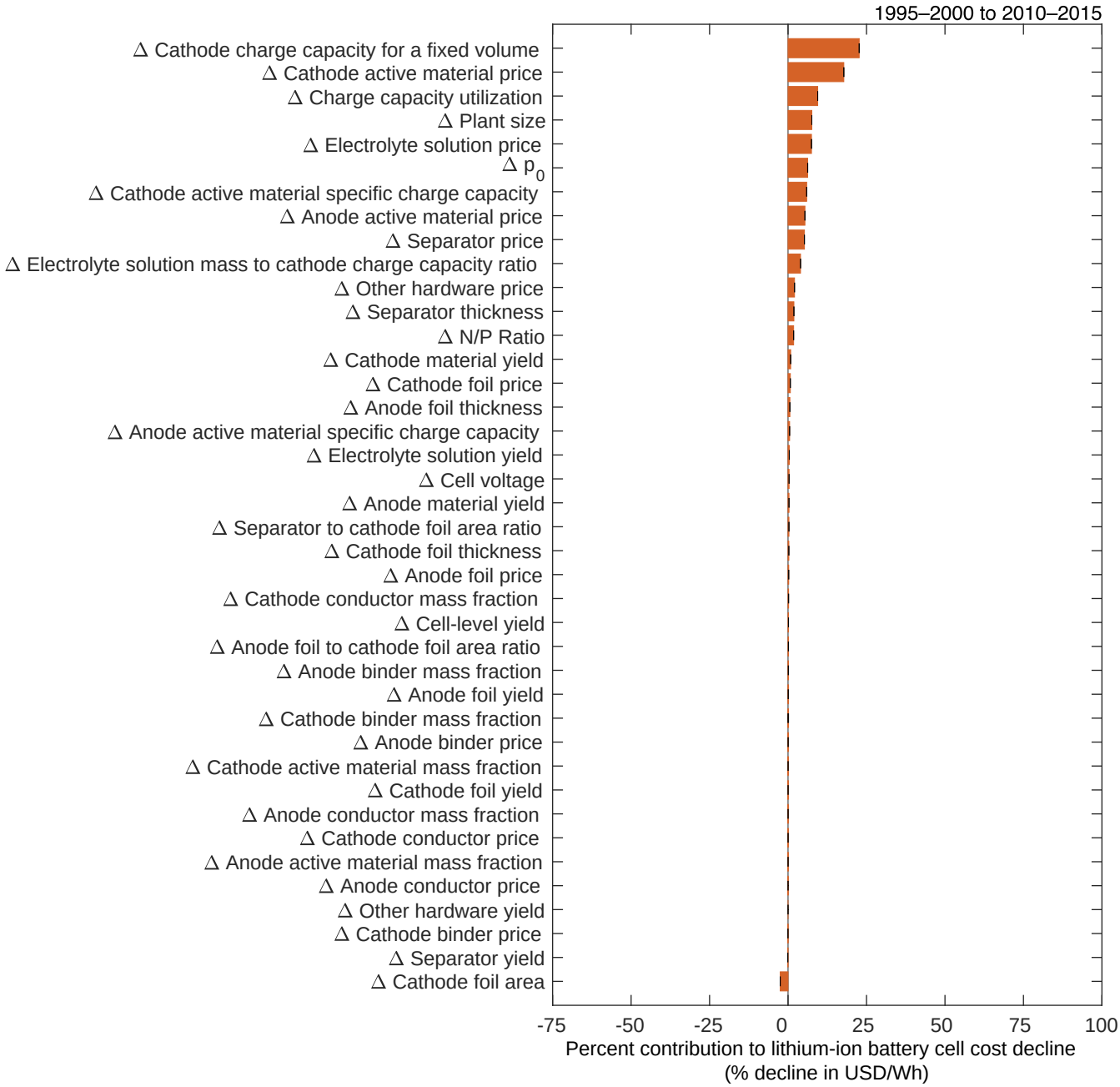

Figure S119: Sensitivity analysis for cathode binder mass fraction ($w_{\text{bin,ca}}$). The value is varied in both periods to the lower and upper bounds given in Table S7, and for each combination, we recompute the contributions of the low-level mechanisms to cost change. The error bars show the minimum and maximum values of the low-level mechanisms' contributions to cost reduction.

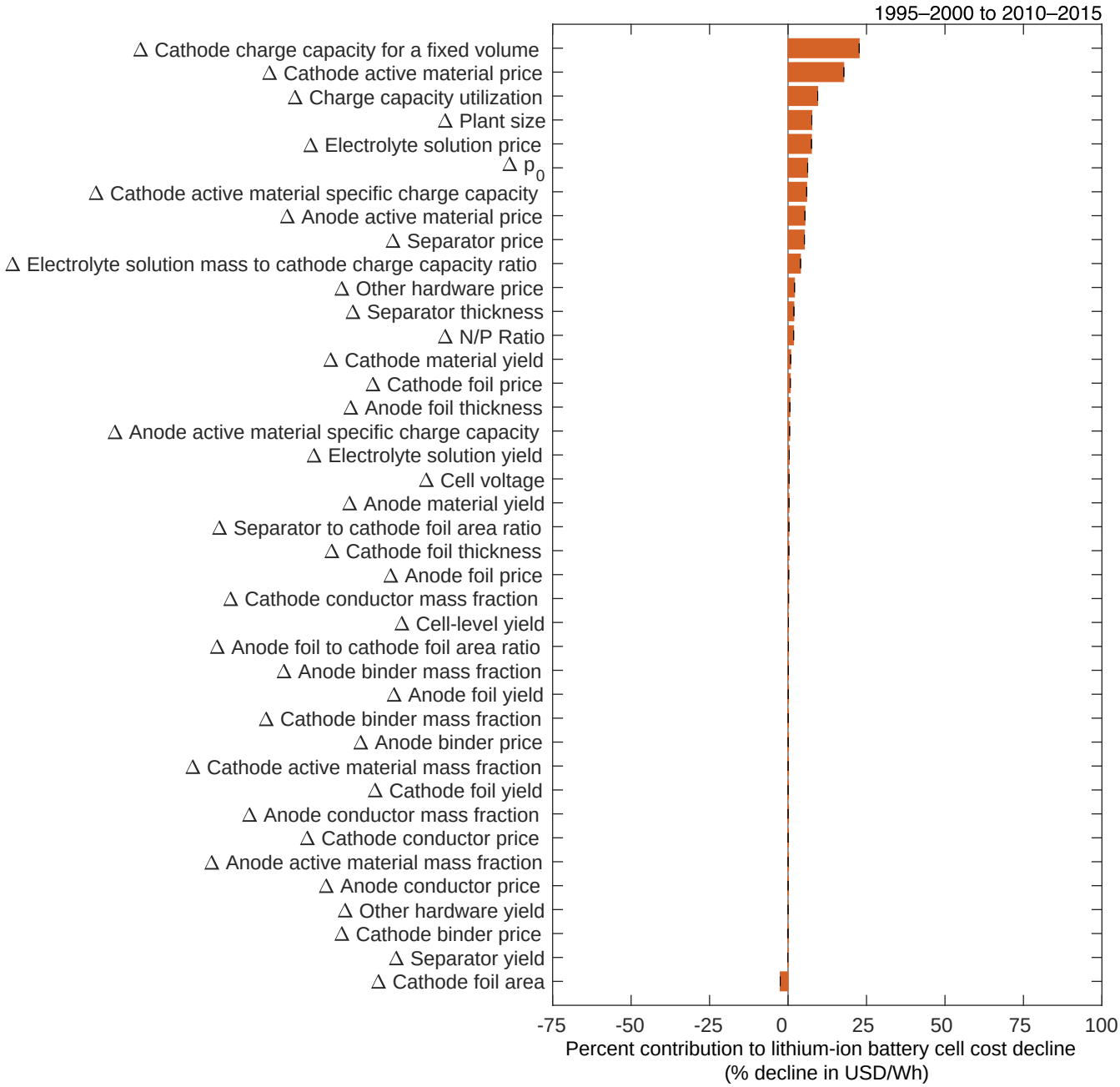

Figure S120: Sensitivity analysis for cathode binder price ($p_{\text{bin,ca}}$). The value is varied in both periods to the lower and upper bounds given in Table S7, and for each combination, we recompute the contributions of the low-level mechanisms to cost change. The error bars show the minimum and maximum values of the low-level mechanisms' contributions to cost reduction.

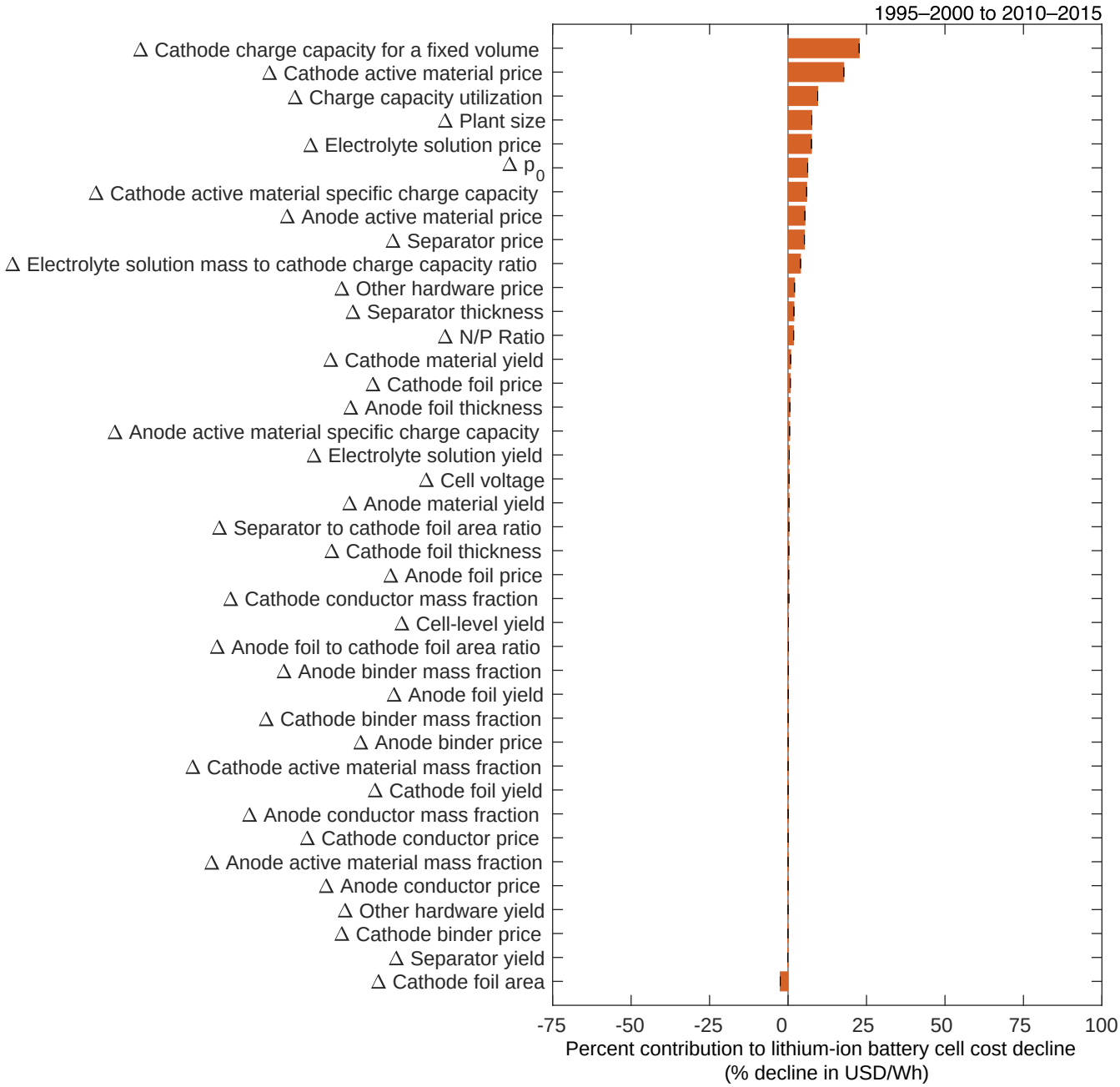

Figure S121: Sensitivity analysis for cathode conductor mass fraction ($w_{\text{con,ca}}$). The value is varied in both periods to the lower and upper bounds given in Table S7, and for each combination, we recompute the contributions of the low-level mechanisms to cost change. The error bars show the minimum and maximum values of the low-level mechanisms' contributions to cost reduction.

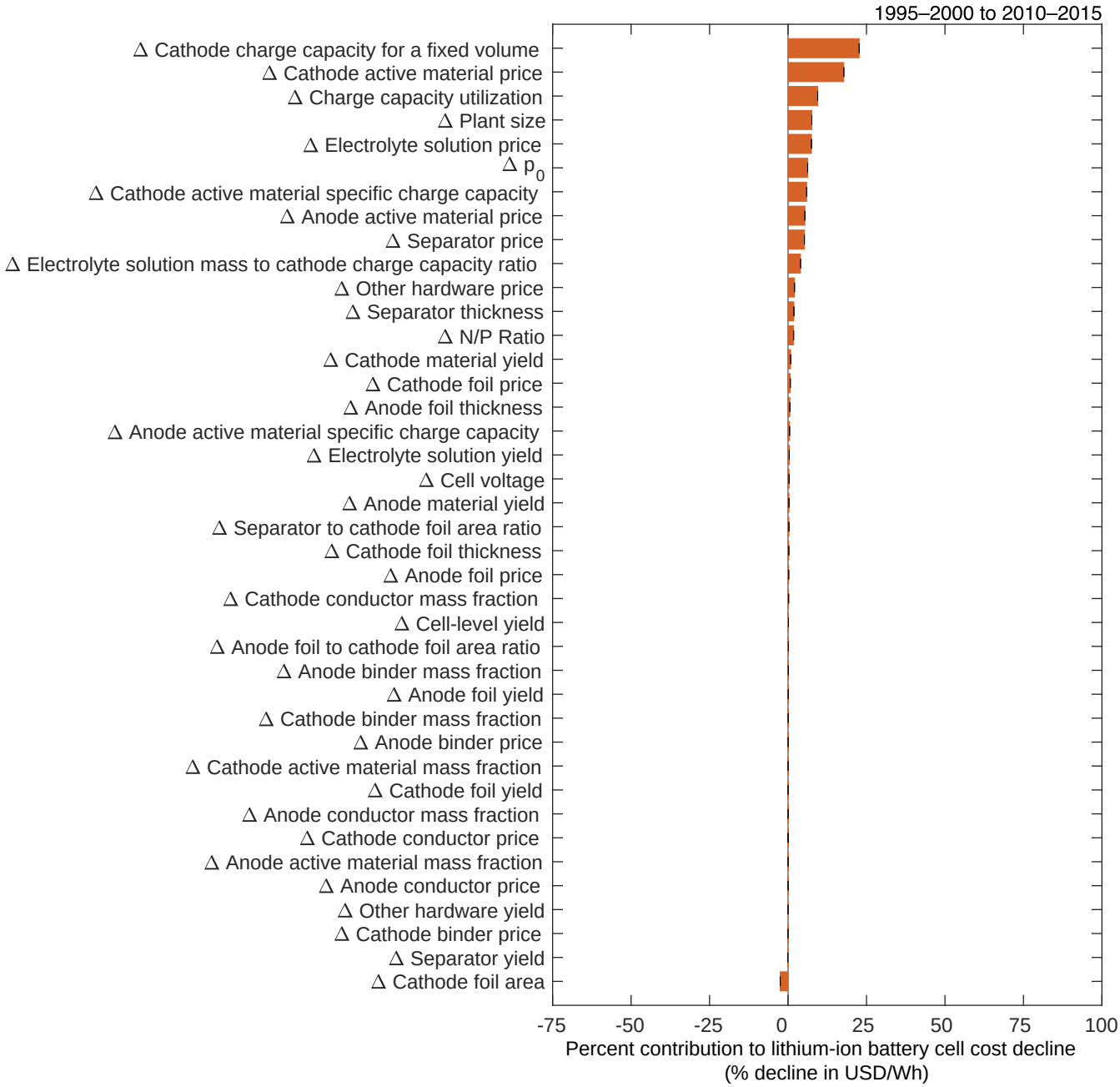

Figure S122: Sensitivity analysis for cathode conductor price ($p_{\text{con,ca}}$). The value is varied in both periods to the lower and upper bounds given in Table S7, and for each combination, we recompute the contributions of the low-level mechanisms to cost change. The error bars show the minimum and maximum values of the low-level mechanisms' contributions to cost reduction.

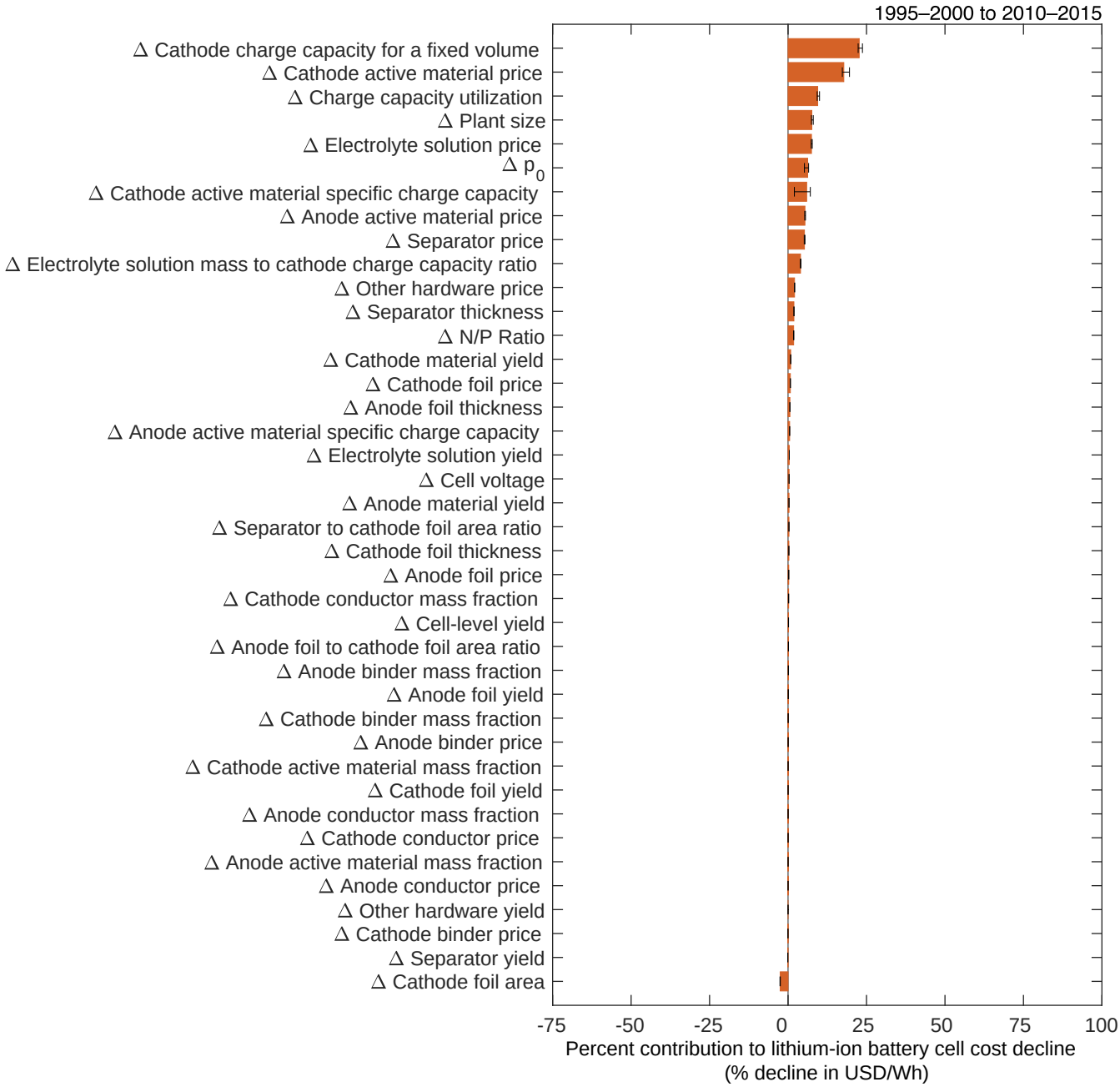

Figure S123: Sensitivity analysis for cathode active material specific charge capacity (q_{ca}). The value is varied in both periods to the lower and upper bounds given in Table S7, and for each combination, we recompute the contributions of the low-level mechanisms to cost change. The error bars show the minimum and maximum values of the low-level mechanisms' contributions to cost reduction.

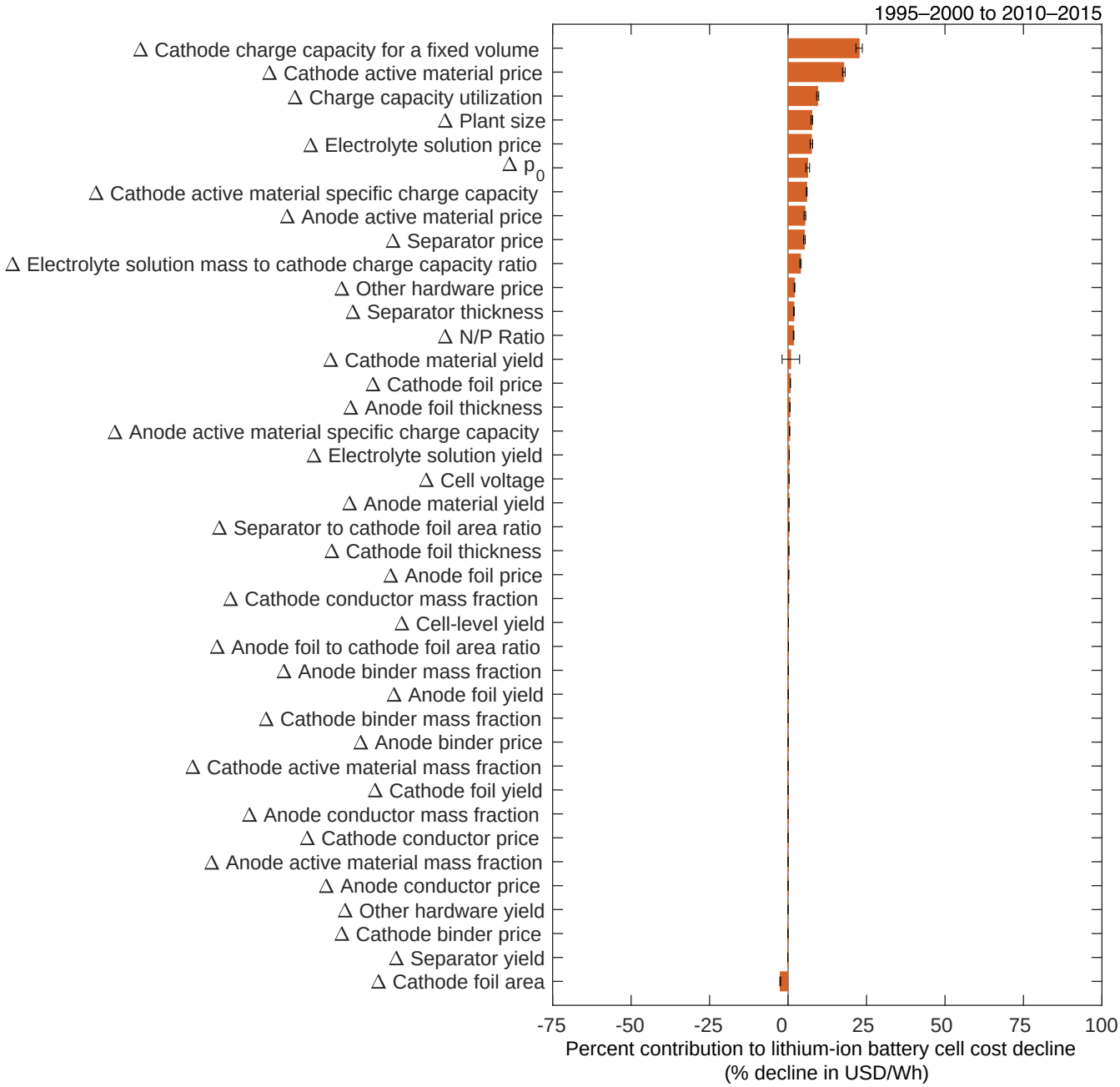

Figure S124: Sensitivity analysis for cathode material yield (y_{ca}). The value is varied in both periods to the lower and upper bounds given in Table S7, and for each combination, we recompute the contributions of the low-level mechanisms to cost change. The error bars show the minimum and maximum values of the low-level mechanisms' contributions to cost reduction.

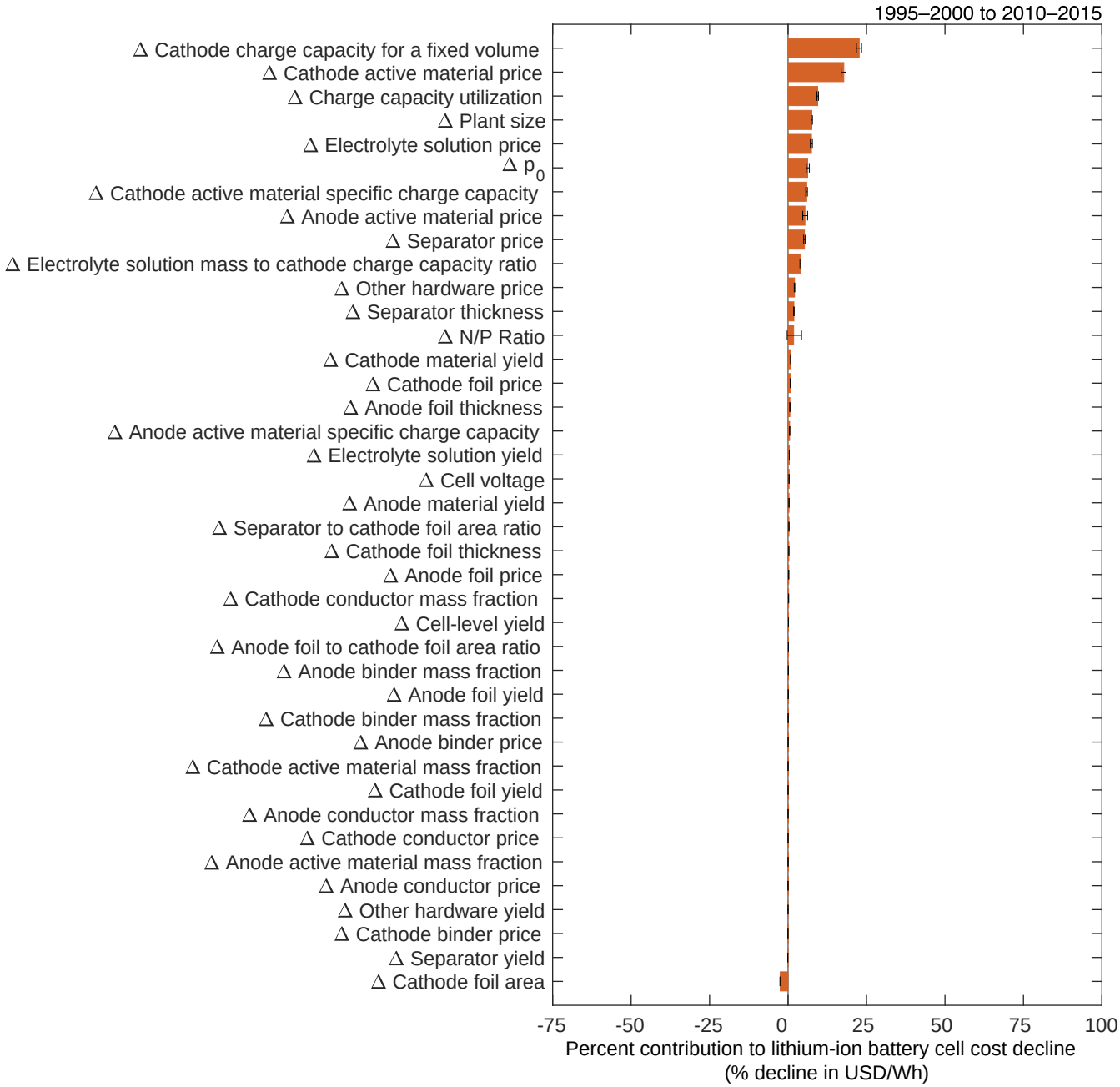

Figure S125: Sensitivity analysis for the N/P ratio ($(\mathrm{N/P})_Q$). The value is varied in both periods to the lower and upper bounds given in Table S7, and for each combination, we recompute the contributions of the low-level mechanisms to cost change. The error bars show the minimum and maximum values of the low-level mechanisms' contributions to cost reduction.

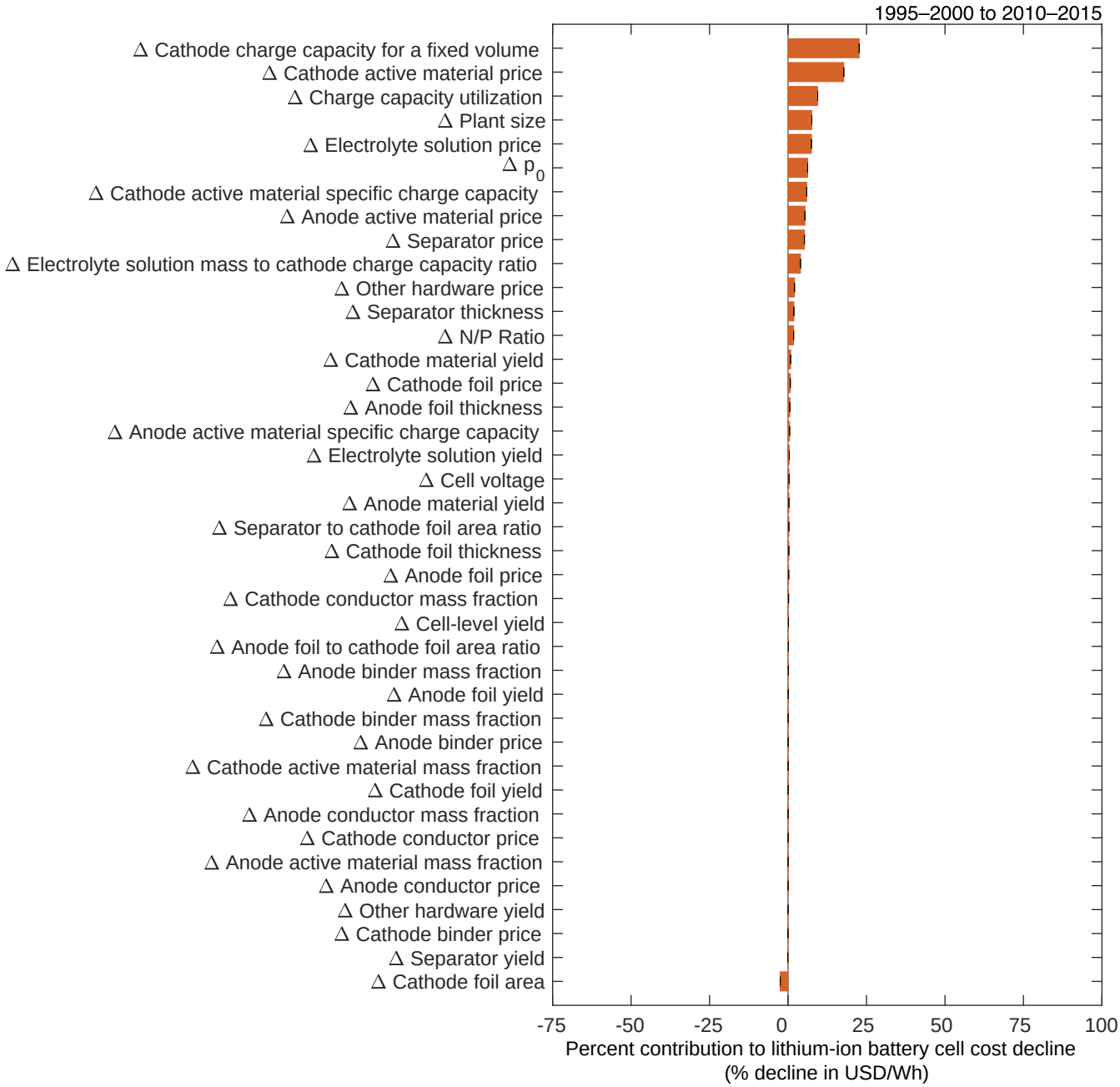

Figure S126: Sensitivity analysis for anode active material mass fraction ($w_{\text{act,an}}$). The value is varied in both periods to the lower and upper bounds given in Table S7, and for each combination, we recompute the contributions of the low-level mechanisms to cost change. The error bars show the minimum and maximum values of the low-level mechanisms' contributions to cost reduction.

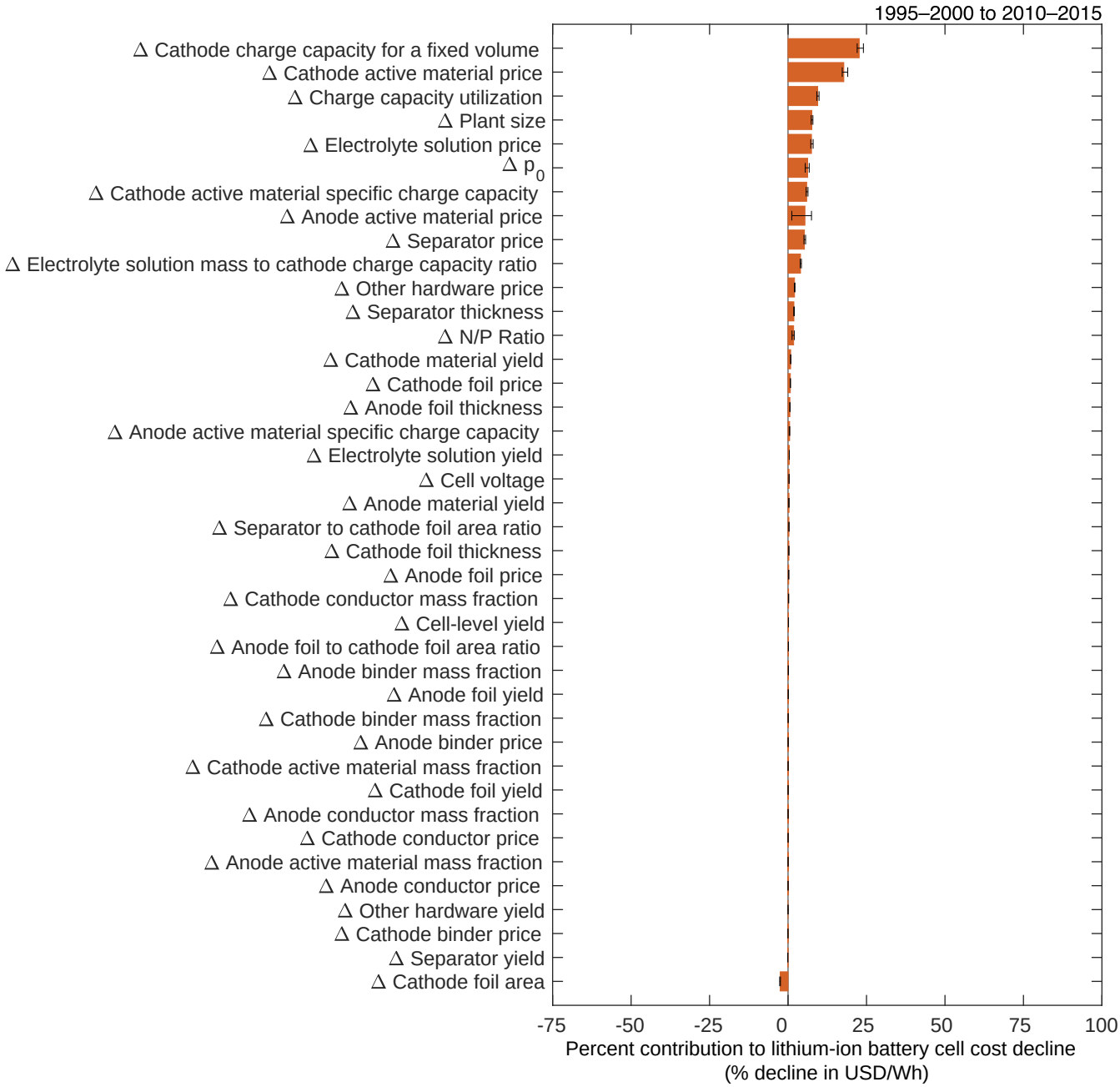

Figure S127: Sensitivity analysis for anode active material price ($p_{\text{act,an}}$). The value is varied in both periods to the lower and upper bounds given in Table S7, and for each combination, we recompute the contributions of the low-level mechanisms to cost change. The error bars show the minimum and maximum values of the low-level mechanisms' contributions to cost reduction.

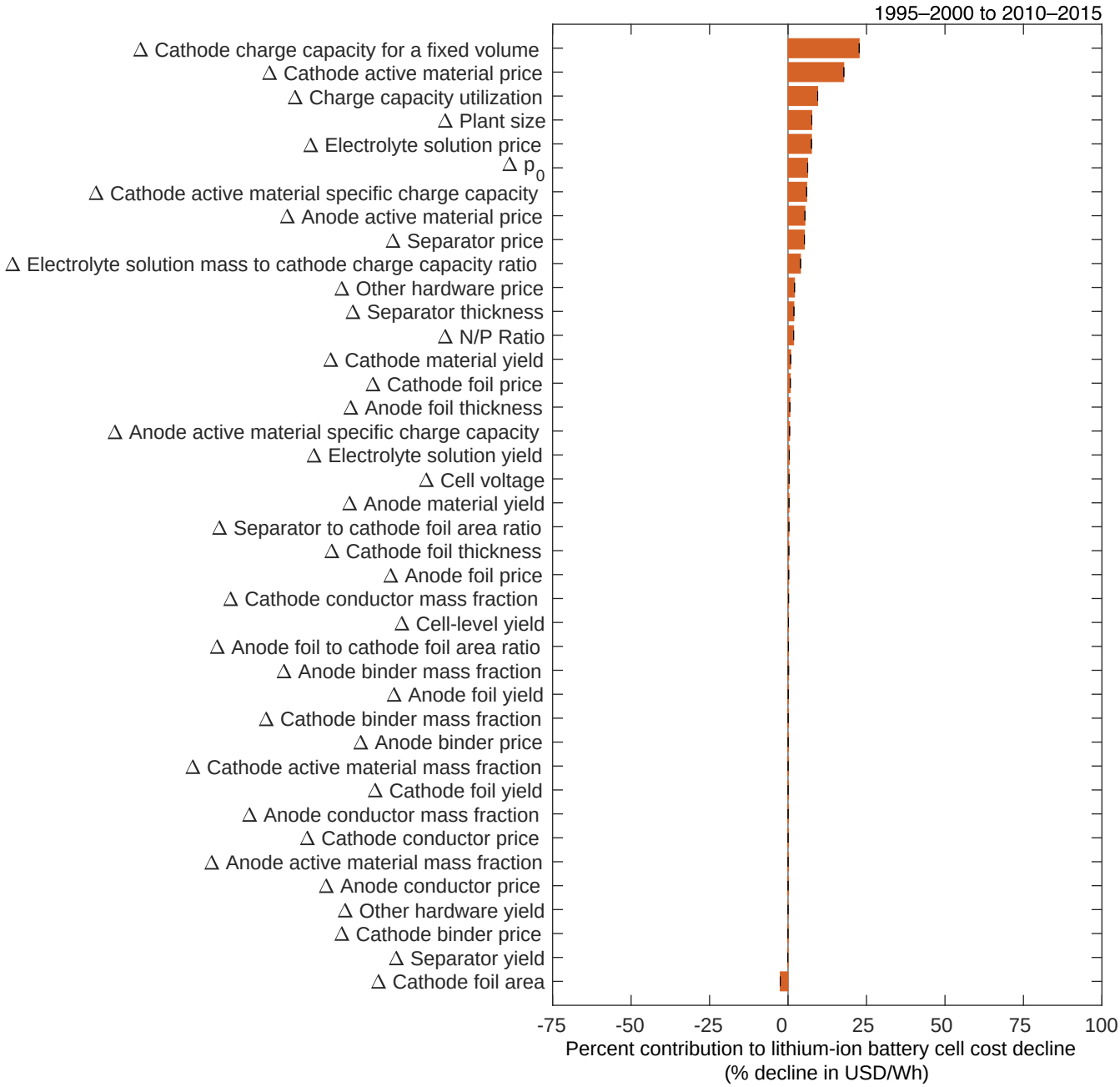

Figure S128: Sensitivity analysis for anode binder mass fraction ($w_{\text{bin,an}}$). The value is varied in both periods to the lower and upper bounds given in Table S7, and for each combination, we recompute the contributions of the low-level mechanisms to cost change. The error bars show the minimum and maximum values of the low-level mechanisms' contributions to cost reduction.

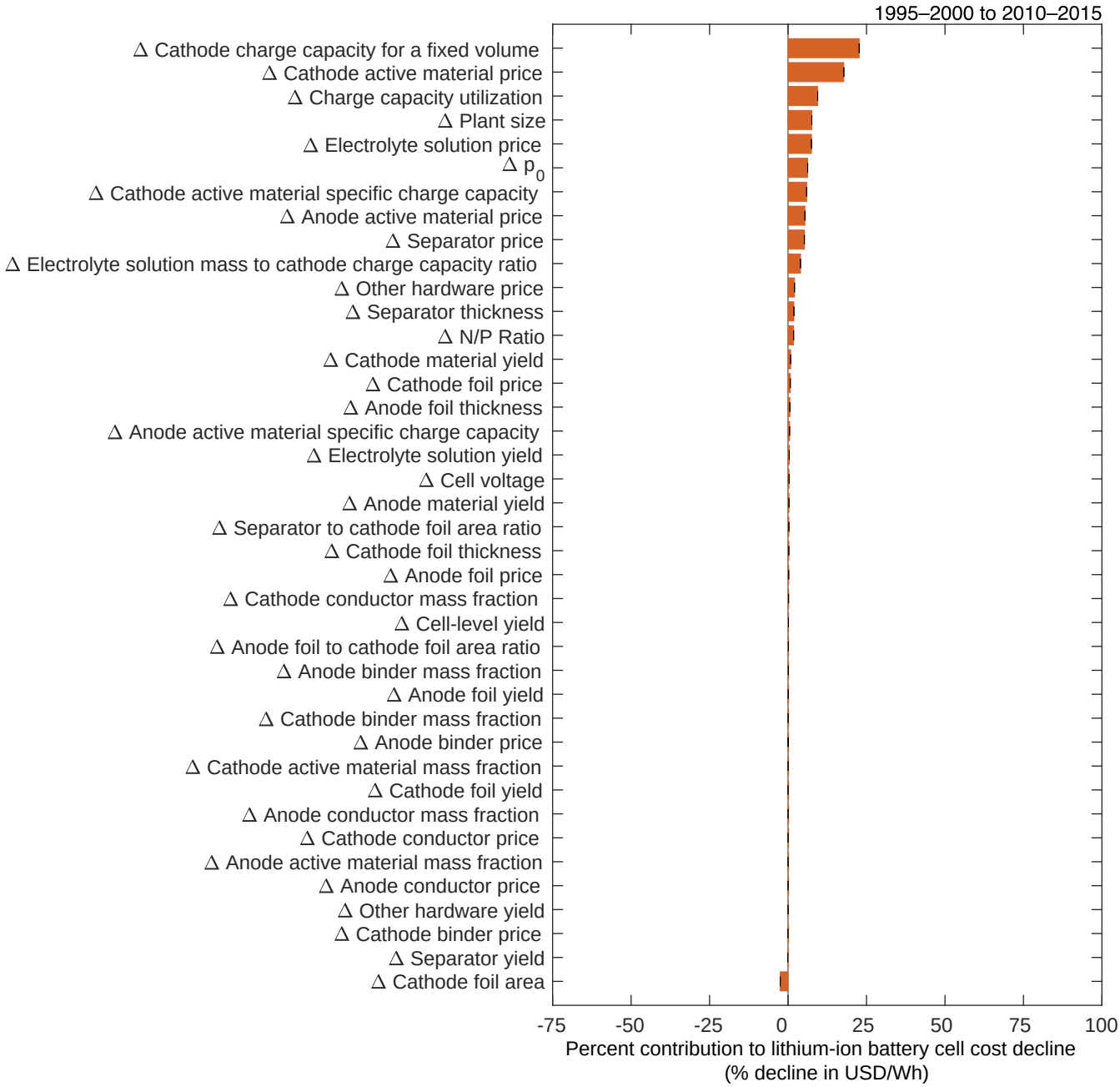

Figure S129: Sensitivity analysis for anode binder price ($p_{\text{bin,an}}$). The value is varied in both periods to the lower and upper bounds given in Table S7, and for each combination, we recompute the contributions of the low-level mechanisms to cost change. The error bars show the minimum and maximum values of the low-level mechanisms' contributions to cost reduction.

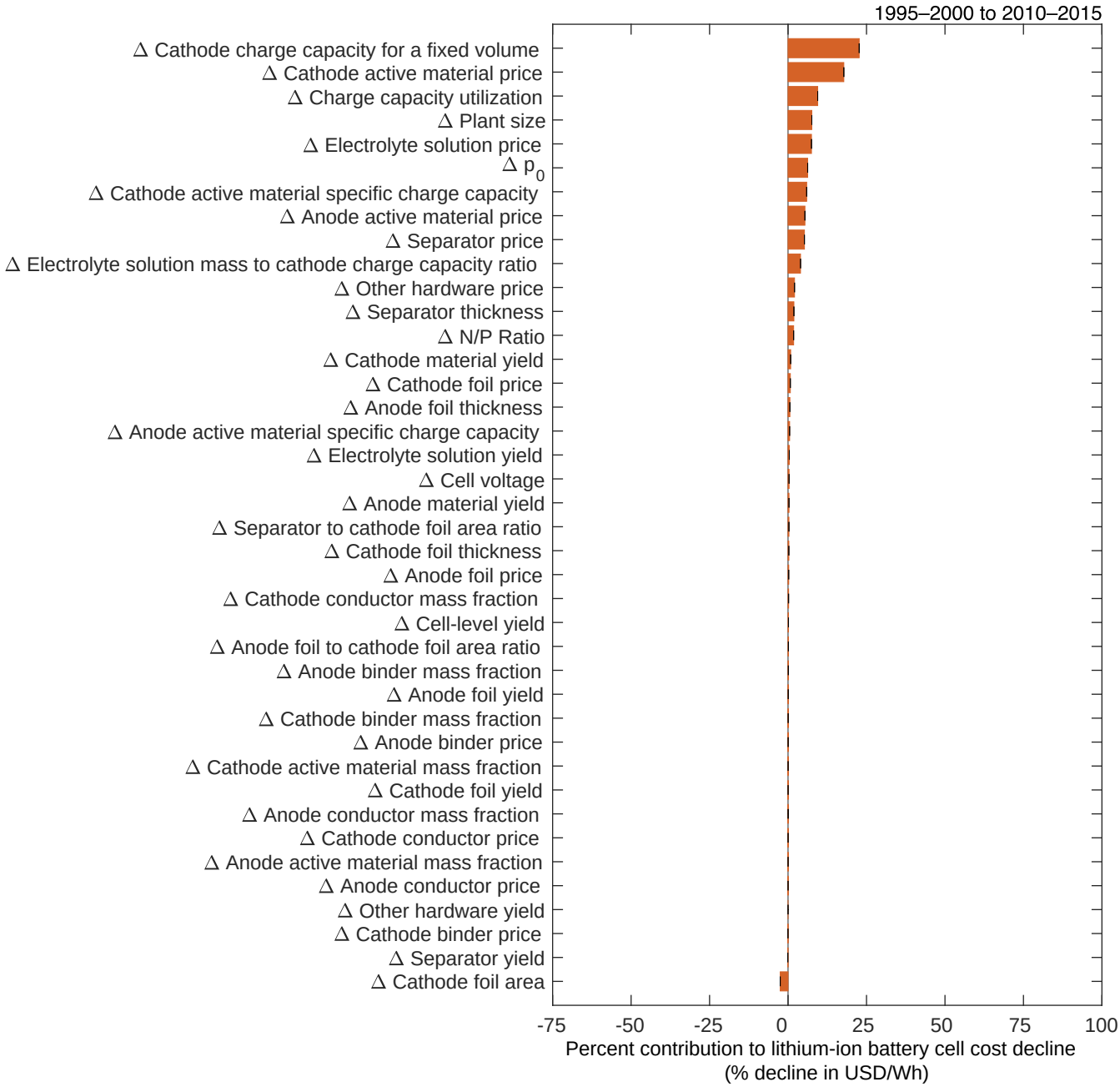

Figure S130: Sensitivity analysis for anode conductor mass fraction ($w_{\text{con,an}}$). The value is varied in both periods to the lower and upper bounds given in Table S7, and for each combination, we recompute the contributions of the low-level mechanisms to cost change. The error bars show the minimum and maximum values of the low-level mechanisms' contributions to cost reduction.

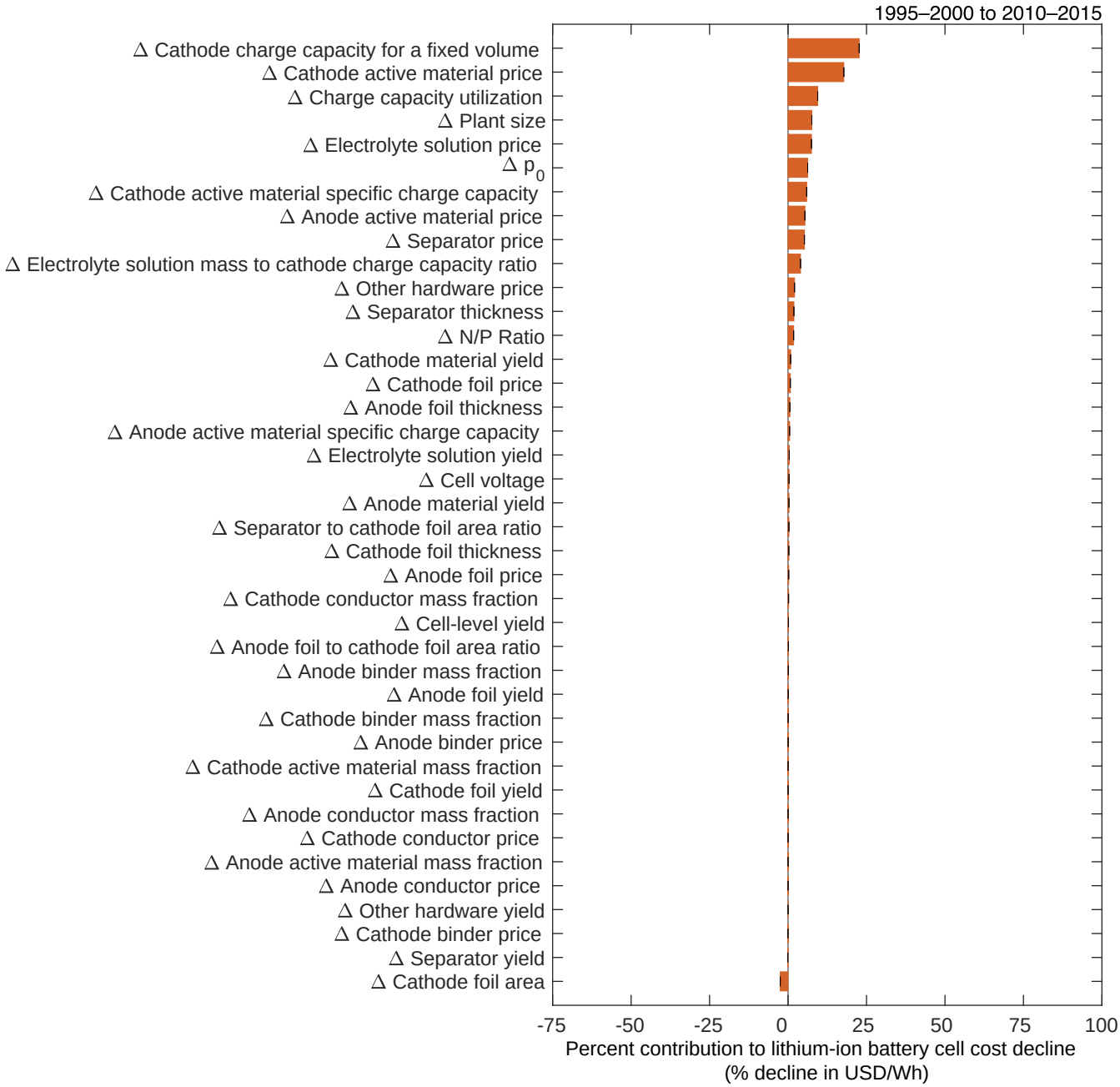

Figure S131: Sensitivity analysis for anode conductor price ($p_{\text{con,an}}$). The value is varied in both periods to the lower and upper bounds given in Table S7, and for each combination, we recompute the contributions of the low-level mechanisms to cost change. The error bars show the minimum and maximum values of the low-level mechanisms' contributions to cost reduction.

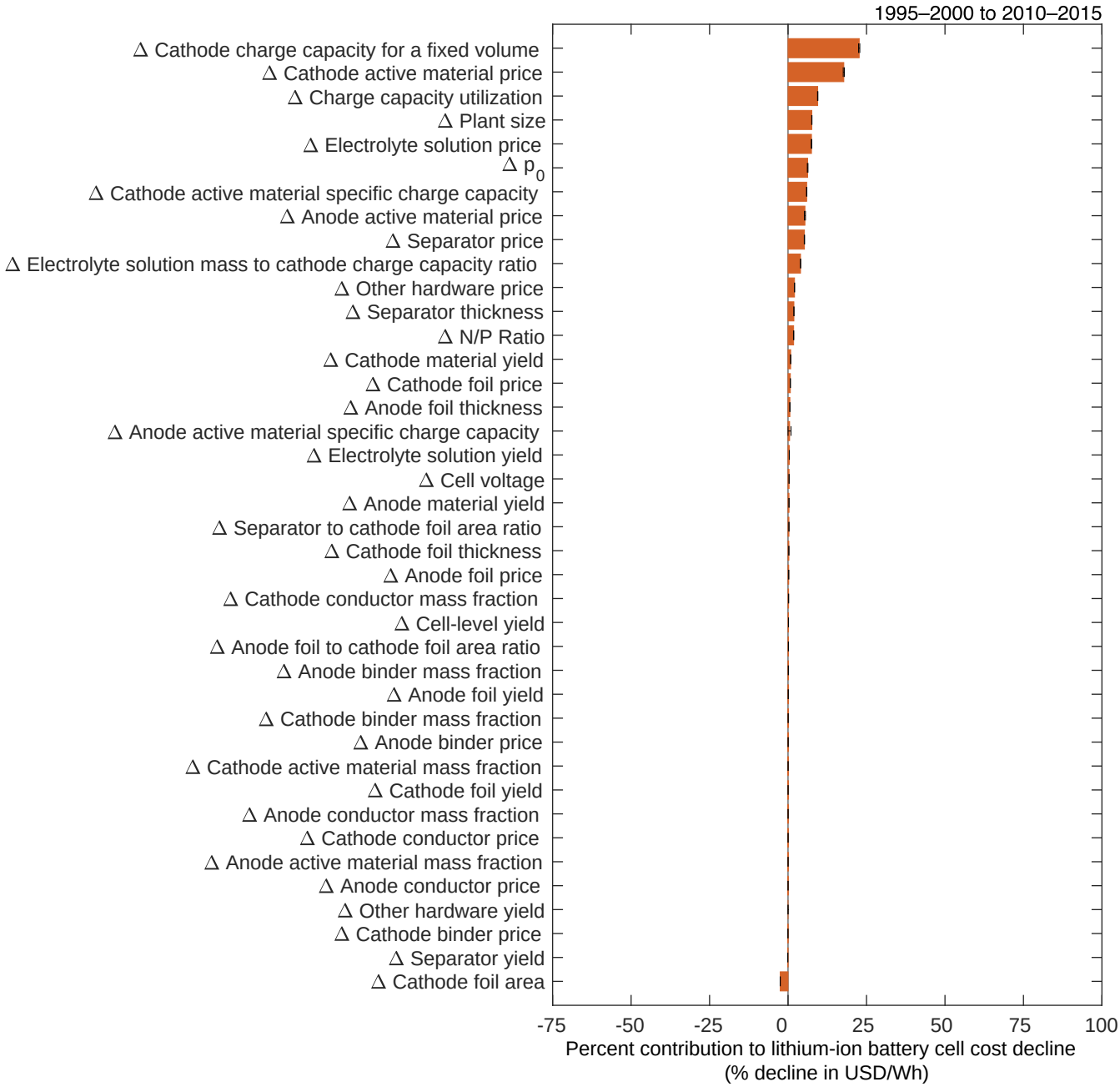

Figure S132: Sensitivity analysis for anode active material specific charge capacity (q_{an}). The value is varied in both periods to the lower and upper bounds given in Table S7, and for each combination, we recompute the contributions of the low-level mechanisms to cost change. The error bars show the minimum and maximum values of the low-level mechanisms' contributions to cost reduction.

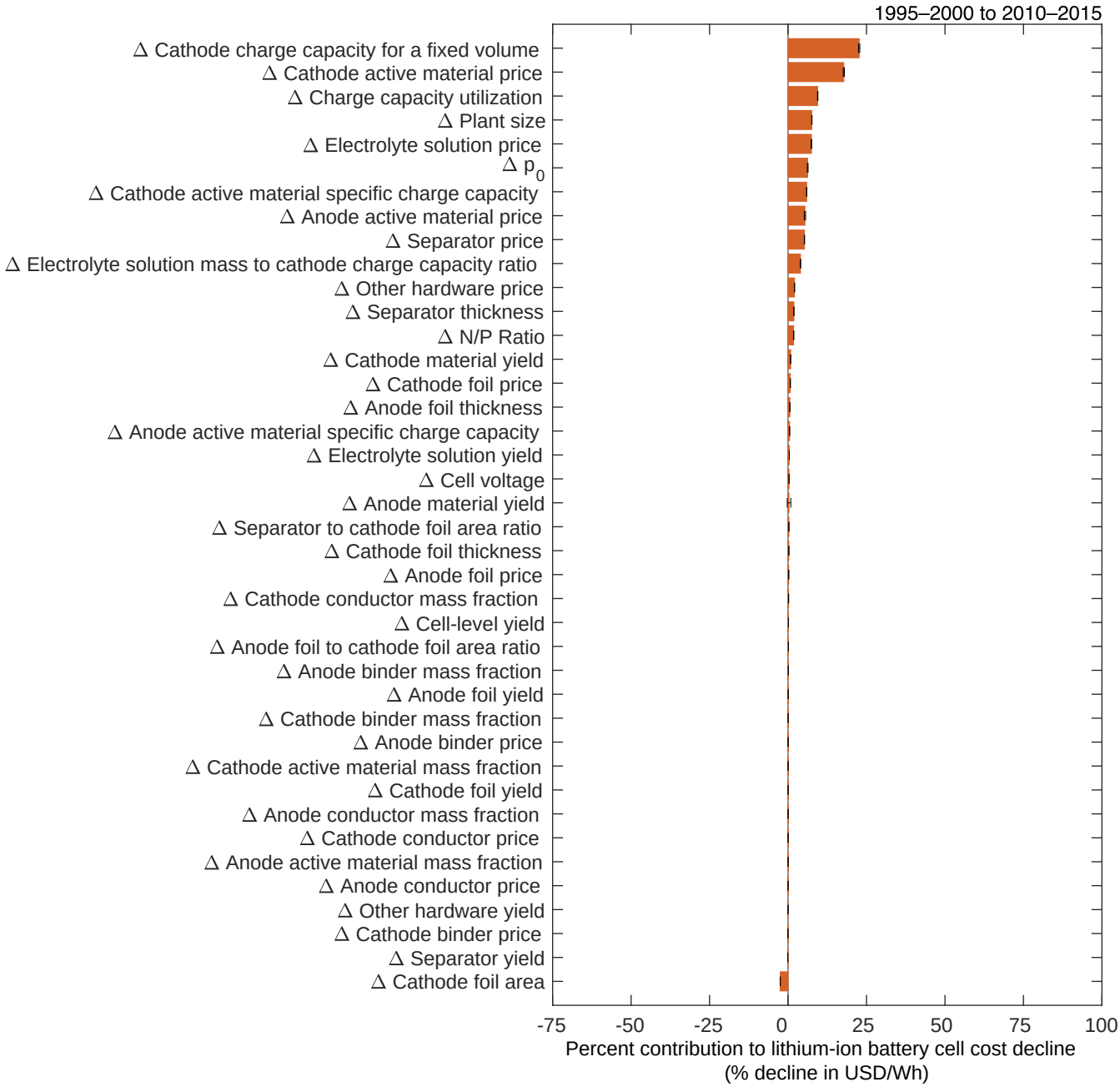

Figure S133: Sensitivity analysis for anode material yield (y_{an}). The value is varied in both periods to the lower and upper bounds given in Table S7, and for each combination, we recompute the contributions of the low-level mechanisms to cost change. The error bars show the minimum and maximum values of the low-level mechanisms' contributions to cost reduction.

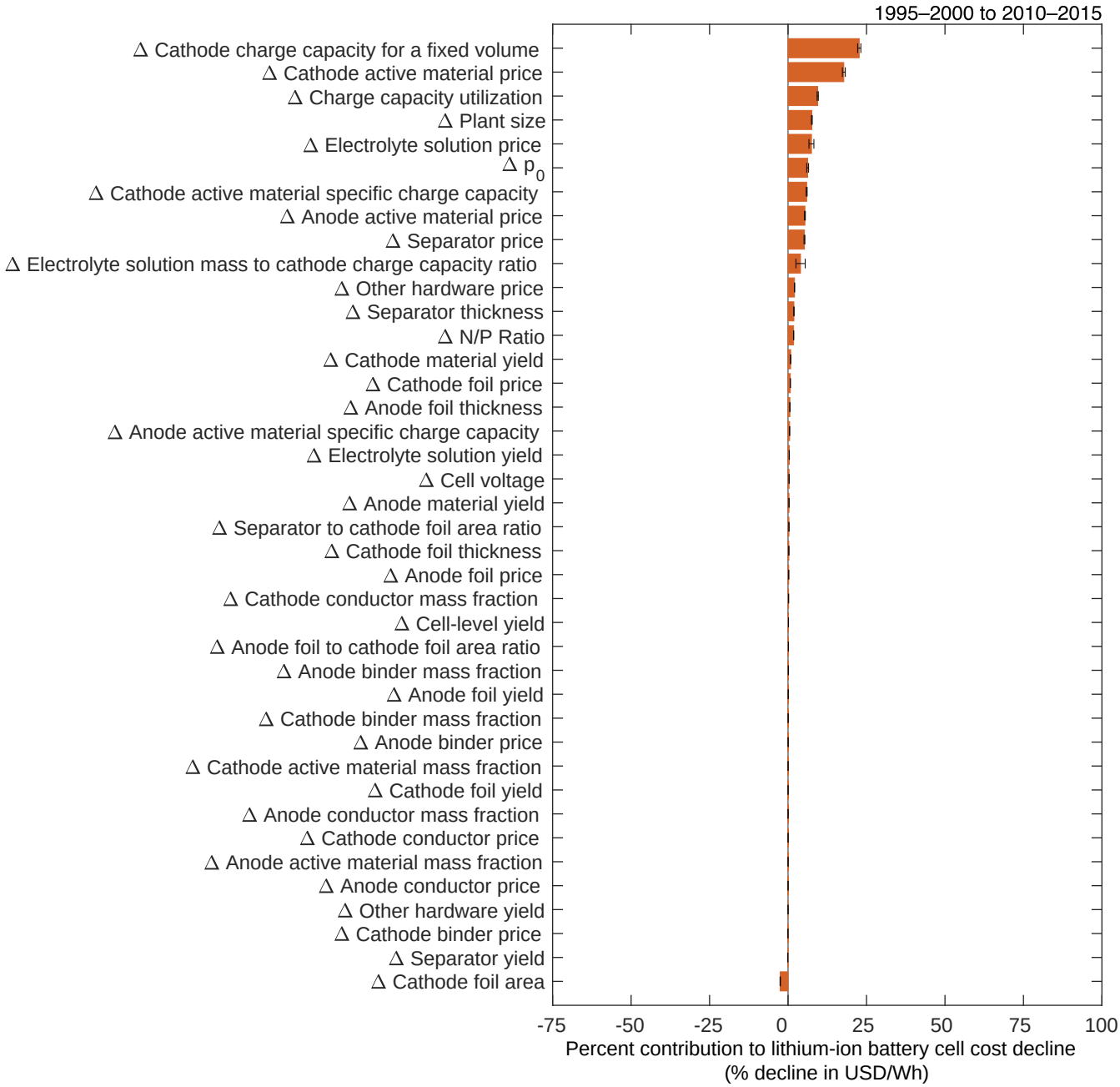

Figure S134: Sensitivity analysis for the ratio of electrolyte solution mass to cathode charge capacity (D_{el}). The value is varied in both periods to the lower and upper bounds given in Table S7, and for each combination, we recompute the contributions of the low-level mechanisms to cost change. The error bars show the minimum and maximum values of the low-level mechanisms' contributions to cost reduction.

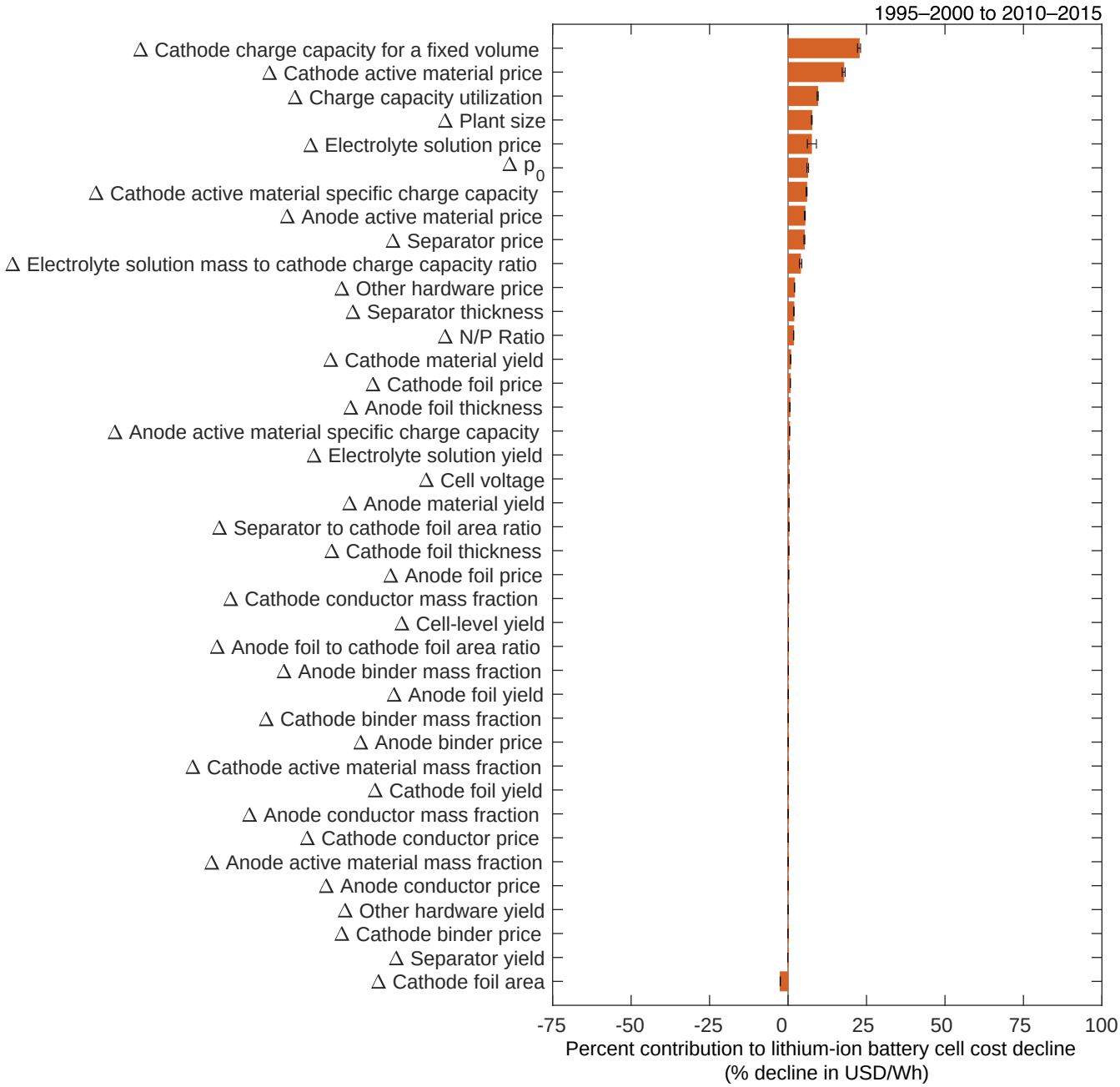

Figure S135: Sensitivity analysis for electrolyte solution price (p_{el}). The value is varied in both periods to the lower and upper bounds given in Table S7, and for each combination, we recompute the contributions of the low-level mechanisms to cost change. The error bars show the minimum and maximum values of the low-level mechanisms' contributions to cost reduction.

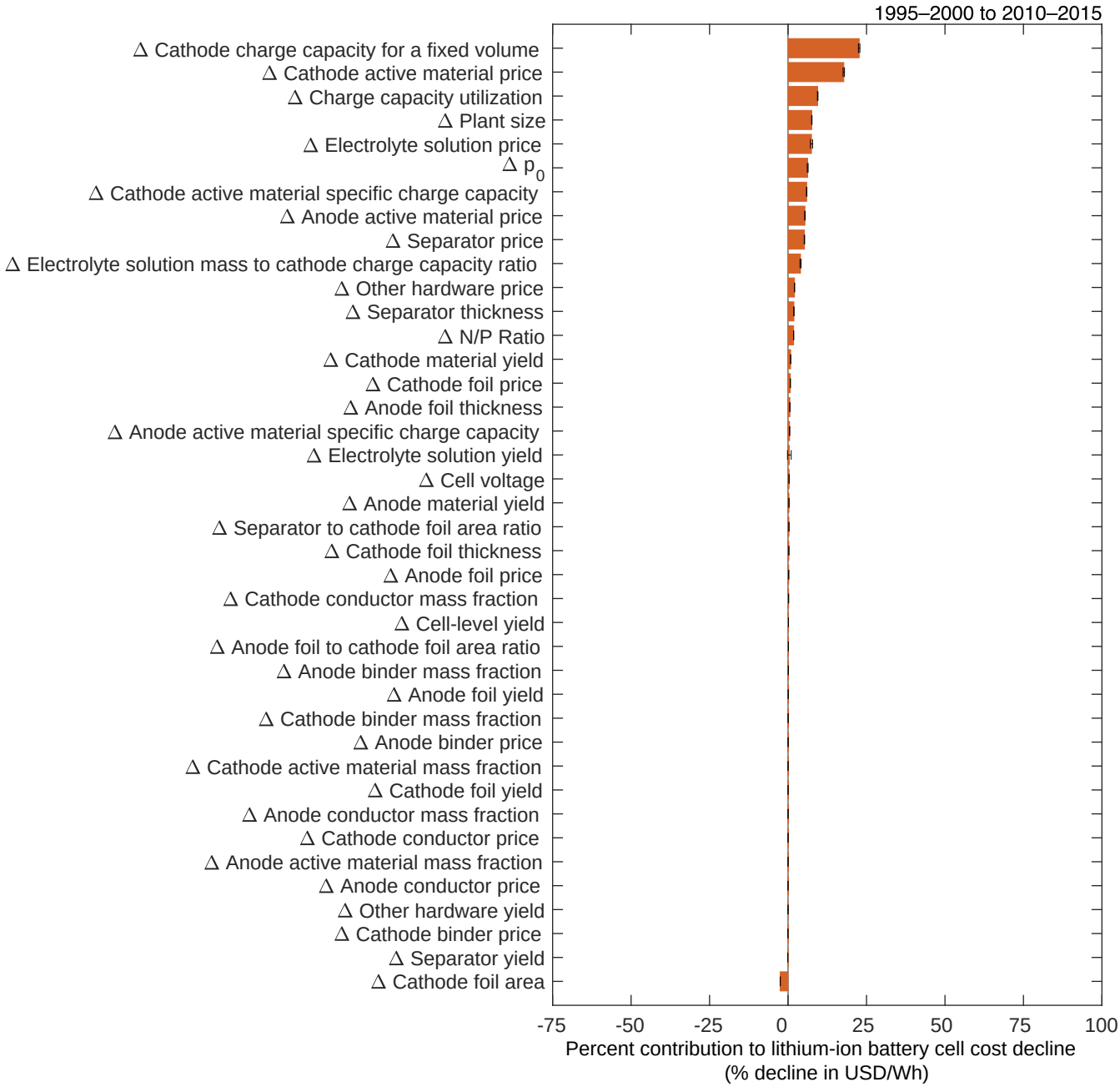

Figure S136: Sensitivity analysis for electrolyte solution yield (y_{el}). The value is varied in both periods to the lower and upper bounds given in Table S7, and for each combination, we recompute the contributions of the low-level mechanisms to cost change. The error bars show the minimum and maximum values of the low-level mechanisms' contributions to cost reduction.

9.2.2 Data-informed sensitivity analysis figures for area-related variables

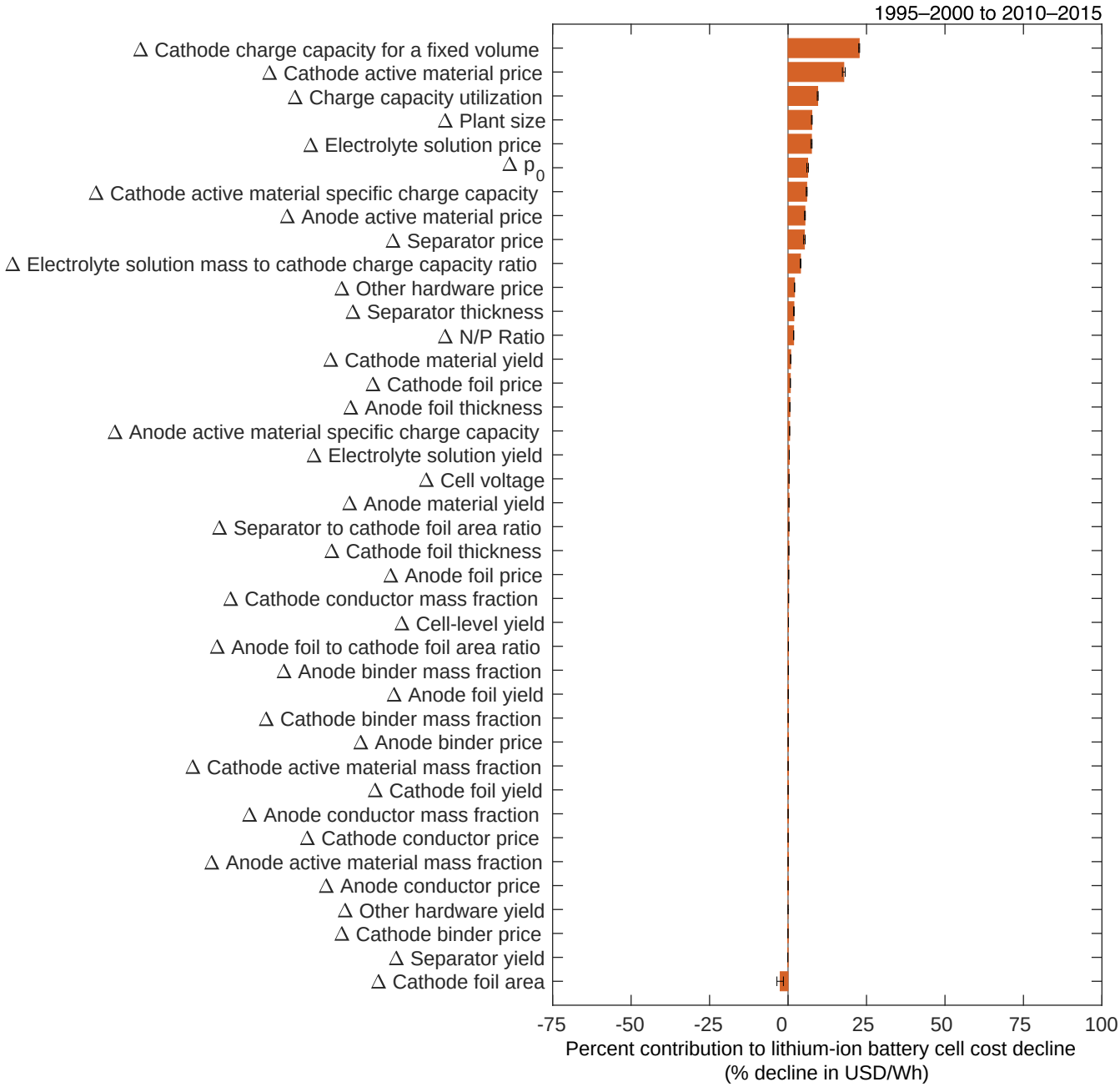

Figure S137: Sensitivity analysis for cathode foil area (a_{Al}). The value is varied in both periods to the lower and upper bounds given in Table S8, and for each combination, we recompute the contributions of the low-level mechanisms to cost change. The error bars show the minimum and maximum values of the low-level mechanisms' contributions to cost reduction.

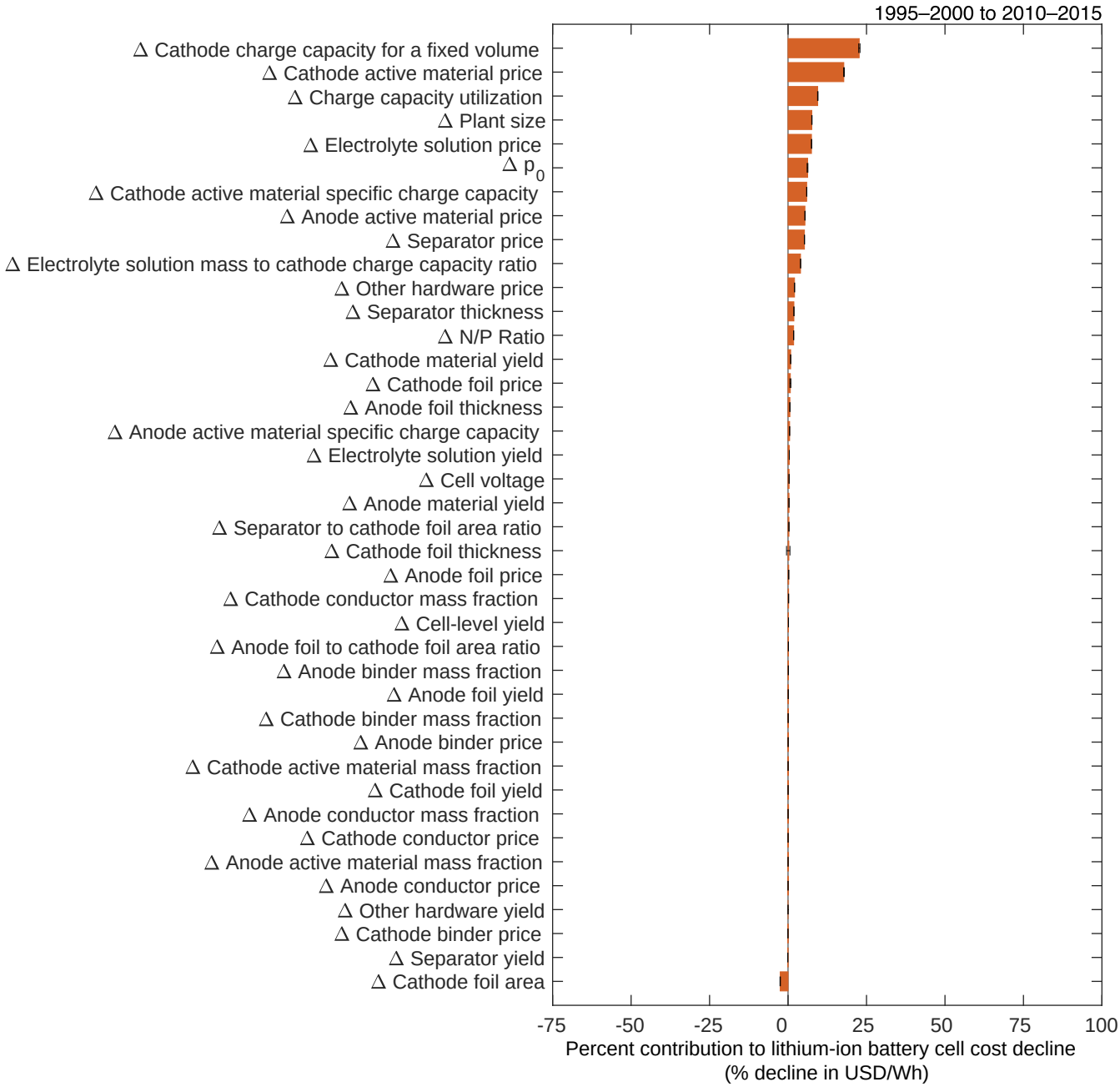

Figure S138: Sensitivity analysis for cathode foil thickness (t_{Al}). The value is varied in both periods to the lower and upper bounds given in Table S8, and for each combination, we recompute the contributions of the low-level mechanisms to cost change. The error bars show the minimum and maximum values of the low-level mechanisms' contributions to cost reduction.

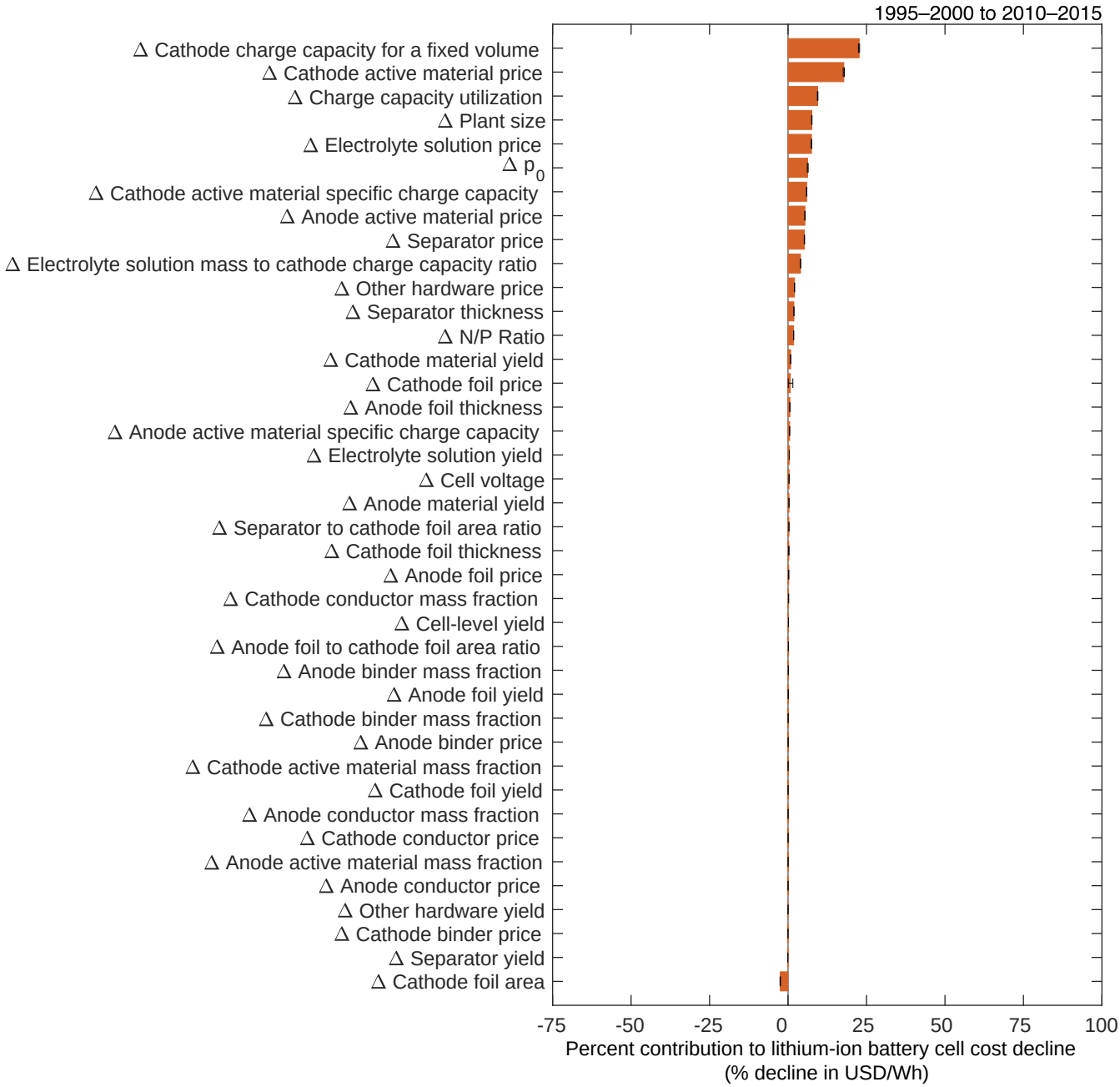

Figure S139: Sensitivity analysis for cathode foil price (p_{Al}). The value is varied in both periods to the lower and upper bounds given in Table S8, and for each combination, we recompute the contributions of the low-level mechanisms to cost change. The error bars show the minimum and maximum values of the low-level mechanisms' contributions to cost reduction.

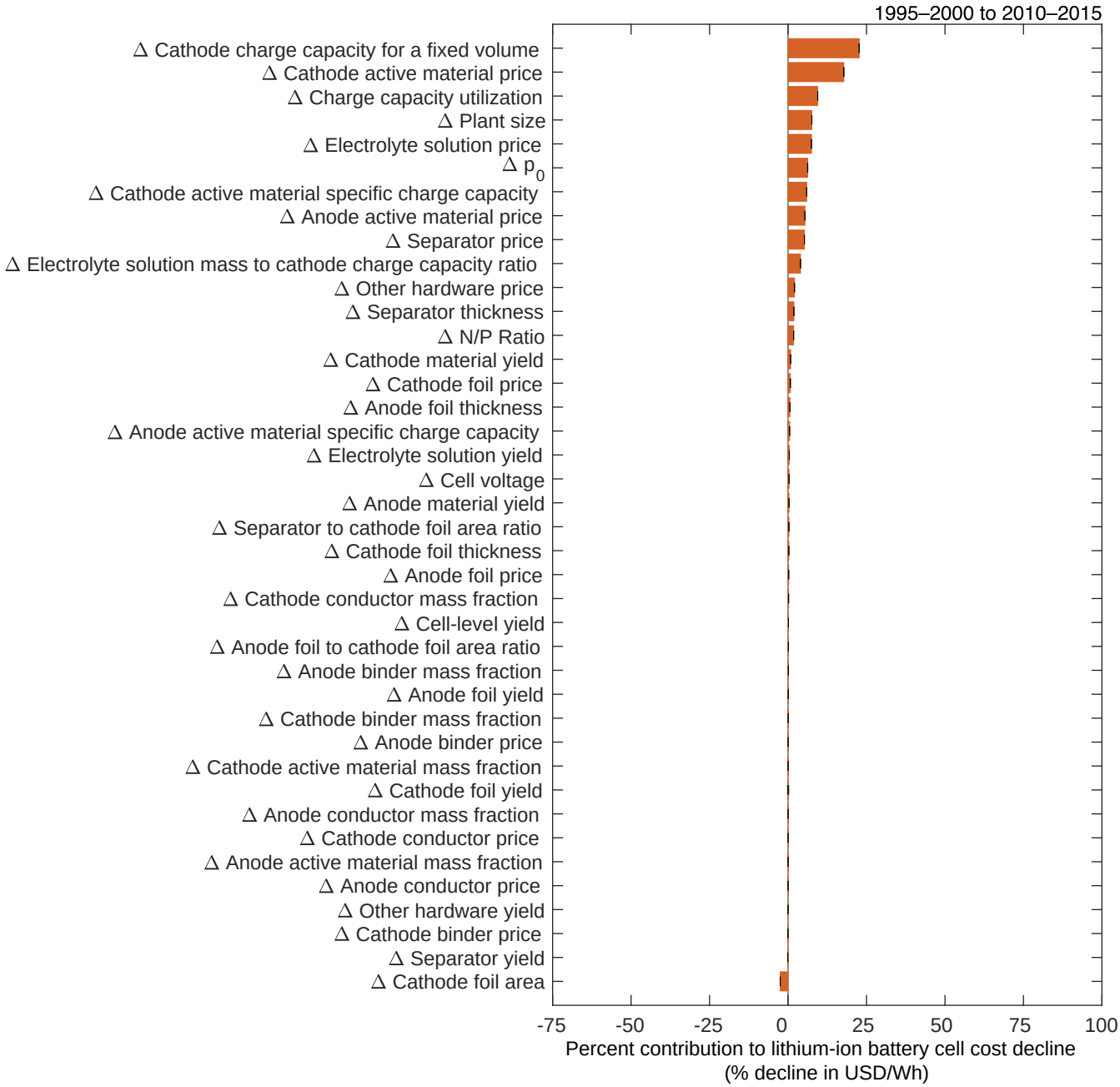

Figure S140: Sensitivity analysis for cathode foil yield (y_{Al}). The value is varied in both periods to the lower and upper bounds given in Table S8, and for each combination, we recompute the contributions of the low-level mechanisms to cost change. The error bars show the minimum and maximum values of the low-level mechanisms' contributions to cost reduction.

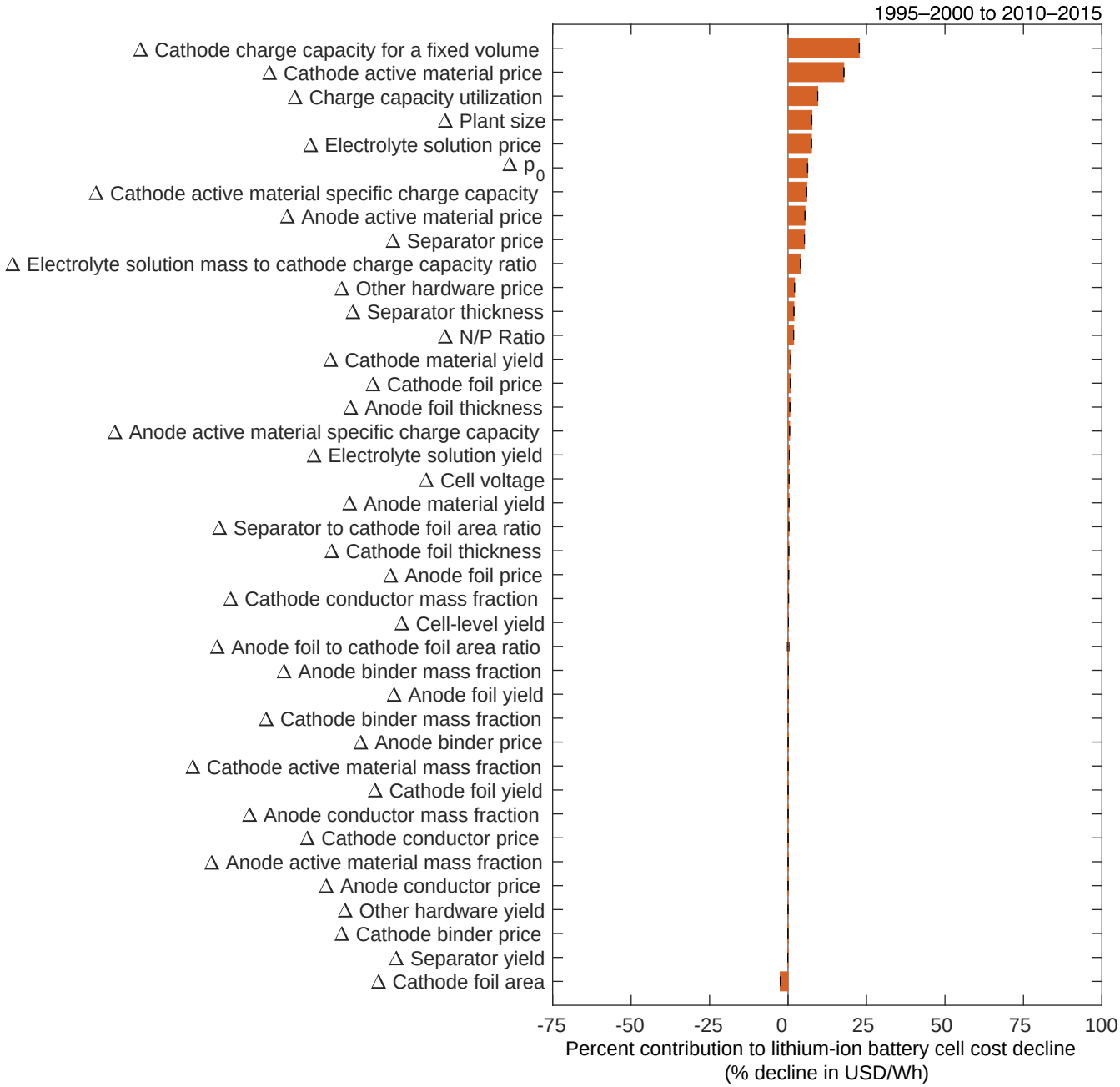

Figure S141: Sensitivity analysis for anode foil to cathode foil area ratio ($(\text{an/ca})_A$). The value is varied in both periods to the lower and upper bounds given in Table S8, and for each combination, we recompute the contributions of the low-level mechanisms to cost change. The error bars show the minimum and maximum values of the low-level mechanisms' contributions to cost reduction.

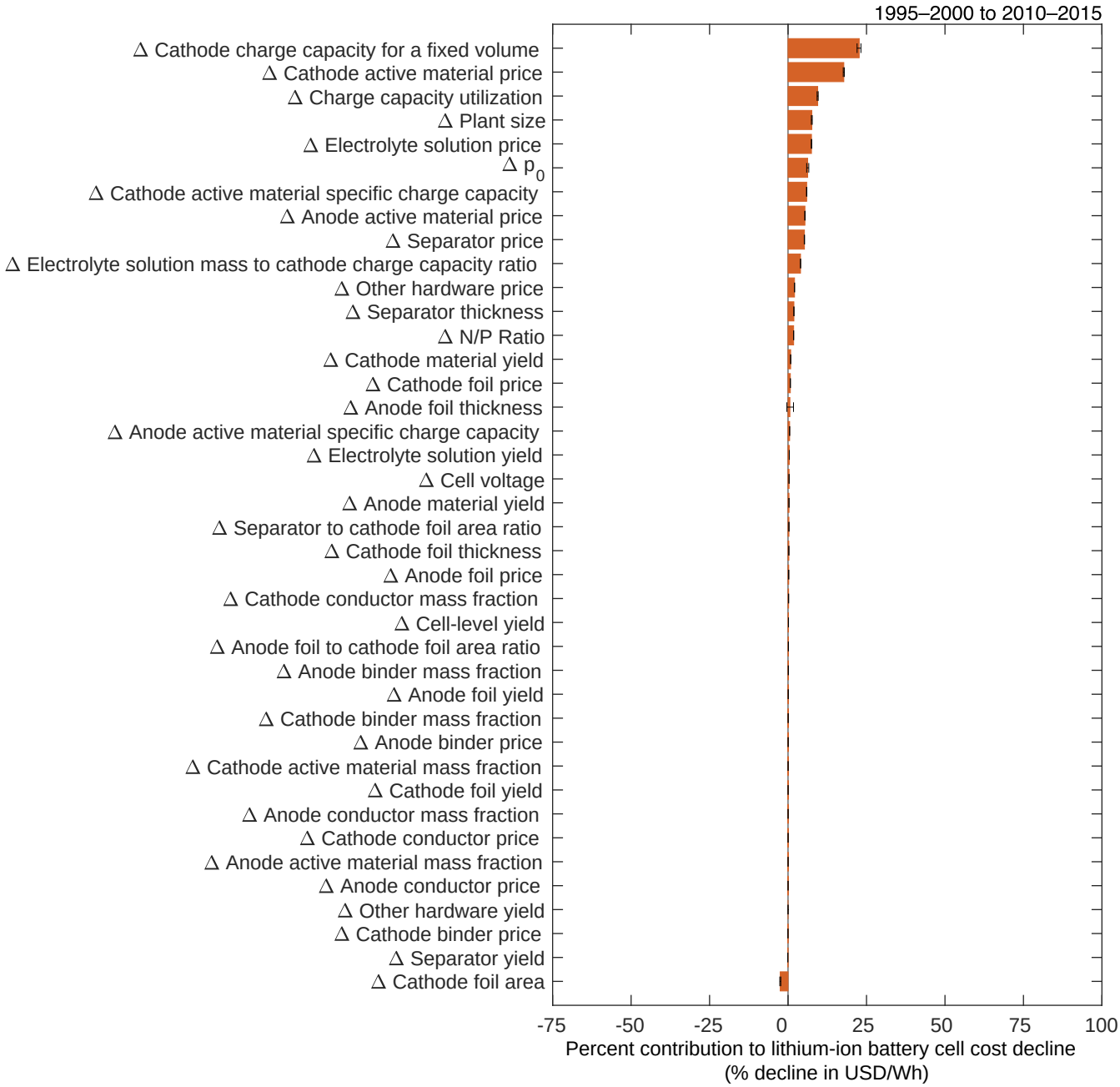

Figure S142: Sensitivity analysis for anode foil thickness (t_{Cu}). The value is varied in both periods to the lower and upper bounds given in Table S8, and for each combination, we recompute the contributions of the low-level mechanisms to cost change. The error bars show the minimum and maximum values of the low-level mechanisms' contributions to cost reduction.

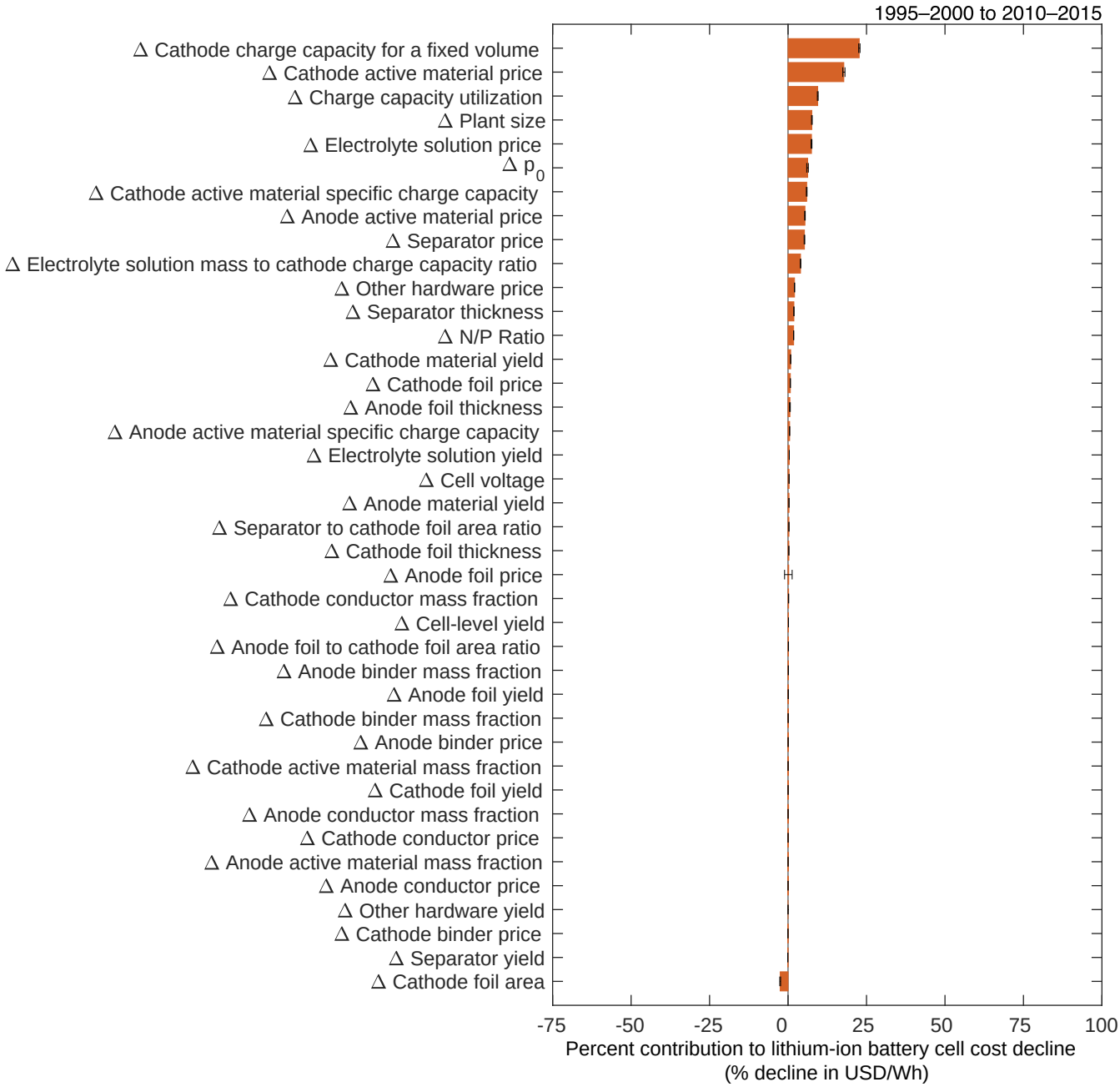

Figure S143: Sensitivity analysis for anode foil price (p_{Cu}). The value is varied in both periods to the lower and upper bounds given in Table S8, and for each combination, we recompute the contributions of the low-level mechanisms to cost change. The error bars show the minimum and maximum values of the low-level mechanisms' contributions to cost reduction.

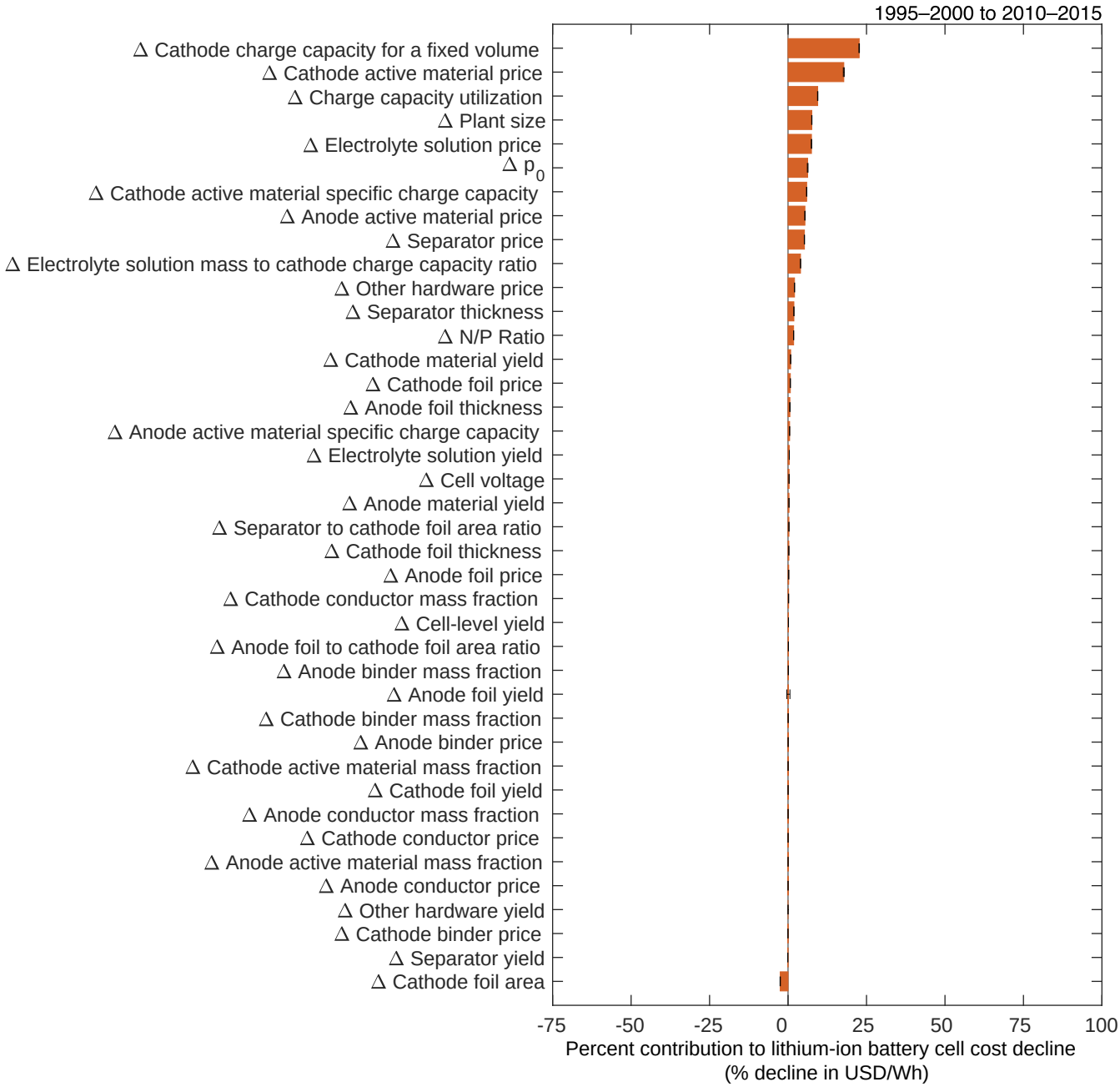

Figure S144: Sensitivity analysis for anode foil yield (y_{Cu}). The value is varied in both periods to the lower and upper bounds given in Table S8, and for each combination, we recompute the contributions of the low-level mechanisms to cost change. The error bars show the minimum and maximum values of the low-level mechanisms' contributions to cost reduction.

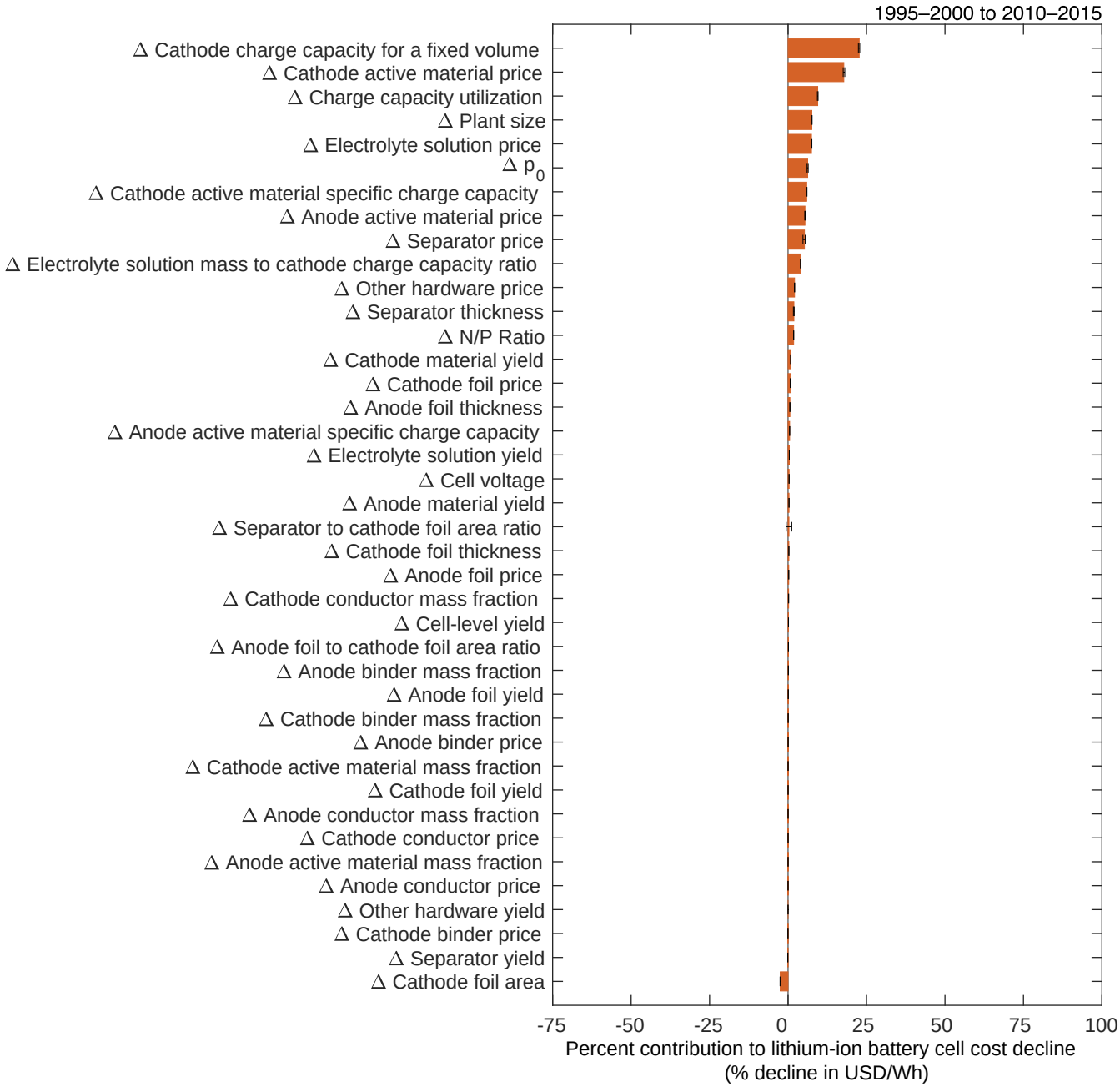

Figure S145: Sensitivity analysis for separator to cathode foil area ratio ($(\text{se/ca})_A$). The value is varied in both periods to the lower and upper bounds given in Table S8, and for each combination, we recompute the contributions of the low-level mechanisms to cost change. The error bars show the minimum and maximum values of the low-level mechanisms' contributions to cost reduction.

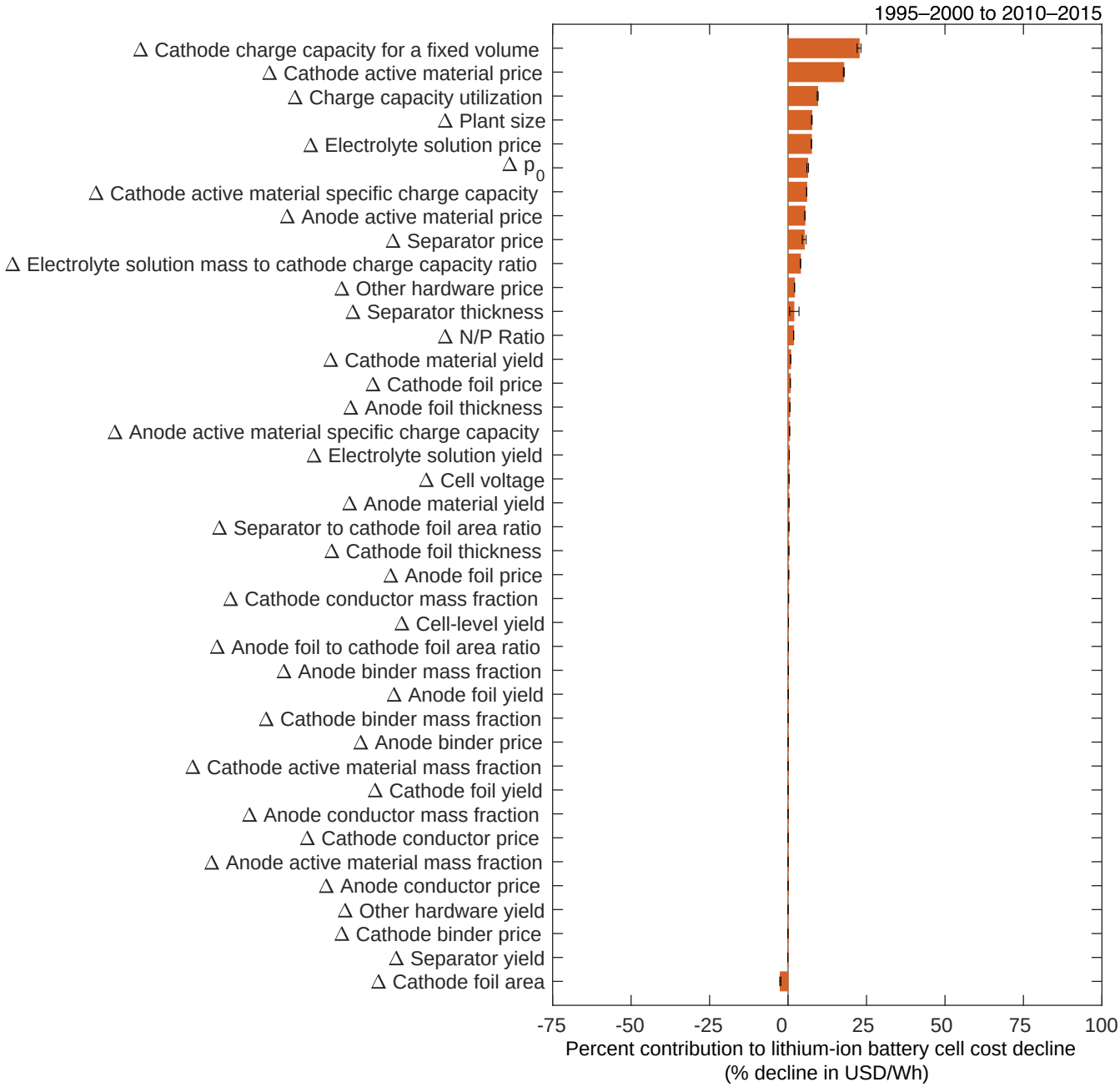

Figure S146: Sensitivity analysis for separator thickness (t_{se}). The value is varied in both periods to the lower and upper bounds given in Table S8, and for each combination, we recompute the contributions of the low-level mechanisms to cost change. The error bars show the minimum and maximum values of the low-level mechanisms' contributions to cost reduction.

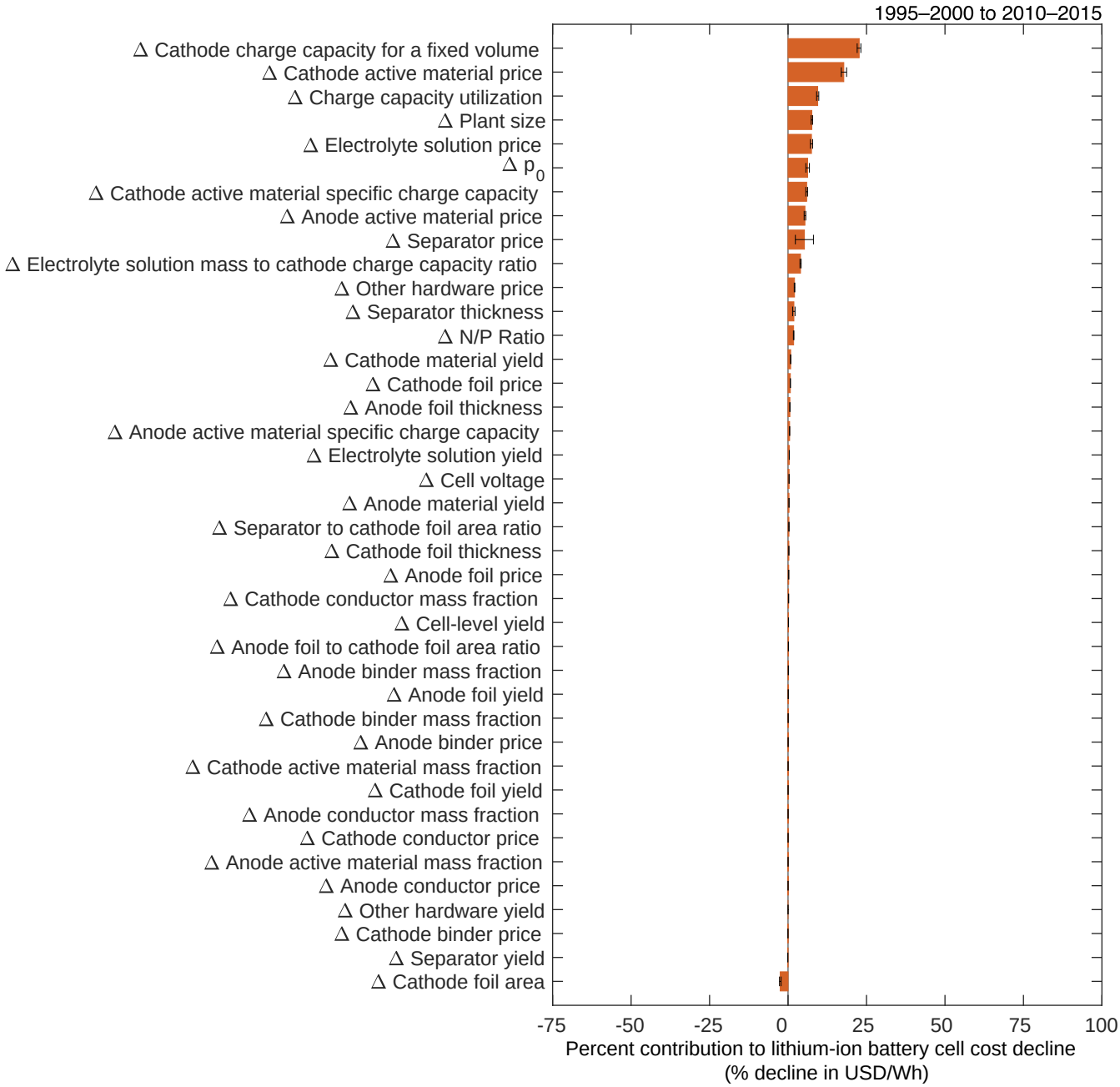

Figure S147: Sensitivity analysis for separator price ($p_{\mathrm{V,se}}$). The value is varied in both periods to the lower and upper bounds given in Table S8, and for each combination, we recompute the contributions of the low-level mechanisms to cost change. The error bars show the minimum and maximum values of the low-level mechanisms' contributions to cost reduction.

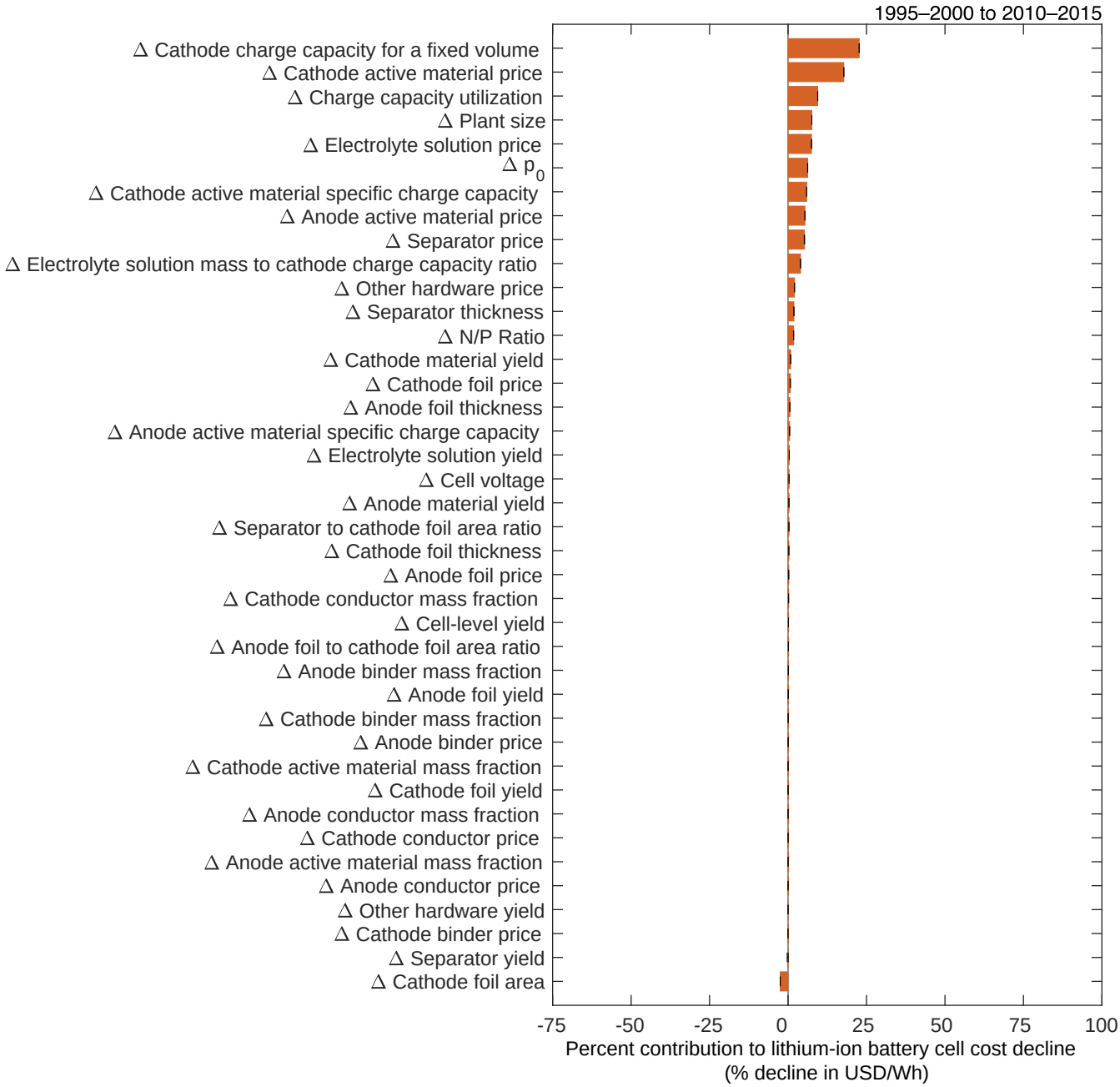

Figure S148: Sensitivity analysis for separator yield (y_{se}). The value is varied in both periods to the lower and upper bounds given in Table S8, and for each combination, we recompute the contributions of the low-level mechanisms to cost change. The error bars show the minimum and maximum values of the low-level mechanisms' contributions to cost reduction.

9.2.3 Data-informed sensitivity analysis figures for other cell cost components and cell-level variables

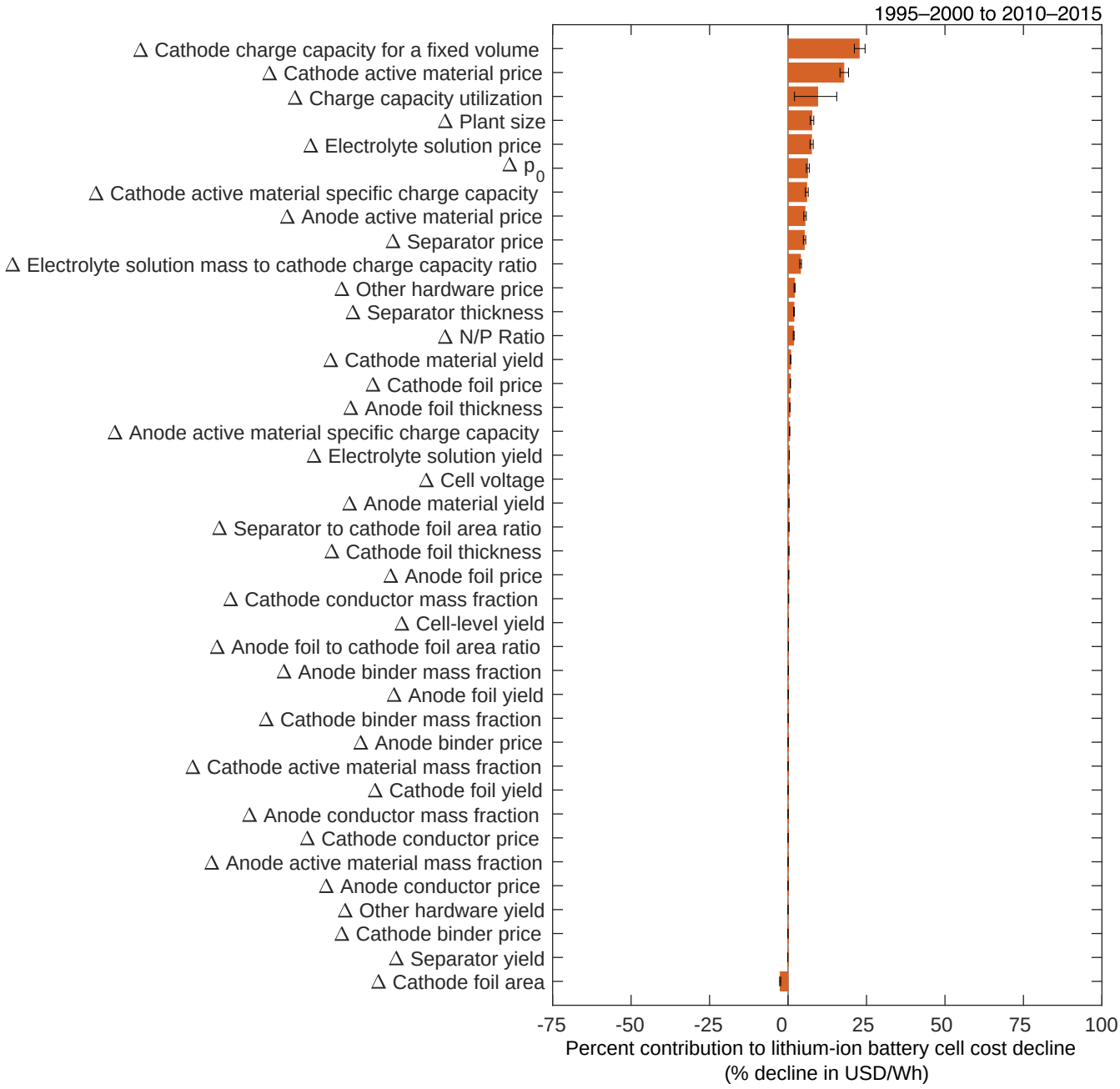

Figure S149: Sensitivity analysis for charge capacity utilization (η_{util}). The value is varied in both periods to the lower and upper bounds given in Table S9, and for each combination, we recompute the contributions of the low-level mechanisms to cost change. The error bars show the minimum and maximum values of the low-level mechanisms' contributions to cost reduction.

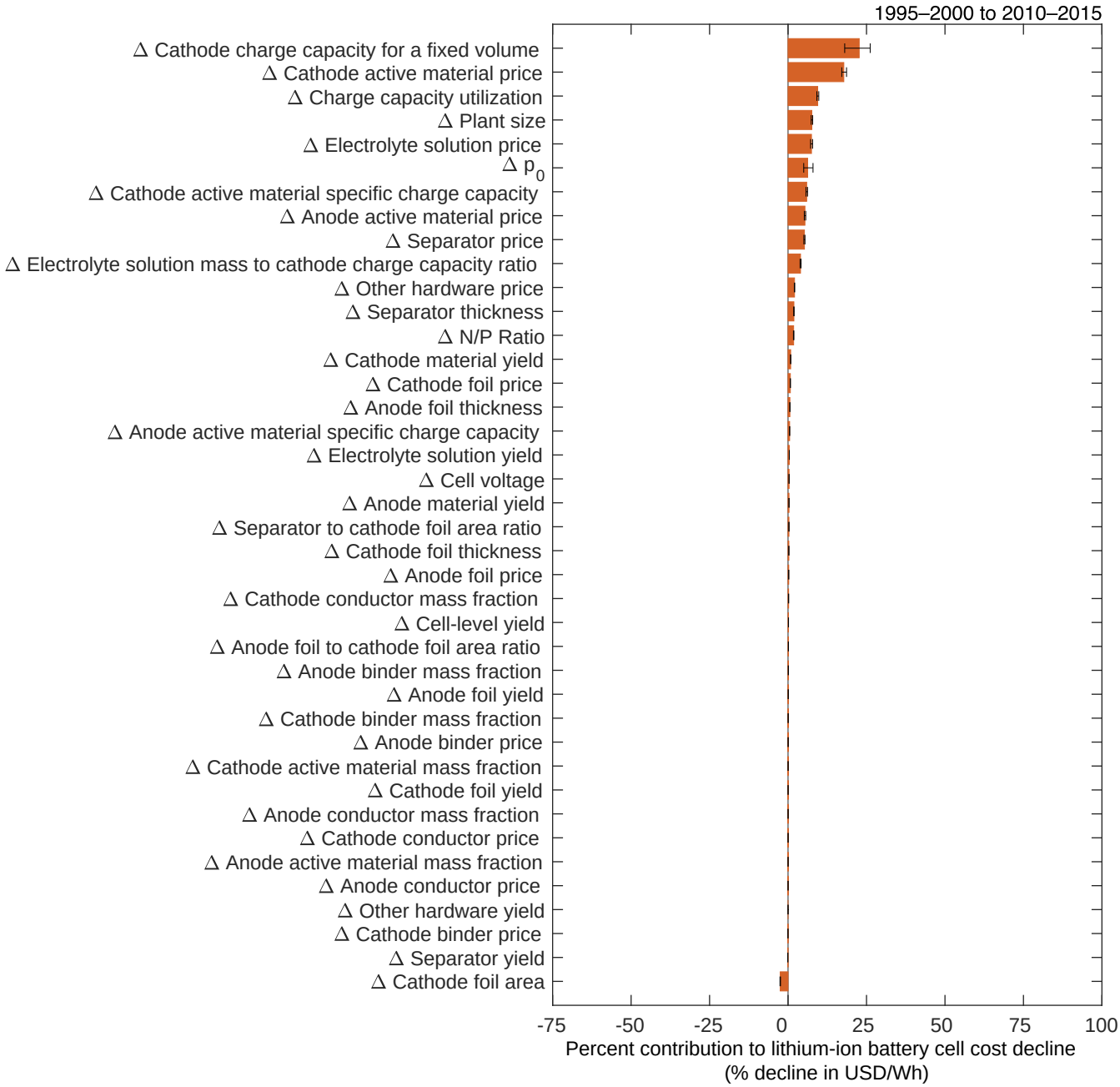

Figure S150: Sensitivity analysis for cathode charge capacity for a fixed volume (Q_{ca}). The value is varied in both periods to the lower and upper bounds given in Table S9, and for each combination, we recompute the contributions of the low-level mechanisms to cost change. The error bars show the minimum and maximum values of the low-level mechanisms' contributions to cost reduction.

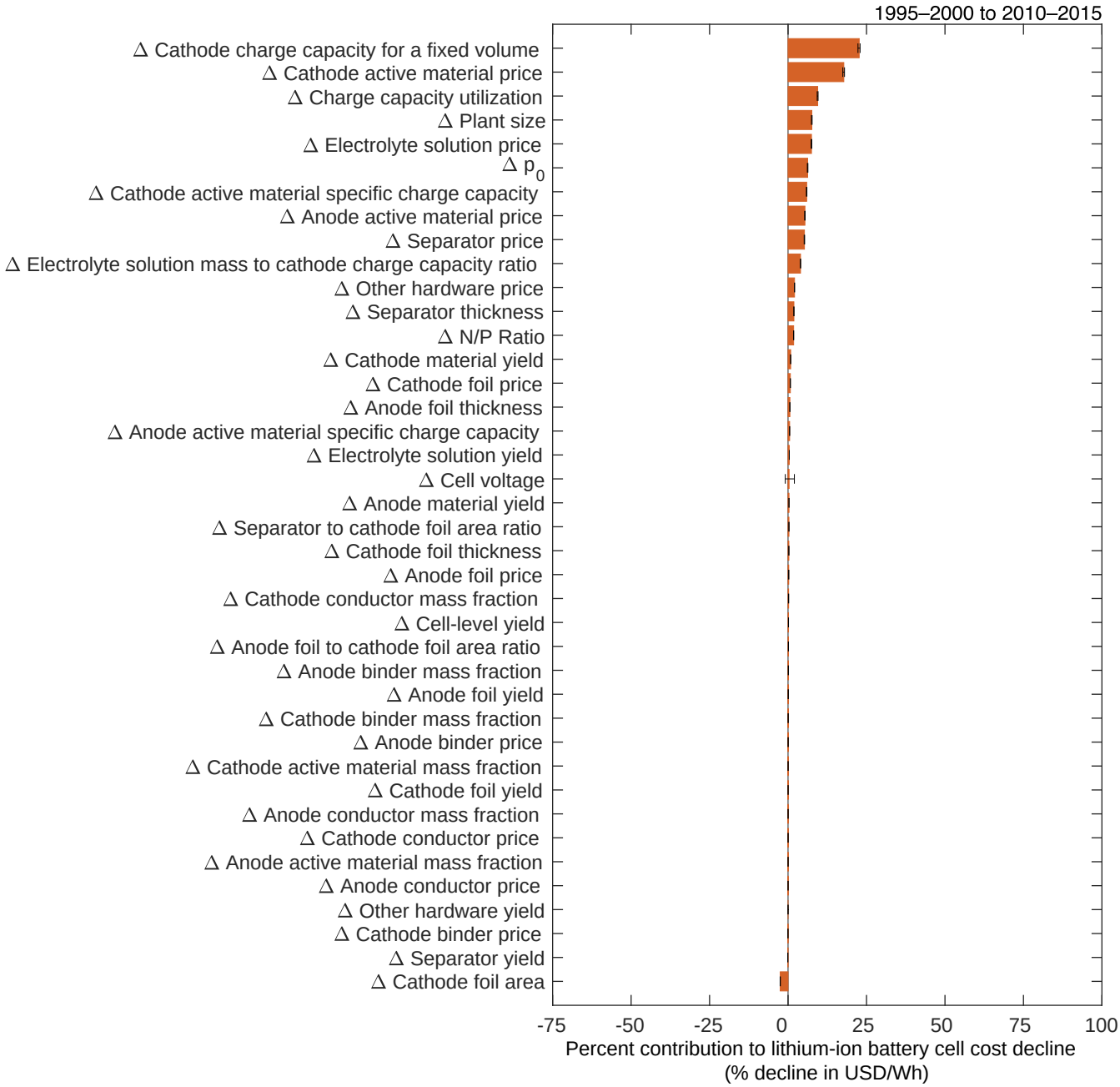

Figure S151: Sensitivity analysis for cell voltage (V). The value is varied in both periods to the lower and upper bounds given in Table S9, and for each combination, we recompute the contributions of the low-level mechanisms to cost change. The error bars show the minimum and maximum values of the low-level mechanisms' contributions to cost reduction.

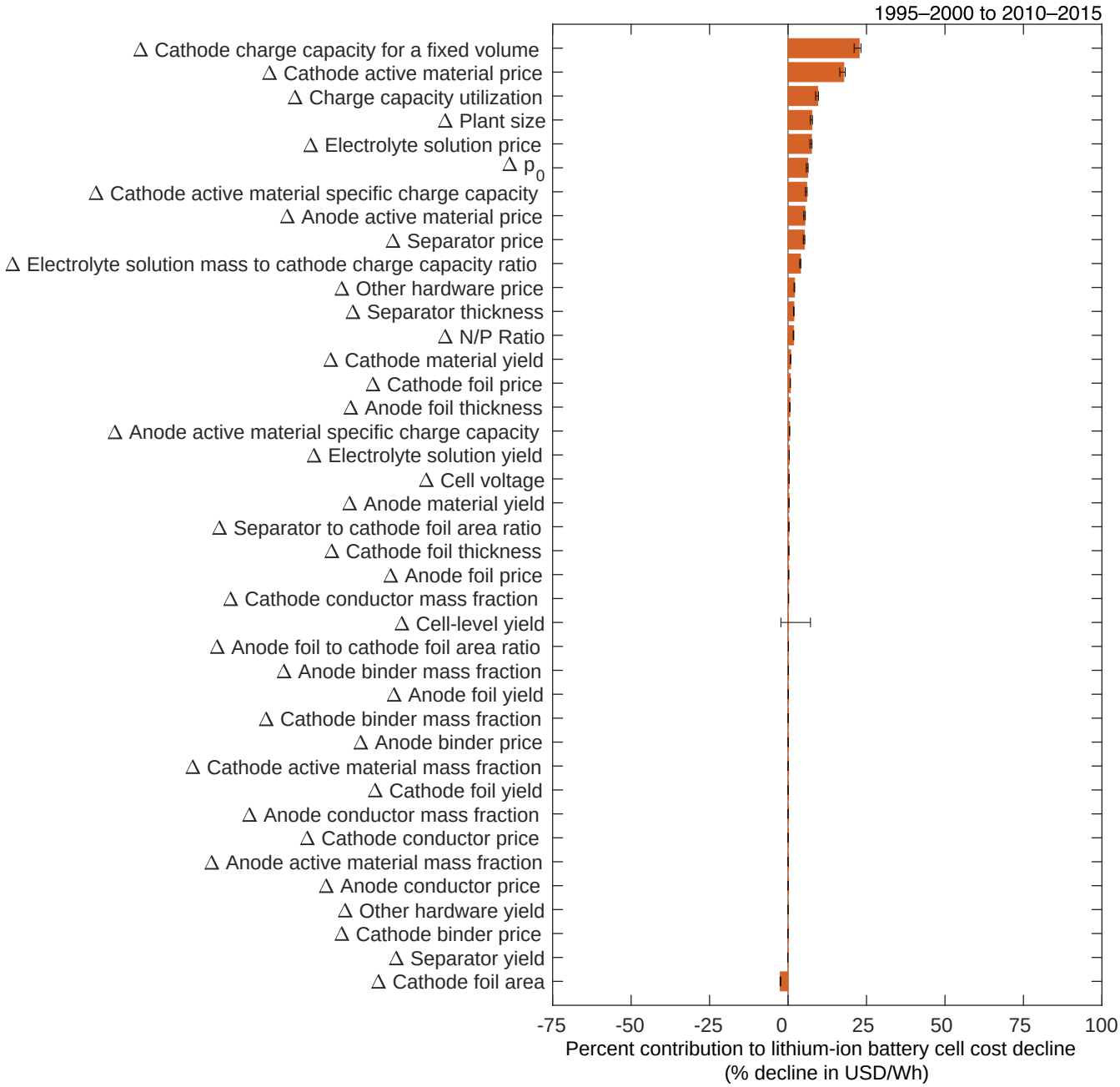

Figure S152: Sensitivity analysis for cell-level yield (y_{cell}). The value is varied in both periods to the lower and upper bounds given in Table S9, and for each combination, we recompute the contributions of the low-level mechanisms to cost change. The error bars show the minimum and maximum values of the low-level mechanisms' contributions to cost reduction.

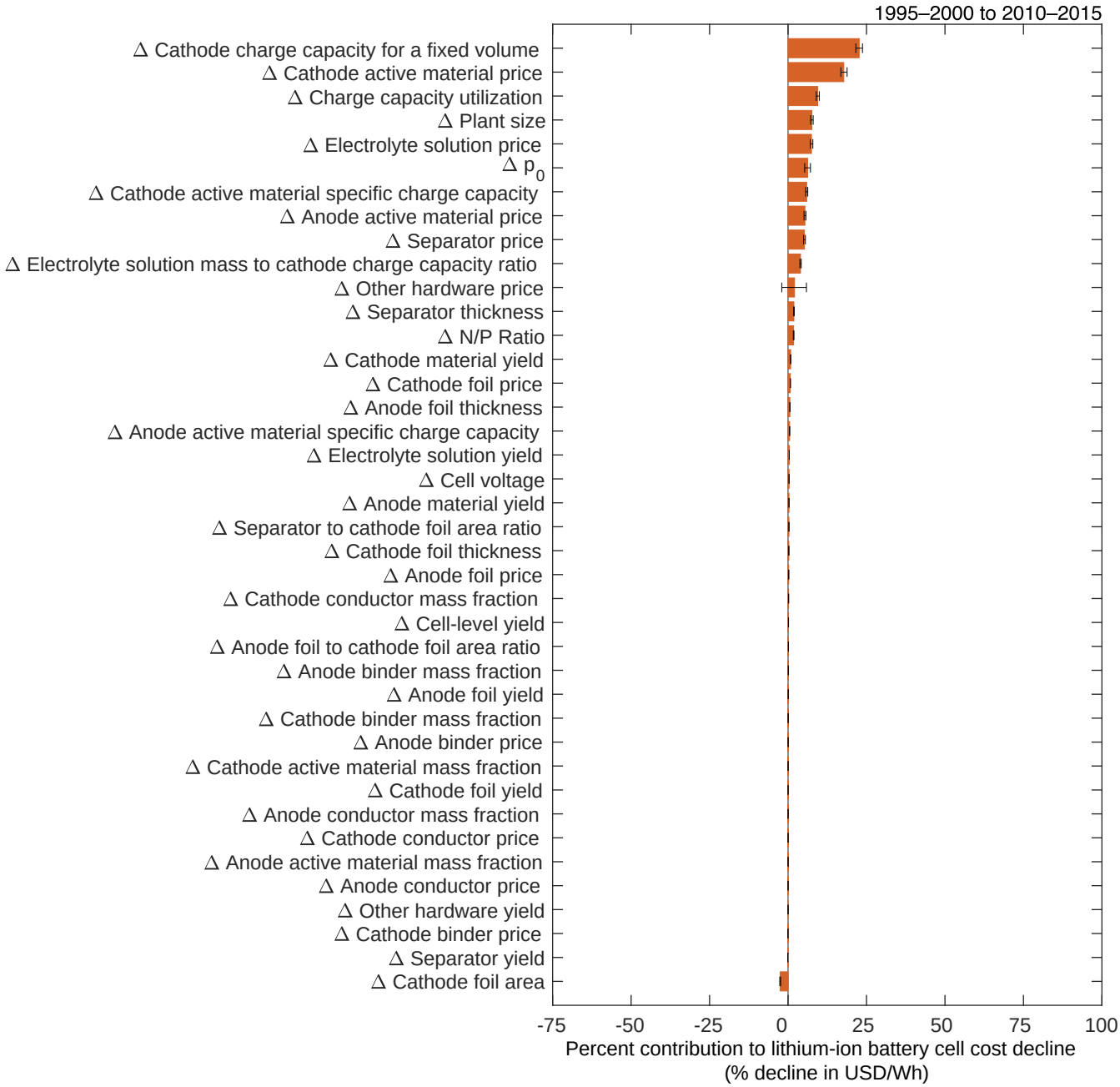

Figure S153: Sensitivity analysis for other hardware price (p_{can}). The value is varied in both periods to the lower and upper bounds given in Table S9, and for each combination, we recompute the contributions of the low-level mechanisms to cost change. The error bars show the minimum and maximum values of the low-level mechanisms' contributions to cost reduction.

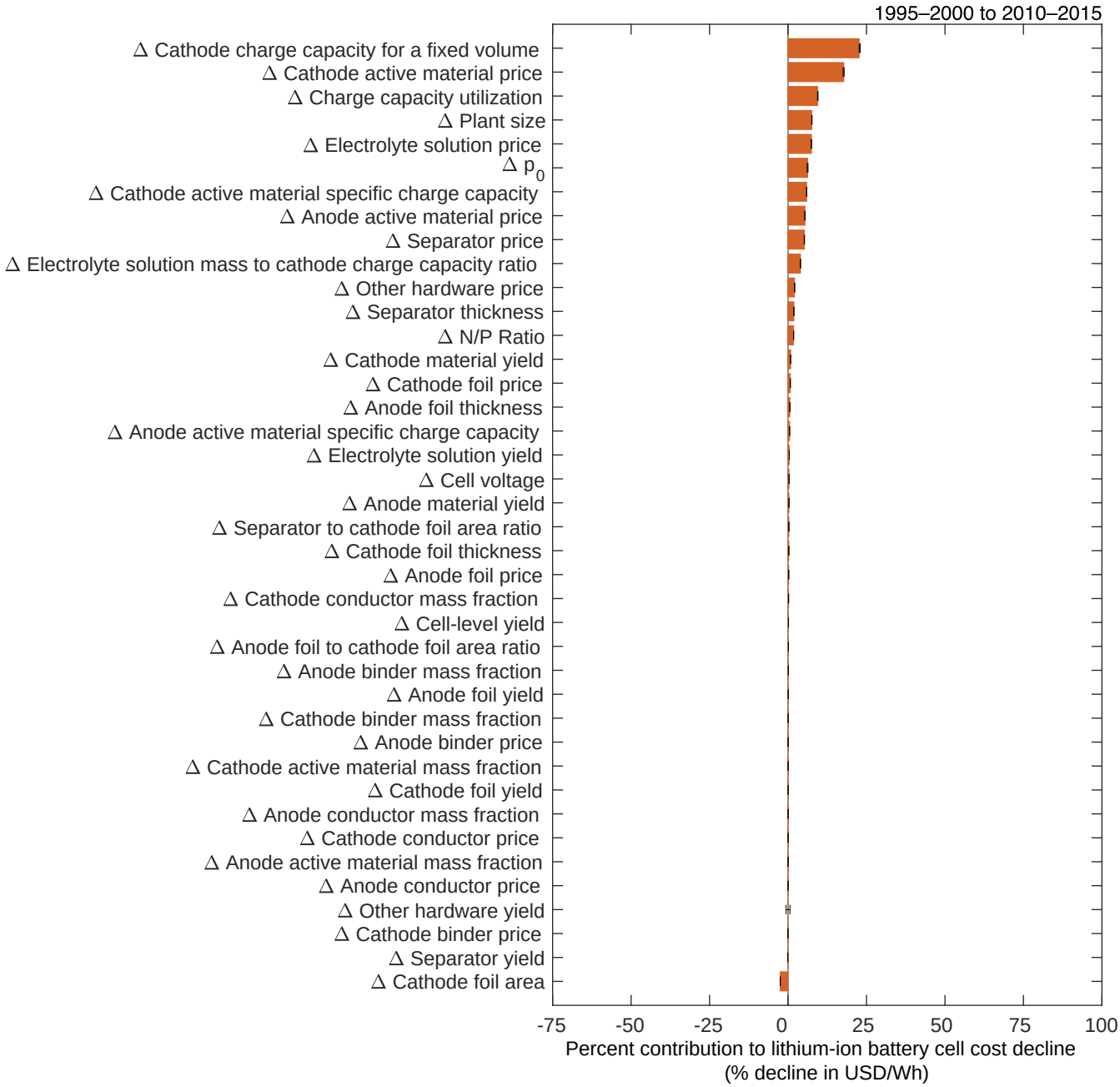

Figure S154: Sensitivity analysis for other hardware yield (y_{can}). The value is varied in both periods to the lower and upper bounds given in Table S9, and for each combination, we recompute the contributions of the low-level mechanisms to cost change. The error bars show the minimum and maximum values of the low-level mechanisms' contributions to cost reduction.

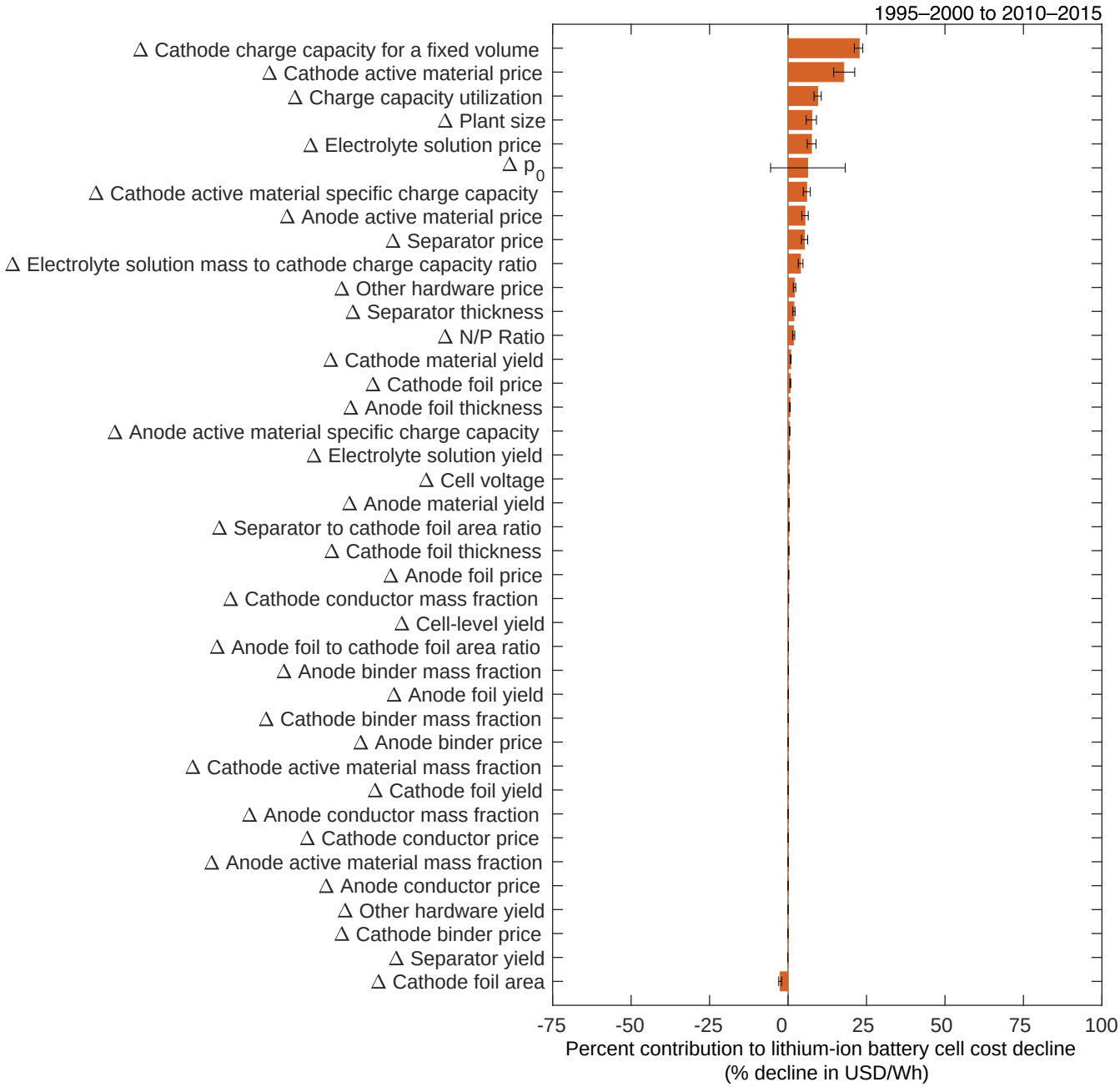

Figure S155: Sensitivity analysis for the material cost fraction (θ). The value is varied in both periods to the lower and upper bounds given in Table S9, and for each combination, we recompute the contributions of the low-level mechanisms to cost change. The error bars show the minimum and maximum values of the low-level mechanisms' contributions to cost reduction.

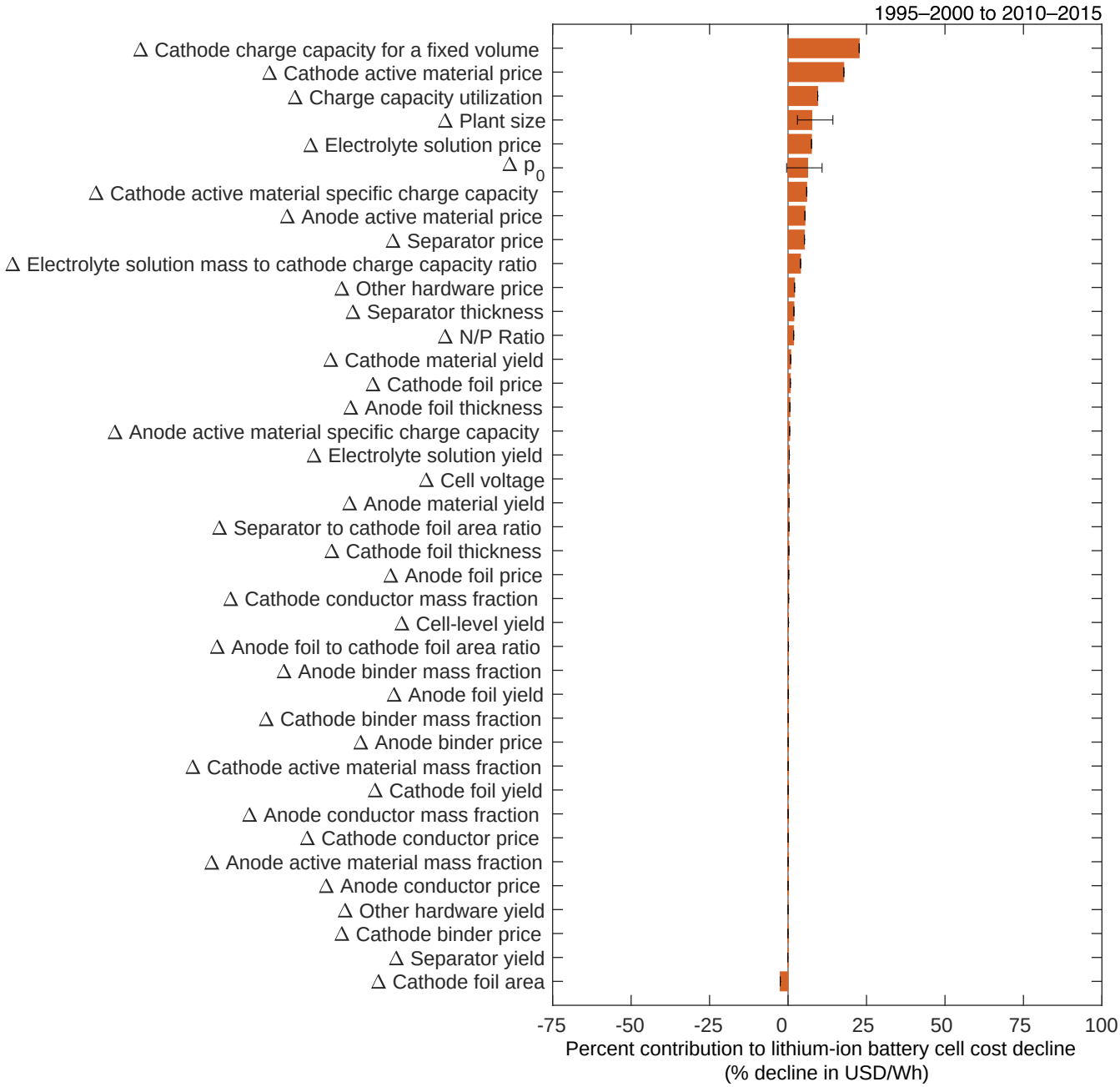

Figure S156: Sensitivity analysis for plant size (K). The value is varied in both periods to the lower and upper bounds given in Table S9, and for each combination, we recompute the contributions of the low-level mechanisms to cost change. The error bars show the minimum and maximum values of the low-level mechanisms' contributions to cost reduction.

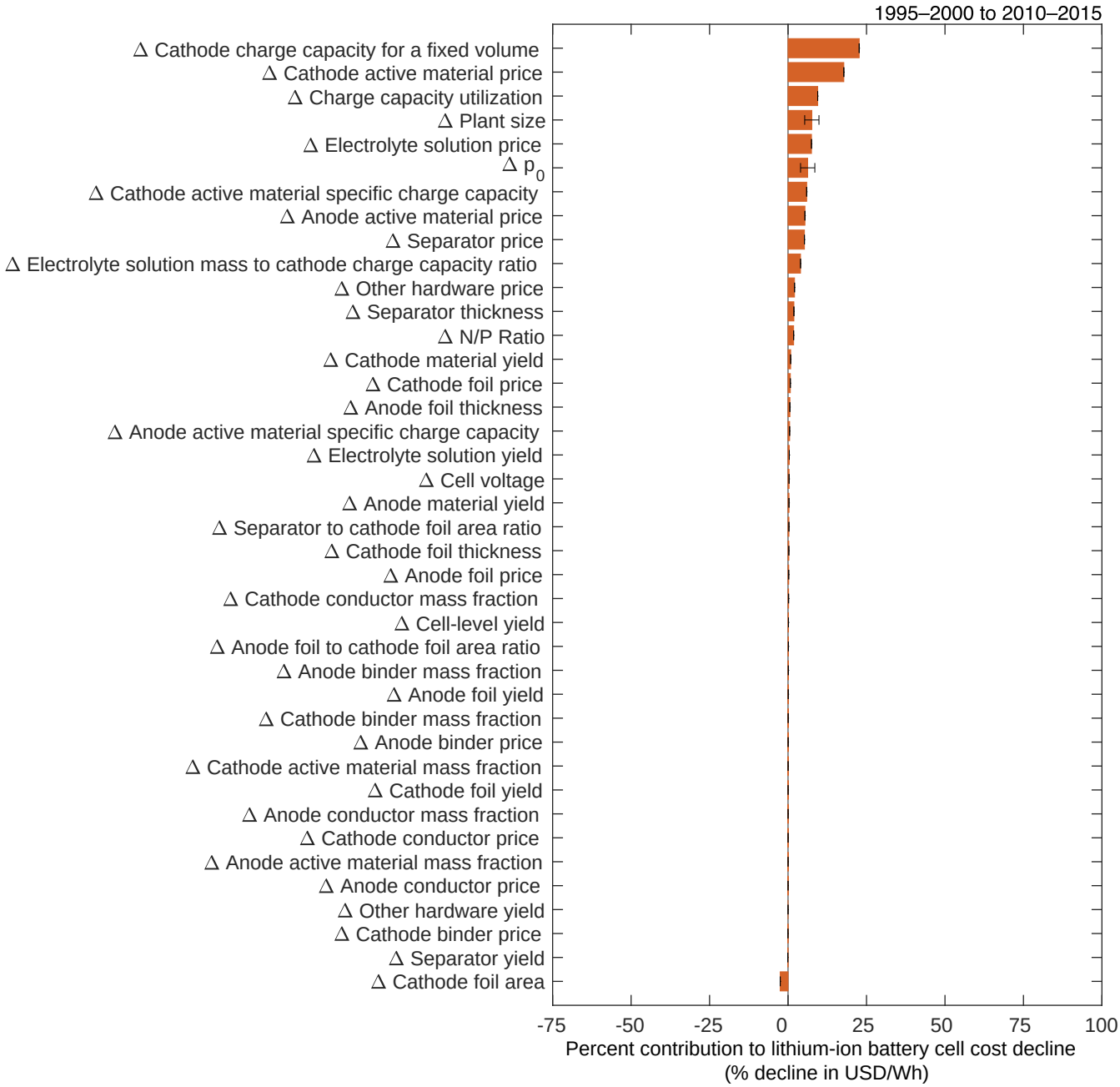

Figure S157: Sensitivity analysis for the scaling factor (b). The value is varied in both periods to the lower and upper bounds given in Table S9, and for each combination, we recompute the contributions of the low-level mechanisms to cost change. The error bars show the minimum and maximum values of the low-level mechanisms' contributions to cost reduction.

9.2.4 Data-informed sensitivity analysis for all variables

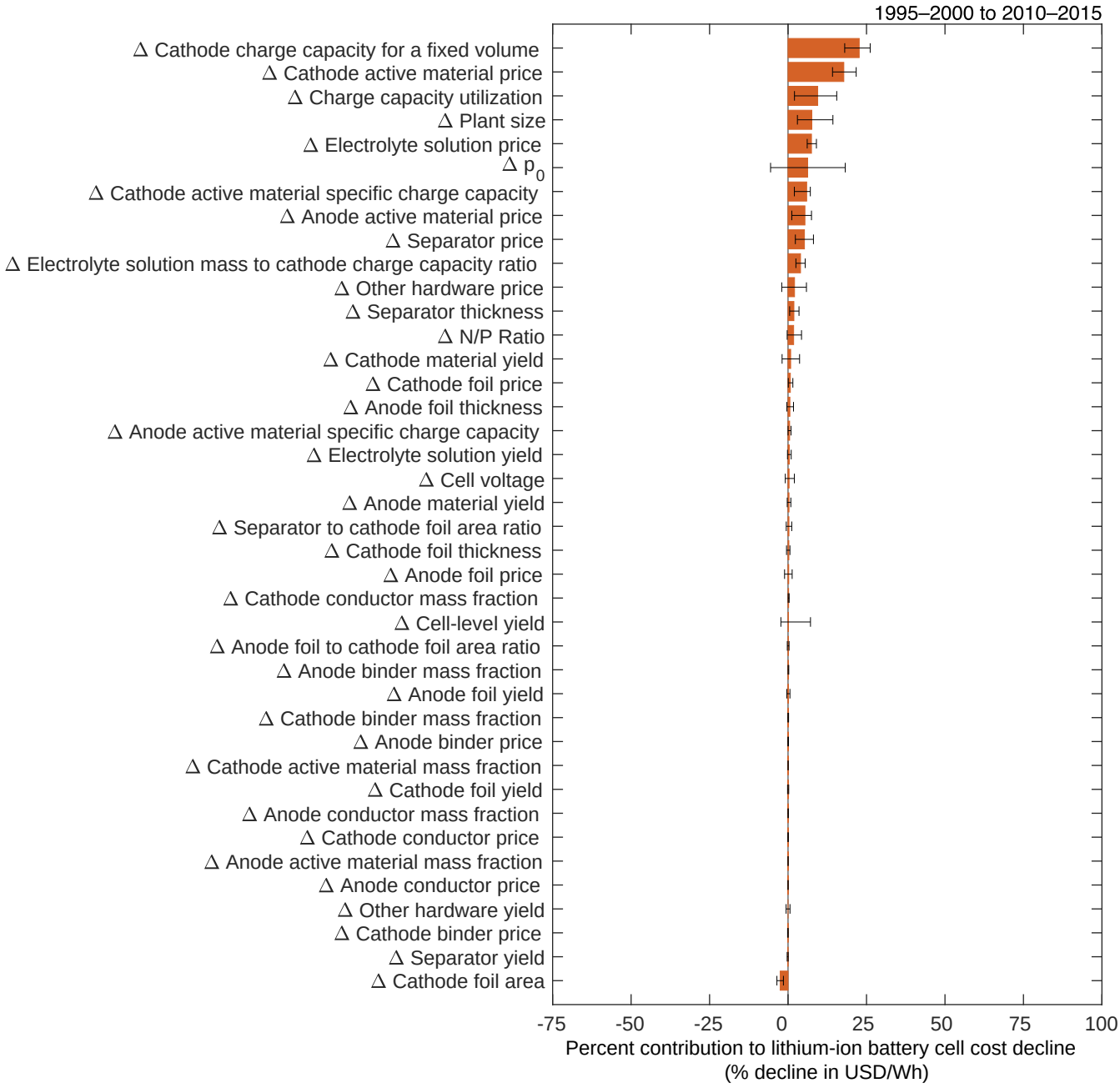

Figure S158: Cost reduction contributions with error bars representing the minimum and maximum values from all scenarios in which variables are varied as given in Tables S7–S9 .

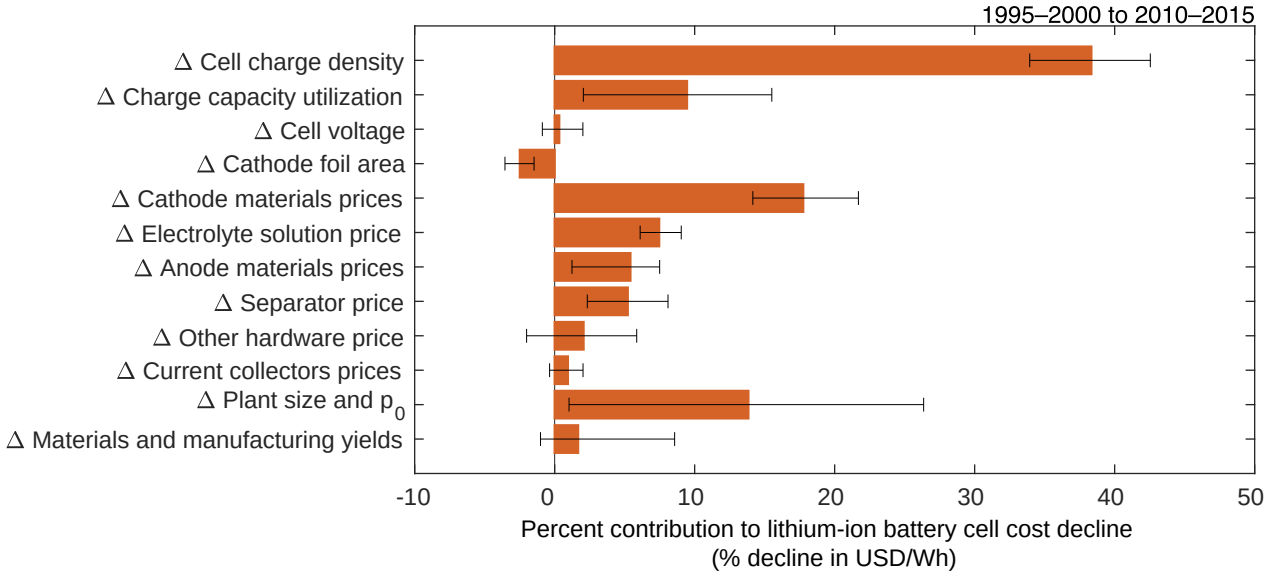

Figure S159: Cost reduction contributions of aggregated low-level cost change mechanisms with error bars representing the minimum and maximum values from all scenarios in which variables are varied as given in Tables S7–S9 .

10 Sensitivity analysis for low-to-high-level mechanism assignments

In this work, we propose a primary assignment for each low-level cost change mechanism to one or more high-level mechanism(s) (see Tables S4–S6). Here we examine how the high-level cost change mechanism results would change given different assignments.

We will first examine the impact of assigning the change in cathode active material price to different high-level mechanisms. In the primary assignment, this price is assigned equally to R&D, EOS, and "other". We could have similarly assigned the change in price entirely to one of these three high-level mechanisms or used different percentages. To examine the extremes, we assign the change in cathode active material price entirely to either R&D, EOS, or "other" and recalculate the high-level mechanism contributions (Figure S160). In all three cases, R&D contributes the plurality of cost change.

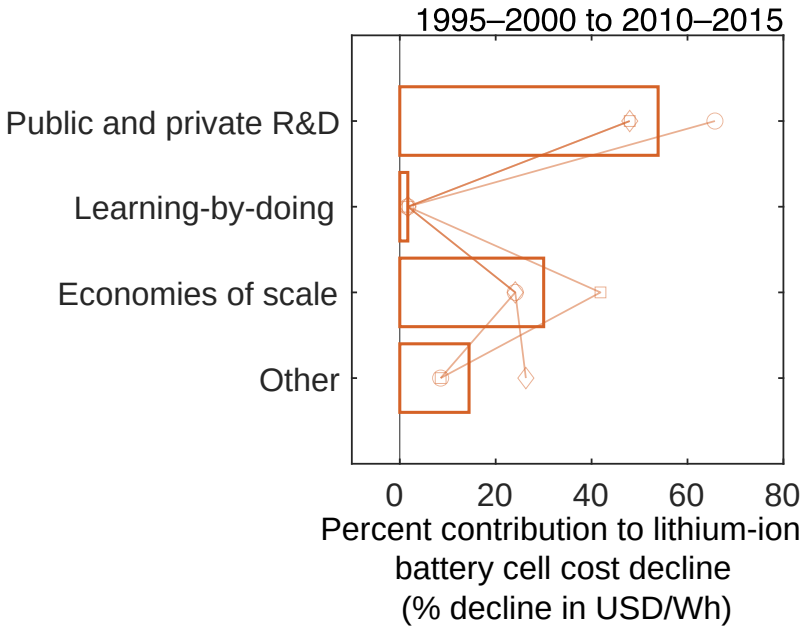

Figure S160: Contributions of high-level mechanisms to the cost decline of 18650-sized lithium-ion cells between period 1 and period 2. The primary assignment results are presented as bars. The results of three alternative assignments of the change in cathode active material price are also plotted, as lines with markers: 100% R&D (◯), 100% EOS (□), and 100% "other" (♢).

We can similarly explore the assignment of the anode active material price change, choosing to categorize it as either entirely R&D, EOS, or "other" (Figure S161). In all three cases, R&D contributes the majority of cost change.

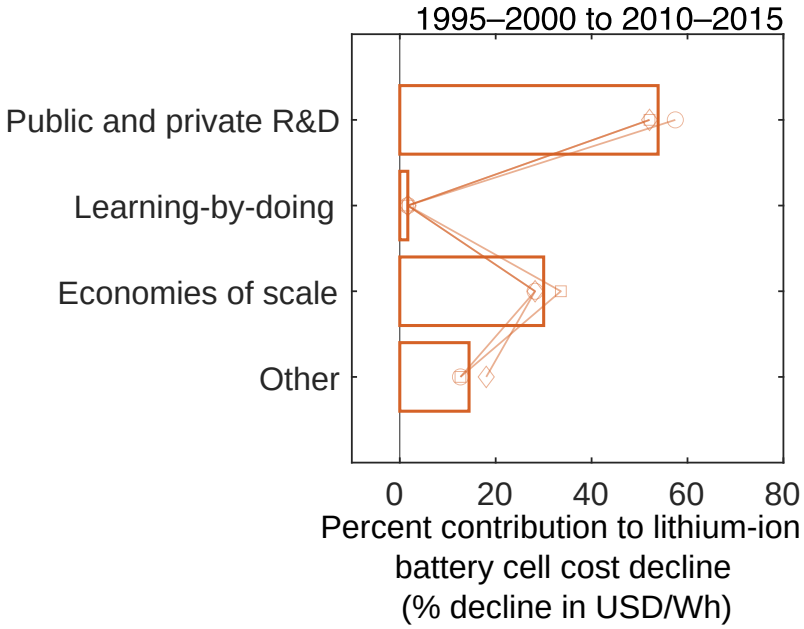

Figure S161: Contributions of high-level mechanisms to the cost decline of 18650-sized lithium-ion cells between period 1 and period 2. The primary assignment results are presented as bars. The results of three alternative assignments of the change in anode active material price are also plotted, as lines with markers: 100% R&D (◯), 100% EOS (□), and 100% "other" (♢).

We can also investigate the impact of assigning the other hardware price change to different high-level mechanisms. The primary assignment categorizes it as partially due to R&D (25%) and partially the result of EOS (75%). We could alternatively assign this change as entirely the result of EOS or "other" (Figure S162). In both cases, the different assignments yield small changes, and the relative contributions of the high-level mechanisms remain unchanged.

In addition, we can explore the combined impact of these various alternative assignments. When all possible combinations of the three aforementioned sets of alternatives are examined, R&D provides the largest contribution in 98% of the cases. (Figure S163).

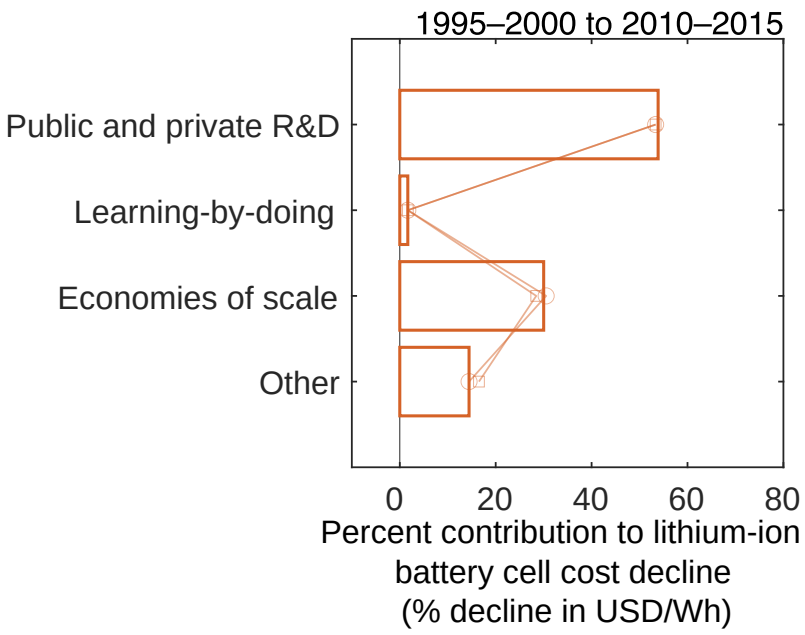

Figure S162: Contributions of high-level mechanisms to the cost decline of 18650-sized lithium-ion cells between period 1 and period 2. The primary assignment results are presented as bars. The results of two alternative assignments of the change in the other hardware price are also plotted, as lines with markers: 100% EOS (◯) and 100% "other" (□).

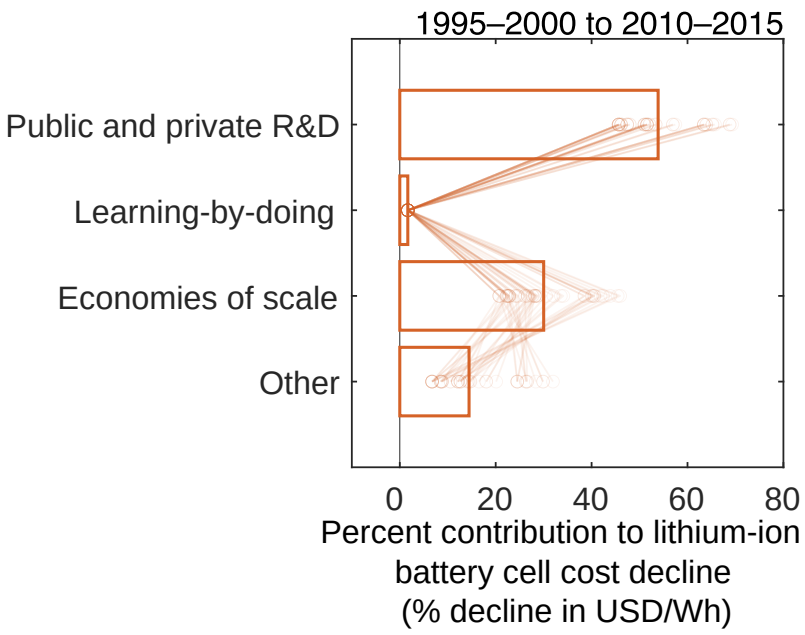

Figure S163: Contributions of high-level mechanisms to the cost decline of 18650-sized lithium-ion cells between period 1 and period 2. The primary assignment results are presented as bars. The results of all combinations of the aforementioned alternative assignments (*i.e.* changes in cathode and anode active material and other hardware prices) are plotted as lines with markers (◯).

11 Assignment of low-level mechanisms to chemistry and materials science research and development

The low-level cost change mechanisms assigned to research and development can be disaggregated into two categories: 1) changes that primarily resulted from advancements in chemistry and materials science, including synthesis, characterization, and processing; and 2) changes that resulted from other research and development, such as design changes. These assignments are given in Tables S10–S12. A complication arises when attempting to assign the increase in cathode charge capacity for a fixed volume as it results from a variety of changes, which include the decreased volume of current collector foils and separators. Between the two representative cell designs considered here, the combined volume of these foils and separators fell by 6%. It is also possible that header volumes fell, but insufficient data were available to reliably estimate this effect. To approximate both influences, the increase in cathode charge capacity was split between factors resulting from chemistry and materials science (90%) and those resulting from design and other changes (10%).

In a sensitivity analysis, we also explore how the estimated contribution to cost decline of advancements in chemistry and material science would change given different assignments. We examine the same extreme cases employed in the analysis that examined the sensitivity of the high-level mechanism estimates to different assignments (see Section 10) and also vary the cathode charge capacity assignment from 85%:15% to 95%:5%. The results of this sensitivity analysis are presented as the error bar in Figure 9.

Table S10: Assignments of mass-related cost contributors employed to examine the influence of chemistry and materials science

Low-level mechanism	**Variable symbol**	**Assignments**	
		Chemistry and materials science	**Other**
Cathode active material mass fraction	$w_{\mathrm{act,ca}}$	100%	0%
Cathode active material price	$p_{\mathrm{act,ca}}$	33%	67%
Cathode binder mass fraction	$w_{\mathrm{bin,ca}}$	100%	0%
Cathode binder price	$p_{\mathrm{bin,ca}}$	0%	100%
Cathode conductor mass fraction	$w_{\mathrm{con,ca}}$	100%	0%
Cathode conductor price	$p_{\mathrm{con,ca}}$	0%	100%
Cathode active material specific charge capacity	q_{ca}	100%	0%
Cathode material yield	y_{ca}	0%	100%
N/P ratio	$(\mathrm{N/P})_Q$	100%	0%
Anode active material mass fraction	$w_{\mathrm{act,an}}$	100%	0%
Anode active material price	$p_{\mathrm{act,an}}$	33%	67%
Anode binder mass fraction	$w_{\mathrm{bin,an}}$	100%	0%
Anode binder price	$p_{\mathrm{bin,an}}$	50%	50%
Anode conductor mass fraction	$w_{\mathrm{con,an}}$	100%	0%
Anode conductor price	$p_{\mathrm{con,an}}$	0%	100%
Anode active material specific charge capacity	q_{an}	100%	0%
Anode material yield	y_{an}	0%	100%
Electrolyte solution mass to cathode charge capacity ratio	D_{el}	100%	0%
Electrolyte solution price	p_{el}	0%	100%
Electrolyte solution yield	y_{el}	0%	100%

Table S11: Assignments of area-related cost contributors employed to examine the influence of chemistry and materials science

Low-level mechanism	**Variable symbol**	**Assignments**	
		Chemistry and materials science	**Other**
Cathode foil area	a_{Al}	0%	100%
Cathode foil thickness	t_{Al}	0%	100%
Cathode foil price	p_{Al}	0%	100%
Cathode foil yield	y_{Al}	0%	100%
Anode foil to cathode foil area ratio	$(\mathrm{an/ca})_A$	0%	100%
Anode foil thickness	t_{Cu}	0%	100%
Anode foil price	p_{Cu}	0%	100%
Anode foil yield	y_{Cu}	0%	100%
Separator to cathode foil area ratio	$(\mathrm{se/ca})_A$	0%	100%
Separator thickness	t_{se}	0%	100%
Separator price	$p_{\mathrm{V,se}}$	0%	100%
Separator yield	y_{se}	0%	100%

Table S12: Assignments of other cell cost contributors and cell-level characteristics employed to examine the influence of chemistry and materials science

Low-level mechanism	Variable symbol	Assignments	
		Chemistry and materials science	Other
Cell-level characteristics			
Charge capacity utilization	η_{util}	100%	0%
Cathode charge capacity for a fixed volume	Q_{ca}	90%	10%
Cell voltage	V	100%	0%
Cell-level yield	y_{cell}	0%	100%
Hardware cost component			
Other hardware price	p_{can}	0%	100%
Other hardware yield	y_{can}	0%	100%
Plant size–dependent characteristics			
p_0	p_0	0%	100%
Plant size	K	0%	100%

12 References

(1) Rohatgi, A. WebPlotDigitizer, version 4.1, Automeris, 2018.

(2) Sakti, A.; Michalek, J. J.; Chun, S.-E.; Whitacre, J. F. A Validation Study of Lithium-Ion Cell Constant c-Rate Discharge Simulation with Battery Design Studio®. *Int. J. Energy Res.* **2013**, *37*, 1562–1568.

(3) In *Handbook of Chemistry and Physics*, 100th ed.; CRC Press, Taylor & Francis Group: 2019.

(4) Johnson, B. A.; White, R. E. Characterization of Commercially Available Lithium-Ion Batteries. *Journal of Power Sources* **1998**, *70*, 48–54.

(5) Juzkow, M. W.; Mayer, S. T. In *The Twelfth Annual Battery Conference on Applications and Advances*, The Twelfth Annual Battery Conference on Applications and Advances, Long Beach, CA, USA, 1997, pp 181–188.

(6) Isaacs, N.; Baker, J.; Bytella, J.; Richardson, K.; Stein, B. In *The 1998 NASA Aerospace Battery Workshop*, The 1998 NASA Aerospace Battery Workshop, ed. by Brewer, J. C., NASA Center for AeroSpace Information: Huntsville, Alabama, 1998, pp 441–479.

(7) Yoshino, A. In *Lithium-Ion Batteries*, Pistoia, G., Ed.; Elsevier: Amsterdam, 2014, pp 1–20.

(8) Pillot, C. Battery Market Development for Consumer Electronics, Automotive, and Industrial: Materials Requirements and Trends, Qinghai EV Rally 2015Xining, China, 2015.

(9) Yoshio, M.; Kozawa, A.; Brodd, R. J. In *Lithium-Ion Batteries*; Springer, New York, NY: 2009, pp 9–48.

(10) Li, M.; Lu, J.; Chen, Z.; Amine, K. 30 Years of Lithium-Ion Batteries. *Advanced Materials* **2018**, *30*, 1800561.

(11) Shokoohi, F. K.; Tarascon, J. M.; Guyomard, D. Rechargeable $LiMn_2O_4$/Carbon Lithium Ion Batteries. *Progress in Batteries and Battery Materials* **1995**, *14*, ed. by Ralph J. Brodd, 199–217.

(12) Amatucci, G. G.; Tarascon, J. M.; Klein, L. C. Cobalt Dissolution in $LiCoO_2$-Based Non-Aqueous Rechargeable Batteries. *Solid State Ionics* **1996**, *83*, 167–173.

(13) Gaines, L.; Cuenca, R. *Costs of Lithium-Ion Batteries for Vehicles*; ANL/ESD-42; Argonne, Illinois: Argonne National Laboratory, 2000, p 73.

(14) Marks, T.; Trussler, S.; Smith, A. J.; Xiong, D.; Dahn, J. R. A Guide to Li-Ion Coin-Cell Electrode Making for Academic Researchers. *J. Electrochem. Soc.* **2010**, *158*, A51–A57.

(15) Yoshio, M.; Noguchi, H. In *Lithium-Ion Batteries*, Yoshio, M., Brodd, R. J., Kozawa, A., Eds.; Springer, New York, NY: 2009, pp 9–48.

(16) Burns, J. C.; Stevens, D. A.; Dahn, J. R. In-Situ Detection of Lithium Plating Using High Precision Coulometry. *J. Electrochem. Soc.* **2015**, *162*, A959–A964.

(17) Aurbach, D.; Markovsky, B.; Rodkin, A.; Cojocaru, M.; Levi, E.; Kim, H.-J. An Analysis of Rechargeable Lithium-Ion Batteries after Prolonged Cycling. *Electrochimica Acta* **2002**, *47*, 1899–1911.

(18) Golubkov, A. W.; Fuchs, D.; Wagner, J.; Wiltsche, H.; Stangl, C.; Fauler, G.; Voitic, G.; Thaler, A.; Hacker, V. Thermal-Runaway Experiments on Consumer Li-Ion Batteries with Metal-Oxide and Olivin-Type Cathodes. *RSC Adv.* **2014**, *4*, 3633–3642.

(19) Liu, J.; Kahaian, A.; Belharouak, I.; Kang, S.; Oliver, S.; Henriksen, S.; Amine, K. *Screening Report on Cell Materials for High-Power Li-Ion HEV Batteries.* ANL-03/16, 811288; Argonne, Illinois: Argonne National Laboratory, 2003.

(20) Broussely, M.; Biensan, P.; Simon, B. Lithium Insertion into Host Materials: The Key to Success for Li Ion Batteries. *Electrochimica Acta* **1999**, *45*, 3–22.

(21) Golubkov, A. W.; Scheikl, S.; Planteu, R.; Voitic, G.; Wiltsche, H.; Stangl, C.; Fauler, G.; Thaler, A.; Hacker, V. Thermal Runaway of Commercial 18650 Li-Ion Batteries with LFP and NCA Cathodes - Impact of State of Charge and Overcharge. *RSC Adv.* **2015**, *5*, 57171–57186.

(22) Sekai, K.; Azuma, H.; Omaru, A.; Fujita, S.; Imoto, H.; Endo, T.; Yamaura, K.; Nishi, Y.; Mashiko, S.; Yokogawa, M. Lithium-Ion Rechargeable Cells with $LiCoO_2$ and Carbon Electrodes. *Journal of Power Sources* **1993**, *43*, 241–244.

(23) Xu, K. Nonaqueous Liquid Electrolytes for Lithium-Based Rechargeable Batteries. *Chem. Rev.* **2004**, *104*, 4303–4418.

(24) Xu, K. Electrolytes and Interphases in Li-Ion Batteries and Beyond. *Chem. Rev.* **2014**, *114*, 11503–11618.

(25) Kalhoff, J.; Eshetu, G. G.; Bresser, D.; Passerini, S. Safer Electrolytes for Lithium-Ion Batteries: State of the Art and Perspectives. *ChemSusChem* **2015**, *8*, 2154–2175.

(26) Schmuch, R.; Wagner, R.; Hörpel, G.; Placke, T.; Winter, M. Performance and Cost of Materials for Lithium-Based Rechargeable Automotive Batteries. *Nat Energy* **2018**, *3*, 267–278.

(27) Winter, M.; Barnett, B.; Xu, K. Before Li Ion Batteries. *Chem. Rev.* **2018**, *118*, 11433–11456.

(28) Kwade, A.; Haselrieder, W.; Leithoff, R.; Modlinger, A.; Dietrich, F.; Droeder, K. Current Status and Challenges for Automotive Battery Production Technologies. *Nature Energy* **2018**, *3*, 290–300.

(29) Megahed, S.; Scrosati, B. Lithium-Ion Rechargeable Batteries. *Journal of Power Sources* **1994**, *51*, 79–104.

(30) Brandt, K. Historical Development of Secondary Lithium Batteries. *Solid State Ionics* **1994**, *69*, 173–183.

(31) Owens, B. B.; Osaka, T. Panel Discussion Future Prospects of Lithium Batteries. *Journal of Power Sources* **1997**, *68*, 173–186.

(32) Moshtev, R.; Johnson, B. State of the Art of Commercial Li Ion Batteries. *Journal of Power Sources* **2000**, *91*, 86–91.

(33) Brodd, R. J.; Tagawa, K. In *Advances in Lithium-Ion Batteries*; Springer, Boston, MA: 2002, pp 267–288.

(34) Krueger, S.; Kloepsch, R.; Li, J.; Nowak, S.; Passerini, S.; Winter, M. How Do Reactions at the Anode/Electrolyte Interface Determine the Cathode Performance in Lithium-Ion Batteries? *J. Electrochem. Soc.* **2013**, *160*, A542–A548.

(35) Meister, P.; Jia, H.; Li, J.; Kloepsch, R.; Winter, M.; Placke, T. Best Practice: Performance and Cost Evaluation of Lithium Ion Battery Active Materials with Special Emphasis on Energy Efficiency. *Chem. Mater.* **2016**, *28*, 7203–7217.

(36) Kasnatscheew, J.; Placke, T.; Streipert, B.; Rothermel, S.; Wagner, R.; Meister, P.; Laskovic, I. C.; Winter, M. A Tutorial into Practical Capacity and Mass Balancing of Lithium Ion Batteries. *J. Electrochem. Soc.* **2017**, *164*, A2479–A2486.

(37) Arora, P.; White, R. E.; Doyle, M. Capacity Fade Mechanisms and Side Reactions in Lithium-Ion Batteries. *J. Electrochem. Soc.* **1998**, *145*, 3647–3667.

(38) Ziegler, M. S.; Trancik, J. E. Re-Examining Rates of Lithium-Ion Battery Technology Improvement and Cost Decline. *Energy Environ. Sci.* **2021**, *14*, 1635–1651.

(39) New JEC Samples No. 5 ($LiCoO_2$) and No. 6 ($LiNiO_2$). *Progress in Batteries & Battery Materials* **1994**, *13*.

(40) *Strategic and Critical Materials Operations Report To Congress: Operations under the Strategic and Critical Materials Stock Piling Act during Fiscal Year 2015*; Fort Belvoir, VA: Office of the Under Secretary of Defense for Acquisition, Technology, and Logistics, US Department of Defense, 2016.

(41) *Strategic and Critical Materials Operations Report To Congress: Operations under the Strategic and Critical Materials Stock Piling Act during Fiscal Year 2016*; Fort Belvoir, VA: Office of the Under Secretary of Defense for Acquisition, Technology, and Logistics, US Department of Defense, 2017.

(42) Brodd, R. J.; Helou, C. Cost Comparison of Producing High-Performance Li-Ion Batteries in the U.S. and in China. *Journal of Power Sources* **2013**, *231*, 293–300.

(43) Ciez, R. E.; Whitacre, J. F. Comparison between Cylindrical and Prismatic Lithium-Ion Cell Costs Using a Process Based Cost Model. *Journal of Power Sources* **2017**, *340*, 273–281.

(44) Henriksen, G. L.; Amine, K.; Liu, J.; Nelson, P. A. *Materials Cost Evaluation Report for High-Power Li-Ion HEV Batteries*; ANL-03/5; Argonne, Illinois: Argonne National Laboratory, 2002, p 70.

(45) Weidner, J. W.; Doyle, M. Report on the Electrolytic Industries for the Year 1999. *J. Electrochem. Soc.* **2000**, *147*, 3953–3974.

(46) Sakti, A.; Azevedo, I. M. L.; Fuchs, E. R. H.; Michalek, J. J.; Gallagher, K. G.; Whitacre, J. F. Consistency and Robustness of Forecasting for Emerging Technologies: The Case of Li-Ion Batteries for Electric Vehicles. *Energy Policy* **2017**, *106*, 415–426.

(47) *Advanced Rechargeable Battery Market Research Program 2007*; Institute of Information Technology, Ltd., 2007.

(48) Nelson, P. A.; Gallagher, K. G.; Bloom, I. D.; Dees, D. W. *Modeling the Performance and Cost of Lithium-Ion Batteries for Electric-Drive Vehicles*; Technical Report ANL-12/55; Argonne, IL: Argonne National Lab, 2011.

(49) Nelson, P. A.; Santini, D. J.; Barnes, J. In, EVS24 International Battery, Hybrid and Fuel Cell Electric Vehicle Symposium, World Electric Vehicle Journal: Stavanger, Norway, 2009; Vol. 3, p 12.

(50) Leamer, E. E. Corrected Expert Report of Edward E. Leamer, Ph.D. 2016.

(51) BatPaC, version 4.0, Argonne, Illinois: Argonne National Laboratory, 2020.

(52) *Mineral Commodity Summaries 1996*; U.S. Geological Survey, 1996.

(53) *Mineral Commodity Summaries 1997*; U.S. Geological Survey, 1997.

(54) *Mineral Commodity Summaries 1998*; Reston, VA: U.S. Geological Survey, 1998.

(55) *Mineral Commodity Summaries 1999*; Reston, VA: U.S. Geological Survey, 1999.

(56) *Mineral Commodity Summaries 2000*; Reston, VA: U.S. Geological Survey, 2000.

(57) *Mineral Commodity Summaries 2001*; Reston, VA: U.S. Geological Survey, 2001.

(58) *Mineral Commodity Summaries 2002*; Reston, VA: U.S. Geological Survey, 2002.

(59) *Mineral Commodity Summaries 2003*; Reston, VA: U.S. Geological Survey, 2003.

(60) *Mineral Commodity Summaries 2004*; Reston, VA: U.S. Geological Survey, 2004.

(61) *Mineral Commodity Summaries 2005*; Reston, VA: U.S. Geological Survey, 2005.

(62) *Mineral Commodity Summaries 2006*; Reston, VA: U.S. Geological Survey, 2006.

(63) *Mineral Commodity Summaries 2007*; Reston, VA: U.S. Geological Survey, 2007.

(64) *Mineral Commodity Summaries 2008*; Reston, VA: U.S. Geological Survey, 2008.

(65) *Mineral Commodity Summaries 2009*; Reston, VA: U.S. Geological Survey, 2009.

(66) *Mineral Commodity Summaries 2010*; Reston, VA: U.S. Geological Survey, 2010.

(67) *Mineral Commodity Summaries 2011*; Reston, VA: U.S. Geological Survey, 2011.

(68) *Mineral Commodity Summaries 2012*; Reston, VA: U.S. Geological Survey, 2012.

(69) *Mineral Commodity Summaries 2013*; Reston, VA: U.S. Geological Survey, 2013.

(70) *Mineral Commodity Summaries 2014*; Reston, VA: U.S. Geological Survey, 2014.

(71) *Mineral Commodity Summaries 2015*; Reston, VA: U.S. Geological Survey, 2015.

(72) *Mineral Commodity Summaries 2016*; Reston, VA: U.S. Geological Survey, 2016.

(73) *Mineral Commodity Summaries 2017*; Reston, VA: U.S. Geological Survey, 2017.

(74) *Mineral Commodity Summaries 2018*; Reston, VA: U.S. Geological Survey, 2018.

(75) *Mineral Commodity Summaries 2019*; Reston, VA: U.S. Geological Survey, 2019.

(76) *Mineral Commodity Summaries 2020*; Reston, VA: U.S. Geological Survey, 2020.